No Restrictions.

ERRATA

PP xv 6th line: "is made" for "in made"

P xii 6th line: "Residual" for "Sample"

P10 equation 2.6, "$\hat{\theta} = \arg\min_{\hat{\theta}} \sum_{i=1}^{n} r_i^2$" for "$\hat{\theta} = \underset{\hat{\theta}}{Minimize} \sum_{i=1}^{n} r_i^2$"

P10 equation 2.9, "$\ldots = \dfrac{\partial S(\hat{\theta})}{\partial \hat{\theta}} = 0$" for "$\ldots = \dfrac{\partial S(\hat{\theta})}{\partial \hat{\theta}} = \dfrac{\partial^2 S(\hat{\theta})}{\partial \hat{\theta}^2} = 2X'X$"

P13 equation 2.13, "$\hat{\theta} = \arg\min_{\hat{\theta}} \sum_{i=1}^{n} \rho(r_i)$" for "$\underset{\hat{\theta}}{Minimize} \sum_{i=1}^{n} \rho(r_i)$"

P14 equation 2.16

"$$\rho(r) = \begin{cases} \frac{1}{2} r^2, & |r| \le a \\ \frac{1}{2} a(2|r| - a), & a < |r| \le b \\ \frac{1}{2} a\left[(|r| - c)^2 / (b - c) + (b + c - a)\right], & b < |r| \le c \\ \frac{1}{2} a(b + c - a), & c \le |r| \end{cases}$$" for "$$\rho(r) = \begin{cases} \frac{1}{2} r^2, & |r| \le a \\ \frac{1}{2} a(2|r| - a), & a < |r| < b \\ \frac{1}{2} a\left[(|r| - c)^2 / (b - c) + (b + c - a)\right], & a < |r| < b \\ \frac{1}{2} a(b + c - a), & c < |r| \end{cases}$$"

P15 last para: "$\hat{\theta} \triangleq (\theta_1, \ldots, \theta_p)'$" for "$\hat{\theta} = (\hat{\theta}_1, \ldots, \hat{\theta}_p)'$"

P16 equation 2.20: "$\hat{\theta}_j = \ldots$" for "$\hat{\theta} = \ldots$"

P16 equation 2.21, "$\hat{\theta} = \arg\min_{\hat{\theta}} \underset{i}{med}\, r_i^2$" for "$\hat{\theta} = \min_{\hat{\theta}} \underset{i}{med}\, r_i^2$"

P23 13th line: "increase" for "increases"

P25 17th line: "uniformly" for "randomly"

P28 2nd line: "highly" for "high"

P80 1st line: "object" for "objects"

P80 4th line: "ambiguity" for "ambiguous"

P85 17th line: "grow" for "grown"

P104 23rd line: "QMDPE" for QMPDE"

P122 19th line: "r_i" for "x_i"

P122 equation 7.3: "$MAD = 1.4826 med_i\{|r_i - med_j r_j|\}$" for "$MAD = 1.4826 med_i\{|x_i - med_j x_j|\}$"

P123 equation 7.4: "$\dfrac{|r_i - med_j r_j|}{MAD_n} < T$" for "$\dfrac{|x_i - med_j x_j|}{MAD_n} < T$"

P124 6th line: "correction" for "correct"

P161 11th line: "objective" for "object"

P168 4th line: "derivative" for "differentive"

P176 7th line: "deviation" for "derivation"

ADDENDUM

Pxviii 7th line: Delete“(in revised form)”; Add “to appear,” before “2004”

P14 1st line: Add “$\sum_{i=1}^{n} \rho(r_i)$ in” before “equation (2.13)”

P18 para 2. Add “(for a detailed description see chapter 7)” after “The preliminary scale”

P22 para 3 1st to 2nd line: Add a quote (“) before “the nature of….” ; Add a quote (”) after “ways”

P40 1st line: Add “by” after “non-negative’

P79 1st line: Delete “the” before “images”
P103 3rd line: Delete “the results of” before “the ground truth”
P107 8th line: Add “(Some others may prefer the term Adaptive-Bandwidth QMDPE—abQMDPE)” before “Instead of using…”

P112 last line: Add “flow” after “optical”
P126: Add under Equation 7.9, “For an explanation of $S_h(x)$ see page 53”;

P134 9th line: Add “Also, the proposed TSSE may underestimate the scale if the underlying distribution is composed of heavily overlapping Gaussians.” after “accurate.”

P147 1st line in last para: Delete “that” after “because”

P154 12th line: Delete “to” before “be”
P178 2nd line: “Delete “by” after “we do”
P181: Add at the end of para 3:

“Our analysis was carried out for the Epanechnikov kernel, which is not differentiable at its borders. It would be interesting to investigate the influence on false peaks if a Gaussian kernel, which is differentiable, is used in the mean shift method.”

P182 6th line: Add “Although (Comaniciu and Meer 2002a) used the joint spatial-range and color space to exploit local property of image data, the dimension of the space in that method is very high (2 for spatial-range and 3 for color space).” after “regions.”

Robust Statistics for Computer Vision: Model Fitting, Image Segmentation and Visual Motion Analysis

by

Hanzi Wang

B.S. (Sichuan University) 1996

M.S. (Sichuan University) 1999

A thesis submitted for the degree of

Doctor of Philosophy

in the

Department of Electrical and Computer Systems Engineering

Monash University

Clayton Victoria 3800

Australia

February 2004

Robust Statistics for Computer Vision: Model Fitting, Image Segmentation and Visual Motion Analysis

by

Hanzi Wang

Contents

List of Figures

Chapter 1. Introduction 1

Chapter 2. Model-Based Robust Methods: A Review 8

Chapter 3. Using Symmetry in Robust Model Fitting 31

Chapter 4. MDPE: A Novel and Highly Robust Estimator 50

Chapter 5. A Novel Model-Based Algorithm for Range Image Segmentation 79

Chapter 6. Variable-Bandwidth QMDPE for Robust Optical Flow Calculation 106

Chapter 7. A Highly Robust Scale Estimator for Heavily Contaminated Data 120

Chapter 8. Robust Adaptive-Scale Parametric Model Estimation for Computer Vision 136

List of Tables

Summary

Robust Statistical methods (such as LMedS and LTS) were first introduced in computer vision to improve the performance of feature extraction algorithms. One attractive feature of traditional robust statistical methods is that they can tolerate up to half of the data points that do not obey the assumed model (i.e., they can be robust to up to 50% contamination). However, they can break down at unexpectedly lower percentages when the outliers are clustered; also, they cannot tolerate more than 50% outliers. This is because that these methods measure only one single statistic: for example, the least median of residuals (for LMedS) or the least sum of trimmed squared of residuals (for LTS), omitting other characteristics of the data. We realised that there are two possible ways to improve the robustness of the methods: (i) to take advantage of special information in the data (e.g., symmetry); (ii) to take advantage of information in the residuals (i.e., the probability density function (pdf) of the residuals). In terms of these aspects, the thesis makes the following contributions:

- To leverage possible symmetry in the data, we adapt the concept of "Symmetry Distance" to formulate an improved regression method, called the Least Trimmed Symmetry Distance (LTSD).

- To exploit the structure in the pdf of residuals, we develop a family of very robust estimators: Maximum Density Power Estimator (MDPE), Quick-MDPE (QMDPE), and variable-bandwidth QMDPE (vbQMDPE) by applying nonparametric density estimation and density gradient estimation techniques in parametric estimation. In these methods, we consider the density distribution of data points in residual space and the size of the residual corresponding to the local maximum of the density distribution in their objective functions. An important tool in our methods is the mean shift method.

- The pdf of the residuals is important for scale estimation (more specifically, the "shape/spread"). By considering distribution of the residuals, and by employing the mean shift method and our proposed mean shift valley method, we develop the Two Step Scale Estimator (TSSE). Furthermore, based on TSSE, we propose a family of novel robust estimators: Adaptive Scale Sample Consensus (ASSC) and Adaptive Scale Sample Consensus (ASRC), which consider both the residuals of inliers and the scale of inliers in the objective functions.

More specifically, the first contribution of this thesis is that we demonstrate the fragility of LMedS and LTS and analyse the reasons that cause the fragility of these methods in the situation when a large percentage of clustered outliers exist in the data. We introduce the concept of Symmetry Distance to model fitting and formulate an improved regression method — the LTSD estimator. Experimental results are presented to show that the LTSD performs better than LMedS and LTS under a large percentage of clustered outliers and large standard variance of inliers.

The traditional robust methods generally assume that the data of interests (inliers) occupy a majority of the whole data. In image analysis, however, the data is often complex and several instances of a model are simultaneously present, each accounting for a relatively small percentage of the data points. To deal with data including multiple structures and a high percentage of outliers (>50%) remains a challenging task. In this thesis, we assume that the inliers occupy a relative majority of the data, by which it is possible that a robust estimator can tolerate more than 50% outliers. A significant contribution of this thesis is that we present a series of novel and highly robust estimators—MDPE, QMDPE and vbQMDPE, which can tolerate more than 80% outliers and is very robust to data with multiple structures, by applying the mean shift algorithm in the space of the pdf of residuals.

When data include multiple structures, two major steps should be taken in the process of robust model fitting: i) robustly estimate the parameters of a model, and ii) differentiate inliers from outliers. Experiments in this thesis show that to correctly estimate the parameters of a model (only) is not enough; to differentiate inliers from outliers, both the estimated parameters of a model and the corresponding scale estimate should be correct.

Having a correct scale of inliers is crucial to the robust behaviour of an estimator. The success of many robust estimators is based on having a correct initial scale estimate or the correct setting of a particular parameter that is related to scale (e.g., RANSAC, Hough Transform, M-estimators etc.). Although there are a lot of papers that propose highly robust estimators, robust scale estimation is relatively neglected in the computer vision community. One major contribution of this thesis is that we investigate the behaviour of several state-of-the-art robust scale estimators for data with multiple structures, and propose a novel robust scale estimator: TSSE. TSSE is very robust to outliers and can resist heavily contaminated data with multiple structures. TSSE is a very general method and can be used to give an initial scale estimate for robust estimators such as M-estimators. TSSE can also be used to provide an auxiliary estimate of scale (after the parameters of a model to fit have been found) as a component of *almost any* robust fitting method such as Hough Transform, MDPE, etc.

Another important contribution of this thesis is that we propose, based on TSSE and RANSAC, another novel and highly robust estimator: ASSC (and a variant of ASSC: ASRC). The ASSC estimator is an important improvement over RANSAC because no priori knowledge concerning the scale of inliers is necessary (the scale estimation is data driven). ASSC can tolerate more than 80% outliers and multiple structures. ASSC is also an improvement over MDPE and its family (QMDPE/vbQMDPE). MDPE and its family only estimate the parameters of a model. In contrast, ASSC can produce the parameters of a model and the corresponding scale as its results.

We used the mean shift algorithm extensively in the robust methods described above. We also directly apply the mean shift method to image segmentation based on image intensity or on image color. One property of the mean shift is that it is sensitive to local peaks (including false peaks). We found in our experiments that there possible are many false peaks if the feature space (such as the intensity/color space or the residual space) is quantized. The occurrence of false peaks may have a negative influence on the performance of methods employing the mean shift. In this thesis, we establish a quantitative relationship between the appearance of false peaks and the value of the bandwidth h. We provide a complete unsupervised peak-valley sliding algorithm for gray-level image segmentation. The general mean shift algorithm considers only the global information (features) of the image, while neglecting the local homogeneity information. We modify the mean shift algorithm so that both local homogeneity and global information are considered.

In order to validate our proposed methods, we have (successfully) applied these methods to a considerable number of important and fundamental computer vision tasks including:

- Model fitting (geometric primitive fitting): (a) line fitting; (b) circle fitting; (c) ellipse fitting; (d) plane fitting, etc.;
- Range image segmentation;
- Robust optical flow calculation;
- Fundamental matrix estimation;
- Grey image segmentation and color image segmentation.

Declaration

February 26, 2004

I declare that:

1. This thesis contains no material that has been accepted for the awards of any other degree or diploma in any university or institute.

2. To the best of my knowledge, this thesis contains no material that has previously published or written by another person except where due reference in made in the text of the thesis.

Signed:

[redacted]

Hanzi Wang

Preface

During my study at Monash University (from June, 2001 to Feb., 2004), a number of papers, which contain material used in this thesis, have been published, accepted, or are currently under review/preparation.

Papers that have been accepted or published:

1. **H. Wang** and D. Suter, "Robust Fitting by Adaptive-Scale Residual Consensus", in 8th European Conference on Computer Vision (**ECCV04**), Prague, pages to appear, May 11-14, 2004.
2. **H. Wang** and D. Suter, "MDPE: A Very Robust Estimator for Model Fitting and Range Image Segmentation", **International Journal of Computer Vision (IJCV)**, pages to appear, 2003.
3. **H. Wang** and D. Suter, "Using Symmetry in Robust Model Fitting", **Pattern Recognition Letters**, **24(16)**, pages 2953-2966, 2003.
4. **H. Wang** and D. Suter, "False-Peaks-Avoiding Mean Shift Method for Unsupervised Peak-Valley Sliding Image Segmentation", in 7th International Conference on Digital Image Computing: Techniques and Applications (DICTA'03), Sydney, pages 581-590, 10-12 Dec. 2003.
5. **H. Wang** and D. Suter, "Color Image Segmentation Using Global Information and Local Homogeneity", in 7th International Conference on Digital Image Computing: Techniques and Applications (DICTA'03), Sydney, pages 89-98, 10-12 Dec. 2003.
6. **H. Wang** and D.Suter, "Variable Bandwidth QMDPE and Its Application in Robust Optic Flow Estimation", in 9th IEEE International Conference on Computer Vision (**ICCV03**), Nice, France, pages 178-183, Oct. 2003.

7. **H. Wang** and D. Suter, "A Model-Based Range Image Segmentation Algorithm Using a Novel Robust Estimator", in 3rd International Workshop on Statistical and Computational Theories of Vision – **SCTV03** (in conjunction with ICCV03), Nice, France, Oct. 2003.

8. D. Suter and **H. Wang**, "Robust Fitting Using Mean Shift: Applications in Computer Vision", in M. Hubert, G. Pison, A. Struyf, and S. Van Aelst, editors, *Theory and Applications of Recent Robust Methods*, Statistics for Industry and Technology. Birkhauser, Basel, to appear, 2004.

9. D. Suter, P. Chen, and **H. Wang**, "Extracting Motion from Images: Robust Optic Flow and Structure from Motion", in Proceedings Australia-Japan Advanced Workshop on Computer Vision, Adelaide, Australia, pages 64-69, 9-11 Sept. 2003.

10. **H. Wang** and D. Suter, "A Novel Robust Method for Large Numbers of Gross Errors", in 7th Int. Conf. on Automation, Robotics and Computer Vision (ICARCV02), Singapore, pages 326-331, December 3-6, 2002.

11. **H. Wang** and D. Suter, "LTSD: A Highly Efficient Symmetry-based Robust Estimator", in 7th Int. Conf. on Automation, Robotics and Computer Vision (ICARCV02), Singapore, pages 332-337, December 3-6, 2002.

Technical Reports:

1. **H. Wang** and D. Suter, "ASSC A New Robust Estimator for Data with Multiple Structures", Technical Report (MECSE-2003-8), Monash University, Sept., 2003.

2. **H. Wang** and D. Suter, "MDPE: A Very Robust Estimator for Model Fitting and Range Image Segmentation", Technical Report (MECSE-2003-3), Monash University, Mar., 2003.

3. **H. Wang** and D. Suter, "Robust Scale Estimation from True Parameters of Model", Technical Report (MECSE-2003-2), Monash University, Mar., 2003.

4. **H. Wang** and D. Suter, "False-Peaks-Avoiding Mean Shift Method for Unsupervised Peak-Valley Sliding Image Segmentation", Technical Report (MECSE-2003-1), Monash University, Mar., 2003.

5. **H. Wang,** A. Bab-Hadiashar, S. Boukir, and D. Suter, "Outliers Rejection based on Repeated Medians", Technical Report (MECSE-2001-1), Monash University, Dec., 2001.

Papers in Revised Form or in Preparation:

1. **H. Wang** and D. Suter, "Robust Adaptive-Scale Parametric Model Estimation for Computer Vision", **IEEE Trans. Pattern Analysis and Machine Intelligence (PAMI)**, 2004. (in revised form)
2. **H. Wang** and D. Suter, "A Novel Robust Estimator for Accurate Optical Flow Calculation", in preparation for Image and Vision Computing.

Acknowledgements

There are many people without whom this thesis could not be finished. I would first like to thank my supervisor—A.Prof. David Suter for his kindly help, advice, support, and encouragement over the years. It is he who did a thorough proof reading and spent countless hours in improving the clarity and the presentation of the thesis as well as my academic papers. I learned many moral standards and beliefs, whether matters relating to academic or non-academic, from David.

I would like to thank my associate supervisor—Prof. Raymond Jarvis who provided me with a clear picture of the research background, the state of art in my research area, and potential new approaches and new directions. His guidance at that stage was so important that helped me to concentrate on my project quickly and determine my path to achieve the goals.

I would like to thank Dr. Alireza Bab-Hadiashar and Dr. Samia Boukir for their valuable discussion and suggestions for the robust statistics part; I would like to thank Prof. Jaesik Min for his kind assistance. I thank Prof. Xiaoyi Jiang and A. Prof. Patrick J.Flynn for their code and results for the range image segmentation part. I thank A. Prof. Michael Black for his valuable suggestions for the optical flow calculation part. I thank Prof. Andrew Zisserman, Dr. Hongdong Li, Kristy Sim, and Haifeng Chen for their kindly help for the fundamental matrix estimation part.

Many thanks to my colleagues from the Digital Perception Laboratory: Dr. Pei Chen, Mr. Daniel Tung, who discussed the theoretical problems with me and provided technical help to me. I also thank Dr. Paul Richardson, Dr. Fang (Fiona) Chen, Dr. Prithiviraj Tissainayagam, Mr. Mohamed Gobara and Mr. James Cheong. I have benefited a lot from their kindly help and support.

I am very grateful to many anonymous reviewers of my journal, conference and workshop papers. Their valuable comments and suggestions provided valuable assistance to revise and improve each of my papers and make the ideas in each paper clearer and more understandable.

I would like to thank many researchers and people that I met at conferences, workshops, and seminars, who motivated and simulated me to pursue a higher level in my study. Thank you for walking with me in my life. Without your inspiration, my study would stay at the orignial level.

Especially, I would like to express my deepest thanks and appreciations to my mother, father, and little sister. They give me constant encouragement, selfless support, and kindly solicitude. Here, I would like to share all my achievements with them.

The research in this thesis was supported by the Australia Research Council (ARC), under the grant A10017082.

Dedication

To my mother, my father and my little sister.

Chapter 1

Introduction

1.1 Background and Motivation

The study of computer vision is a strongly interdisciplinary one. This study is new, rapidly growing and complex since it brings together several disciplines including Computer Science, Artificial Intelligence, Physics, Graphics, Psychology, Physiology, etc. The purpose of computer vision is to develop theories and algorithms to automatically extract and analyse useful information from an observed image, image set, or image sequence.

One major task of computer vision and image analysis involves the extraction of "meaningful" information from images or image sequences using concepts akin to regression and model fitting. The range of applications is wide: it includes: robot vision, automated surveillance (civil and military) and inspection, biomedical image analysis, video coding, motion segmentation, human-machine interface, visualization, historical film restoration etc.

Parametric models play a vital role in many activities in computer vision research. When engaged in parametric fitting in a computer vision context, it is important to recognise that data obtained from the image or image sequences may be inaccurate. It is almost unavoidable that data are contaminated (due to faulty feature extraction, sensor noise, segmentation errors, etc) and it is also likely that the data will include multiple structures. Thus, it has been widely acknowledged that all algorithms in computer vision should be robust for accurate estimation (Haralick 1986). This rules out a simple-minded application of the least squares (LS) method. To fit a model to noisy data (with a large number of outliers and multiple structures) is still one major and challenging task within the computer vision communities.

Robust regression methods are a class of techniques that can tolerate gross errors (outliers) and has a high breakdown point. Robust Statistical methods were first introduced in computer vision to improve the performance of feature extraction algorithms. These methods can tolerate (in various degrees) the presence of data points that do not obey the assumed model. Such points are called "outliers."

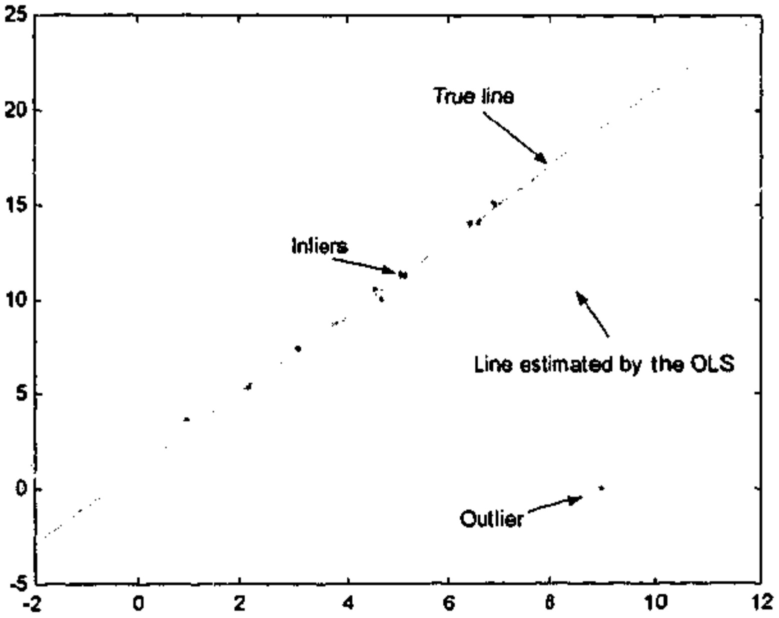

Figure 1.1: The OLS estimator may breakdown when even one outlier exists in the data.

The definition of robustness in this context often is focused on the notion of the *breakdown point*. The breakdown point of an estimator may be roughly defined as the smallest percentage of outlier contamination that can cause the estimator to produce arbitrarily large values ((Rousseeuw and Leroy 1987), pp.9). Breakdown point is one important quality of an estimator when we evaluate how robust an estimator is to outliers. The more robust an estimator is, the higher its breakdown point is. The breakdown point, as defined in statistics, is a worst-case measure. A zero breakdown point only means that there exists one (at least) potential configuration for which the estimator will fail. The LS estimator has a breakdown point of 0%, because only one single extreme outlier is sufficient to force the LS estimator to produce arbitrarily large values (see Figure 1.1).

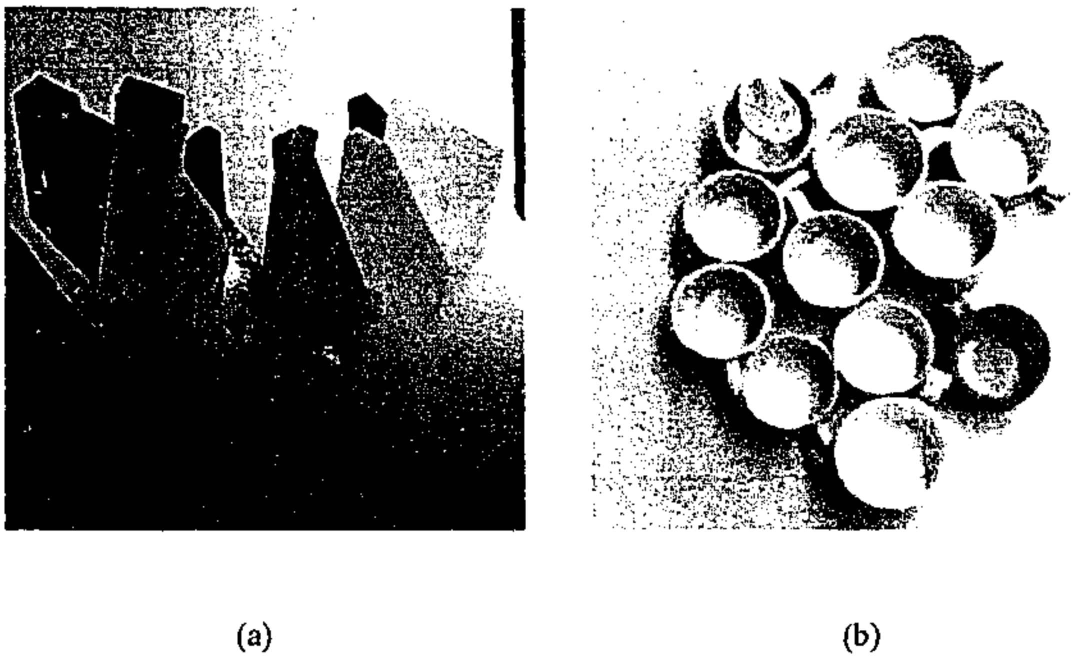

(a) (b)

Figure 1.2: Examples that many instances of a model can be simultaneously present in one image: (a) there are many planar surfaces (i.e., instances of a planar model) in the range image, (b) there are many cups (the rim of a cup can be roughly treated as a circle model) in the color image.

Two frequently used robust techniques are the least median of squares (LMedS) (Rousseeuw 1984) and the M-estimators (Huber 1981). One attractive feature of LMedS and M-estimators is that it can tolerate up to half of the data points being arbitrarily bad. In computer vision and image analysis, however, the data is often complex and several instances of a model are simultaneously present, each accounting for a relative small percentage of the data points (see Figure 1.2). We call this case "data with multiple structures". Thus it will rarely happen that a given population achieves the critical size of 50% of the total population and, therefore, techniques that have been touted for their high breakdown point (e.g., LMedS and other traditional robust methods from statistics) are no longer reliable candidates, being limited to a 50% breakdown point. Only robust methods designed with this special nature of the visual data in mind can achieve satisfactory results.

To design an efficient robust method for computer vision tasks, several characteristics that are distinct from those (mostly) addressed by the statistical community must be taken into account:

- **Pseudo-outliers.** In a given image, there are usually several populations of data (i.e., multiple structures). Some parts correspond to one object in a scene and other parts will correspond to other, rather unrelated, objects. When attempting to fit a model to this data, one must consider the population belonging to the related object as inliers and other populations as outliers - the term *pseudo-outlier* has been coined (Stewart 1995). In computer vision tasks, it rarely happen that a given population achieves the critical size of 50% of the total population and, therefore, techniques that have been touted for their high breakdown point (e.g., the Least Median of Squares) are no longer reliable candidates from this point of view.

- **Large data sizes.** Modem digital cameras exist with around 4 million pixels per image. Image sequences, typically at up to 50 frames per second, contain many images. Thus, computer vision researchers typically work with data sets in the tens of thousands of elements, *at least*, and data sets in the 10^6 and 10^9 range are not uncommon.

- **Unknown sizes of populations and unknown location.** Computer vision requires fully automated analysis in, generally, rather unstructured environments. Thus, the sizes and locations of the populations involved, will fluctuate greatly. Moreover, there is no "human in the loop" to select regions of the image dominated by a single population, or to adjust various thresholds. In contrast, statistical problems studied in most other areas usually have a single dominant population plus some percentage of outliers (typically mis-recordings - not the pseudo-outliers mentioned above). Typically a human expert is there to assess the results (and, if necessary, crop the data, adjust thresholds, try another technique etc.).

- **Emphasis on fast calculation.** Most tasks in computer vision must be performed "on-the-fly". Offline analysis that takes seconds, let alone minutes or hours, is usually a luxury afforded by relatively few applications.

These rather peculiar circumstances have lead computer vision researchers to develop their own techniques that perform in a robust fashion (perhaps "empirically robust" should be used, as few have formal proved robust properties, though many trace their heritage to techniques that do have such proved properties). These include ALKS (Lee, Meer et al. 1998), RESC (Yu, Bui et al. 1994), and MUSE (Miller and Stewart 1996). However, it has to be admitted that a complete solution, addressing all of the above problems, is far from being achieved. Indeed, none of the techniques, with present hardware limitations, are really "real-time" when applied to the most demanding tasks. None have been *proved* to reliably tolerate high percentages of outliers and, indeed, we have found with our experiments that RESC and ALKS, although clearly better than the Least Median of Squares, in this respect, are not always reliable. As we stated in the summary of this thesis, one can improve upon these approaches by using extra information such as symmetry in the data or the residual distribution.

This thesis addresses various problems in computer vision - specifically, robust model fitting, range image segmentation, image motion estimation, fundamental matrix calculation, and grey/color image segmentation. The **major contributions** of this thesis come in following forms: **(a)** a new symmetry-based robust method; **(b)** several novel highly robust methods with experimentally demonstrated advantages; **(c)** a novel highly robust scale estimation technique; **(d)** several practical techniques applying the proposed robust methods to solve "real" computer vision problems including range image segmentation, optical flow calculation and fundamental matrix estimation; and **(e)** a couple of algorithms for grey/color image segmentation. A more subtle contribution of this thesis is that we, in looking at applying the mean shift for histogram-based image segmentation, noticed a quantizing effect that produces false peaks. We develop a theory to predict/avoid false peaks and this theory is applicable in all situations where one quantizes feature space (e.g., the residual space) before applying the mean shift. The methods/techniques developed in this thesis can be beneficial to both the statistics and the computer vision communities.

1.2 Thesis Outline

There are a wide range of topics covered in this thesis (model fitting; range image segmentation; optical flow calculation; fundamental matrix estimation; grey/color image segmentation). Thus, previous related work is reviewed or introduced when it is necessary.

In **Chapter 2**, several state-of-the-art robust techniques are reviewed. These robust techniques include both those developed in the statistics field (such as M-Estimators, Repeated Median, LMedS, and LTS) and those developed in the computer vision community (such as Hough Transform, RANSAC, MINPRAN, MUSE, ALKS, and RESC). **Chapter 3** addresses the fragility of traditionally employed robust methods (LMedS and LTS) when data involve clustered outliers, and analyses the reasons that cause the fragility of these methods. Furthermore, the symmetry information in the data is exploited and the concept of "Symmetry Distance" is introduced to model fitting. An improved regression method — the LTSD is proposed. **Chapter** 4 takes advantage of structure information in the pdf of the residuals in order to achieve higher robustness. By employing nonparametric density estimation and density gradient techniques, and by considering the distribution of probability density in the residual space, a novel and highly robust estimator, MDPE, is proposed. Extensive experimental comparisons have been carried out to show the advantages of MDPE compared with five frequently used robust methods (LMedS, Hough Transform, RANSAC, ALKS, and RESC). **Chapter 5** begins by reviewing several state-of-the-art range image segmentation algorithms. Then a novel model-based range image segmentation algorithm, derived from Quick-MDPE, is proposed. Segmentation is a complicated task and it requires more than a simple application of a robust estimator. Actually, our proposed algorithm tackles many subtle issues and thereby provides a framework for those who want apply their robust estimators to the task of range image segmentation. In **Chapter 6**, we introduce the problem of optical flow calculation. Then, a modified QMDPE employing the variable bandwidth technique (vbQMDPE) is applied to compute the optical flow. Because vbQMDPE has a higher robustness to outliers than LMedS and LTS, the experiments on both synthetic and real image sequences show very promising results.

Having a correct scale of inliers is important to the robust behaviour of a lot of estimators. However, robust scale estimation is relatively neglected. Thus, **Chapter 7** investigates the behaviour of several state-of-the-art robust scale estimators for data with multiple structures, and, by exploiting the information of shape distribution of residuals, proposes a novel robust scale estimator: TSSE. **Chapter 8** proposes, based on TSSE, a novel robust estimator: ASSC and its variant ASRC. Experiments on model fitting, range image segmentation and fundamental matrix estimation show that the proposed method is very robust to data with discontinuities, multiple structures and outliers. In **Chapter 9**, we directly apply the mean shift algorithm to grey/color image segmentation. In the process, we identify an issue that affects the mean shift method when the data is heavily quantized. We also solve a couple of practical problems: (i) we propose a quantitative relationship between the appearance of false peaks and the value of the bandwidth h, which is applicable for many methods employing the mean shift; (ii) we introduce the local homogeneity into the mean shift algorithm. These result in two algorithms for grey/color image segmentation. Finally, **Chapter 10** summarizes what we have done and identifies what remain to be challenging problems: suggesting future research work.

Chapter 2

Model-Based Robust Methods: A Review

The history of seeking a robust method that can resist the effects of gross errors, i.e. outliers, in fitting models is long. Since data contamination is usually unavoidable - (due to such cases as faulty feature extraction, sensor noise and failure, segmentation errors, multiple structures, etc.), there has recently been a general recognition that all algorithms should be robust for accurate estimation. As pointed out by (Meer, Mintz et al. 1991), a robust estimator should have followed properties:

- Good efficiency at the assumed noise distribution.
- Reliability in the presence of various types of noise.
- High breakdown point.
- Time complexity is not much greater than that of the Least Squares method.

Because linear models play a very important role in most modern robust methods and many modern techniques are developed based on linear regression methods, this chapter commences with reviewing a most frequently applied linear regression method: the LS method. Several state-of-the-art robust techniques are then reviewed.

2.1 The Least Squares (LS) Method

Linear regression analysis is an important tool in most applied science including computer vision. The least squares method is one of the most famous linear regression methods and it has been used in many scientific fields for a long time.

The classical linear model can be described in the following form [(Rousseeuw and Leroy 1987), pp.1]:

$$y_i = x_{i1}\theta_1 + \ldots + x_{ip}\theta_p + e_i \qquad (i = 1,\ldots,n) \tag{2.1}$$

where the variable y_i is the response variable; and the variables $x_{i1},\ldots,x_{ip}$ are the explanatory variables. The error term e_i is usually assumed to be normally distributed with mean zero and standard deviation σ.

We have n sets of observations on y_i and $(x_{i1},\ldots,x_{ip})$, for i=1,...n:

$$(Y,X) = \begin{pmatrix} y_1 & x_{11} & \cdots & x_{1p} \\ \cdot & \cdot & & \cdot \\ \cdot & \cdot & & \cdot \\ \cdot & \cdot & & \cdot \\ y_n & x_{n1} & \cdots & x_{np} \end{pmatrix} \tag{2.2}$$

where Y=($y_1,\ldots,y_n$)' is a n-vector; X=($x_{(1)},\ldots, x_{(p)}$) is a n-by-p matrix and $x_{(i)} = (x_{i1},\ldots,x_{in})$' is a n-vector.

Equation (2.1) can be rewritten using matrix notation as follows:

$$Y = X\theta + e \tag{2.3}$$

Using regression analysis, we can obtain regression coefficients $\hat{\theta} = (\hat{\theta}_1 \cdots \hat{\theta}_p)'$ from the observation data (Y, X). $\hat{\theta}$ is the estimate of θ. Applying $\hat{\theta}$ to the explanatory variables $(x_{i1},\ldots,x_{ip})$, we can obtain:

$$\hat{y}_i = x_{i1}\hat{\theta}_1 + ... + x_{ip}\hat{\theta}_p \quad (2.4)$$

where $\hat{y}_i$ is the estimated value of y_i. Usually, this estimated value is not exactly the same as the actually observed value. The difference between the estimated value $\hat{y}_i$ and actually observed value y_i is the residual r_i for the i'th set of observed data.

$$r_i = y_i - \hat{y}_i \quad (2.5)$$

The ordinary least squares regression estimator can be written as follows:

$$\hat{\theta} = \underset{\hat{\theta}}{\text{Minimize}} \sum_{i=1}^{n} r_i^2 \quad (2.6)$$

Equation (2.6) is the well-known LS equation. From equation (2.6), we can see the least squares estimator estimates the optimized $\hat{\theta}$ by minimizing of the sum of the squared residuals.

If we let:

$$S(\hat{\theta}) = \sum_{i=1}^{n} r_i^2 \quad (2.7)$$

Then, we have:

$$S(\hat{\theta}) = r'r = (Y-X\hat{\theta})'(Y-X\hat{\theta}) = Y'Y + \hat{\theta}'X'X\,\hat{\theta} - 2\hat{\theta}'X'Y \quad (2.8)$$

Differentiating $S(\hat{\theta})$ w.r.t. $\hat{\theta}$, we obtain:

$$2X'X\hat{\theta} - 2X'Y = \frac{\partial S(\hat{\theta})}{\partial \hat{\theta}} = \frac{\partial^2 S(\hat{\theta})}{\partial \hat{\theta}^2} = 2X'X \quad (2.9)$$

From equation (2.9), we obtain the normal equation [(Rao and Toutenburg 1999), *pp*.24]:

$$X'X\hat{\theta} = X'Y \quad (2.10)$$

When X'X is not singular, the regression coefficients $\hat{\theta}$ can be estimated by:

$$\hat{\theta} = (X'X)^{-1}X'Y \tag{2.11}$$

The LS estimator is highly efficient and achieves optimum results under Gaussian distributed noise. Although the LS method has the advantages of low computational cost and high efficiency, it is extremely sensitive to outliers (gross errors or samples belonging to another structure and distribution).

2.2 Outliers and Breakdown Point

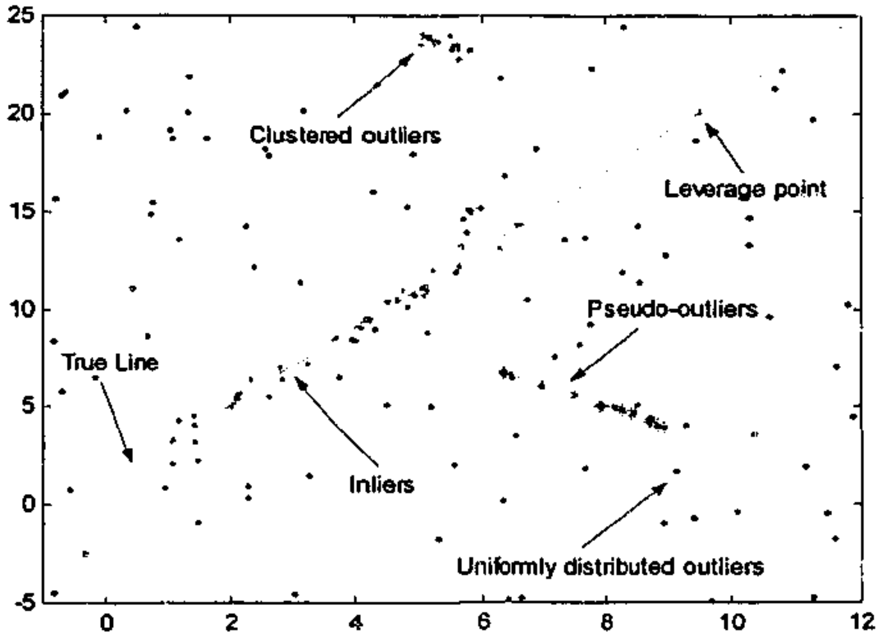

Figure 2.1: The types of outliers.

Outliers can be grossly defined as: "the data points that lie far from the majority of the data". Before we discuss the behavior of robust estimators, it is beneficial to investigate the various types of outliers that one can encounter. Outliers frequently happen in the data in computer vision tasks. Outliers could potentially lead to negative effects on the accuracy of the results. Even more, outliers could seriously spoil the results of one method that is not robust to outliers. Although a lot of new statistical techniques have been developed to tolerate the effect of outliers within recent years, their advantages remain only when the data involve certain types of outliers.

Loosely speaking, outliers can be classified into following four types:

- Leverage points — the outliers in explanatory variables.
- Clustered outliers — the outliers that are clustered.
- Randomly distributed outliers — the outliers that are randomly distributed.
- Pseudo outliers — the data points from structures that are extraneous to a particular single parametric model fit, i.e., data that are inliers to one structure will be pseudo outliers to another.

"Leverage point" means that the point is outlying relative to the explanatory variable x_i, but not relative to the response variable y_i. Leverage points do not always lead to negative results. When a leverage point lies close to a regression line, it is a "good leverage point" (as shown in Figure 2.1) and can lead to a good effect on the results. However, the leverage point is far away the regression line, it is a "bad leverage point" (i.e., outlier). Clustered outliers often bring seriously negative effects to the results It has been experimentally shown that it is relatively harder to resist the effects of clustered outliers than those of randomly distributed outliers (see chapter 3 and 4). Most theories are proposed assuming that outliers are uniformly distributed. The theories that consider clustered outliers are relatively less.

One characteristic to distinguish pseudo outliers from gross outliers and clustered outliers is that pseudo outliers are coherent and structured. Pseudo outliers have structures while gross outliers and clustered outliers do not have. Pseudo outliers often appear in the data including multiple structures. Because multiple structures frequently happen in computer vision tasks, studying the effects of pseudo outliers (multiple structures) has been popular in computer vision community (Yu, Bui et al. 1994; Miller and Stewart 1996; Lee, Meer et al. 1998; Bab-Hadiashar and Suter 1999).

To seek an estimator with high breakdown point is one of the most important topics among the statistics and computer vision community. The breakdown point of an estimator may be roughly defined as the smallest percentage of outlier contamination that can cause the estimator to produce arbitrarily large values. Let Z be any sample of n data points (x_I, y_I),

…, (x_n, y_n), $Z = \{z_1, \ldots, z_n\}$ and $z_i = \{x_i, y_i\}$. For $m \le n$, the finite-sample breakdown point of a regression estimator T can be written as [(Rousseeuw and Leroy 1987), pp.10]:

$$\varepsilon_n^*(T,Z) = \min\left\{\frac{m}{n};\ \sup_{Z^* \in Z_m} \left\|T_n(Z^*)\right\| = \infty\right\} \tag{2.12}$$

Because one single outlier is sufficient to force the LS estimator to produce arbitrarily large value, the LS estimator has a breakdown point of 0%.

In order to reduce the influence of outliers, many robust estimators with high breakdown point have been developed during the past three decades. In the next sections, several modern robust estimators, developed by both statistics and computer vision communities will be reviewed.

2.3 Traditional Robust Estimators from Statistics

A lot of robust estimators have been developed within the statistics community and applied to computer vision field. Among these robust estimators, the family of M-estimators is one class of the most popular robust regression methods.

2.3.1 M-Estimators and GM-Estimators

The theory of M-estimators was firstly developed by Huber in 1964 and several years later. It was successfully generalized as a robust regression method (Huber 1973; Huber 1981). The essence of M-estimators is to replace the squared residuals r_i^2 in equation (2.6) by a symmetric function ρ of the residuals:

$$\underset{\hat{\theta}}{\text{Minimize}} \sum_{i=1}^{n} \rho(r_i) \tag{2.13}$$

where $\rho(r_i)$ is a robust loss function with a unique minimum when residual r is zero. The purpose of introducing the loss function $\rho(r_i)$ is to reduce the effects of outliers.

Let the derivative of $\rho(r_i)$ be $\psi(r_i)$, then differentiating equation (2.13), we obtain

$$\sum_{i=1}^{n} \psi(r_i / \hat{\sigma}) x_i = 0 \tag{2.14}$$

where $\hat{\sigma}$ is the variance related to residuals. The solution of equation (2.14) could be found using iterative minimization and various equation solving algorithms (Li 1985).

M-estimators can be classified into three types based on the influence function $\psi(r_i)$ (Holland and Welsch 1977; Stewart 1997):

1. Monotone M-estimators. This type of M-estimators has nondecreasing, bounded $\psi(r)$ functions [(Huber 1981), Chapter 7]. The loss functions can be written as:

$$\rho(r) = \begin{cases} \frac{1}{2} r^2, & |r| \le c \\ \frac{1}{2} c(2|r| - c), & c < |r| \end{cases} \tag{2.15}$$

2. Hard Redescenders. This type of M-estimators forces $\psi(r)$=0 when $|r| > c$ (c is a threshold). That is to say, a residual will lose its effects on the results when the absolute of the residual is larger than c (Hampel, Rousseeuw et al. 1986a). The loss functions $\rho(r)$ can be written as:

$$\rho(r) = \begin{cases} \frac{1}{2} r^2, & |r| \le a \\ \frac{1}{2} a(2|r| - a), & a < |r| < b \\ \frac{1}{2} a\left[(|r| - c)^2 / (b - c) + (b + c - a)\right], & a < |r| < b \\ \frac{1}{2} a(b + c - a), & c < |r| \end{cases} \tag{2.16}$$

3. Soft Redescenders. This type of M-estimators have not a finite rejection point c. The type of M-estimators force $\psi(r)$=0 when $|r| \to \infty$.

$$\rho(r) = \frac{1}{2}(1+f)\log(1+r^2/f) \tag{2.17}$$

Although the M-estimators are robust to outliers with respect to response variables, they are not efficient in resisting the outliers with respect to explanatory variables (see equation (2.1)). Therefore, the generalized M-estimators (GM-estimators) were developed to reduce the effects of outliers with respect to explanatory variables. GM-estimators used weight function *w* to resist the influence of outliers with respect to explanatory variables.

Mallows (Mallows 1975) presented the following GM-estimators:

$$\sum_{i=1}^{n} w(x_i)\psi(r_i/\hat{\sigma})x_i = 0 \tag{2.18}$$

Hill developed the following equation (Hill 1977):

$$\sum_{i=1}^{n} w(x_i)\psi(r_i/w(x_i)\hat{\sigma})x_i = 0 \tag{2.19}$$

Unfortunately, it has been proved that the breakdown point of GM-estimators is only 1/(1+*p*), where *p* is the dimension of explanatory variables (Maronna, Bustos et al. 1979). That means when *p*=2, the highest breakdown point of GM-estimators is only 33.333%. When *p* increases, the breakdown point will correspondingly diminish.

2.3.2 The Repeated Median (RM) Estimator

Before the development of the repeated median estimator, it was controversial whether it was possible to find a robust estimator with a high breakdown point of 50%. In 1982, Siegel proposed the repeated median (RM) estimator (Siegel 1982). The repeated median estimator has an attractive characteristic in that it can obtain a 50% breakdown point.

The repeated median method can be summarized as follows: For any *p* observations, $(x_{i1}, y_{i1}),\ldots,(x_{ip}, y_{ip})$, let the solution parameter vector be denoted by $\hat{\theta} = (\hat{\theta}_1,\ldots,\hat{\theta}_p)'$. The *j*th coordinate of this vector is denoted by $\theta_j(i_1,\ldots,i_p)$. Then the repeated median estimator is written as:

$$\hat{\theta} = \underset{i_1}{med}(\ldots(\underset{i_{p-1}}{med}(\underset{i_p}{med}\,\theta_j\,(i_1,\ldots,i_p)))\ldots) \tag{2.20}$$

The repeated median estimator is effective for problems with small p. However, the time complexity of the repeated median estimator is $O(n^p \log^p n)$, which prevents the method being useful in applications where p is even moderately large.

2.3.3 The Least Median of Squares (LMedS) Estimator

Rousseeuw proposed the least median of squares (LMedS) in 1984 (Rousseeuw 1984). The LMedS method has the following assumptions:

- The signal to estimate should occupy the majority of all the data points, that is, more than 50% data points should belong to the signal to estimate (some traditional methods such as RM, LTS, etc., also have the same assumption).
- The correct fit will correspond to the one with the least median of squared residuals. This criterion is not always true when the data includes multiple structures and clustered outliers, and when the variance of inliers is large (see chapter 2 and 3).

The LMedS method is based on the simple idea of replacing the sum in least sum of squares formulation by a median. LMedS finds the parameters to be estimated by minimizing the median of squared residuals corresponding to the data points. The LMedS estimate can be written as:

$$\hat{\theta} = \min_{\hat{\theta}} \underset{i}{med}\, r_i^2 \tag{2.21}$$

A drawback of the LMedS method is that no explicit formula exists for the solution of equation (2.21) – the exact solution can only be determined by a search in the space of all possible estimates. This space is very large. One can consider all estimates determined by all possible p-tuples of data points. There are $O(n^p)$ p-tuples and it takes $O(n\log n)$ time to find the median of the residuals of the whole data for each p-tuple. Thus it costs $O(n^{p+1}\log n)$ for the LMedS method. The cost will thus increase very fast with n and p.

In practice, only an approximate LMedS, based upon random sampling, can be implemented for any problem of a reasonable size – we generally refer to this approximate version when we use the term LMedS (a convention adopted by most other authors as well). In order to reduce the time complexity of the LMedS method to a feasible value, a Monte Carlo type technique (described as follows) is usually employed.

A p-tuple is "clean" if it consists of p good observations without contamination by outliers. One performs, m times, random selections of p-tuples, where one chooses m so that the probability (P) that at least one of the m p-tuples is "clean" is almost 1. Let ε be the fraction of outliers contained in the whole set of points. The probability P can be expressed as follows:

$$P=1-(1-(1-\varepsilon)^{p})^{m} \tag{2.22}$$

Thus one can determine m for given values of ε, p and P by:

$$m=\frac{\log(1-P)}{\log[1-(1-\varepsilon)^{p}]} \tag{2.23}$$

For example, if there are 50 percent of data contaminated by outliers, i.e. $\varepsilon = 0.5$, and if we require $P = 0.99$; then, for circle fitting, p=3, we obtain m=35; and for ellipses fitting, if we let p=5, then we obtain m=145.

The LMedS method has excellent global robustness and high breakdown point (i.e., 50%). Over the last two decades, LMedS has been growing in popularity. For example, Kumar and Hanson used the least median of squares to solve the pose estimation problem (Kumar and Hanson 1989); Roth and Levine employed it for range image segmentation (Roth and Levine 1990); Meer et. al. applied it for image structure analysis in the piecewise polynomial field ; Zhang used the least median squares in conic fitting (Zhang 1997); and Bab-Hadiashar and Suter employed it for optic flow calculation (Bab-Hadiashar and Suter 1998).

However, the relative efficiency of the LMedS method is poor when Gaussian noise is present in the data. As Rousseeuw noted (Rousseeuw and Leroy 1987), the LMedS method has a very low convergence rate: it is of order $n^{-1/3}$, which is much lower than the convergence rate of order $n^{-1/2}$ of M-estimators. To compensate this deficiency, Rousseeuw improved the LMedS method by carrying out a weighted least square procedure after the initial LMedS fit. The weights are chosen based on the initial LMedS fit.

The preliminary scale estimate is given by:

$$S = 1.4826(1+\frac{5}{n-p})\sqrt{\underset{i}{med}\, r_i^2} \tag{2.24}$$

where r_i is the residual of i'th sample.

The weight function W_i which will be assigned to the i'th data point is given by:

$$W_i = \begin{cases} 1 & r_i^2 \le (2.5S)^2 \\ 0 & r_i^2 > (2.5S)^2 \end{cases} \tag{2.25}$$

The data points corresponding to W_i=0 are likely to be outliers and will not be considered in the further weighted least squares estimate. The data points having W_i=1 are inliers and will be used for determining the final variance estimates $\hat{\sigma}$.

Finally, $\hat{\sigma}$ is given by the weighted least squares

$$\hat{\sigma} = \min_{\hat{\theta}} \sum_{i=1}^{n} W_i r_i^2 \tag{2.26}$$

There are different ways in which a method can be robust. The robustness we have been discussing is global robustness. However, the LMedS method may be locally unstable when fitting models to data. This means that a small change in the data can greatly alter the output. This behaviour is not desirable in computer vision and has been noticed by Thomas (Thomas and Simon 1992). In comparison, M-estimators have better local stability.

2.3.4 The Least Trimmed Squares (LTS) Estimator

The least trimmed squares (LTS) method was introduced by Rousseeuw to improve the low efficiency of LMedS (Rousseeuw 1984; Rousseeuw and Leroy 1987). The LTS estimator can be mathematically expressed as:

$$\hat{\theta} = \min_{\hat{\theta}} \sum_{i=1}^{h} (r^2)_{i:n} \tag{2.27}$$

where $(r^2)_{1:n} \leq \cdots \leq (r^2)_{n:n}$ are the ordered squared residuals, h is the trimming constant. The LTS method uses h data points (out of n) to estimate the parameters. The coverage value, h, may be set from $n/2$ to n. The aim of LTS estimator is to find the h-subset with smallest least squares residuals and use the h-subset to estimate parameters of models. The breakdown point of LTS is $(n-h)/n$. When h is set $n/2$, the LTS estimator has a high breakdown value of 50%.

The advantages of LTS over LMedS are:

- It is less sensitive to local effects than LMedS, i.e. it has more local stability.
- LTS has better statistical efficiency than LMedS. It converges like $n^{-1/2}$.

The implement of the LTS method also uses random sampling because the number of all possible h-subsets (C_n^h) grows fast with n. There are two commonly employed ways to generate a h-subset:

1. Directly generate a random h-subset from the n data points.
2 Firstly generate a random p-subset. If the rank of this p-subset is less than p, randomly add data points until the rank is equal to p. Next, use this subset to compute parameters $\hat{\theta}_j$ (j=1,...p) and residuals r_i (i=1,...,n). Sort the residuals into $|r(\pi(1)| \leq \cdots \leq |r(\pi(h)| \leq \cdots \leq |r(\pi(n)|$, and h-subset is set to: H:={$\pi(1),...,\pi(h)$}.

Although the first way is easier than the second, the h-subset yielded by the first method may contain a lot of outliers. Indeed, the chance of generating a "clean" h-subset by method (1) tends to zero with increasing n. In contrast, it is easier to find a "clean" p-subset without outliers. Therefore, method (2) can generate more (good) initial subset with size h than method (1).

Like LMedS, the efficiency of LTS can be improved by adopting a weighted least squares refinement as the last stage.

2.4 Robust Estimators Developed within the Computer Vision Community

Although many robust estimators were developed in statistics during the past decades, most of them can only tolerate 50% outliers. In computer vision tasks, it frequently happe:ıs that outliers and pseudo-outliers occupy the absolute majority of the data. Therefore, the requirement in these robust estimators that outliers occupy less than 50% of all the data points is far from being satisfied for the real tasks in computer vision. A good robust estimator should be able to correctly find the fit when outliers occupy a higher percentage of the data (more than 50%). Also, ideally, the estimator should be able to resist the influence of all types of outliers (e.g., uniformly distributed outliers, clustered outliers and pseudo-outliers).

Recently, many efforts have been made in computer community to find robust estimators, which can tolerate more than 50% outliers. Among these high robust estimators, the frequently used estimators are Hough Transform (Hough 1962), RANSAC (Fischler and Rolles 1981), MINPRAN (Stewart 1995), MUSE (Miller and Stewart 1996), ALKS (Lee, Meer et al. 1998), and RESC estimator (Yu, Bui et al. 1994). In the following sub-sections, we will introduce these robust estimators. We commence with the explanation of *breakdown point* as it is often interpreted by the computer vision community.

2.4.1 Breakdown Point in Computer Vision

In the statistical literature (Huber 1981; Rousseeuw and Leroy 1987), there are a number of precise definitions of robustness and of robust properties: including the aforementioned "breakdown point" (see section 2.2)– which is an attempt to characterize the tolerance of an estimator to large percentages of outliers. Loosely put, such estimators should still perform reliably even if up to 50% of the data do not belong to the model we seek to fit (in statistics, these "outliers" are usually false recordings or other "wrong" data).

Estimators, such as the Least Median of Squares, that have a proven breakdown point of 0.5, have been much vaunted; particularly since this is generally viewed to be the best achievable. It would be desirable to place all estimators on such a firm theoretical footing by, amongst other things, defining and proving their "breakdown-point. However, in practice, it is usually not possible to do so. Moreover, one can question whether the current definitions of such notions are appropriate for the tasks at hand – in order to yield mathematical tractability, they may be too narrow/restrictive. For example, does one care if there is one single, *unlikely* if not impossible, configuration of data that will lead to the breakdown of an estimator if all practical examples of data can be reliably tackled? Moreover, as appealing as it is to quote theoretical results, it may mean little in practice. Taking for example the Least Median of Squares estimator: the estimator is too costly to implement and so everyone implements an *approximate* version of that estimator – no such proofs exist (nor can they) assuring a precise breakdown point for such approximate versions of the estimators. Not to mention the fact that there *are* data sets, having less than 50% outliers, where even the true Least Median of Squares will provably fail (for example clustered outliers—see section 3.2); of course such configurations are carefully excluded by the careful phrasing of the formal proofs of robustness. Yet clustered outliers, perhaps unlikely in the mainstream statistical examples, *are* somewhat likely in computer vision tasks when we consider the notion of pseudo-outliers (Stewart 1997) – data belonging to a second "object" or "objects" within the image.

Several techniques (e.g., RANSAC, Hough transform) have experimentally proven themselves as reliable workhorses (tolerating very high percentages of outliers – usually much over 50%). We may say that these have an empirically determined very high breakdown point, meaning that these are "unlikely" to breakdown and can usually tolerate extremely high levels of outliers (much in excess of 50%).

Although the breakdown point in statistics is proved to be bounded by 0.5 [(Rousseeuw and Leroy 1987), pp.125], the proof also shows that they require the robust estimator has a unique solution (more technically, they require affine equivariance). When outliers (including pseudo-outliers associated with multiple structures) occupy more than 50% of the whole data, a robust method may return one of the multiple valued solutions (Yu, Bui et al. 1994).

As Stewart said (Stewart 1999): the nature of computer vision problem alters the performance requirements of the robust estimators in a number of ways. The optimum breakdown point of 0.5 must be surpassed in some domains. A robust estimator with more than 0.5 breakdown point is possible. That is, a robust estimator may have a higher than 0.5 breakdown point if we relax the single solution requirement, and permit the case of multiple solutions to exist (Yu, Bui et al. 1994; Stewart 1995; Lee, Meer et al. 1998). This can be done through the use of RANSAC or Hough Transform, or through adaptive techniques based on scale estimates such as ALKS and MUSE, etc (Stewart 1999). Though none of them have a theoretically proven breakdown point higher than 0.5, plausible arguments, supported by experiments, suggest that they do in practice.

Thus, in this thesis, though we are motivated by the appealing notion of strictly provable robustness in the form of high breakdown point, we follow a growing tradition of authors (Yu, Bui et al. 1994; Stewart 1995; Lee, Meer et al. 1998) that present estimators, that have empirically demonstrated robust qualities and are supported by plausible arguments, based (as is, we might emphasize, the approximate Least Median of Squares technique used by many statisticians and other scientists alike) on the similarity of the proposed technique to estimators that do have provably high breakdown points.

2.4.2 Hough Transform (HT) Estimator

The Hough Transform was developed first to detect simple curves such as lines and circles (Hough 1962). The basic Hough Transform is a voting technique. A typical implementation of the technique is to count the number of data features that are mapped into each cell in quantized parameter space. The Hough Transform has attracted a great deal of attention, and many improvements have been made, like the generalized Hough Transform, the probabilistic Hough Transform and the hierarchical Hough Transform (Illingworth and Kittler 1988; Leavers 1993).

The Hough transform has been recognized as being a powerful tool in shape analysis, model fitting, motion segmentation, which gives good results even in the presence of noise and occlusion. Major shortcomings of the Hough Transform are excessive storage requirements and computational complexity. Typically, the storage space and time complexity required is about $O(N^p)$, where p is the dimension of parameter space and N is the number that each parameter space is quantized into. Another problem of the Hough Transform is its limited precision. Generally speaking, increasing the quantization number of each parameter space will lead to a higher precision; however, this will also increases the computational cost. Finally, though the Hough Transform can be successfully applied to estimate multiple structures, one might have to solve many practical problems in multi-modal parameter space. In effect, the hard problems have been deferred to the analysis of parameter space. Though the Hough Transform tends to demonstrate robustness in the presence of relatively high percentages of outliers, no formal proof of robustness (in terms of breakdown point) seems to exist until very recently: we become aware of the work of (Goldenshluger and Zeevi 2004), where the authors formalized the statistical properties of the HT methodology and determined the breakdown point of the HT estimator.

2.4.3 Random Sample Consensus (RANSAC) Estimator

Fischler and Bolles (Fischler and Rolles 1981) provided a generate-and-test paradigm: RANdom Sample Consensus (RANSAC). They used the minimum number of data points, a p-subset (p is the dimension of parameter space), necessary to estimate the parameters of the model. RANSAC, for its high robustness to outliers and ease to carry out, has been widely employed in many computer vision tasks. The algorithm of RANSAC can be described as follows:

1 Randomly choose a p-subset from the given n data points. This step has the similar place to that used in LMedS, LTS, ALKS, etc. in that all of these estimators employ a random sampling scheme.

2 Using this p-subset to determine the parameters of the model. Then, determine the number of data points that are within some error tolerance of the model.

3 If the number is greater than a threshold, use the p-subset to determine a new model by the least squares method and output the parameters of the model as results.

4 Otherwise, randomly choose a new p-subset and repeat step 1 and 2. If no consensus with the threshold or more members has been found after running the predetermined number of trails, either terminate the program or compute the parameters of the model with the largest consensus set found.

From the procedure of RANSAC described above, we can see the RANSAC method need three predetermined parameters:

- The error tolerance.
- The number of subsets to try.
- The threshold, which indicates whether or not the correct model has been found.

If the predetermined parameters are correct, RANSAC is very robust to outliers and can tolerate more than 50% outliers experimentally. However, if the predetermined parameters or some of them (for example, the error tolerance) are wrong, the achievements of RANSAC will be corrupted.

2.4.4 Minimize the Probability of Randomness (MINPRAN) Estimator

The MINPRAN estimator is one kind of robust estimator that has a higher than 50% breakdown point (Stewart 1995). It can find a model in the data involving more than 50%

outliers without prior knowledge about error bounds. In contrast, the Hough Transform and RANSAC techniques need a priori knowledge about the inlier bound of the correct fit.

The MINPRAN estimator is similar to the LMedS/LTS estimator but it outperforms the LMedS/LTS estimator in the following ways:

- The MINPRAN estimator can find correct fit that involves less than 50% of the data. The prerequisite of this achievement is that inliers need to be close to the correct fit and outliers are randomly distributed.
- It does not "hallucinate" fits when there is not any model in the data. (The MINPRAN estimator outputs nothing, not even a false fit, when there is no model in the data). This is different from most other robust estimators such as M-estimators, LMedS, LTS, etc.
- The LMedS/LTS estimators always use 50% of the data (for LMedS, see section 2.3.3) or *h* data points out of *n* data points (for LTS, see section 2.3.4) regardless of the true percentage of the inliers in the whole data. MINPRAN, however, will identify and use all inliers. Therefore, the MINPRAN estimator can yield more accurate results than the LMedS and LTS estimators.

However, MINPRAN assumes that the outliers are randomly distributed within a certain range. This makes MINPRAN less effective in extracting multiple structures and clustered outliers. At the same time, it occasionally finds the fits that actually bridge small magnitude discontinuities.

2.4.5 Minimum Unbiased Scale Estimator (MUSE) and Adaptive Least kth Order Squares (ALKS) Estimator

Miller and Stewart proposed the minimum unbiased scale estimator (MUSE) in 1996 (Miller and Stewart 1996). MUSE was designed to extract surfaces that contained less than 50% of the data without a priori knowledge about the percentage of the inliers and to detect the small-scale discontinuities in the data. MUSE is based on the LMedS method, but it improves LMedS and can accurately estimate fits when the data contain multiple surfaces.

MUSE randomly selects p-subsets and then estimates fits based on these p-subsets. It then calculates the unbiased estimate of the scale for each fit's k smallest residuals, where k is set to all possible values and satisfies $1 \le k \le N\text{-}p$; Then the smallest scale estimate over all possible k is chosen as the representative value of the hypothesized fits. Finally, the fit from the p-subset with the smallest scale estimate is chosen as the optimum fit. The scale estimate can be written as:

$$s_k = \frac{r_{k:N}}{E[u_{k:N}]} \tag{2.28}$$

where $r_{k:N}$ is the kth ordered absolute residual, and $E[u_{k:N}]$ can be approximated by:

$$E[u_{k:N}] \approx \Phi^{-1}((1+\frac{k}{N+1})/2) \tag{2.29}$$

where $\Phi^{-1}[.]$ is the argument of the normal cumulative density distribution.

Because the scale estimate is biased, a correction is taken to eliminate the bias by normalizing the s_k. The unbiased minimum scale estimate can be written as:

$$\varphi = \frac{\min_k s_k}{E[\min v_{k'} \mid k' = \arg\min_k s_k]} \tag{2.30}$$

where v_k is the kth scale estimate.

Because it takes $O(n^3)$ time to calculate $E[\min v|k]$, these are pre-calculated and stored in a table, which will be used when MUSE is carried out.

Inspired by MUSE, Lee and Meer provided the adaptive least kth order squares (ALKS) estimator (Lee, Meer et al. 1998). ALKS is based on the least kth order squares (LKS) [(Rousseeuw and Leroy 1987), pp.124]. LKS procedure is similar to those of the LMedS estimator. The difference between LKS and LMedS is in that LKS uses k data points out of n data points ($p<k<n$), while LMedS uses half of the n data points. The breakdown point of LKS is $\min(k/n, 1\text{-}k/n)$. Because it is impossible for a robust estimator using a one-step procedure to have a breakdown point exceeding 50%, ALKS uses multi-step procedure (in

each step, ALKS employs LKS with different k value) and recovers the fit to the relative majority of the data without any priori knowledge about the scale of inliers.

ALKS uses k data points out of n data points. The robust estimate of the noise scale can be written as:

$$\hat{s}_k = \frac{\hat{d}_{k\,\min}}{\Phi^{-1}[\frac{1+k/n}{2}]} \tag{2.31}$$

where $d_{k\min}$ is the half-width of the shortest window containing k residuals.

This estimate of noise scale is only valid when the k is not very large or very small. After $\hat{s}_k$ is estimated, the variance of the normalized error is computed as follows:

$$\mathrm{E}_k^2 = \frac{1}{q_k - p}\sum_{i=1}^{q_k}\left(\frac{r_{i,k}}{\hat{s}_k}\right)^2 = \frac{1}{\hat{s}_k^2}\frac{\sum_{i=1}^{q_k} r_{i,k}^2}{q_k - p} = \frac{\hat{\sigma}_k^2}{\hat{s}_k^2} \tag{2.32}$$

ALKS assumes that the optimum value of k should yield the smallest E_k^2.

In order to estimate the correct k, a random sampling technique, similar to that used in LMedS and RANSAC, is also employed in ALKS. The ALKS method can deal with data with multiple structures, but it cannot resist the influence of the extreme outliers.

The authors of MUSE and those of ALKS consider robust scale estimate in their methods and they both can obtain a greater than 50% breakdown point. MUSE and ALKS can perform better than LMedS and M-estimators at small-scale discontinuities. However, MUSE needs a lookup table for the scale estimate correction; ALKS is limited in its ability to handle extreme outliers. Another problem we found in ALKS is its instability under a small percentage of outliers.

2.4.6 Residual Consensus (RESC) Estimator

Yu et al. presented a high robust estimator for range image segmentation and reconstruction (Yu, Bui et al. 1994). Because this method considers residual consensus, it is called RESC. RESC greatly improves the robustness of an estimator to outliers. Although there have been some estimators appearing in the literature (such as Hough Transform and RANSAC) that might tolerate more than 50% outliers, RESC claims that it can reach a high breakdown point which can tolerate more than 80% outliers. This attractive characteristic of the RESC method is achieved by using a histogram compression approach for residual consensus.

The basic idea of the RESC method is that if a model is correctly fitted, the residuals of inliers should be small and, at the same time, the histogram of the residuals should concentrate within a small range in the lower part of the histogram. In the RESC method, a histogram compression technique plays an important role in residual consensus. The histogram compression technique works as follows:

1. Estimate the original histogram of residuals with as many histogram columns (says 2000) as possible. The estimated histogram of residuals will be used for compression in the following steps.

2. Decide the column width of the compressed histogram. The width is chosen where the first column of the compressed histogram can contain *p* percent of all data points. The value of *p* is experimentally chosen as 12. Then the number *v* of consecutive columns in the original histogram can be easily determined (these consecutive columns of the original histogram will contain *p* percent of the data points).

3. Then every *v* columns in the original histogram is compressed into one column in the compressed histogram.

From the details of the histogram compression, we can see that the column width of the compressed histogram depends on the noise level, which will change for different types of data. Instead of using only residual information in its objective function, the RESC method considers two factors in its objective function: the number of inliers and the residuals of the inliers.

The RESC method defined its objective function as:

$$\psi = \frac{1}{v^{\beta}} \sum_{i=1}^{m} h_i^{\alpha} / i^{\beta} \tag{2.33}$$

where i is the ith column in the compressed histogram; h_i is the number of points in the ith column. α and β are coefficients which determine the relative importance of h_i and i. They are empirically determined as: α =1.3; and β =1.0. ψ is also called histogram power.

The procedure of the RESC method is as follows:

1. Randomly choose k sets of p-subset from the whole data points. A modified genetic algorithm is used by the RESC method to improve the speed.
2. Calculate the residuals and compress the histogram of the residuals.
3. Select a p-subset from the k sets whose histogram power is the highest.
4. Determine the standard variance of the residuals.
5. Label the points of this primitive and remove them from the whole data points.
6. Remove the outliers in the labelled region.
7. Repeat step 1-6 until all signals are extracted.

The RESC method is very robust to noise. It finds the parameters by the p-subset corresponding to the maximum of the histogram power. However, a disadvantage of the RESC method is that it needs user to tune many parameters for the optimal performance.

2.5 Conclusion

In this chapter, we have reviewed several traditional and state-of-the-art robust estimators, with their advantages and disadvantages. In the following chapters, we will, by using the extra information inside the residuals, proposed novel efficient robust methods and apply them to computer vision tasks.

Chapter 3

Using Symmetry in Robust Model Fitting

3.1 Introduction

The pattern recognition and computer vision communities often employ robust methods for model fitting (Fischler and Rolles 1981; Rousseeuw 1984; Rousseeuw and Leroy 1987; Zhang 1997; Danuser and Stricker 1998; Stewart 1999). It is common to employ "regression analysis" to undertake such tasks (Rousseeuw and Leroy, 1987). In particular, high breakdown-point methods such as Least Median of Squares (LMedS) and Least Trimmed Squares (LTS) have often been used in situations where the data are contaminated with outliers. LMedS and LTS are based on the idea that the correct fit will correspond to the one with the least median of residuals (for LMedS), or the least sum of trimmed squared residuals (for LTS). The essence of the argument claiming a high breakdown point for the LMedS is that if the uncontaminated data are in the majority, then the median of the squared residuals should be unaffected by the outliers, and thus the median squared residual should be a reliable measure of the quality of the fit. Likewise, since the LTS method relies only on (the sum of squares of) the *h* smallest residuals, for some choice of the parameter *h*, it is thought that this should be robust to contamination so long as *h* data points, at least, belong to the true fit.

However, though the breakdown point of these methods can be as high as 50% (they can be robust to up to 50% contamination), they can break down at unexpectedly lower percentages when the outliers are clustered. Due to the affects of clustered outliers, the correct fit may not correspond to the fit with the least median of squared residual (for LMedS) or the least trimmed squared residuals (for LTS). It is worth mentioning that this phenomenon is not limited to LMedS, and LTS. It also happens to most other robust estimators such as random sample consensus—RANSAC (Fischler and Rolles 1981), residual consensus estimator—RESC (Yu, Bui et al. 1994), adaptive least k squares estimator—ALKS (Lee, Meer et al. 1998), etc. The mechanism of the breakdown in these robust estimators is similar to that of the LMedS and LTS (see chapter 4).

This illustrates a general principle: most robust methods only depend upon a single statistical property (the sum of the trimmed squared residuals or the median of the squared residuals, for example) and these methods ignore many other properties that the data, or the residuals to the fit, should have. The key to salvaging the robustness of LMedS and LTS (and some other robust estimators), even in the presence of clustered outliers, can be that one looks beyond the standard definition of the robust methods to incorporate other measures and statistics into the formulation. In this chapter, we restrict ourselves to one such property – symmetry.

Symmetry is very common and important in our world. When we will fit circles, ellipses, or any symmetric object, one of the most basic features in the model is symmetry. In our method, we introduce the concept of symmetry distance (SD) and thereby we propose, by taking advantage of the symmetry information in the visual data, an improved method, called the least trimmed symmetry distance (LTSD). The symmetry we employ, in this context, is that of symmetry about a central point (central with respect to the shape of interest). The LTSD method is influenced not only by the sizes of the residuals of data points, but also by the symmetry of the data points and has applications where one is trying to fit a symmetric model (e.g. circle and ellipses). Experimental results show that the LTSD approach gives better results than the LMedS method and the LTS method in situations where a large percentage of clustered outliers and large standard variance in inliers are encountered.

The main contributions of this chapter are as follows:

1. We illustrate situations where LMedS and LTS to fail to correctly fit the data in the presence of clustered outliers, and analyze the reasons that cause the breakdown of these two methods. This provides an important cautionary note when employing these two robust estimators in situations where the outliers are clustered.

2. We introduce the concept of symmetry distance (SD) into model fitting. The concept of SD in computer vision is not novel. However it is a novel concept in the fiel.: of model fitting. Based on Su et al.'s *point symmetry distance* (Su and Chou 2001), we propose a novel symmetry distance and apply it to model fitting.

3. We experimentally show that the proposed method works better than LMedS and LTS under a large percentage of clustered outliers for both simulated and real data.

This chapter is organized as follows: in section 3.2, the factors that cause both LMedS and LTS to fail to fit a model under a large percentage of clustered outliers are explored. In section 3.3, a novel symmetry distance measure is given and our proposed method is developed in section 3.4. Experiments demonstrating the utility of the approach (for circle fitting and ellipses fitting) are given in section 3.5. Finally, some conclusions and future work are summarized in section 3.6.

3.2 Dilemma of the LMedS and the LTS in the Presence of Clustered Outliers

The LMedS method and the LTS method are based on the idea that the correct fit is determined by a simple statistic: the least median of the squared residuals (for LMedS), or by the least sum of trimmed squared residuals (for LTS); and that such a statistic is not influenced by the outliers.

Consider the contaminated distribution defined as follows (Haralick 1986; Hampel, Rousseeuw et al. 1986b):

$$F=(1-\varepsilon)F_0+\varepsilon H \quad (3.1)$$

where F_0 is an inlier distribution, and H is an outlier distribution.

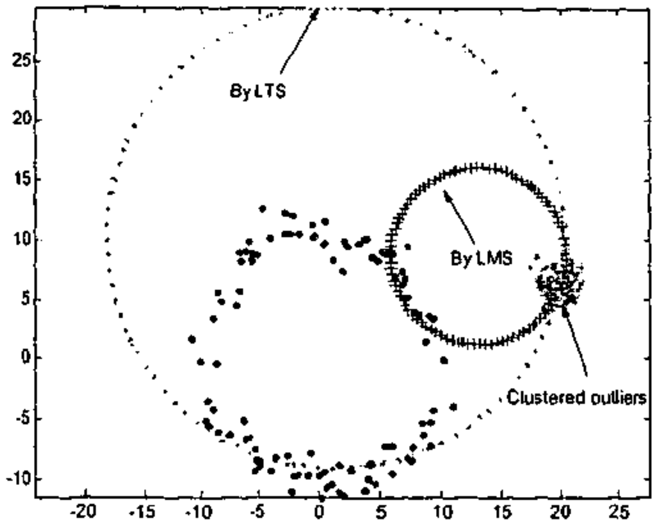

Figure 3.1: An example where LMedS and LTS (h is set to $0.5n$) fail to fit a circle yet there are under 44.5% outliers – though, of course, the outliers are clustered.

Equation (3.1) is also called the *gross error model.* When the standard variance of F_0 is small (<<1) and that of H is large or H is uniform distributed, the assumptions leading to the robustness of LMedS or LTS, are true. However, when F_0 is "scattered", i.e. the standard variance of F_0 is big, and H is clustered distributed with high density, the assumption is not always true.

Let us investigate an example. In Figure 3.1, F_0 (bivariate normal with unit variance) including 100 data points were generated by adding the noise to samples of a circle with radius 10.0 and center at (0.0, 0.0). Then 80 clustered outliers were added, possessing a spherical bivariate normal distribution with one unit standard variance and mean (20.0, 6.0). As Figure 3.1 shows, both LMedS and LTS failed to fit the circle: LMS returned the result with a radius equal to 7.4239 and the center was located at (13.1294, 8.6289). The results obtained by LTS were: the radius equalled 19.3069 and the center was at (1.1445, 10.1470).

It is important to point out that the failure is inherent, and not simply an artefact of our implementation. Let us check the median of the residuals (for LMedS) and the sum of trimmed squared residuals (for LTS) and we will understand why LMedS and LTS failed to fit to the circle. The median of residuals of the perfect fit is 5.7928. However the median of residuals of final result by the LMedS method is 5.1479.

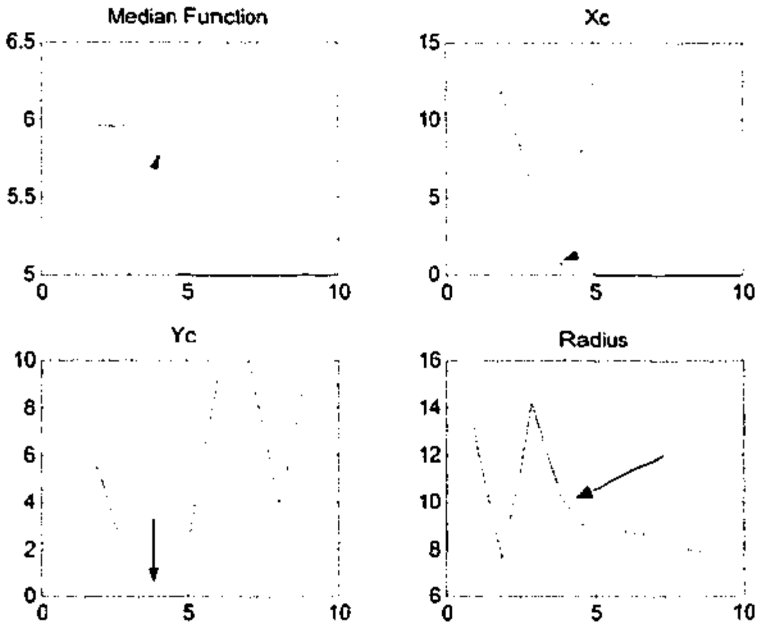

Figure 3.2: LMedS searches for the "best" fit with the least median of residuals.

Figure 3.2 shows the time evolution of the parameters: median of residuals (top left), centre of the fitted circle (x coordinate and y coordinate in the top right and bottom left, respectively), and the radius of the fitted circle (bottom right) as LMedS searches for the "best" fit with the least median of residuals. (Note: the iterations pass by the correct fit (pointed out by arrows) proceeding to fits with even lower median of residuals.) In fact, during the searching procedure, the LMedS estimator consistently minimizes the median of the residuals, starting with initial fits that have a larger median residual than the true fit, but successively finding fits with lower median residuals – proceeding to even lower median residuals than that possessed by the true fit.

The reason that LTS failed is similar. LTS finds the fit with smallest trimmed squared residuals. The value of the least sum of trimmed squared residuals obtained is 32.6378. However, the same statistic for the "true fit" is 58.6688. Clearly, LTS has "correctly", by its criterion, obtained a "better" fit (but in fact, the wrong one). The problem is not with the implementation but with the criterion

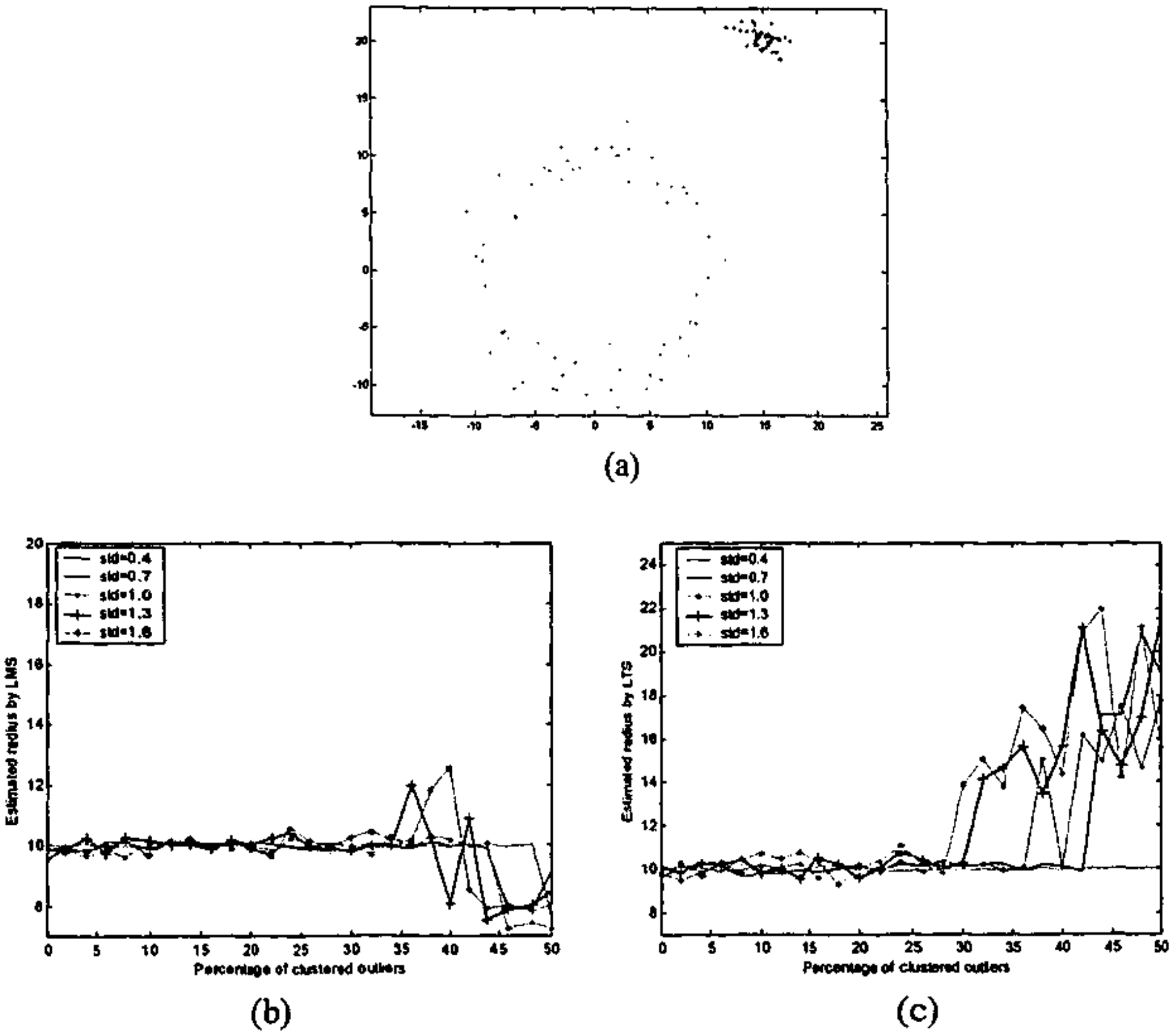

Figure 3.3: Breakdown Plot: (a) One case of the distribution of data; The results of LMedS (b) and LTS (c) in circle fitting will be affected by the standard variance of inliers and percentages of clustered outliers.

Now, let us consider another example showing that the results of the LMedS and the LTS are affected by the standard variance of the inliers. We generated a circle with radius 10.0 and center at (0.0, 0.0). In addition, clustered outliers were added to the circle with mean (20.0, 6.0) and unit standard variance. In total, 100 data points were generated. At first, we assigned 100 data to the circle without any outliers. Then we repeatedly moved two points from the circle to the clustered outliers until 50 data were left in the circle. Thus, the percentage of outliers changed from 0 to 50%. In addition, for each percentage of clustered outliers, we varied the standard variance of the inliers from 0.4 to 1.6 with a step size of

0.3. Figure 3.3 (a) illustrates one example of the distribution of the data, with 38% clustered outliers and the standard variance of inliers 1.3.

From Figure 3.3 (b), we can see that when the standard variance of inliers is no more than 1.0, LMedS can give the right results under a high percentage of outliers (more than 44%). However, when the standard variance of inliers is more than 1.0, LMedS does not give the right result even when the percentage of outliers is less then 40%. From Figure 3.3 (c), we can see when the standard variance of inliers is 0.4, the LTS estimator can correctly give the results even under 50% clustered outliers; while when the standard variance of inliers is 1.6, LTS does not give the right results even when only 30 percent of the data are outliers.

From the discussion above, we now see several conditions under which LMedS and LTS failed to be robust. A crucial point is: these methods measure only one single statistic: the least median of residuals or the least sum of trimmed squared of residuals, omitting other characteristics of the data. If we look at the failures, we can see that the results lost the most basic and common feature of the inliers with respect to the fitted circle—symmetry.

In the next section, we will introduce the concept of symmetry distance into robust regression methods and propose an improved method, called the Least Trimmed Symmetry Distance (LTSD), by which the better performance is acquired even when data include clustered outliers.

3.3 The Symmetry Distance

Symmetry is considered a pre-attentive feature that enhances recognition and reconstruction of shapes and objects (Attneave 1995). Symmetry exists almost everywhere around us. A square, a cube, a sphere, and a lot of geometric patterns show symmetry. Architecture usually displays symmetry. Symmetry is also an important parameter in physical and chemical processes and is an important criterion in medical diagnosis. Even we human beings show symmetry, (for instance, our faces and bodies are roughly symmetrical between right and left). One of the most basic features in the shapes of models we often fit/impose on our data, e.g. circles and ellipsis, is the symmetry of the model.

Symmetric data should suggest symmetric models and data that is symmetrically distributed should be preferred as the inlier data (as opposed to the outliers). For decades, symmetry has widely been studied in computer vision community. For example, considerable efforts have been focused on the detection of symmetry in images in regard to mirror symmetries (Marola 1989; Nalwa 1989) and in regard to circular symmetries (Bigun 1988; Reisfeld, Wolfson et al. 1992); Kirby etc. used the symmetric features of images for image compression (Kirby and Sirovich 1990); Zabrodsky treated symmetry as a continuous feature and applied it in finding the orientation of symmetric objects (Zabrodsky, Peleg et al. 1995); Skewed symmetries in 3D structures have been extensively studied (Oh, Asada et al. 1988; Ponce 1990; Gross and Boult 1994). Symmetry has also been treated as a feature in cluster analysis (Su and Chou 2001). More detailed definitions of symmetry can be found in (Zabrodsky 1993). We demonstrate here that symmetry can also be used as a feature to enhance the performance of robust estimators when fitting models with symmetric structure.

3.3.1 Definition of Symmetry

There are many kinds of symmetry in existence in the world. Generally speaking, symmetry can be classified into the following four basic types, which are shown in Figure 3.4, (Zabrodsky 1993; Zabrodsky, Peleg et al. 1995):

1. Mirror-symmetry: if an object is invariant under a reflection about a line (for 2D) or a plane (for 3D).
2. C_n-symmetry: if an object is invariant under rotation of $\frac{2\pi}{n}$ radians about its center (for 2D) or a line passing through its center (for 3D).
3. D_n-symmetry: if an object has both mirror-symmetry and C_n-symmetry.
4. Circular-symmetry: if an object has C_∞-symmetry.

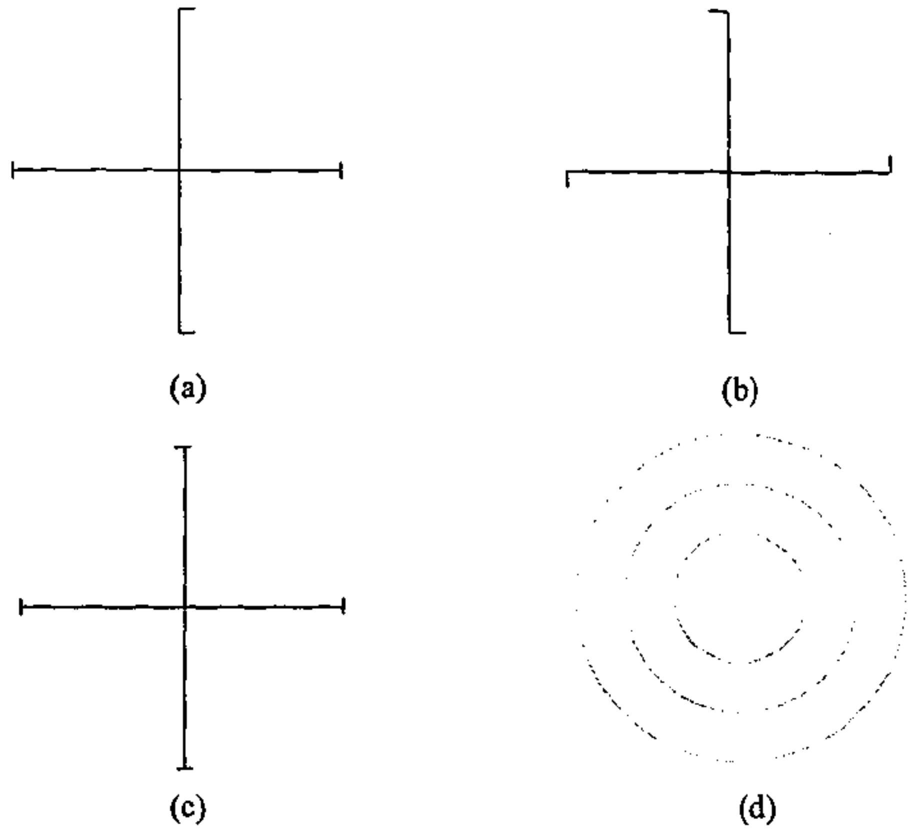

Figure 3.4: Four kinds of symmetries: (a) mirror-symmetry; (b) C_4-symmetry; (c) D_4-symmetry; (d) circular symmetry.

3.3.2 The Symmetry Distance

The exact mathematical definition of symmetry (Weyl 1952; Miller 1972) is insufficient to describe and quantify symmetry found both in the natural world and in the visual world.

Su and Chou proposed a symmetry distance measure based on the concept of "*point symmetry*" (Su and Chou 2001). Given *n* points x_i, $i = 1,...n$ and a reference vector *C* (e.g. the centroid of the data), the point symmetry distance between a point x_j and *C* is defined as follows:

$$d_s(x_j, C) = \min_{\substack{i=1,...,N \\ and\ i \neq j}} \frac{\|(x_j - C) + (x_i - C)\|}{\|x_j - C\| + \|x_i - C\|} \qquad (3.2)$$

From equation (3.2), we can see that the point symmetry distance is non-negative definition. In essence, the measure tries to "balance" data points with others symmetric about the centroid – for example, x_i=($2C$-x_j) exists in the data, $d_s(x_j,C)$=0.

However, according to (3.2), one point could be used repeatedly as the "balancing point" with respect to the center. This does not seem to properly capture the notion of symmetry. In order to avoid one point being used as a "symmetric point" more than one time by other points, we refine the point symmetry distance between a point x_j and C as follows:

$$D_s(x_j, C) = \min_{\substack{i=1,\ldots N \\ and\ i\neq j \\ and\ i\notin \Re}} \frac{\|(x_j - C) + (x_i - C)\|}{\|x_j - C\| + \|x_i - C\|} \tag{3.3}$$

where $\Re$ is a set of points that have been used as "symmetric point".

Based on the concept of "point symmetry distance", we propose a non-metric Symmetry Distance (*SD*). Given a pattern x consisted of n points x_1,... x_n and a reference vector C, the symmetry distance of the pattern x with respect to the reference vector C is:

$$\mathrm{SD_n(x,C)} = \frac{1}{n}\sum_{i=1}^{n} D_s(x_i, C) \tag{3.4}$$

When the *SD* of a pattern is equal to 0.0, the pattern is perfect symmetric; when the *SD* of a pattern is very big, the pattern has little symmetry.

3.4 The Least Trimmed Symmetry Distance (LTSD) Method

We proposed a new method, which couples the LTS method with the symmetry distance measure defined in sub-section 3.3.2. That is, besides residuals, we also choose symmetry distance as a criterion in the model fitting. For simplicity, we call the proposed method LTSD (Least Trimmed Symmetry Distance). Mathematically, the LTSD estimate can be written as:

$$\hat{\theta} = \arg\min_{\theta, C} SD_h(x, C) \tag{3.5}$$

Only h data points with the smallest sorted residuals are used to calculate the symmetry distance. The estimated parameters correspond to the least symmetry distance.

The specific details of the proposed method are given as follows:

1. Set repeat times (RT) according to equation (2.23). Initialise h with $[(n+p+1)/2] \leq h \leq n$. If we want LTSD to have a high breakdown point, say 50%, we can set $h=(n+p+1)/2$.

2. Randomly choose p-subsets, and extend to h-subset H_I by the method (2) in sub-section 2.3.4.

3. Compute $\hat{\theta}_I$ by LS method based on H_I. Compute symmetry distance SD_I based on $\hat{\theta}_I$ and H_I using equation (3.4) in sub-section 3.3.2 and using the centre of the fit (circle or ellipse) as the reference vector C. Decrement RT and if RT is smaller than 0, go to step 4, otherwise, go to step 2. We calculate the parameters $\hat{\theta}$ based on h-subset instead of p-subset in order to improve the statistical efficiency.

4. Finally, output $\hat{\theta}$ with the lowest SD.

3.5 Experimental Results

In this section, we will show several examples using the proposed method to fit a model with symmetrical structures. Circle fitting and ellipses fitting have been very popular topics in the computer vision field. One of the obvious characteristics of circles and ellipses is that they are symmetric. We first present an example of circle fitting; then we present a relatively more complicated example of ellipse fitting. The results are compared with those of the LMedS method and the LTS method.

3.5.1 Circle Fitting

In Figure 3.5, about 45 percent clustered outliers were added to the original circle data. Since LMedS and LTS only rely on the residuals of the data points, their results were affected by the standard variance of the inliers and percentages of the clustered outliers. Therefore, they failed to fit the circle under a high percentage of clustered outliers (see Figure 3.1). However, because the LTSD method considers the symmetry of the object, this enables LTSD find the right model (see Figure 3.5): the true centre and radius of the circle are respectively (0.0,0.0) and 10.0; by the LTSD method, we obtained centre (-0.23, 0.01) and radius10.06.

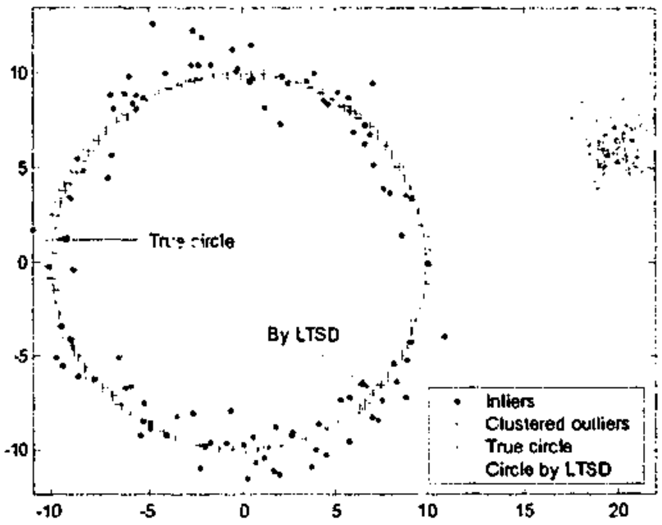

Figure 3.5: Using the symmetry of the circle, the LTSD method found the approximately right results under 44.5% clustered outliers.

Another example showing the advantages of the proposed method is given in Figure 3.6 (a) (corresponding to Figure 3.3 (a)). From Figure 3.6 (a), we can see that when the outliers are clustered, the LMedS and LTS broke down under very low percentages of outliers, in this case, they both broke down under 38% outliers! In comparison to the LMedS and LTS methods, the proposed method gives the most accurate results. The proposed method is affected less by the standard variance of the inliers and the percentages of the clustered outliers. Figure 3.6 (b) shows that the radius found by the LTSD method in circle fitting (true radius is 10.0) changed less under different standard variance of the inliers and percentages of clustered outliers. In comparison to Figure 3.3 (b) and (c), the fluctuation of the radius found by the LTSD method is smaller. Even when 50 percent clustered outliers exist in the data and the standard variance of inliers is 1.6, the results did not (yet) break down. However, both the LMedS and the LTS broke down.

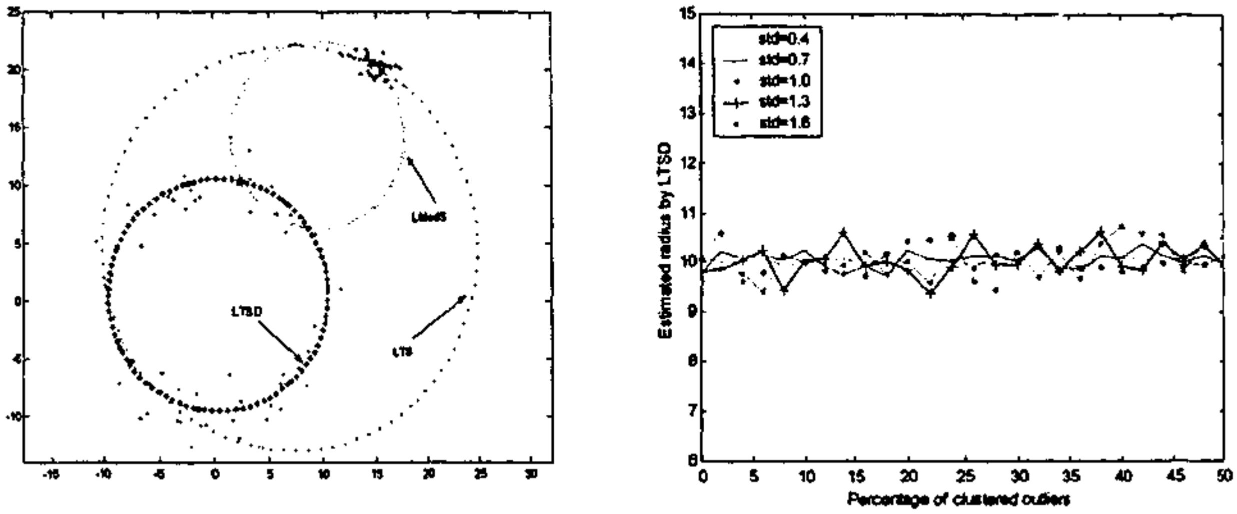

(a)

(b)

Figure 3.6: (a) A comparative result of the LTSD, LMedS, and LTS with 38% clustered outliers; (b) the results of the LTSD method is affected less by the standard variance of inliers and percentages of clustered outliers.

3.5.2 Ellipse fitting

Ellipses are one of most common and important primitive models in computer vision and pattern recognition, and often occur in geometric shapes, man-made and natural scenes. Ellipse fitting is a very important task for many industrial applications because it can reduce the data and benefit the higher level processing (Fitzgibbon, Pilu et al. 1999). Circles may be projected into ellipses under perspective projection. Thus ellipses are frequently used in computer vision for model matching (Sampson 1982; Fitzgibbon, Pilu et al. 1999; Robin 1999). In this subsection, we apply the proposed robust method—LTSD to ellipses fitting.

A general conic equation can be written as follows:

$$ax^2 + bxy + cy^2 + dx + ey + f = 0 \tag{3.6}$$

where *(a,b,c,d,e,f)* are the parameters needed to find from the given data. When $b^2 < 4ac$, the equation above corresponds to ellipses.

The ellipse can also be represented by its more intuitive geometric parameters:

$$\frac{(x\cos\theta + y\sin\theta - x_c\cos\theta - y_c\sin\theta)^2}{A^2} + \frac{(-x\sin\theta + y\cos\theta + x_c\sin\theta - y_c\cos\theta)^2}{B^2} = 1 \tag{3.7}$$

where (x_c, y_c) is the center of the ellipse, A and B are the major and minor axes, and θ is the orientation of the ellipse.

The relation between *(a,b,c,d,e,f)* and (x_c, y_c, A, B, θ) can be written as (Robin 1999):

$$\begin{cases} x_c = \dfrac{be - 2cd}{4ac - b^2} \\ y_c = \dfrac{bd - 2ae}{4ac - b^2} \\ \{A, B\} = 2\sqrt{\dfrac{-2f}{a + c \pm f\sqrt{b^2 + (\dfrac{a-c}{f})^2}}} \\ \theta = \dfrac{1}{2}\tan^{-1}\dfrac{b}{a-c} \end{cases} \tag{5.3}$$

It is convenient to find *(a,b,c,d,e,f)* first by the given data and then convert to (x_c, y_c, A, B, θ).

As illustrated in Figure 3.7 and Table 3.1, 200 data were generated with 40% clustered outliers. The outliers were compacted within a region of radius 5 and center at (20.0, 5.0). The ellipse had a standard variance 0.8, major axis 10.0, minor axis 8.0, center (0.0,0.0), and orientation to horizon direction θ is 0.0 degree. The results of LTS and LMedS were seriously affected by the clustered outliers. However, the LTSD method worked well.

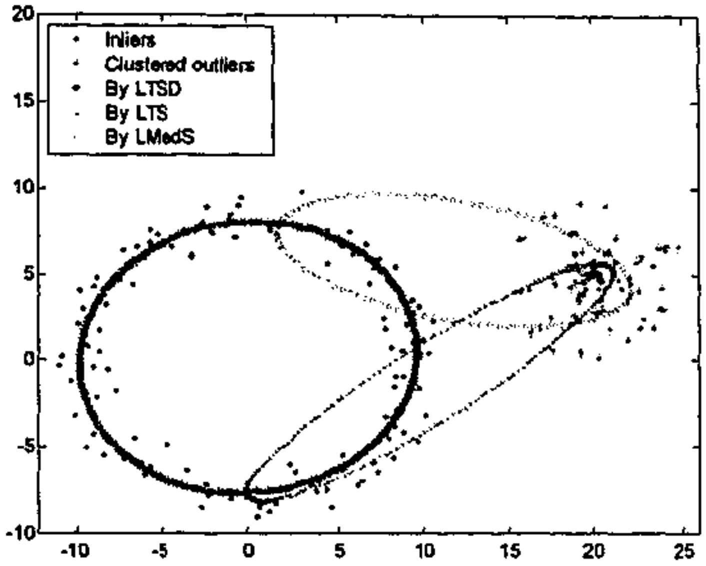

Figure 3.7: Comparison of the results obtained by the LTSD method, LTS and LMedS in ellipse fitting under 40% clustered outliers.

	xc	*yc*	Major axis	Minor axis	θ(deg)
True value	0.0	0.0	10.0	8.0	0.0
The LTSD method	-0.125	-0.145	9.760	7.810	6.355
The LTS method	19.786	5.162	3.328	3.035	34.129
The LMedS method	9.560	5.208	11.757	3.679	-3.307

Table 3.1: Comparison of the estimated parameters by the LTSD, LTS, and LMedS methods in ellipses fitting under 40% clustered outliers.

Next, we will apply the LTSD method to real images.

3.5.3 Experiments with Real Images

The first example is to fit an ellipse in an image of a mouse pad, shown in Figure 3.8. The edge image was obtained by using Canny operator with threshold 0.07. In total, 310 data points were in the edge image (Figure 3.8 (b)). The clustered outliers, due to the flower, occupy 50% of the data. Three methods (the LTSD, LTS and LMedS) were applied to detect the mouse pad edge. As shown in Figure 3.8 (c), both LTSD and LTS correctly found the edge of the mouse pad. However, LMedS fails to detect the edge of the mouse pad. This is because under the condition that the standard variance of inliers is small, the statistical efficiency of LTS is better than LMedS.

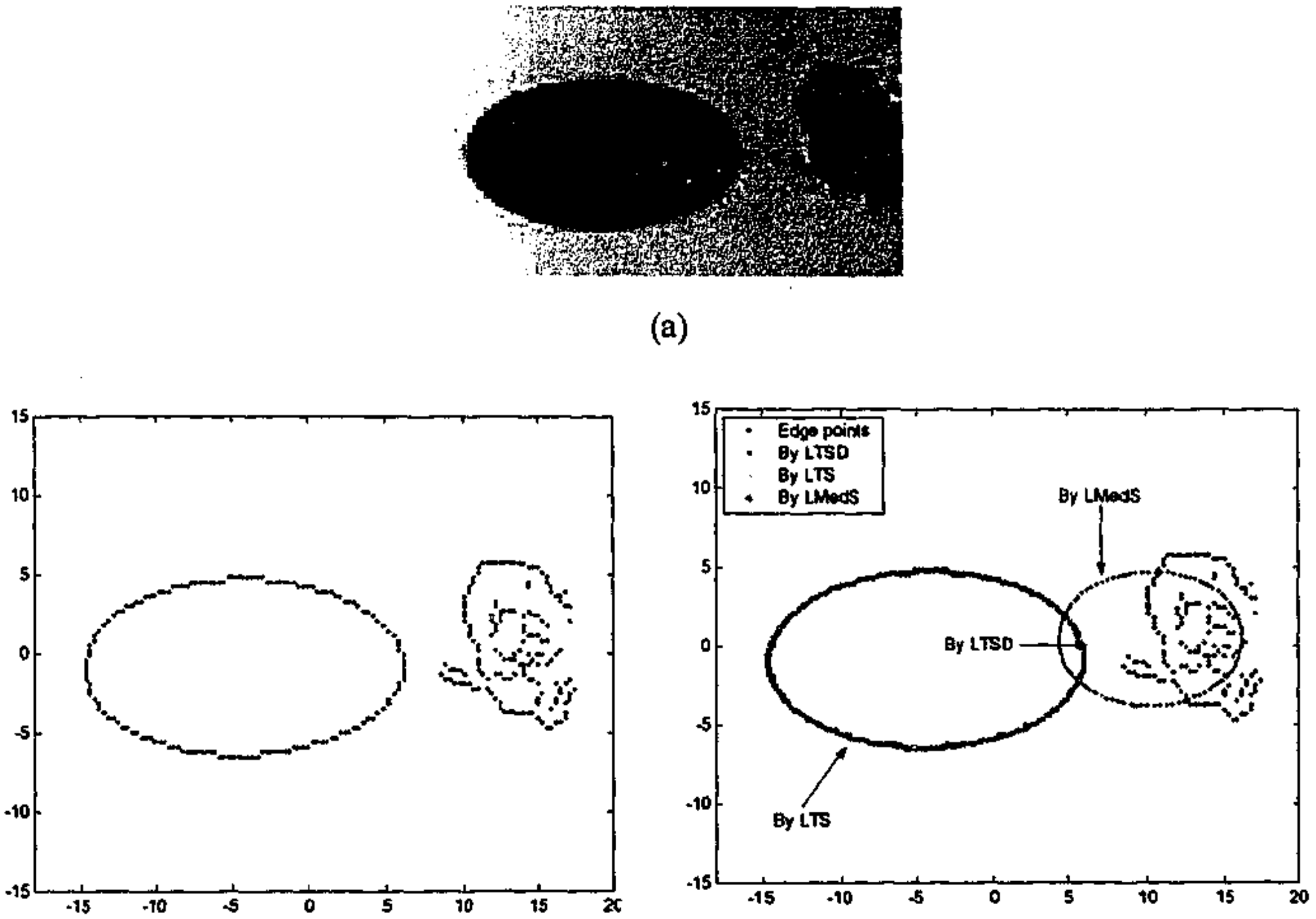

(a)

(b)

(c)

Figure 3.8: Fitting a mouse pad (a) a mouse pad with some flower; (b) the edge image by using Canny operator; (c) the results obtained by the LTSD, LTS and LMedS methods.

Figure 3.9 shows the use of the LTSD method to fit an ellipse to the rim of a cup. Figure 3.9 (a) gives a real cup image. After applying the Prewitt operator, the edge of the cup is detected is shown in Figure 3.9 (b). We can see that there is a high percentage (about 45%) of clustered outliers existing in the edge image, external to the rim of the cup (the ellipse we shall try to fit), mainly due to the figure on the cup. However, the rim of the cup has a symmetric elliptical structure. Figure 3.9 (c) shows that the LTSD method correctly finds the ellipse in the opening of the cup, while both the LTS and the LMedS fail to correctly fit the ellipse.

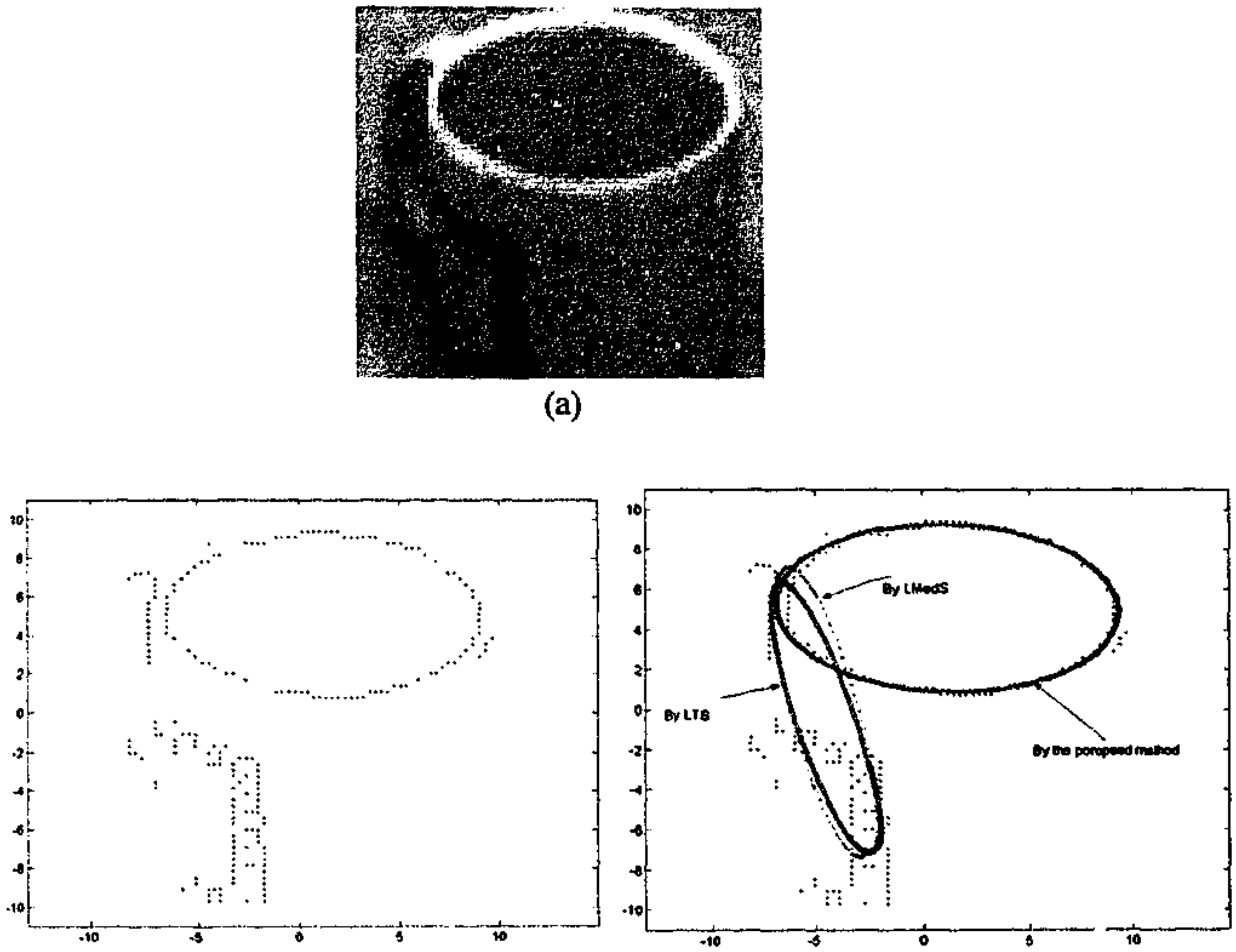

(a)

(b)

(c)

Figure 3.9: Fitting the ellipse in a cup (a) a real cup image; (b) the edge of the cup by applying Prewitt operator; (c) comparative results obtained by the LTSD, LTS and LMedS methods

3.5.4 Experiments for the Data with Uniform Outliers

Finally, we investigated the characteristics of the LTSD under uniform outliers. We generated 200 data points with 40% uniform outliers (see Figure 3.10). The ellipse had a standard variance 0.5, major axis 10.0, minor axis 8.0, center (0.0, 0.0), and orientation to horizon direction θ is 0.0 degree. The uniform outliers were randomly distributed in a rectangle with left upper corner (-20.0, 20.0) and right lower corner (20.0, -20.0). We repeated the performance 100 times and the averaged results were shown in Table 3.2. We can see the LTSD method can also work well in uniform outliers.

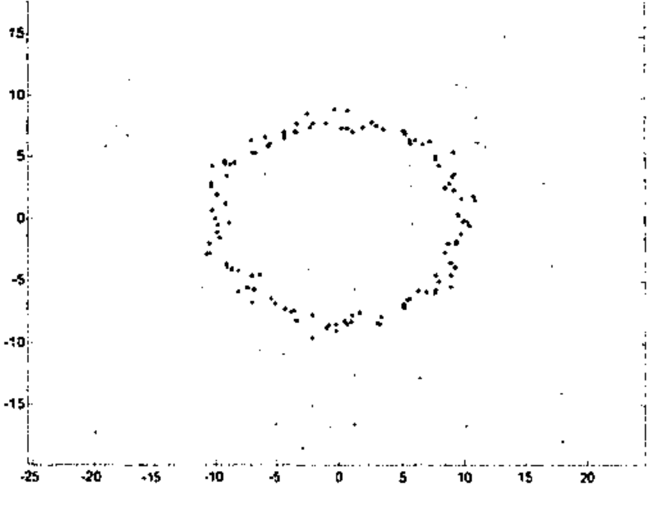

Figure 3.10: An ellipse with 40% randomly distributed outliers.

	xc	yc	Major axis	Minor axis	θ (deg)
True value	0.0	0.0	10.0	8.0	0.0
The LTSD method	-0.107	0.121	10.005	8.024	-1.119
The LTS method	-0.009	0.120	9.877	7.959	-2.117
The LMedS method	0.007	0.002	9.987	8.062	-0.981

Table 3.2: Comparison of the estimated parameters by the LTSD, LTS, and LMedS methods in ellipses fitting with 40% randomly distributed outliers.

3.6 Conclusion

The fragility of traditionally employed robust estimators: LMedS and LTS, in the presence of clustered outliers, has been demonstrated in this chapter (a similar story applies more widely – see chapter 4). These robust estimators can break down at surprisingly lower percentage of outliers when the outliers are clustered. Thus this chapter provides an important cautionary note to the computer vision community to carefully employ robust estimators when outliers are clustered. We also proposed a new method that incorporates symmetry distance into model fitting. The comparative study shows that this method can achieve better performance than the least median of squares method and the least trimmed squares method especially when large percentages of clustered outliers exist in the data and the standard variance of inliers is large. The price paid for the improvement in fitting models is an increase of the computational complexity due to the complicated definition of symmetry distance. It takes about O(n^2) time to compute symmetry distance (SD) for each p-subset. The proposed method can be applied to the fitting of other symmetric shapes and to other fields.

Unfortunately, LTSD was especially designed for spatially symmetric data distributions. For inlier distributions that are not spatially symmetric (including structures that, though they may be symmetric, have large amounts of missing or occluded data so that the visible inliers are not symmetric), the LTSD is not a good choice (Note: for this kind of data, we have developed other novel highly robust estimators that will be presented in the following chapters). However, the LTSD does provide a feasible way to greatly improve the achievements of conventional estimators -the LMedS and the LTS, especially, when the data contain inliers (with symmetry) with large variance and are contaminated by large percentage of clustered outliers.

In the next chapter, we will take advantage of the information in the structure of the pdf of residuals, and propose a more general highly robust estimator: MDPE, which can be widely applied in many computer tasks and is applicable for missing data, data with occlusion, and data without symmetry. The same motivation is also behind several improved methods: QMDPE and vbQMDPE (in chapter 5 and chapter 6).

Chapter 4

MDPE: A Novel and Highly Robust Estimator

4.1 Introduction

Many robust estimators (such as M-estimators, LMedS, LTS, etc.) have been developed in the statistics field. However, they assume that inliers occupy an absolute majority of the whole data, and thus, they will breakdown for data involving an absolute majority of outliers. Obviously, the requirement for 50% or more data belonging to inliers may not be always satisfied, e.g., when the data contain multiple surfaces, when data from multiple views are merged, or when there are more than 50% noise data points existing in the data. For these cases, we need to find a more robust estimator that can tolerate more than 50% outliers.

This chapter presents a novel robust estimator (MDPE). This estimator applies nonparametric density estimation and density gradient estimation techniques in parametric estimation ("model fitting"). The goals in designing MDPE are: it should be able to fit signals corresponding to less than 50% of the data points and be able to fit data with multi-structures. In developing MDPE, we make the common assumption that the residuals of the inliers are contaminated by Gaussian noise (although the precise nature of the noise distribution is not that essential, depending only upon zero mean and unimodality). We also assume that the signal (we seek to fit) occupies a relative majority of the data – that is, there are no other populations, belonging to valid structures, that singly has a larger population. In other words, if there are multiple structures, we seek to fit the largest structure (in terms of population of data – which is often related to but not necessarily identical to geometric size). Of course, in a complete application of MDPE, such as the range segmentation algorithm presented in the next chapter, one can apply the estimator serially to identify the largest structured population, remove it, and then seek the largest in the remaining population etc.

Key components of MDPE are: Probability Density estimation in conjunction with Mean Shift techniques (Fukunaga and Hostetler 1975). The mean shift vector always points towards the direction of the maximum increase in the probability density function (see section 4.2). Through the mean shift iterations, the local maximum density, corresponding to the mode (or the center of the regions of high concentration) of data, can be found.

MDPE optimizes an objective function that measures more than just the size of the residuals. It considers the following two factors at the same time:

- The density distribution of the data points (in residual space) estimated by the density estimation technique.
- The size of the residual corresponding to the local maximum of the probability density distribution.

If the signal is correctly fitted, the densities of inliers should be as large as possible; at the same time, the center of the high concentration of data should be as close to zero as possible in the residual space. Thus, both the density distribution of data points in residual space and the size of the residual corresponding to the local maximum of the density distribution, are considered as important characteristics in the objective function of MDPE.

MDPE can tolerate a large percentage of outliers and pseudo-outliers (empirically, usually more than 85%) and it can achieve better performance than other similar robust estimators.

To demonstrate the performance of MDPE, we compare, based upon tests on both synthetic and real images, MDPE with other five popular robust estimators (from both statistics and computer vision field): Hough Transform (HT), Random Sampling Consensus (RANSAC), Least Median of Squares (LMedS), Residual Consensus (RESC), and Adaptive Least kth Order Squares (ALKS). Experiments show that MDPE has a higher robustness to outliers and fewer errors than the other five estimators.

The contributions of this chapter can be summarized as follows:

- We apply nonparametric density estimation and density gradient estimation techniques in parametric estimation.
- We provide a novel estimator, MDPE, which can usually tolerate more than 85% outliers although it is simple and easy to implement.
- The performance of MDPE has been compared with those of five other popular methods, including "traditional" ones (RANSAC, Hough Transform, and LMedS) and recently proposed ones (RESC and ALKS).

The organization of this chapter is as follows: density gradient estimation and the mean shift method are introduced in section 4.2. Section 4.3 describes the MDPE method. Comparative experimental results of MDPE and several other robust estimators are contained in section 4.4. Finally, we conclude with a summary and a discussion of further possible work in section 4.5.

4.2 Nonparametric Density Gradient Estimation and Mean Shift Method

There are several nonparametric methods available for probability density estimation: the histogram method, the naive method, the nearest neighbor method, and kernel estimation (Silverman 1986). The kernel estimation method is one of the most popular techniques used in estimating density. Given a set of n data points $\{X_i\}_{i=1,\ldots,n}$ in a d-dimensional

Euclidian space R^d, the multivariate kernel density estimator with kernel K and window radius (band-width) h is defined as follows ((Silverman 1986), p.76)

$$\hat{f}(x) = \frac{1}{nh^d} \sum_{i=1}^{n} K(\frac{x - X_i}{h}) \tag{4.1}$$

The kernel function $K(x)$ should satisfy some conditions ((Wand and Jones 1995), p.95).

There are several different kinds of kernels. The Epanechnikov kernel ((Silverman 1986), p.76) is one optimum kernel which yields minimum mean integrated square error (MISE):

$$K_e(\mathrm{X}) = \begin{cases} \frac{1}{2} c_d^{-1} (d+2)(1 - \mathrm{X}^T \mathrm{X}) & \mathit{if}\, \mathrm{X}^T \mathrm{X} < 1 \\ 0 & \mathit{otherwise} \end{cases} \tag{4.2}$$

where c_d is the volume of the unit d-dimensional sphere, e.g., c_1=2, c_2=π, c_3=4π/3.

The estimate of the density gradient can be defined as the gradient of the kernel density estimate (4.1):

$$\hat{\nabla} f(x) \equiv \nabla \hat{f}(x) = \frac{1}{nh_d} \sum_{i=1}^{n} \nabla K(\frac{x - X_i}{h}) \tag{4.3}$$

According to (4.3), the density gradient estimate of the Epanechnikov kernel can be written as:

$$\hat{\nabla} f(x) = \frac{n_x}{n(h^d c_d)} \frac{d+2}{h^2} \left(\frac{1}{n_x} \sum_{X_i \in S_h(x)} [X_i - x] \right) \tag{4.4}$$

where the region $S_h(x)$ is a hypersphere of the radius h, having the volume $h^d c_d$, centered at x, and containing n_x data points.

The mean shift vector $M_h(x)$ is defined as

$$\mathrm{M}_h(\mathrm{x}) \equiv \frac{1}{n_x} \sum_{X_i \in S_h(x)} [X_i - x] = \frac{1}{n_x} \sum_{X_i \in S_h(x)} X_i - x \tag{4.5}$$

Equation (4.4) can be rewritten as:

$$\mathrm{M}_{\mathrm{h}}(\mathrm{x}) \equiv \frac{h^2}{d+2} \frac{\hat{\nabla} f(x)}{\hat{f}(x)} \tag{4.6}$$

Equation (4.6) firstly appeared in (Fukunaga and Hostetler 1975). Equation (4.5) shows that the mean shift vector is the difference between the local mean and the center of the window. Equation (4.6) shows the mean shift vector is an estimate of the normalized density gradient. The mean shift is an unsupervised nonparametric estimator of density gradient. One characteristic of the mean shift vector is that it always points towards the direction of the maximum increase in the density.

The Mean Shift algorithm can be described as follows:

1. Choose the radius of the search window
2. Initialize the location of the window.
3. Compute the mean shift vector $M_h(x)$.
4. Translate the search window by $M_h(x)$.
5. Step 3 and step 4 are repeated until convergence.

The converged centers (or windows) correspond to modes (or centers of the regions of high concentration) of data represented as arbitrary-dimensional vectors. The proof of the convergence of the mean shift algorithm can be found in (Comaniciu and Meer 2002a). Since its introduction by Fukunaga and Hostetler (1975), the mean shift method has been extensively exploited and applied, for its ease and efficiency, in low level computer vision tasks such as video tracking (Comaniciu, Ramesh et al. 2000), image filtering (Comaniciu and Meer 1999a), clustering (Cheng 1995; Comaniciu and Meer 1999b) and image segmentation (Comaniciu and Meer 1997; Comaniciu and Meer 2002a).

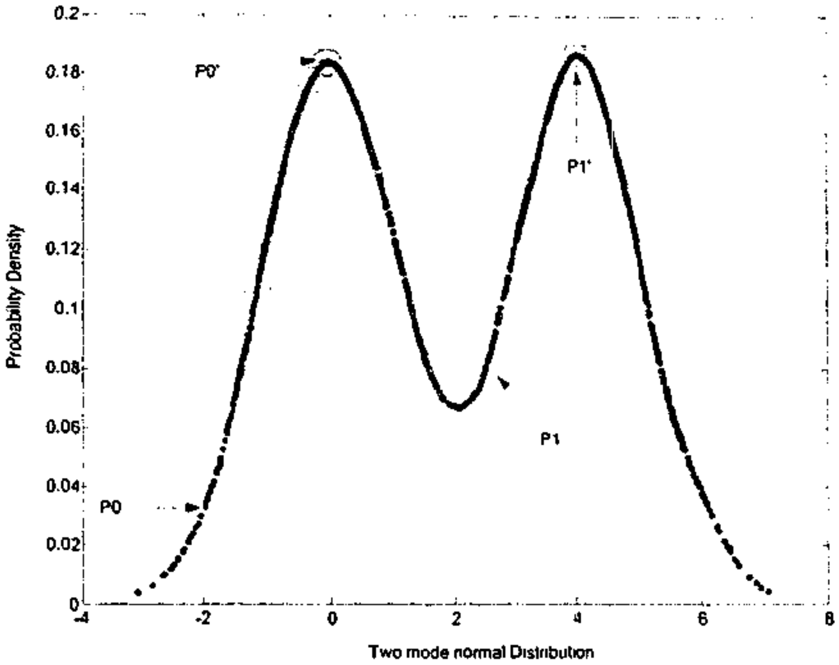

Figure 4.1: One example where the mean shift estimator found the local maximum of the probability densities.

To illustrate the mean shift method, two sets of samples from normal distributions were generated, each having 1000 data points and with unit variance. One had a distribution with zero mean, and the other had a mean of 4.0 (see Figure 4.1). These points were distributed along the abscissa but here we choose to plot only the corresponding probability density at those data points). We selected two initial points as the centers of the initial windows: P0 (-2.0) and P1 (2.5). The search window radius was chosen as 1.0. After applying the mean shift algorithm, the mean shift estimator automatically found the local maximum densities (the centers of converged windows). Precisely, P0' located at -0.0305, and P1' with 4.0056. The centers (P0' and P1') of the converged windows correspond to the local maximum probability densities, that is, the two modes.

4.3 Maximum Density Power Estimator—MDPE

4.3.1 The Density Power (DP)

Random sampling techniques have been widely used in a lot of methods, for example, RANSAC, LMedS, RESC, ALKS, etc (see chapter 2). Each uses the random sampling techniques to choose p points, called a p-subset, to determine the parameters of a model for that p-subset (p equals 2 for a line, 3 for a circle or plane, 6 for a quadratic curve), and finally outputs the parameters determined by the p-subset with the minimum or maximum of the respective objective function. They differ in their objective functions used to rank the p-subsets. Here we define a new objective function.

When a model is correctly fitted, there are two criteria that should be satisfied:

(1) Data points on or near the model (inliers) should be as many as possible;

(2) The residuals of inliers should be as small as possible.

Most objective functions of existing methods consider either one of the criteria or both. RANSAC (Fischler and Rolles 1981) applies criterion (1) into its optimization process and outputs the results with the highest number of data points within an error bound; The Least squares method uses criterion (2) as its objective function, but minimizes the residuals of all data points without the ability to differentiate the inliers from the outliers; MUSE, instead of minimizing the residuals of inliers, minimizes the scale estimate provided by the kth ordered absolute residual. RESC combines both criteria into its objective function, i.e., the histogram power. Among all these methods, RESC obtains the highest breakdown point. It seems that it is preferable to consider both criteria in the objective function.

The new estimator we introduce here, MDPE, also considers these two criteria in its objective function. We assume the residuals of the inliers (good data points) satisfy a zero mean, smooth and unimodal distribution: e.g., a Gaussian-like distribution. If the model to fit is correctly estimated, the data points on or near the fitted structure should have a higher probability density; and at the same time, the center of the converged window by the mean shift procedure (corresponding to the highest local probability density) should be as close to zero as possible in residual space. According to the above assumptions, our objective function ψ_{DP} considers two factors: (1) the densities $\hat{f}(X_i)$ of all data points within the converged window W_c and (2) the center Xc of the converged window. Thus $\psi_{DP} \propto \sum_{X_i \in Wc} \hat{f}(X_i)$ and $\psi_{DP} \propto \frac{1}{|Xc|}$. We define the probability density power function as follows:

$$\psi_{DP} = \frac{\left(\sum_{X_i \in W_c} \hat{f}(X_i) \right)^{\alpha}}{\exp(|Xc|)} \tag{4.7}$$

where Xc is the center of the converged window W_c obtained by applying the mean shift procedure. α is a factor that adjusts the relative influence of the probability density to the residual of the point corresponding to the center of the converged window. α is empirically set to 1.0. Experimentally, we have found the above form to behave better than various other alternatives having the same general form.

If a model is found, $|Xc|$ is very small, and the densities within the converged window are very high. Thus our objective function will produce a high score. Experiments, presented in the next section, show that MDPE is a very powerful method for data with a large percentage of outliers.

4.3.2 The MDPE Algorithm

As Lee stated (Lee, Meer et al. 1998), any one-step robust estimator cannot have a breakdown point exceeding 50%, but estimators adopting multiple-step procedures with an apparent breakdown point exceeding 50% are possible.

MDPE adopts a multi-step procedure. The procedure of MDPE can be described as follows:

(1) Choose a search window radius h, and a repetition count m. The value m can be chosen according to equation (2.23).

(2) Randomly choose one p-subset, estimate the model parameters by the p-subset, and calculate the signed residuals of all data points.

(3) Apply the mean shift steps in the residual space with initial window center zero. Notice that the mean shift is employed in one-dimensional space – signed residual space. The converged window center C can be obtained by the mean shift procedure in section 4.2.

(4) Calculate the densities (using equation 4.1) corresponding to the positions of all data points within the converged window with radius h in the residual-density space.

(5) Calculate the density power according to equation (4.7).

(6) Repeat step (2) to step (5) m times. Finally, output the parameters with the maximum density power.

The results are from one p-subset, corresponding to the maximum density power. In order to improve the statistical efficiency, a weighted least square procedure [(Rousseeuw and Leroy 1987), p.202] is carried out after the initial MDPE fit. However, a more robust scale estimator TSSE (which was proposed at the later stage—see chapter 7) can also be employed.

Instead of estimating the fit involving the absolute majority in the data set, MDPE finds a fit having a relative majority of the data points. This makes it possible, in practice, for MDPE to obtain a high robustness that can tolerate more than 50% outliers.

4.4 Experiments and Analysis

Next, we will compare the abilities of several estimators (MDPE, RESC, ALKS, LMedS, RANSAC, and Hough Transform) to deal with data with a large percentage of outliers. We choose RANSAC and Hough Transform as two methods to compare with, because they are very popular methods and have been widely applied in computer vision. Provided with the correct error tolerance (for RANSAC) or bin size (for Hough Transform), they can tolerate more than 50% outliers. Although LMedS has only 0.5 breakdown point and cannot tolerate more than 50% outliers, it needs no prior knowledge of the variance of inliers. RESC and ALKS are two relatively new methods and represent modern developments in robust estimation. We also note that RANSAC, LMedS, RESC, ALKS, and MDPE all adopt similar four-step procedures: randomly sampling; estimating the parameter candidate for each sample; evaluating the quality of each candidate; outputting the final parameter estimate with the best quality measure.

In this section, we will investigate the characteristics of the six methods under clustered outliers and different percentages of outliers. We also investigate the time complexity of the five comparative methods (LMedS, RANSAC, ALKS, RESC, and MDPE). We produce the breakdown plot of the six methods, and test the influence of the choice of window radius on the MDPE. Unless we specify, the window radius h for MDPE will be set at 2.0 for the experiments in this section.

4.4.1 Experiment 1

In this experiment, the performance of MDPE in line fitting and circle fitting will be demonstrated and its tolerance to large percentages of outliers will be compared with five other popular methods: RANSAC, Hough Transform, LMedS, RESC, and ALKS. The time complexity of the five methods (except for Hough Transform) will also be evaluated and compared. We will show that some methods break down. We can (and have) checked whether such a breakdown is an artifact of implementation (e.g. randomly sampling) or whether the breakdown is the result of the objective function for that method scoring wrong fit "better" than the true one—see discussions later (sub-section 4.4.1.1) .

4.4.1.1 Line Fitting

We generated four kinds of data (step, three-step, roof, and six-line), each with a total of 500 data points. The signals were corrupted by Gaussian noise with zero mean and standard variance σ. Among the 500 data points, α data points were randomly distributed in the range of (0, 100). The i'th structure has n_i data points.

(a) Step: x:(0-55), y=30, n_1=65; x:(55-100), y=40, n_2=30; α=405; σ=1.5.

(b) Three-step: x:(0-30), y=20, n_1=45; x:(30-55), y=40, n_2=30; x:(55-80), y=60, n_3=30; x:(80-100), y=80, n_4=30; α=365; σ=1.

(c) Roof: x:(0-55), y=x+30, n_1=35; x:(55-100), y=140-x, n_2=30; α=435; σ=1.

(d) Six-line: x:(0-25), y=3x, n_1=30; x:(25-50), y=150-3x, n_2=20; x:(25-50), y=3x-75, n_3=20; x:(50-75), y=3x-150, n_4=20; x:(50-75), y=225-3x, n_5=20; x:(75-100), y=300-3x, n_6=20; α=370; σ=0.1.

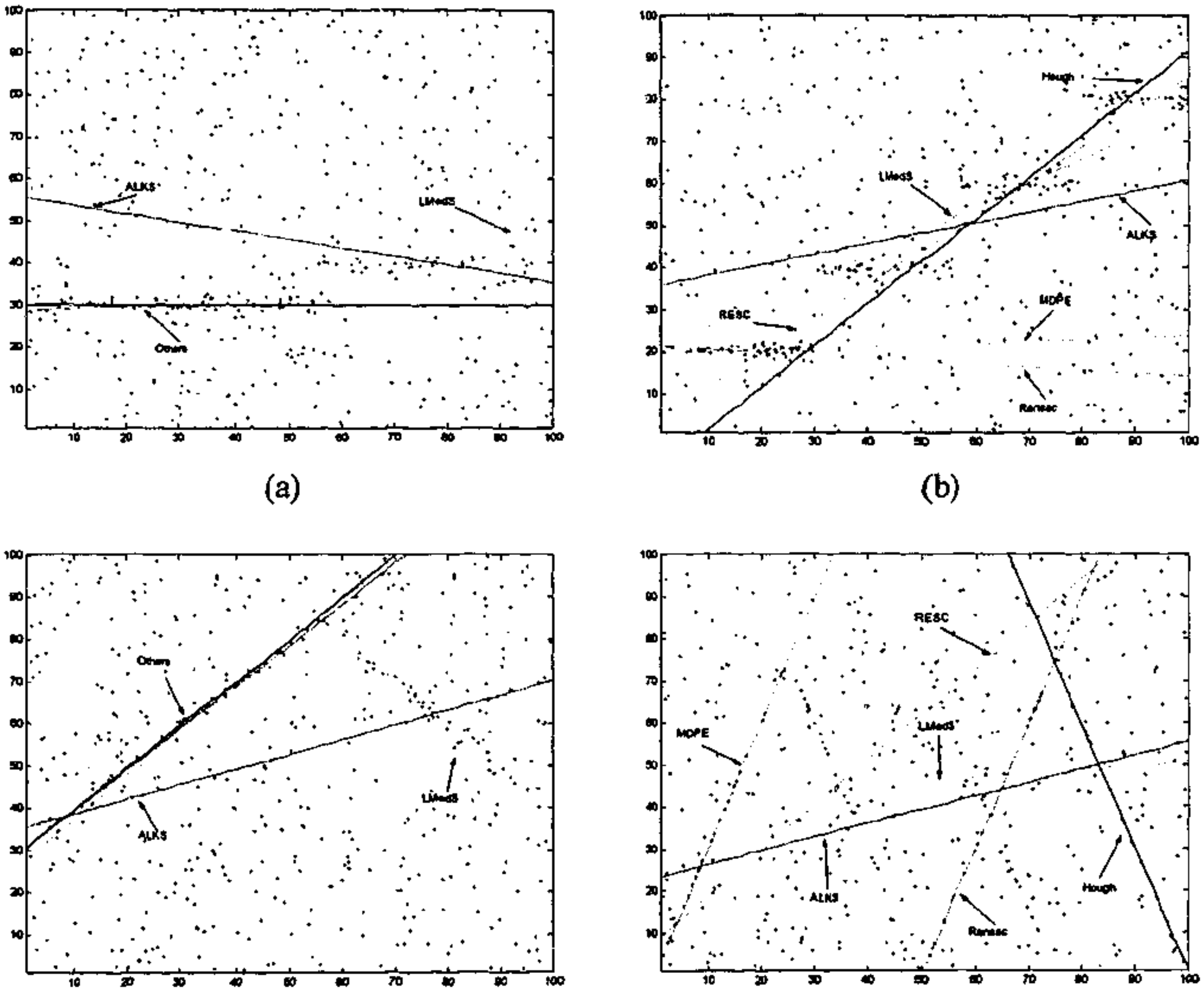

(a)

(b)

(c)

(d)

Figure 4.2: Comparing the performance of six methods: (a) fitting a step with a total of 87% outliers; (b) fitting three steps with a total of 91% outliers; (c) fitting a roof with a total of 93% outliers; (d) fitting six lines with a total of 94% outliers.

From Figure 4.2, we can see that because LMedS has only a 0.5 breakdown point, it cannot resist more than 50% outliers. Thus, LMedS failed to fit all the four signals: The ALKS, RESC and MDPE approaches all have higher robustness, compared with LMedS, to outliers. However, the results show that ALKS is not applicable for the signals with such large percentages of outliers because it failed in all four cases. RESC, although having a very high robustness, fitted one model, but failed three. The Hough Transform could not correctly fit the step signals, which happen to fall near an inclined line, with large percentages of outliers. Provided with the correct error bound of inliers, RANSAC correctly fitted three signals, but failed one. Only the MDPE method correctly fitted all the four signals. The MDPE didn't breakdown even with 94% outliers. In Figure 4.2 (d), we can see, although MDPE, Hough Transform, and RANSAC did not breakdown, they found different lines in the six-line signal (according to their own criterion).

Among these six methods, MDPE, RESC and RANSAC are similar to each other. They all randomly choose *p*-subsets and try to estimate parameters by a *p*-subset corresponding to the maximum value of their object function. Thus, their objective functions are the core that determines how much robustness to outliers these methods have. RANSAC considers only the number of data points falling into given error bound of inliers; RESC considers the number of data points within the mode and the residual distributions of these points; MDPE considers not only the density distribution of the mode, which is assumed having Gaussian-like distribution, in the residual space, but also the size of the residual corresponding to the center of the mode.

It is important to point out that the failures of RESC, ALKS, LMedS, and RANSAC, and Hough Transform in some of or all of the four signals is inherent and not simply an artefact of our implementation. Let us check the criteria of RESC and we will understand why RESC failed to fit to the three signals. The objective function of RESC for the correct fit is 7.0 (for one-step signal), 5.8 (for three-steps signal) and is 4.4 (for six-lines signal). However, the objective function of RESC for the estimated parameters is 7.6 for a step, 8.1 for three steps and 5.3 the six-line signal. In fact, during the searching procedure, the RESC estimator consistently maximizes its objective function—histogram power, starting with initial fits that have a smaller histogram power, but successively finding fits with higher histogram power – proceeding to even higher histogram power than that possessed by the true fit. The failures of RANSAC, LMedS and ALKS have a similar nature: for example, the median of residuals of the true fit is 16.8, 29.2 and 97.0 for a step, three steps and six lines respectively. However the median of residuals of final result by the LMedS method is 16.3, (for a step), 15.5 (for three steps) and 23.4 (for six lines). The problem is not with the implementation but with the criterion.

4.4.1.2 Circle Fitting

The proposed MDPE is a general method that can be easily applied to fit other kinds of models, such as circles, ellipsis, planes, etc. Figure 4.3 shows the ability of the MDPE to fit circles under 95% outliers. Five circles were generated, each with 101 data points and σ=0.1. 1500 random outliers were distributed at range (-75 - 75). Thus, for each circle, it has 1904 outliers (404 pseudo-outliers plus 1500 random outliers). The MDPE method gave more accurate results than LMedS, RESC, and ALKS. The Hough Transform and RANSAC also correctly fit the circles when provided with correct bin size (for Hough Transform) and error bound of inliers (for RANSAC). The three methods (MDPE, Hough Transform, and RANSAC) fitted three different circles according to their own criterion.

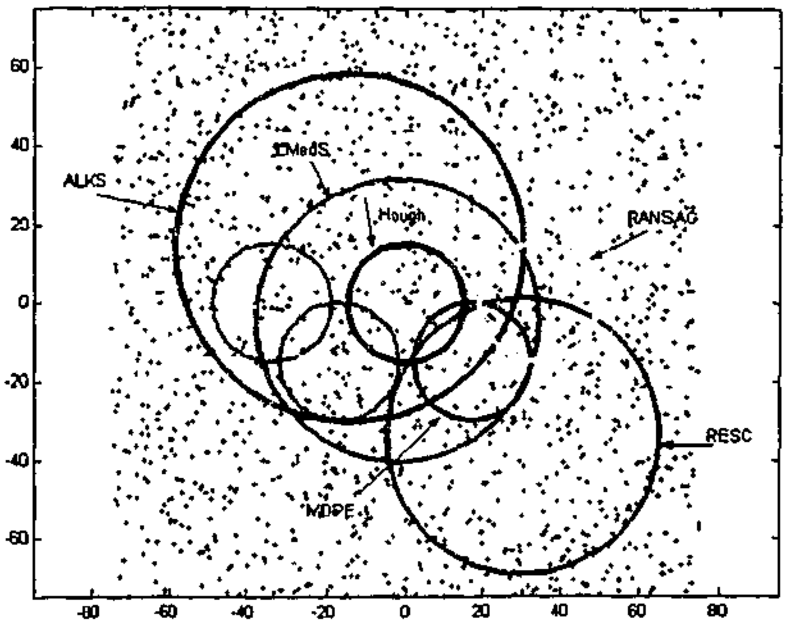

Figure 4.3: One example of fitting circles by the six methods. The data had about 95% outliers.

4.4.1.3 Time Complexity

It might be interesting to compare the time complexity between the different methods. In this experiment, we will compare the speed of MDPE, RESC, ALKS, LMedS, and RANSAC. We do not consider the Hough Transform, because the speed of Hough transform depends on the dimension of parameter space, the range of each parameter, and the bin size. It also uses a different framework (voting in parameter space), compared with the other five methods (which use sampling techniques).

In order to make the speed of each method comparable, the same simple random sampling technique was used for all five methods. Although some other sampling techniques exist, such as guided sampling (Tordoff and Murray 2002) and GA sampling (Roth and Levine 1991; Yu, Bui et al. 1994), and the speed of each method by adopting these sampling techniques can be improved; we adopted the simple randomly sampling technique because:

(1) It has been widely used in most robust estimators (such as LMedS, LTS, RANSAC, ALKS, MUSE, MINPRAN, etc.).

(2) It is easy to perform.

	A Step	Three Steps	A Roof	Six Lines	Five Circles
Percentages of outliers	87%	91%	93%	94%	95%
Number of Sampling: *m*	500	1000	1500	2000	3000
MDPE	7.3	15.1	20.1	28.4	73.4
RESC	12.6	23.8	35.4	47.3	82.2
ALKS	6.4	13.7	19.8	26.7	126.8
LMedS	0.6	1.3	2.0	3.0	14.6
RANSAC	0.7	1.2	1.6	2.5	14.0

Table 4.1: The comparison of time complexity for the five methods (all time in seconds).

We used the signals above (a step, three steps, a roof, six lines, and five circles) to test speed of the five methods. We repeated the experiments on each signal 10 times, and the mean time of each method for each signal was recorded. We performed them all in complete MATLAB code (programming in C code with optimisation will make the methods faster).

From Table 4.1, we can see that LMedS and RANSAC have similar speed and they are faster than MDPE, RESC, and ALKS. MDPE is about 35% faster than RESC. The speed of MDPE is close to that of ALKS in line fitting but faster than ALKS in the five-circles fitting. ALKS is also faster than RESC in line fitting, but slower than RESC in circle fitting. We noted that the time complexity of ALKS, compared with MDPE and RESC, is slower in the five-circle signal (2005 data points) than in the line signals (505 data points). This is because the ALKS procedure used *m* *p*-subsets for each value of *k* (as recommended by Lee and Meer, the number of different *k* is equal to 19). Thus, when the number of data points and sampling times is increased, the increase of time complexity of ALKS in sorting the residuals of the data points (mainly) is higher than that of RESC in compressing histogram, and that of MDPE in calculating density power.

4.4.2 Experiment 2

In the previous experiment, we investigated the characteristics of the six methods to fit data with multiple structures. In this experiment, we will explore the abilities of the six methods to fit data with clustered outliers. We generated a line (y=x-1) corrupted by Gaussian noise with zero mean and standard variance σ_1. The line had n data points. Among the total 500 data points, α data points were randomly distributed in the range of (0, 100.0), and β clustered outliers were added to the signals, possessing a spherical bivariate normal distribution with standard variance σ_2 and mean (80.0, 30.0).

(a) γ=100, σ_1=1.0; α=200; β=200; σ_2=5.0.

(b) γ=100, σ_1=1.0; α=200; β=200; σ_2=2.0.

(c) γ=275, σ_1=1.0; α=0; β=225; σ_2=1.0.

(d) γ=275, σ_1=5.0; α=0; β=225; σ_2=1.0.

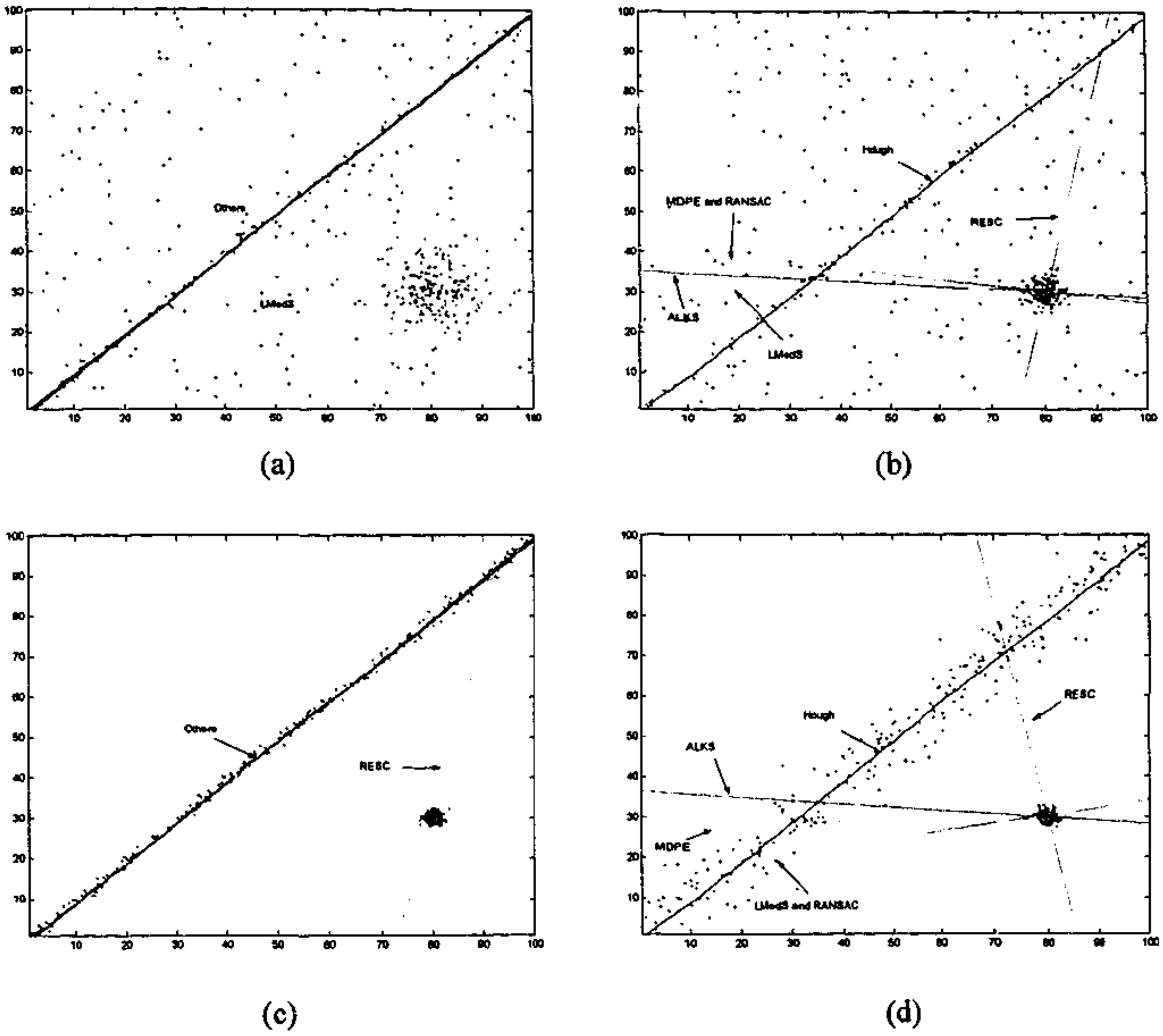

(a)

(b)

(c)

(d)

Figure 4.4: Experiment where the six methods are fitting a line with clustered outliers. The standard variance of both clustered outliers and inliers will affect the results of the six methods.

Figure 4.4 shows that both the standard variance of clustered outliers σ_2 and the standard variance of inliers to the line σ_1 will decide the accuracy of the results estimated by the six methods. When σ_1 is small and σ_2 is large, all methods except for LMedS can correctly fit the line although a large number of clustered outliers existed in the data (see Figure 4.4 (a)). The LMedS failed because it cannot tolerate more than 50% outliers. When the standard variance of clustered outliers is small, i.e., the outliers are densely clustered within a small range; the ability of MDPE, RESC, ALKS, and RANSAC to resist the influence of clustered outliers will be greatly reduced (see Figure 4.4 (b)). As shown in Figure 4.4 (c) and Figure 4.4 (d), the standard variance of inliers to the line will also affect the accuracy of the results by LMedS, MDPE, RESC, ALKS, and RANSAC. When σ_1 was 5.0 (Figure 4.4 (d)), all the five methods failed to fit the line even with only 45% clustered outliers.

The Hough Transform, to our surprise, showed excellent performance to resist clustered outliers. It succeeded to fit all the four signals despite clustered outliers. We note that the Hough Transform adopts a different framework to the other five methods: it uses a voting technique in parameter spaces instead of residual space. It would seem that the objective functions of all other methods fail to score the correct solutions highly (for MDPE, RESC, and RANSAC) or lowly (for LMedS and ALKS) enough when there are large numbers of very highly clustered outliers. This has been noted before with the LMedS (Wang and Suter 2003a; also see chapter 3) and is presumably one reason why the proofs of high breakdown point specifically stipulates rather generally distributed outliers.

4.4.3 Experiment 3

It is important to know the characteristics of the various methods when the signals were contaminated by different percentages of outliers. In this experiment, we will draw the "breakdown plot" and compare the abilities of the six methods to resist different percentages of outliers (in order to avoid crowding, each sub-figure in Figure 4.5 includes three methods). We generated step signals (y=Ax+B) as follows:

Signals: line 1: x:(0-55), A=0, B=30, n_1 will be decreased with the increase of uniformly distributed outliers α, line 2: x:(55-100), A=0, B=60, n_2=25; for both lines: σ=1.

In total 500 points. 15 clustered outliers centred at (80, 10) with unit variance were added to the signals. At the beginning, n_1 = 460, α=0, so the first signal had an initial 8% outliers; then every repeat of the experiment 5 points was moved from n_1 to uniform outliers (α) ranging over (0-100) until n_1=25. Thus the percentage of outliers in the data points changed from 8% to 95%. The whole procedure above was repeated 20 times.

As Figure 4.5 illustrated, the LMedS first broke down (at about 50% of outliers) among all these six estimators. ALKS broke down even when outliers comprised less than 80%; RESC began to break down when outliers comprised more than 88% of the total data.

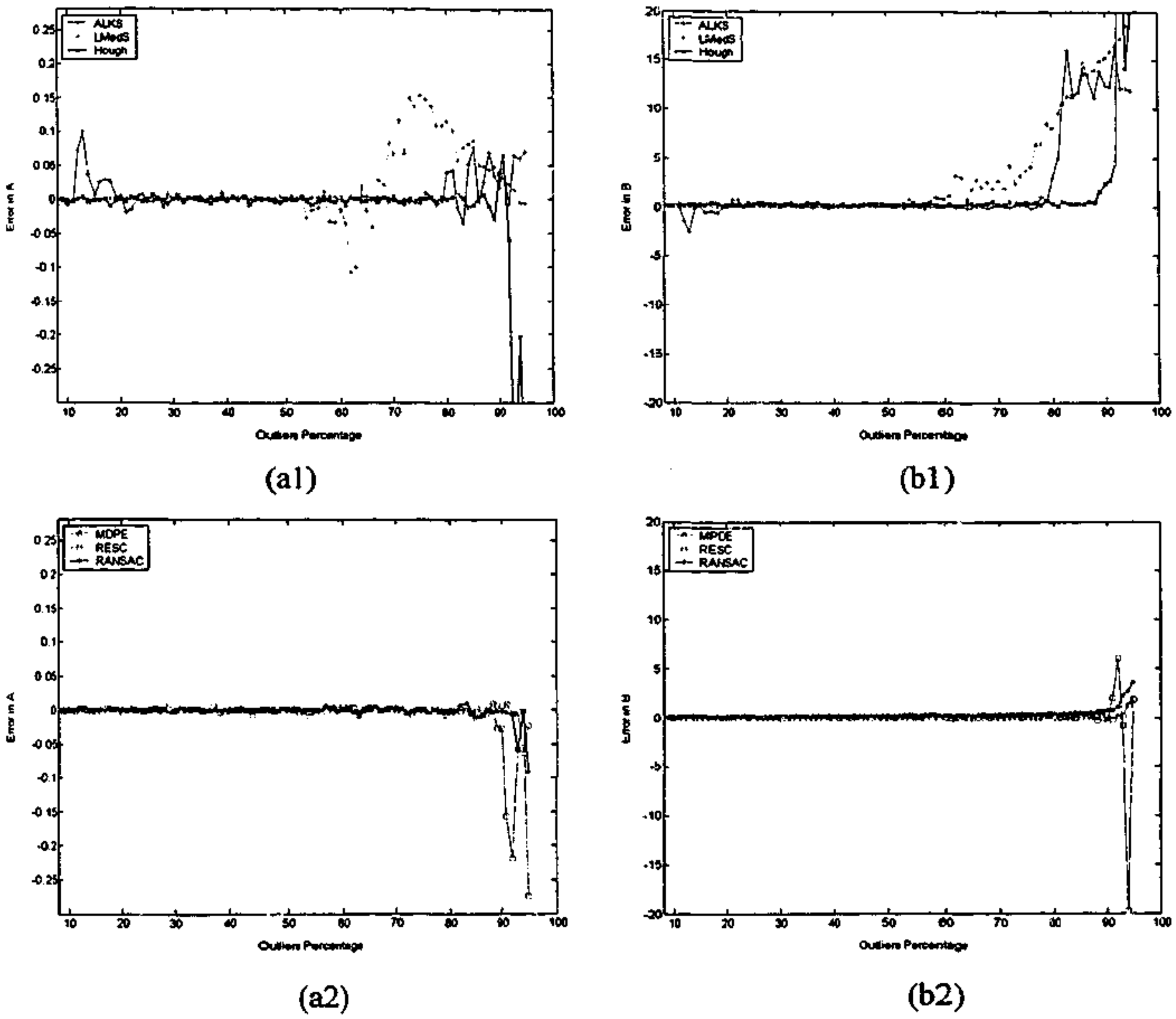

(a1)

(b1)

(a2)

(b2)

Figure 4.5: Breakdown plot for the six methods: (a1) and (a2) error in A vs. outlier percentage; (b1) and (b2) error in B vs. outlier percentage.

From Figure 4.5, we can also see that, provided with the correct error bound (for RANSAC) and with a "good" bin size (for Hough Transform), RANSAC and Hough Transform can tolerant more than 50% outliers. RANSAC began to break down at 92% outliers; Hough transform began to break down when outliers have more than 88% (broke down at 89% or more outliers). However, the performance of RANSAC is largely dependent on the correct choice of error tolerance. If the error tolerance deviated from the correct error tolerance, RANSAC will completely breakdown (see experiment subsection

4.4.4.2). Similarly, the good performance of Hough Transform is largely dependent on the choice of accumulator bin size. If the bin size is wrongly given, Hough Transform will also breakdown (this phenomenon was also pointed out by Chen and Meer (Chen and Meer 2002)).

In contrast, MDPE has the highest robustness among the six methods. MDPE began to break down only at 94% outliers. However, even at 94% and 95% outliers, MDPE had still, loosely speaking, about 75% correct estimation rate out of the 20 times.

Another thing we noticed is that ALKS has some obvious fluctuations in the results when the outliers are less than 30%, while the other five do not have this undesirable characteristic. This may be because the robust estimate of the noise variance is not valid for small or large *k* values (*k* is the optimum value to be determined by the data).

Among all these six methods, MDPE and RANSAC have similar accuracy. They are more accurate than RESC, ALKS, and LMedS. The accuracy of the Hough Transform greatly depends on the accumulator bin size in each parameter space. Generally speaking, the larger the bin size is, the lower accuracy the Hough Transform may have. Thus, in order to obtain higher accuracy, one needs to reduce the bin size. However, this will lead to an increase in storage requirements and computational complexity. Also, one can have a bin size that is too small (theoretically, each bin receives less votes and in the limit of very small bin size, no bin will have more than 1 vote!).

4.4.4 Experiment 4

The problem of the choice of window radius in the means shift, i.e., bandwidth selection, has been widely investigated during the past decades (Silverman 1986; Wand and Jones 1995; Comaniciu, Ramesh et al. 2001; Comaniciu and Meer 2002a). Comaniciu and Meer (2002a) suggested several techniques for the choice of window radius:

1. The optimal bandwidth should be the one that minimizes AMISE;

2. The choice of the bandwidth can be taken as the center of the largest operating range over which the same results are obtained for the same data.
3. The best bandwidth maximizes a function that expresses the quality of the results.
4. User provides top-down information to control the kernel bandwidth.

Next we will investigate the influence of the choice of window radius on the results of MDPE.

4.4.4.1 The Influence of the Window Radius and the Percentage of Outliers on MDPE

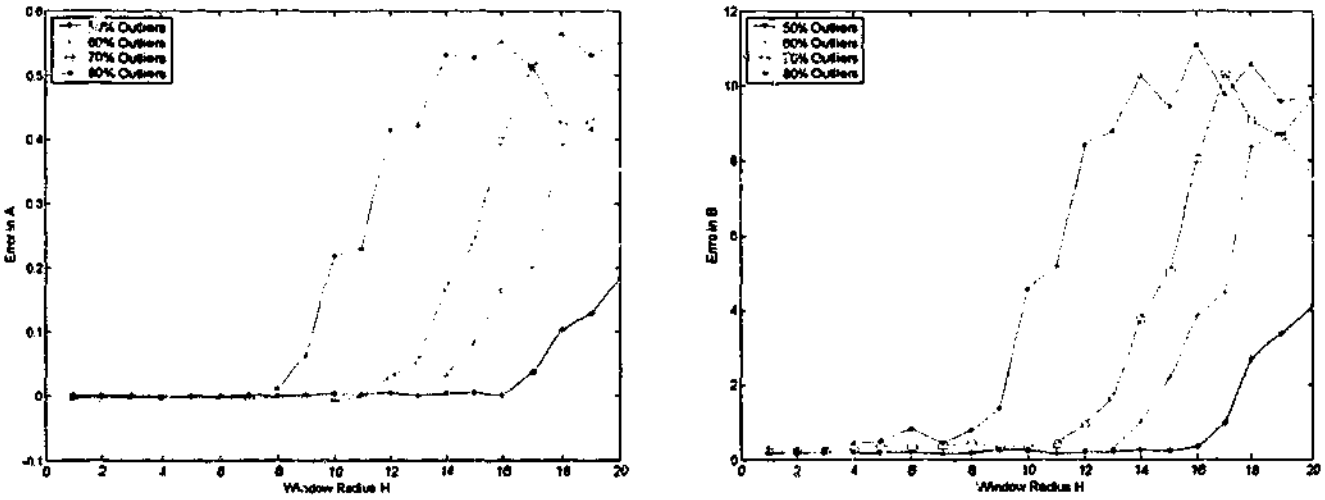

Figure 4.6: The influence of window radius and percentage of outliers on the results of the MDPE.

Although the MDPE has showed its powerful ability to tolerate large percentage of outliers (including pseudo-outliers), its success is decided by the correct choice of window radius *h*. If *h* is chosen too small, it is possible that the densities of data points in the residual space may not be correctly estimated (the density function is a noisy function with many local peaks and valleys), and some inliers may possibly be neglected; on the other hand, if *h* is set too large, the window will include all the data points including inliers and outliers; all peaks and valleys of the density function will also be smoothed out. In order to investigate the influence of the choice of window radius *h* and percentage of outliers on the estimated results, we generated a step signal: $y=Ax+B$, where A=0, B=30 for x:(0-55),

n_1=100; and A=0, B=70 for x:(55-100), n_2=80. . The line was corrupted by Gaussian noise with a unit variance. In total, 500 data points were generated. Uniformly distributed outliers in the range (0-100) were added to the signal so that the data respectively included 50%, 60%, 70% and 80% outliers (including uniformly distributed outliers and pseudo outliers). To investigate the effect of window size in MDPE, the window radius h was set from 1 to 20 with increasing step by 1 each time. The results were repeated 20 times.

Figure 4.6 shows that the absolute errors in A and B increase with the window radius h (when h is larger than some range) because when the radius becomes larger, it is possible that more outliers were included within the converged window. The percentage of outliers has influence on the sensitivity of the results to the choice of window radius: when the data include a higher percentage of outliers, the results are relatively more sensitive to the choice of window radius; in contrast, when there are a less percentage of outliers in the data, the results are relatively less sensitive to the choice the window radius.

4.4.4.2 The Influence of the Choice of Error Tolerance on RANSAC

We notice that RANSAC has an important parameter—error tolerance (i.e. error bound of inliers), the correct choice of which is crucial for the method's success in model fitting. The purpose of error tolerance in RANSAC has some similarity to the window radius h in MDPE: they both restrict immediate consideration of the data within some range; MDPE uses the densities of the data within the converged window; RANASC uses the number of the data within error tolerance. It would be interesting to investigate the sensitivity of the results to the choice of the error bounds in RANSAC. We used the same signal as used in Figure 4.6 and the results were repeated 20 times.

As Figure 4.7 show, RANSAC has little robustness to the choice of different error bound. When the error bound deviated from the true value (which is assumed as a priori knowledge), RANSAC totally break down. Moreover, the result of RANSAC is very sensitive the choice of error bound, regardless of the percentages of outliers that are included in the data: even when data included 50% outliers, RANSAC still broke down when the error bound was wrongly provided. This is different to the behaviour of MDPE.

As shown in Figure 4.6, when the data include 50% of outliers, the results of MDPE showed robustness for a large range of *h* (from1 to 15).

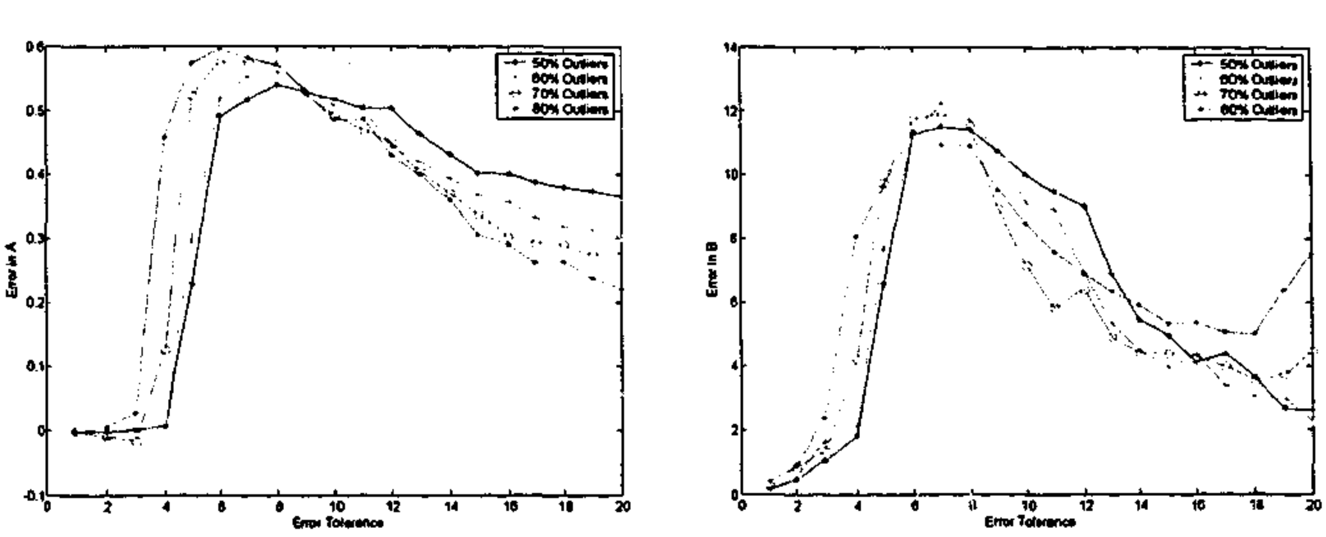

Figure 4.7: The influence of the choice of error bound on the results of RANSAC.

4.4.4.3 The Relationship between the Noise Level of Signal and the Choice of Window Radius for MDPE

Next, we will investigate the relationship between the noise level of inliers and the choice of window radius. We use the step signal with 70% outliers that is used in Figure 4.6. But we change the standard variance of the step signal from 1 to 4, with interval 1.

Figure 4.8 shows that the results are similar when the noise levels of the step signal are set from 1 to 3. However, when the standard variance of the signal is increased to 4, the tolerance range to the choice of window radius has an obvious reduction; and the fluctuation in the estimated parameters is larger for higher noise level in the signal than lower one. In fact, we have noticed that, not surprisingly, when the noise level is too large, the accuracy of all methods that are used for comparison is low. The breakdown point of these methods will decrease with the increase of noise level of signal.

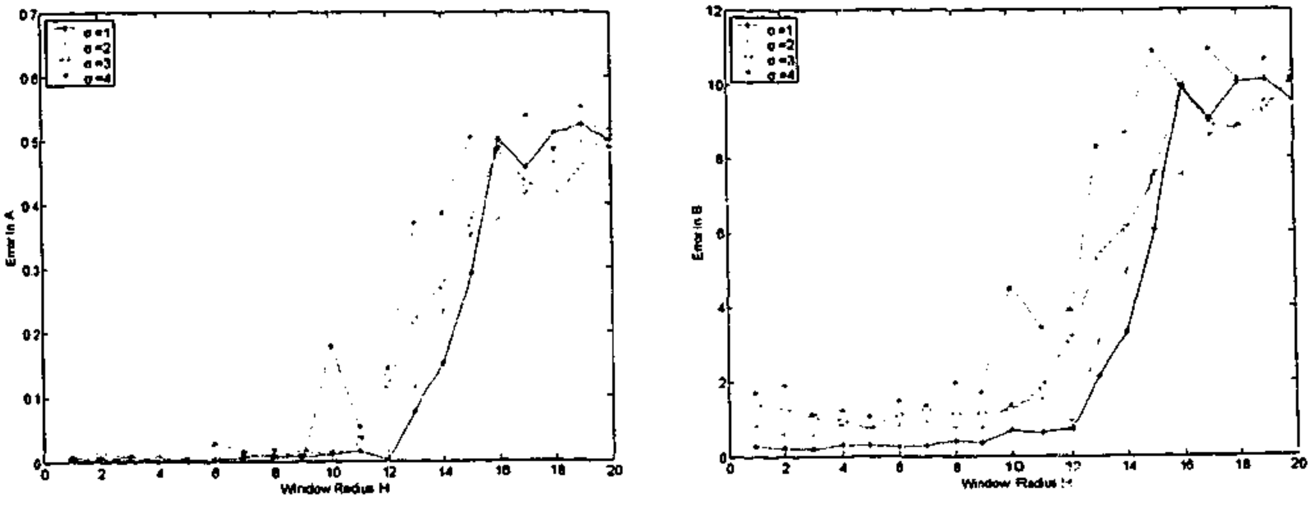

Figure 4.8: The relationship between the noise level of signal and the choice of window radius in MDPE.

4.4.5 Experiments on Real Images

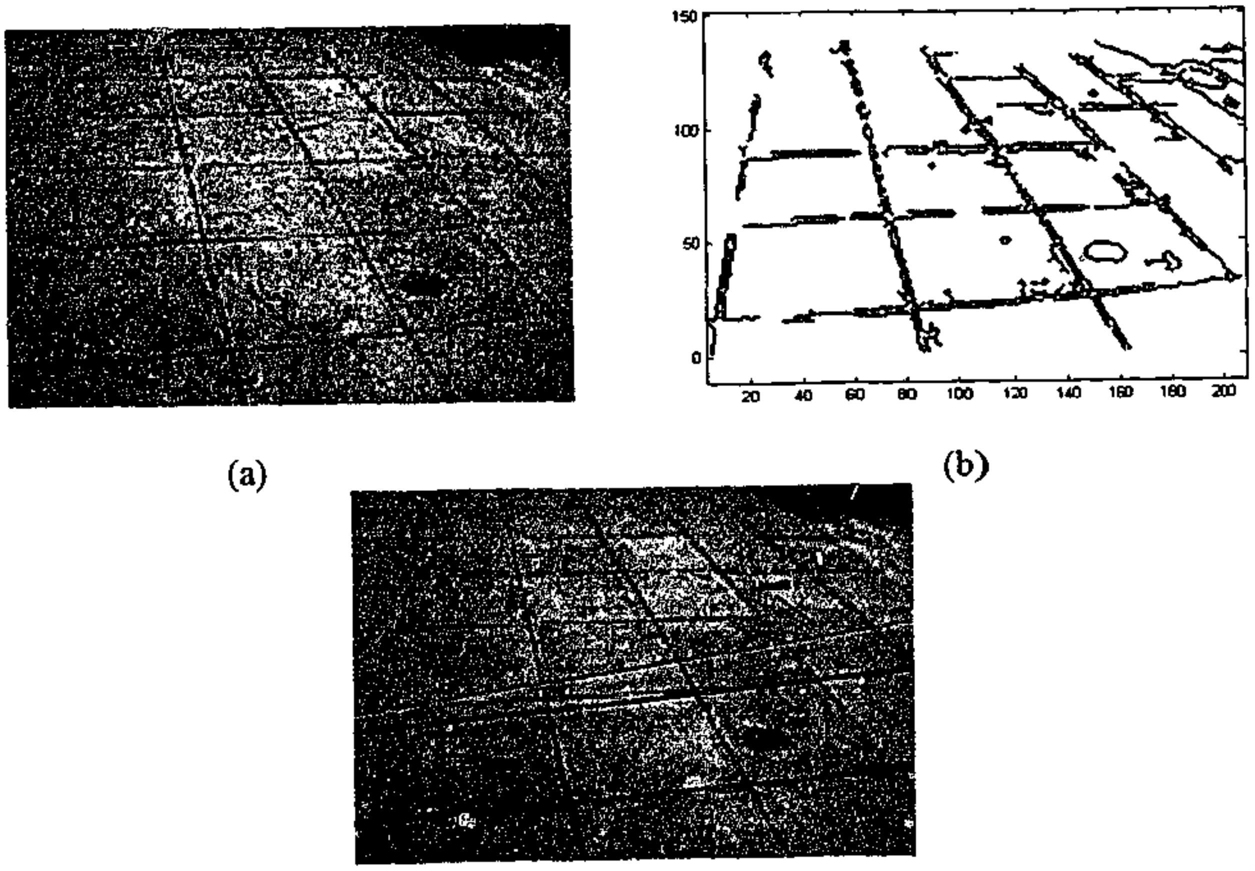

(a)

(b)

(c)

Figure 4.9: Fitting a line (a) one real pavement; (b) the edge image obtained by using Canny operator; (c) the results of line fitting obtained by the six methods.

In this experiment, we will give two real images to show the ability of MDPE to tolerate large percentage of outliers.

The first example is to fit a line in the pavement shown in Figure 4.9. The edge image was obtained by using Canny operator with threshold 0.15 and included 2213 data points (shown in Figure 4.9 (b)). There were about 85% outliers (most belonging to pseudo-outliers which had structures and belonged to other lines) in the data. Six methods (MDPE, RESC, ALKS, LMedS, RANSAC, and Hough Transform) were applied to fit a line in the pavement. As shown in Figure 4.9 (c), ALKS and LMedS failed to correctly fit a line in the pavement; while the other four methods correctly found a line.

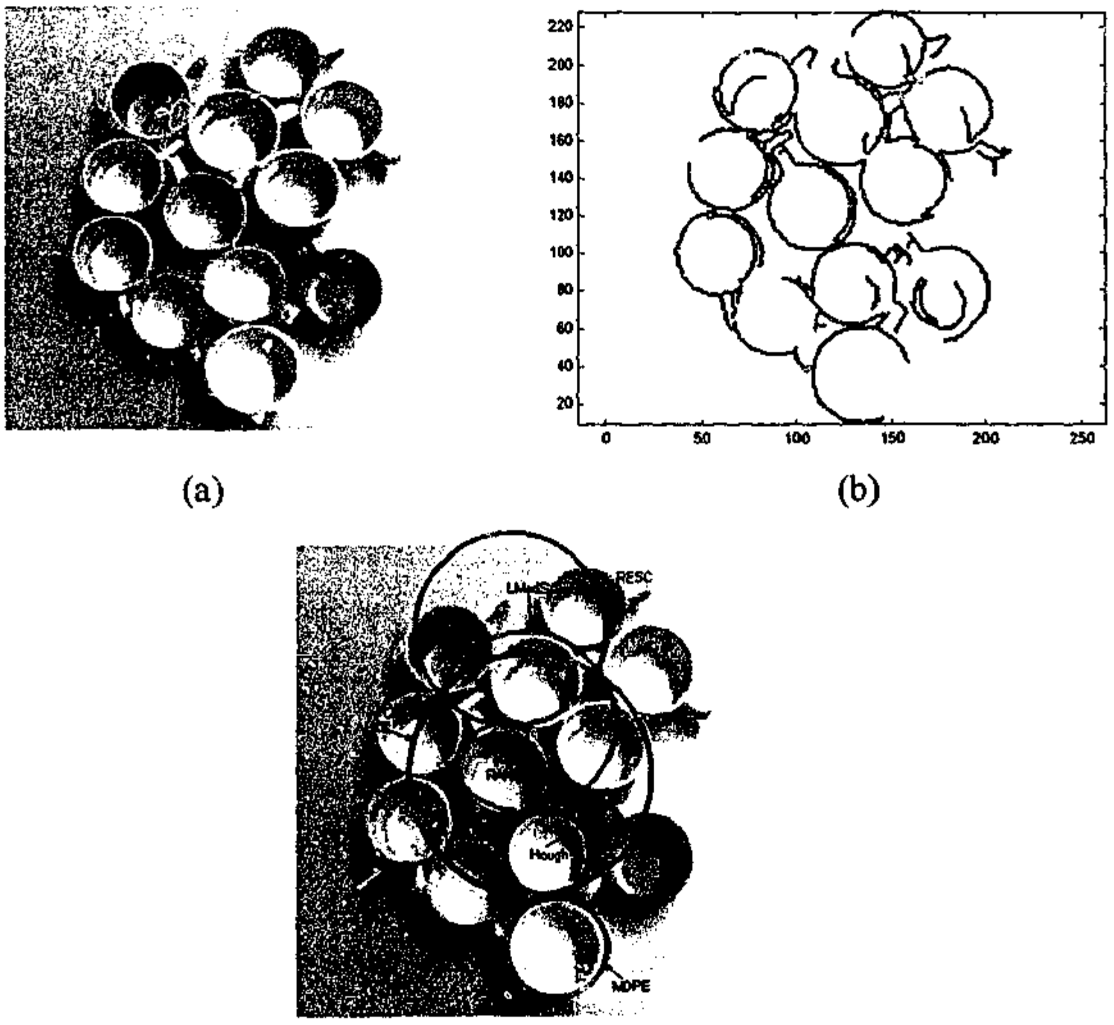

(a)

(b)

(c)

Figure 4.10: Fitting a circle edge. (a) twelve cups; (b) the edge image obtained by using Canny operator; (c) the results of circle fitting obtained by the six methods.

The second example is to fit a circle edge of one cup out of twelve cups. Among the total 1959 data points, the inliers corresponding to each cup were less than 10% of the total data points. This is another multiple-solution case: the fitted circle can correspond to any cup in the twelve cups. As shown in Figure 4.10, MDPE, RANSAC, and Hough Transform all correctly found a cup edge (the result of RANSAC was relatively lower accurate than that of MDPE), but each method found a different circle (Note: as these are not synthetic data, we do not have the correct error bound for RANSAC and bin size for Hough Transform. We empirically chose the error bound for RANSAC and bin size for Hough Transform so that the performance was optimized). However, all other three methods (RESC, ALKS, and LMedS), which are closer to MDPE in spirit, failed to fit the circle edge of a cup.

4.5 Conclusion

In this chapter, we introduce a new and highly robust estimator (MDPE). MDPE is similar to many random sampling estimators: we randomly choose several p-subsets, and we calculate the residuals for the fit determined by each p-subset. However, the crux of the method is that we apply the mean shift procedure to find the local maximum density of these residuals. Furthermore, we evaluate a density power measure involving this maximum density. The final estimated parameters are those determined by the one p-subset corresponding to the maximum density power over all of the evaluated p-subsets. Our method, and hence our definition of maximum density power, is based on the assumption that when a model is correctly fitted, its inliers in residual space should have a higher probability density, and the residual at the maximum probability density of inliers should have a low absolute value. This captures the dual notions that: the data points having lower residuals should be as many as possible, and that the residuals should be as small as possible. In that sense, our method combines the essence of two popular estimators: Least Median of Squares (low residuals) and RANSAC (maximum number of inliers). However, unlike RANSAC, MDPE scores the results by *the densities of data points* falling into the converged window *and on the size of residual* of the point corresponding to local maximum density. Contrast this also with the Least Median of Squares, which uses a single statistic (the median).

The result of our innovation is a highly robust estimator. The MDPE can tolerate more than 85% outliers, and has regularly been observed to function well with even more than 90% outliers.

We also compared our method with several traditional (RANSAC, Hough Transform and LMedS) and recently provided methods (RESC and ALKS). From our experimental analysis, it is hard to say if any method has a clear advantage. LMedS and RANSAC are the fastest among the six methods. However, the apparent breakdown point of LMedS is lower; and RANSAC needs a priori knowledge of the error bounds. The results of RANSAC are very sensitive the choice of error bounds, even when the percentage of outliers is low. The Hough Transform shows excellent performance when the data include clustered outliers. However, the space requirement and time complexity is high when the dimension of parameters is high and high accuracy is required. Among recently proposed estimators: MDPE, RESC, and ALKS; MDPE has the highest robustness to outliers. ALKS shows less robustness and instability when the percentage of outliers is small. However, it is completely data driven. Although RESC needs user to adjust some parameters, it is also a highly robust estimator. So, we can see each method has some advantages and disadvantages.

When the percentage of outliers is very large or there are many structures in the data (pseudo-outliers), one problem in carrying out *all of* the methods which use random sampling techniques is: the number of p-subsets to be sampled, m, will be huge. Fortunately, several other sampling techniques, such as guided sampling (Tordoff and Murray 2002) and GA sampling (Roth and Levine 1991; Yu, Bui et al. 1994), appeared during recent years. Investigation of sampling techniques is beyond the scope of this thesis but should be addressed in future work

In the latter part of construction of MDPE, the authors became aware of (Chen and Meer 2002). This work has some similar ideas to our work in that both methods employ kernel density estimation technique. However, their work places emphasis on the projection pursuit paradigm and on data fusion. Moreover, they use an M-estimator paradigm (see section 2 in the paper). Though there are nice theoretical links between M-estimator versions of robust estimators and kernel density estimation, as referred to in that paper, the crucial fact remains that LMedS and RANSAC type methods have a higher breakdown point (especially in higher dimension).

Thus, though their work employs kernel density estimation that is also a key to our own approach, the differences are significant:

(1) The spaces considered are different: in their methods, they considered their mode of the density estimate in the projection space along the direction of parameter vector. MDPE considers the density distribution of the mode in the residual space.

(2) The implication of the mode is different: they sought the mode that corresponds to the maximum density in the projection space, which maximizes the projection index. MDPE considers not only the density distribution of the mode, which is assumed having Gaussian-like distribution, in the residual space, but also the size of the residual corresponding to the center of the mode.

(3) They used a variable bandwidth technique that is proportional with the MAD scale estimate. However, as Chen and Meer said, MAD may be unreliable when the distribution is multi-modal, which may cause problems with the bandwidth estimation. We used a fixed bandwidth technique to estimate the density distribution. The relationship between the choice of the bandwidth and the results of MDPE is investigated in this chapter. Furthermore, we also employed the variable bandwidth technique in the modified version of MDPE (see chapter 6), in TSSE (chapter 7) and in ASSC (chapter 8).

(4) In their method, the computational complexity is greatly increased for higher dimensions because the search space is much larger with the increase of the dimension of parameter space. Thus, a more efficient search strategy is demanded for higher dimension in their method. In our method, like RESC, ALKS, LMedS, etc., one-dimensional residual space is analyzed rather than multi-dimensional parameter space. The time complexity of MDPE (and RESC, ALKS, LMedS, etc.) is related to the randomly sampling times, which will be affected by both the dimension of the parameter space and the percentage of outliers.

(5) Because their method employed a projection pursuit technique, more supporting data points ((Chen and Meer 2002), pp.249) are needed to yield reliable results. Thus, they randomly choose the data points in one bin from the upper half of the ranking (by the number of points inside each bin) followed by region growing to reach more data points. In MDPE, we randomly choose p-subsets from the whole data each time, and calculate the parameters by the p-subset and then the residuals of all data points by the obtained parameters.

At this point in time, it is difficult to compare the performance of the two approaches.

We do not prove that our method has a high breakdown point in a rigorous way. However, we must point out that, despite impressions that may be obtained by reading much of the literature, particularly that aimed more at the practitioner, more traditionally accepted techniques still have their shortcomings in similar ways. For example, though it is often cited that Least Median of Squares has a proven breakdown point of 50%, it is often overlooked that all practical implementations of Least Median of Squares are an approximate form of Least Median of Squares (and thus only have a weaker guarantee of robustness).

Indeed, the robustness of practical versions of Least Median of Squares hinges on the robustness of two components (and in two different ways): the robustness of the median residual as a measure of quality of fit and the robustness of the random sampling procedure to find at least one residual distribution whose median is not greatly affected by outliers. Our procedures, like many other procedures, share the second vulnerability as we also rely on random sampling techniques.

The first vulnerability is sometimes disregarded for practical versions of Least Median of Squares, because robustness is viewed as being guaranteed by virtue of the proof of robustness for the ideal Least Median of Squares.

However, two comments should be made in this respect. Firstly, that proof relies on assumptions regarding the outlier distribution and it can easily be shown that clustered outliers will invalidate that proof. Secondly, there is an inherent "gap" between a proof for an ideal procedure and what one can say about an approximation to that procedure. We believe that our method of scoring the fits better protects against the vulnerabilities that structure in the outliers expose. We have presented empirical evidence to support that.

Chapter 5

A Novel Model-Based Algorithm for Range Image Segmentation

5.1 Introduction

Perception of surfaces in the images has played a very important role in image understanding and three-dimensional object recognition. Because range images contain three-dimensional geometric information, the difficulties of recognizing three-dimensional objects in range images are greatly reduced.

Range images are the images that can provide 3D distance information, related to a known reference coordinate system, to surface points on the objects (in the images) in a scene. Each pixel in a range image contains 3D geometry information. Thus, the value of the pixel corresponds to a depth/range measurement (i.e., in the 'z' direction); and the coordinate of the pixel in 3D can be written as (x, y, z), where (x, y) is the image coordinate of the pixel.

Currently, range images have been widely applied in the fields such as autonomous navigation and medical diagnosis.

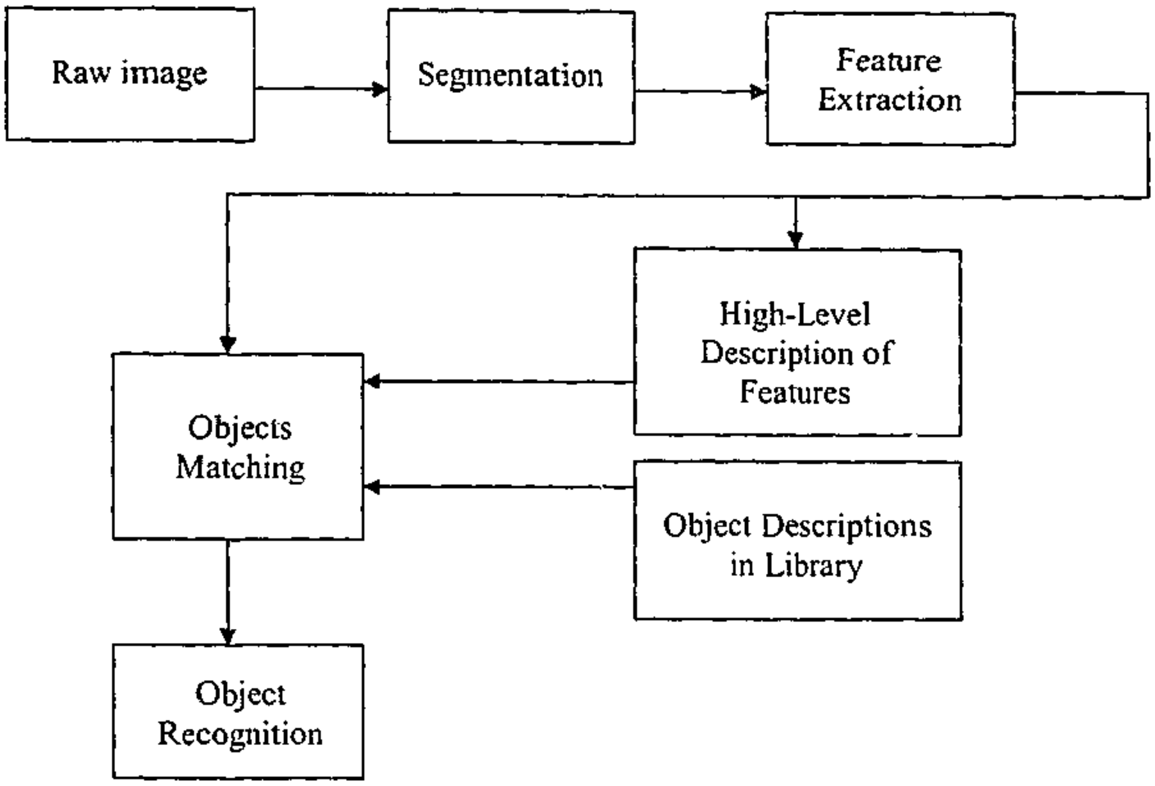

Figure 5.1: The simplified 3D recognition systems

Although various 3D objects recognition systems have been developed in recent years, there are common aims in these systems [(Suk and Bhanddarkar 1992), pp.10]:

- Robustness of the recognition process. The systems should be able to recognize objects with noise, occlusion, and ambiguous.

- Generality of representation. The systems should be able to handle different types of objects.

- Flexibility in control strategy.

- Speed and Efficiency. Speed is a critical factor. It will affect whether or not the systems can recognize the objects on real time. This factor is especially important in robot systems.

As Figure 5.1 illustrates, we can see that to segment range images is the first step in order to extract features and recognize a three dimensional object. Therefore whether or not we can correctly segment the range images is the important factor that affects the recognition of a three-dimensional object.

Image segmentation is to segment the image into some meaningful non-overlapping homogeneous regions whose union is the entire image. If we let R to be the whole image, R_1, R_2,..., R_n to be the segmented regions, then, according to Gonzalez [(Gonzalez. and Woods. 1992), pp.458], segmentation of an image can be described as follows:

1. $\bigcup_{i=1}^{n} R_i = R$
2. R_i is a connected region for all i=1,2,$\cdots$,n.
3. $R_i \bigcap R_j = \Phi$ when $i \neq j$
4. $P(R_i)$=TRUE for all i=1,2,....,n
5. $P(R_i \bigcup R_j)$=FALSE when $i \neq j$

where Φ is the null set and $P(R_i)$ is the logical judge over the points in the set R_i.

There has been general agreement on what results an image segmentation system should achieve [(Haralick and Shapiro 1992), pp.509]:

- The segmented regions of an image should be uniform and homogeneous considering some characteristic, e.g., models of the objects in the image.
- Region interiors should contain as less holes as possible.
- Boundaries of regions should be smooth and accurate.

It is very difficult to achieve all these properties at the same time by one segmentation method. To evaluate the performance of a method for image segmentation, Hoover suggested to use following five types of metrics (Hoover, Jean-Baptiste et al. 1996):

1. ***Correct detection.*** If there are more than T percent of the pixels in the segmented region correctly assigned, the region is correctly detected.

2. ***Over segmentation.*** If there are more than T percent of the pixels in a segmented region that should be assigned to other regions, the detected region is called over segmented.

3. ***Under segmentation.*** If a segmented region contains more than one surface, (which should be assigned to different regions,) the detected region is called under segmented.

4. ***Missing a region.*** If a region is not contained in any region of correct detection, over segmentation, or under segmentation in the segmented image, the region is missed.

5. ***Noisy region.*** If a region in the segmented image does not belong to any region of correct detection, over segmentation, or under segmentation, it is classified as noise.

where T is a threshold and can be specified by user according to the accuracy requirement of a system.

There are many three-dimensional image segmentation methods published in the literature. Generally speaking, these segmentation methods can be classified into two major classes:

1. Edge-based segmentation techniques (Ghosal and Mehrotra 1994; Wani and Batchelor 1994).

2. Region-based segmentation techniques or clustering techniques (Hoffman and Jain 1987; Jiang and Bunke 1994; Fitzgibbon, Eggert et al. 1995).

In edge-based segmentation methods, it is important to correctly extract the discontinuities—surface discontinuities (boundaries and jumps) and orientation discontinuities (creases and roofs), which will be used to guide the followed segmentation process. The main difficulties that edge-based segmentation techniques meet are:

- The effectiveness of these methods will be greatly reduced when range images contain noise;

- When the edge operator mask size is increased, the computational time will be greatly increased.

- When the edge pixels detected by edge operator are not continuous (especially in noisy image), it will be difficult to link these discontinuous pixels.

- Also, the reliability of the crease edge detectors makes edge-based methods questionable.

Region-based techniques have wider popularity than edge-based techniques. The essence of region growing techniques is that it segments range images based on the similarities of feature vectors corresponding to pixels in range images. The region-based techniques first estimate the feature vectors at each pixel, and then aggregate the pixels that have similar feature vectors; and at the same time, separate the pixels whose feature vectors are dissimilar, to form a segmented region.

However, region-based methods also have some problems:

- They have many parameters to control the processing of the region growing. Most of these parameters need to be predetermined.

- The choice of initial region greatly affects the performance of most region-based methods. When the seeds are placed on a boundary or on a noise corrupted part of the image, the results will break down.

- The region boundaries are often distorted because of the noise in the range images.

- In clustering-based methods, to adaptively estimate the actual number of clusters in the range image is difficult.

Another way of classifying a segmentation approach is that which uses the notion of model-driven (top-down). The model-driven methods are appealing because it has been proved that these methods have similarities to the human cognitive process (Neisser 1967;

Gregory 1970). The model-based methods can directly extract the required primitives from the unprocessed raw range images. Model-based methods, in particular, robust model based approaches, have been attracting more and more attention (Roth and Levine 1990; Yu, Bui et al. 1994; Stewart 1995; Miller and Stewart 1996; Lee, Meer et al. 1998). These methods are very robust to noisy or occluded data.

Next, we will review several state-of-the-art methods of segmentation in section5.2. Then we modify the MDPE to produce a quicker version, called QMDPE (Quick-MDPE), and evaluate its achievements in section 5.3. In section 5.4, we present a model-based method based on the QMDPE for segmentation of rage images. The performance of the proposed method is compared to that of several other state-of-the-art range image segmentation methods in section 5.5. We conclude in section 5.6.

5.2 A Review of Several State-of-the-Art Methods for Range Image Segmentation

In this section, four methods (UB, UE, USF, WSU) will be reviewed. The USF (Hoover, Jean-Baptiste et al. 1996) and UE (Fitzgibbon, Eggert et al. 1995) algorithms segment range images by iteratively growing regions from seed regions. However, the WSU (Hoffman and Jain 1987; Flynn and Jain 1991) algorithm employs a clustering technique in its segmentation process. The UB (Jiang and Bunke 1994) algorithm is in region growing framework, but it is based on straight-line segmentation in scan lines. Next the four methods will be reviewed in detail.

5.2.1 The USF Range Segmentation Algorithm

The USF algorithm (Hoover, Jean-Baptiste et al. 1996) can be described as follows:

1. Compute the normal of each range pixel.

   First, a growing operation is carried out in a n-by-n window from the pixel of interest. The distances between the pixels (to grow) and their four-connected pixels must be less than a threshold; otherwise, the pixels will be ignored. The normal is found by either an Eigen method (Duda and Hart 1973; Goldgof, Huang et al. 1989) or a method solving a set of nine plane equations.

2. Choose the seed points.

   The pixel with smallest interior measure, corresponding to the residual error of the plane equation fit to the entire n-by-n window, is chosen as a seed point.

3. Using the seed point to grow the region.

   Four criteria for pixels joining the region must be satisfied:

   (a) The point is connected to the region grown so far.

   (b) Angle between normal of pixel and that of region grown so far is less than a threshold T_1.

   (c) Perpendicular distance between pixel and plane grown so far is within a threshold T_2.

   (d) Distance of pixel and four-connected neighbor already in the grown region is less than a threshold T_3.

The region is recursively grown until no pixel left to join that region. Then a new region begins to grown from the next seed point available. If a region's final size is less than a threshold T_4, the region and its pixels are ignored and will be dealt with during the post-process step.

5.2.2 The WSU Range Segmentation Algorithm

The WSU algorithm is first presented by Hoffman and Jain (Hoffman and Jain 1987). Flynn and Jain improved the WSU algorithm and applied it to 3D object recognition (Flynn and Jain 1991). WSU can be used not only for planar surfaces but also for quadric surfaces. The details of the WSU algorithm can be described as follows:

1 Labelling the jump edge pixels. The distances (d_j, j=1,2,...,8) in z between a range pixel and its eight neighbouring pixels are measured. If d_j for all eight points is greater than a predetermined threshold, the pixel is labelled as a jump edge pixel.

2 Estimating the surface normal of each range pixel. The surface normal of each range pixel is estimated using k-by-k neighbouring points (but not including jump edge pixels). A principal component technique (Flynn and Jain 1988) is employed to estimate the surface normal because this technique can accommodate data contaminated with noise.

3 Sampling on a regular grid is performed to yield a data set less than 1000 in size. The normal information and position information of each sampled data point is used to form six vectors. Then a clustering algorithm (Jain and Dubes 1988) is employed in the six dimensional space (corresponding to the six vectors).

4 Assigning the range pixels to clusters. Each range pixel is assigned to the corresponding closest cluster center. The connected component algorithm is used to avoid assigning the same labels to regions that are not connected.

5 An edge-based merge step is performed. This step will merge the regions where the average angle between the surface normals of range pixels on one side of the edge and their neighbours on the other side is less than a predetermined threshold.

6 A principal component procedure is performed to distinguish planar regions from non-planar regions. The non-planar regions will be ignored in further processing.

7 If regions have similar parameters and are adjacent, they will be merged.

8 Unlabeled pixels on each segment are merged into the region.

9 Step 6, 7 and 8 are repeated until the result has no change.

5.2.3 The UB Range Segmentation Algorithm

The UB segmentation method was developed based on the observation that if a line is used to scan the image, the points that belong to a planar surface will form a straight line segment. On the other hand, if the points are on the same straight line segment, they will surely belong to the same planar surface. Unlike other region growing algorithms which use seeds to grow the regions, the UB segmenter uses straight line segments as growing primitives. This greatly reduces the data dimension to be dealt with in the growing process and makes the algorithm very fast.

The UB algorithm can be described as follows (Jiang and Bunke 1994):

1. A median filter is employed as a preprocessing step to reduce the noise level of an image.

2. Scan the image by scan line and divide the data on each scan line into straight line segments.

3. Using a link-based data structure, find the neighborhood of each line segment.

4. Select the best seed region by the following process. First choose a small number of neighboring line segments (three in (Jiang and Bunke 1994)) in a seed region. If any line segment is shorter than a predetermined threshold, this candidate region is discarded. The optimal seed region is one with the smallest error among the errors computed by a least square plane fitting for each candidature.

5. The growing process is performed. In the UB algorithm, the initial guess is a set of line segments. A line segment is added to the region if the perpendicular distance between its two end points and the plane of the region is within a threshold. This process is continued until no more line segments can be added to this region.

6. The process of seed region finding (step 4) and region growing (step 5) is iterated until no seed region can be found.

7. A post-processing step is applied to yield clean edges between regions.

5.2.4 The UE Range Segmentation Algorithm

The UE algorithm (Fitzgibbon, Eggert et al. 1995) is similar to the USF algorithm. They both belong to the class of region growing algorithms. The UE algorithm contains the following main steps:

1. Normal Calculation.

   A 5-by-5 window is used to estimate the normal of each range pixel. A normal and a depth discontinuity are detected using a predetermined normal threshold and depth threshold.

2. A discontinuity preserving smoothing is performed with multiple passes for greater smoothing.

3. H-K based segmentation for initialization.

   The Gaussian (H) and mean (K) curvature of each pixel is estimated. Using the combined signs of the pair (H, K), one can judge the surface type of each range pixel. Each pixel and its eight-connected pixels of similar labeling are grouped to form initial regions. Then dilation and erosion are performed to fill small unknown areas and remove small regions.

4. Region growing.

   A least squares surface fitting procedure is performed in the initial regions obtained above. Then each region is in turn grown. To join the region, a point needs satisfy the following requirements:

   (a) The point is eight-connected to the region grown so far.

   (b) The perpendicular distance between the pixel and plane grown so far is within a threshold.

   (c) The angle between normal of the pixel and that of region grown so far is less than a threshold.

   (d) The point is closer to current surface than any other possible surfaces it may be assigned to.

   (e) The normal of the pixel is in better agreement with the current surface than any other possible surface it may be assigned to.

   After expansion, the surface is refitted using these new points. Then a contraction of the region boundary is performed.

5. Region boundary refinement.

A pixel is added to a region during expansion if:

(a) The point is eight-connected to the region grown so far.

(b) The point-to-plane distance is less than a threshold.

(c) The point is on the one side of a decision surface.

5.2.5 Towards to Model-Based Range Image Segmentation Method

Although the edge-based methods and region-based methods are popular in the computer vision community, it is difficult for these methods to directly extract specified primitives. The model-driven (top-down) methods are appealing because they can directly extract the required primitives from the unprocessed raw range images. The features that are used in model-driven methods are primitives. So the matching takes place very early in the recognition process. In the model-based methods, primitive geometric features are matched instead of similar features that are used in region-based methods. Then matches are checked for local consistency by using some geometric constraints, e.g. distance, normal, etc. Because of the introduction of robust statistics into some model-based methods, the model-based segmentation methods are very robust to noisy or occluded data.

Next, we will present an efficient model-based method for range image segmentation.

5.3 A Quick Version of the MDPE—QMDPE

As shown in chapter 4, MDPE has a very high robustness and can tolerate a large percentage of outliers including gross noise and pseudo-outliers. However, the time needed to calculate the densities $\hat{f}(X_i)$ of all data points within the converged window W_c is large when the number of the data points is very large. It takes $O(n)$ time to calculate the density $\hat{f}(X_i)$ at one point X_i. If there are nw data points within the converged window W_c, the time complexity of computing the probability density power function ψ_{DP} is $O(n*nw)$. In range image processing, *nw* may be tens of thousands to hundreds of thousands in size. For such a huge number of range data points, MDPE is not computationally efficient. A quicker version of MDPE with a similar higher breakdown point to outliers is needed for range image segmentation.

In this section, we will modify our MDPE to produce a quicker version, called QMDPE.

5.3.1 QMDPE

MDPE measures the entire probability densities of all data points within the converged mean shift window. However, QMDPE uses only the density of the point in the center of the converged window. QMDPE, like MDPE, also assumes inliers occupy a relative majority, with Gaussian-like distribution, of the data points. Thus, when a model to fit is correctly estimated, the center of the converged window (*Xc*) in residual space should be as close to zero as possible; and the probability density $\hat{f}(X_c)$ of the point at *Xc* should be as high as possible. Thus we define the probability density power function, which uses only one point's probability density, as follows:

$$\psi_{DP} = \frac{\left(\hat{f}(Xc)\right)^{\alpha}}{\exp(|Xc|)} \qquad (5.1)$$

where α is a factor that adjusts the relative influence of the probability density to the residual of the point corresponding to the center of the converged window. It is empirically determined to get the best performance. We adjusted the value of α by comparing the results in both synthetic data and real image data used in section 4.4, and set it to be 2.0 for optimal achievement (we note that the empirically best value of α in equation (5.1) for QMDPE is different to that in equation (4.7) for MDPE, where α is set to 1.0).

Because only the probability density on the point corresponding to the center of the converged window needs to be calculated, the time cost to compute the probability density power in QMDPE is greatly reduced when the number of data is very large (for example, range image data).

5.3.2 The Breakdown Plot of QMDPE

Now, we compare the tolerance of QMDPE (to outliers) with that of other estimators (including LMedS, ALKS, RESC, RANSAC, Hough Transform, and MDPE) using the data in section 4.4.3 (the results of those estimators are shown in Figure 4.5). From Figure 5.2 (the experiments were repeated 20 times and results were averaged), we can see that the QMDPE began to breakdown when outliers involved more than 92% of the data. However, even when outliers occupied more than 92% of the data, QMDPE still acted reasonably reliably (about 70%, loosely speaking, correct). The percentage of outliers at which the QMDPE began to break down is higher than that of LMedS (51%), ALKS (80%), RESC (89%), and Hough Transform (89%) methods; QMDPE and the RANSAC have similar performance. However, RANSAC needs a priori knowledge about the error bound of inliers; QMDPE needs no prior knowledge about the error bounds. Although its robustness to outliers is a little lower than that of MDPE, the QMDPE algorithm is faster than MDPE because it saves time in calculating the probability density power for each randomly sampled *p*-subset.

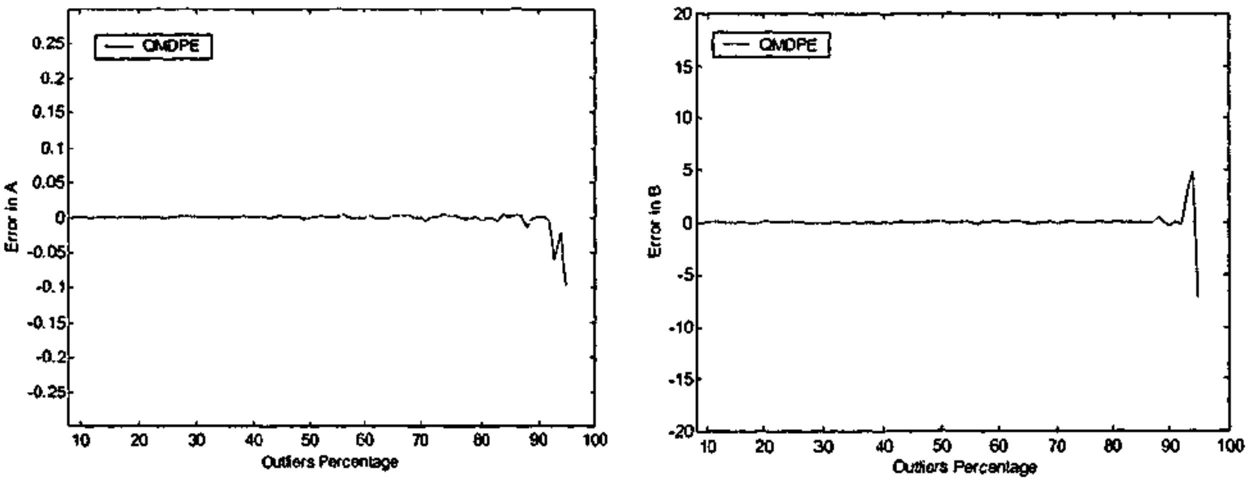

(a)

(b)

Figure 5.2: Breakdown plot for the QMDPE method: (a) error in A vs. outlier percentage; (b) error in B vs. outlier percentage.

5.3.3 The Time Complexity of QMDPE

	A Step	Three Steps	A Roof	Six Lines	Five Circles
QMDPE	5.8	12.1	16.6	23.0	61.4

Table 5.1: The time complexity of QMDPE (in seconds).

Compared with Table 4.1, Table 5.1 shows the time complexity of QMDPE. We can see that QMDPE is slower than LMedS and RANSAC. However, the speed of QMDPE is faster than that of MDPE, RESC, and ALKS. QMDPE is about 20% faster than MDPE and almost 100% faster than RESC in line fitting. Of course, the time complexity of these methods may change, to some extent, for different types of signal (for example, RESC is slower than ALKS in the analysis of the four line signal but faster than ALKS in five circle signal; QMDPE is much faster than MDPE in our experiments with range image data). It is not practical to compare the time complexity of all methods for all types of signals. The above will give the reader some rough idea of the time complexity of each method.

5.3.4 The Influence of Window Radius on the Results of QMDPE

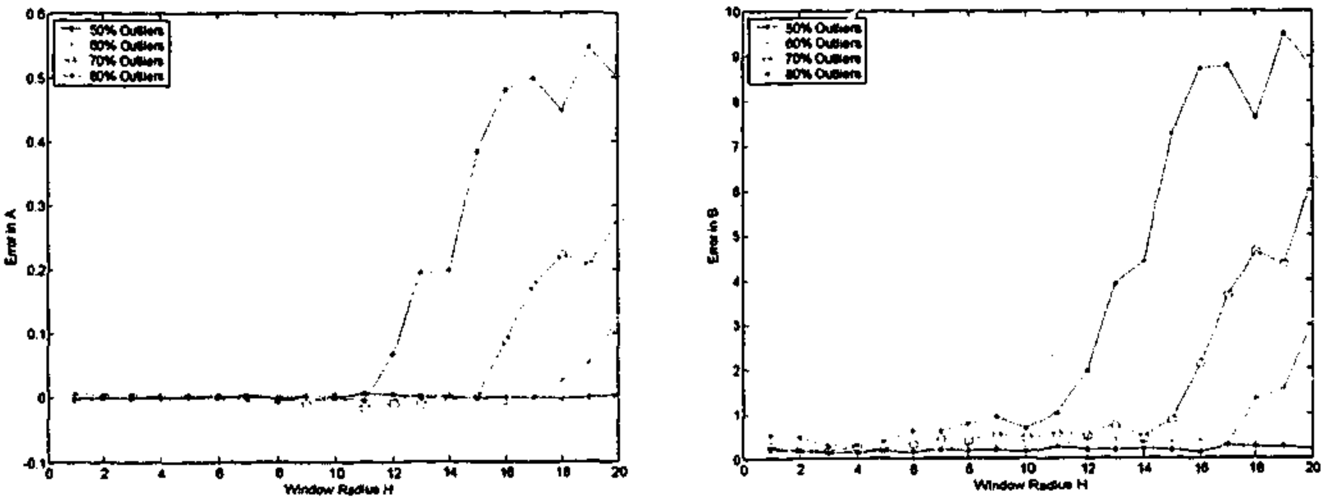

Figure 5.3: The influence of window radius on the results of the QMDPE.

Now, we will investigate the influence of window radius on the results of the QMDPE. From Figure 5.3, we can see that, although the percentage of outliers also has an affect on the choice of window radius (the results are relatively more sensitive to the choice of window radius when the outliers are greater in number), the results of QMDPE show less sensitivity to the choice of window radius *h* than the results of MDPE (see Figure 4.6). The reason is: the window radius *h* plays two roles in MDPE. First, *h* is related to the density estimation; Second, the density power in MDPE will count all points' densities within the converged window (where *h* is the radius of the window). However, because we use only one point to estimate the density power, *h* is only used for density estimation in QMDPE.

5.4 Applying QMDPE to Range Image Segmentation

A good estimator is generally only one component of a complete scheme to successfully tackle meaningful computer vision tasks. Segmentation requires more than a simple-minded application of an estimator, no matter how good that estimator is. Several difficulties faced with applying a statistical estimator to this task must be considered in designing a method for segmentation.

5.4.1 From Estimator to Segmenter

To test the utility of QMDPE, we apply it to range image segmentation. The range images were generated by using an ABW structured light scanner and all ABW range images have 512x512 pixels. These ABW range images can be obtained from the USF database (available at http://marathon.csee.usf.edu/seg-comp/SegComp.html).

However, segmentation is a (surprisingly) complex task and an estimator cannot simply be directly applied without considering the following factors:

1. The computational cost.

   QMDPE is an improved (in speed) MDPE. Its computational cost is much less than MDPE's computational cost. Even so, for a range image with a large number of data points (262,144 data points in our case), employing a hierarchical structure in our algorithm greatly optimizes the computational speed.

2. Handling of intersections of surfaces.

When two surfaces intersect, points around the intersection line may possibly be assigned to either surface (see Figure 5.5). In fact, the intersection line is on both surfaces and the data points are inliers to both surfaces. Additional information (such as the normal to the surface at each pixel) should be used to handle data near the intersection line.

3. Handling virtual intersection.

   It is popular in model-based methods to directly estimate parameters of a primitive; and classify data points belonging to the primitive according to the estimated parameters. The data points on the surface will then be masked out and not be processed in later steps. However, sometimes two surfaces do not actually intersect, but the extension of one surface is intersected by the other surface. In this case, the connected component algorithm (Lumia, Shapiro et al. 1983) should be employed.

4. Removal of the isolated outliers.

   When all surfaces are estimated, some isolated outliers, due to the noise introduced by range image camera, may remain. At this stage, a post processing procedure should be made to eliminate the isolated outliers.

The originators of other novel estimators (e.g. ALKS, RESC, MUSE, MINPRAN) have also applied their estimators to range image segmentation, but they have not generally tackled all of the above issues. Hence, even those interested in applying ALKS/RESC, or any other estimator, to range image segmentation may find several of the components of our complete implementation independently useful.

5.4.2 A New and Efficient Model-Based Algorithm for Range Image Segmentation

Shadow pixels may occur in an ABW range image. These points cannot give range information and thus will not be processed.

There are four levels in the hierarchy we used in our algorithm. The bottom level of the hierarchy contains 64x64 pixels that are obtained by using regular sampling on the original image. The top level (i=4) of the hierarchy is the original image (512x512). The level i=2 and the level i=3 of the hierarchy have 128x128 and 256x256 pixels respectively. We begin with bottom of the hierarchy (i=1), i.e., the 64x64 regular sampled range image.

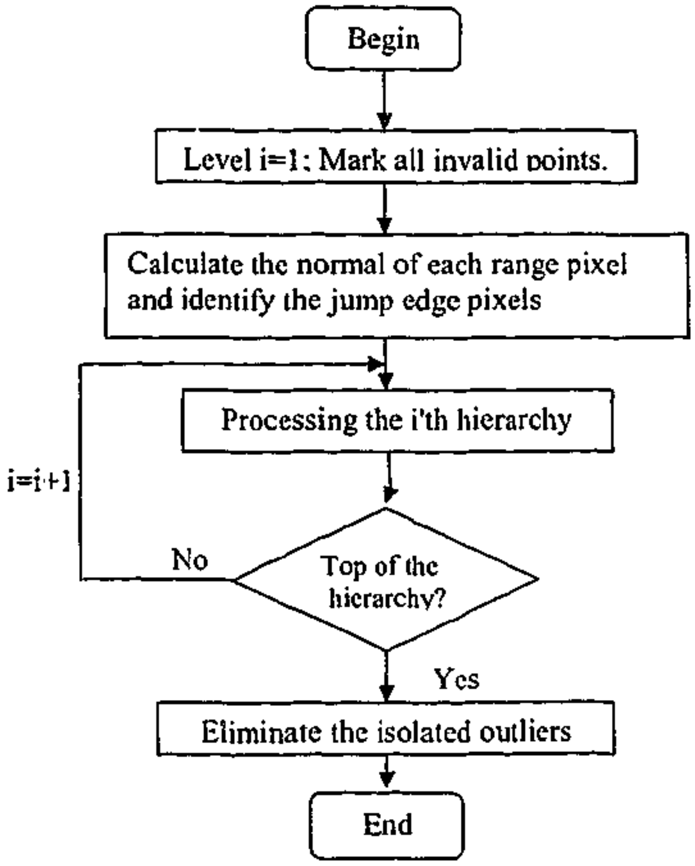
Begin
Level i=1: Mark all invalid points.
Calculate the normal of each range pixel and identify the jump edge pixels
Processing the i'th hierarchy
i=i+1
No
Top of the hierarchy?
Yes
Eliminate the isolated outliers
End

Figure 5.4: The structure of the proposed range image segmentation algorithm

For unlabelled points in the top hierarchy, we use the connected component algorithm to get the maximum connected component (leaving out the invalid points). Thus, the data for current hierarchical level can be obtained by regularly sampling on the maximum connected component. For the connected points whose number is below a threshold, we marked them as noise. The structure of the proposed algorithm is shown in Figure 5.4.

The detailed steps of the proposed method can be described as follows:

1. Mark all invalid points. For example, shadow pixels may occur in a structured light scanner (e.g. ABW) image, these points will not be processed in the next steps.

2. Calculate the normal of each range pixel and identify the jump edge pixels.

Although the QMDPE algorithm was designed to fit the data despite noise and multiple structures, it requires that the data points of the model should occupy a relative majority of the whole data. This can be satisfied in a lot of range images (and the presented algorithm can deal with the whole image as raw image). However, for some very complicated range images (those with many objects and surfaces), this requirement is not always satisfied. Using the information provided by the jump edge will help to coarsely segment the range image to some small regions (each may include several planes).

3. Employ a hierarchal sampling technique.

   The proposed algorithm employs a hierarchal structure based on the fact that when an image is regularly sampled, the main details will remain while some minor details may be lost.

4. Apply the QMDPE to obtain the parameters of the estimated primitive.

   For the current level in the hierarchy, we use the whole sampled image as the data to deal with. We apply the QMDPE algorithm to that data which yields the plane parameters. The inliers corresponding to the estimated plane parameters are then identified by employing an auxiliary scale estimator. (For historical reason, we employed a revised Median scale estimator: $s = \alpha(1+\frac{5}{n-3})\sqrt{\underset{i}{med}(r_i^2)} + \beta$, where α and β were experimentally set as 1.8 and 0.2 for optimum. However, an improved robust scale estimator TSSE – see chapter 7, can be used to estimate the scale of inliers).

   At this stage, it is difficult to tell which plane, of any two intersecting planes, the data that are on or near the intersection line belong to. Note: this case is not considered in the popular range image segmentation methods employing robust estimators such as RESC, MUSE and ALKS. We handle this case in the next step.

5. Using normal information.

   When the angle between the normal of the data point that has been classified as an inlier, and the estimated plane normal, is less than a threshold value (T-angle, 40 degree in our case), the data point is accepted for step 5. Otherwise, the data point is rejected and is classified as a "left-over point" for further processing. As shown in Figure 5.5, when we did not consider the normal information, the range image was over segmented because of the intersection of two planes (pointed out by the arrow in Figure 5.5 (b) and (c)). As comparison, we obtain the right result when we considered the normal information (see Figure 5.5 (d) and (e)).

6. Using the connected component algorithm to extract the maximum connected component and label them.

   The remaining unlabeled inliers will be used in the next loop for further processing.

7. Select the connected component for processing in the next loop.

   For all unlabeled data points, we use jump edge information and connected component analysis to extract the component with the maximum number of the connected data points for the next loop. When the number of the data points belonging to the maximum connected component is larger than a threshold (T-cc), we repeat step 4-6. Otherwise, we stop this hierarchy and go to the *next* higher level in the hierarchy until the top of the hierarchy (512-by-512).

8. Finally, we eliminate the isolated outliers and assign them to the majority of their eight-connected neighbors.

Compared with current popular methods (region-based and edge-based methods), our proposed method is a model-based top-down technique. Our method directly extracts the required primitives from the raw images, and it deals with the whole image as raw image. Our method is very robust to noisy or occluded data due to the adoption of robust estimator QMDPE. Because we adopt hierarchical technique, this makes the proposed method computationally efficient and makes it possible to deal with large size range images with only small extra computational cost.

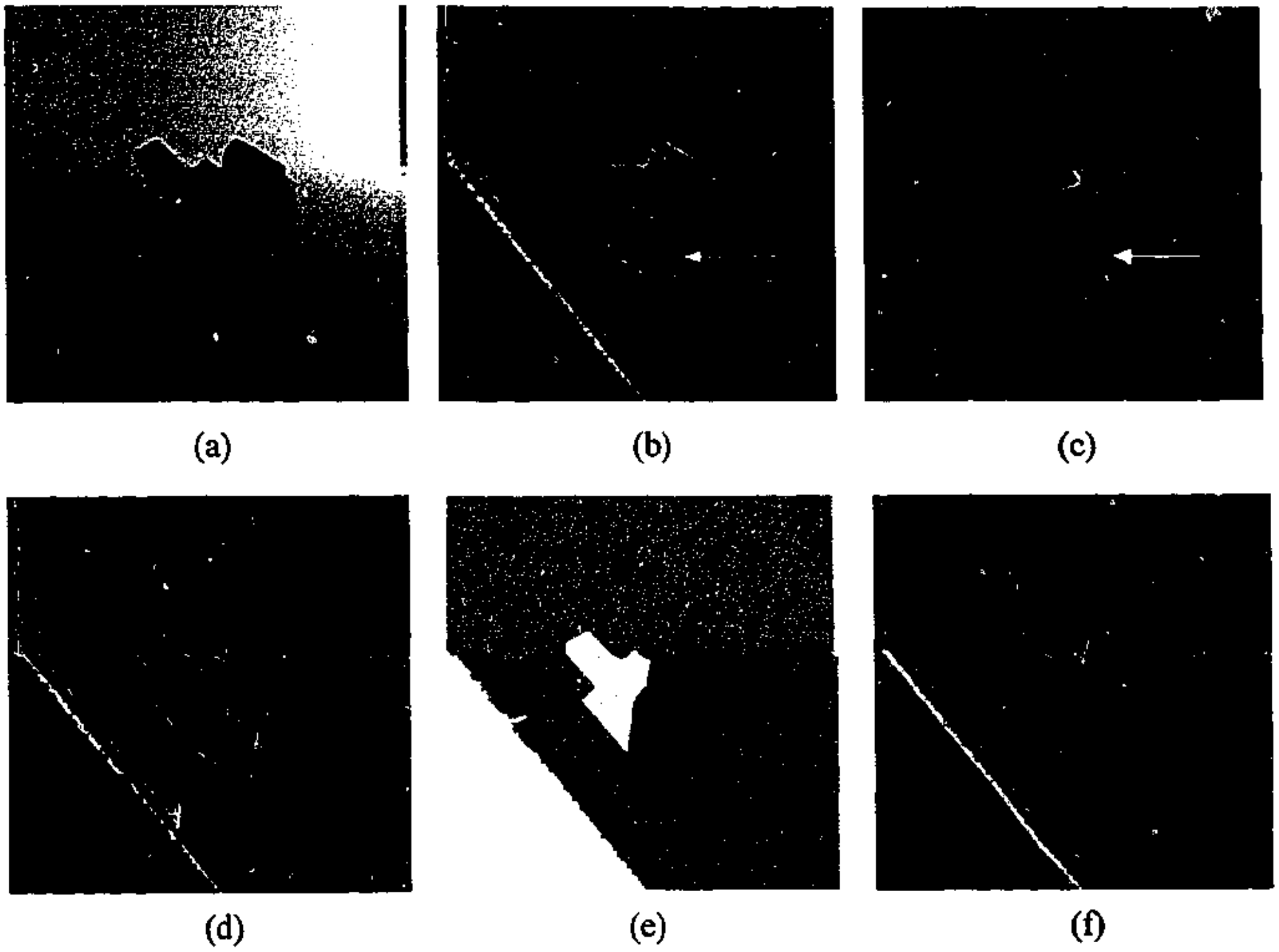

Figure 5.5: A comparison of using normal information or not using normal information. (a) Range image (ABW test.10 from the USF database); (b) The segmentation result without using normal information; (c) The points near or on the intersection of two planes may be classified to both planes without considering normal information; (d, e) The result using normal information; (f) The ground truth result.

5.5 Experiments in Range Image Segmentation

In this section, we will show how to use our method to segment range images. Since one main advantage of our method, over the traditional methods, is that it can resist the influence of noise, we put some randomly distributed noise into the range images (Note, as the whole image is dealt with at the beginning of the segmentation, there is also a high percentage of pseudo-outliers existing in the data).

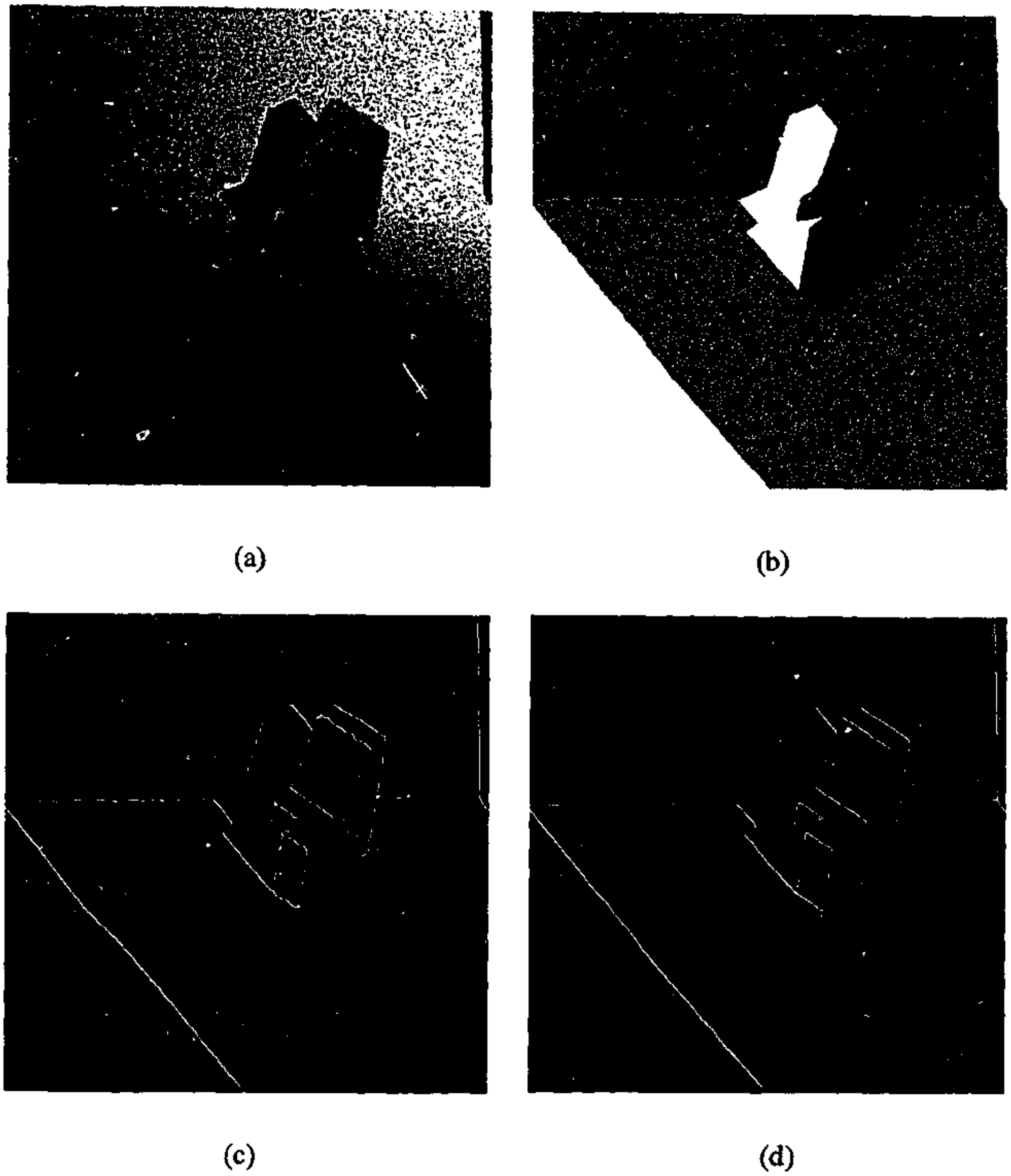

Figure 5.6: Segmentation of ABW range image (test.28) from the USF database. (a) Range image with 15% random noise; (b) Segmentation result by the proposed method; (c) The edge image of the result by the proposed method; (d) The edge image of the ground truth result.

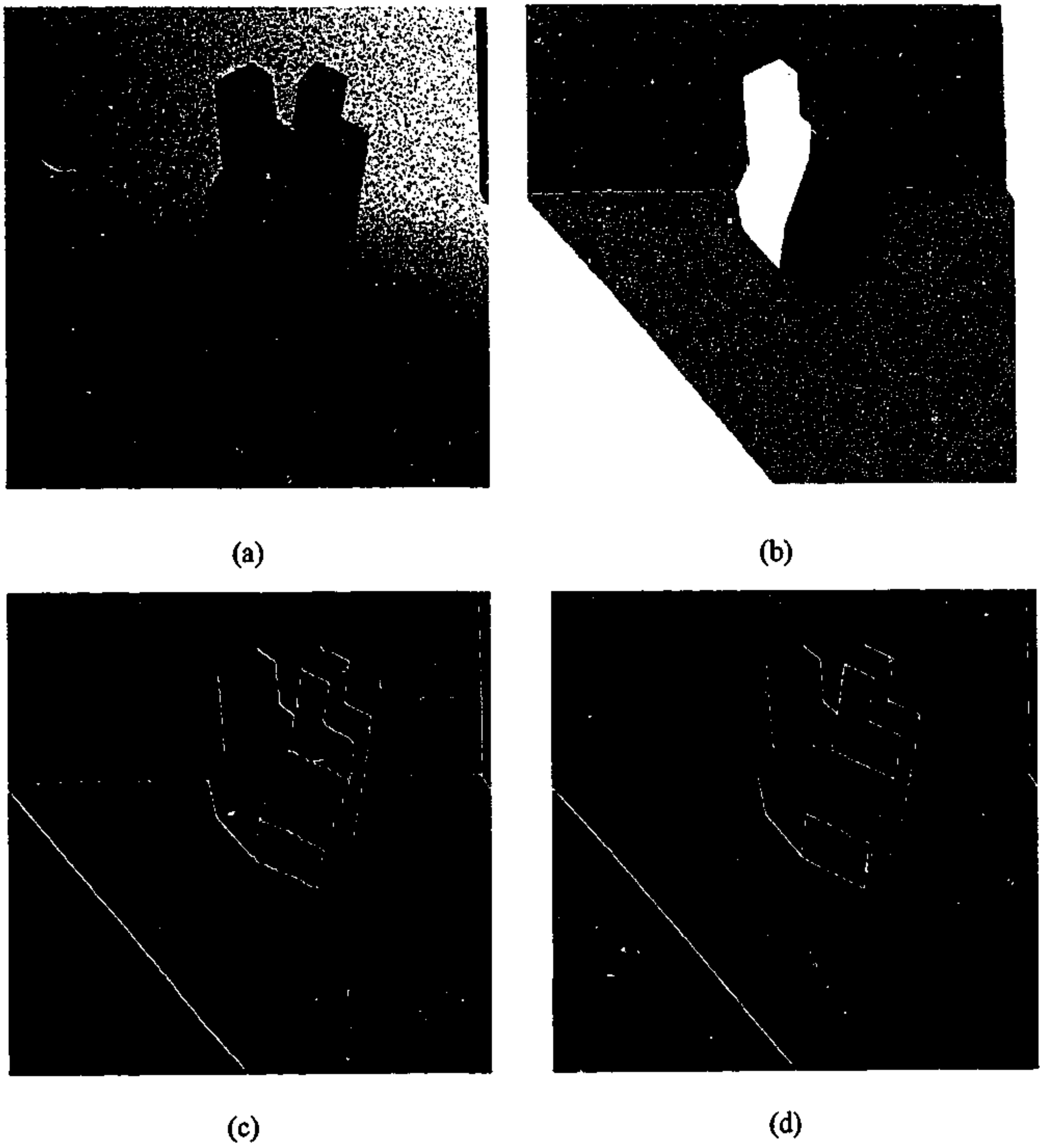

(a)

(b)

(c)

(d)

Figure 5.7: Segmentation of ABW range image (test.27) from the USF database. (a) Range image with 15% random noise; (b) Segmentation result by the proposed method; (c) The edge image of the result by the proposed method; (d) The edge image of the ground truth result.

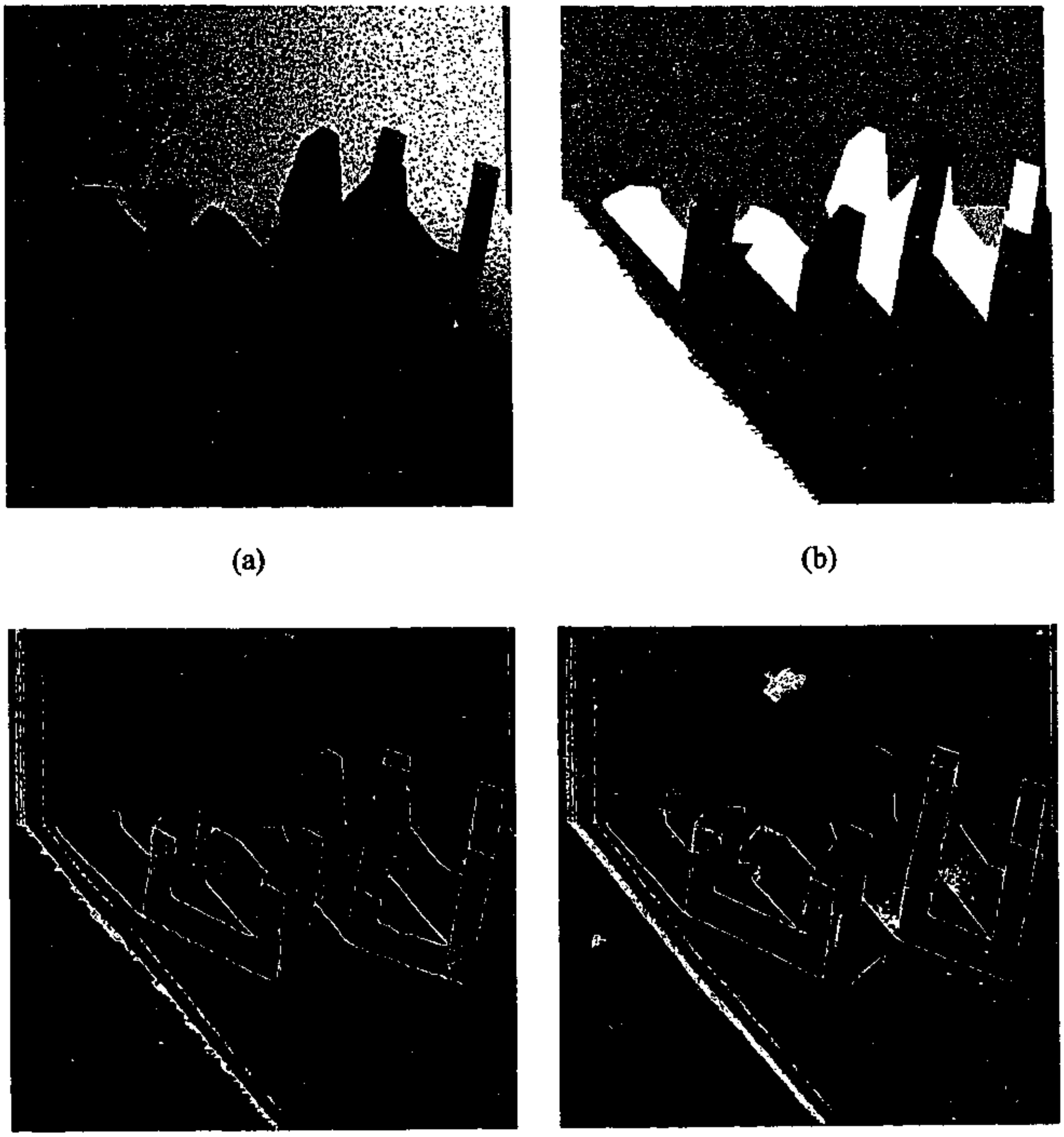

(a) (b)

(c) (d)

Figure 5.8: Segmentation of ABW range image (test.13) from the USF database. (a) Range image with 15% random noise; (b) Segmentation result by the proposed method; (c) The edge image of the result by the proposed method; (d) The edge image of the ground truth result.

In Figure 5.6, Figure 5.7, and Figure 5.8 (a), we add 15% randomly distributed noise, i.e. 39322 noisy points were added to each range image taken from the USF ABW range image database (test28, test27, and test13). As shown Figure 5.6, Figure 5.7, and Figure 5.8 (b) and (c), our method can resist the influence of large number of noise corrupted points. The main surfaces were recovered by our proposed method. Only a slight distortion appeared on some boundaries of neighbouring surfaces. In fact, the accuracy of the range data, and the accuracy of normal at each range point, will have an effect on the distortion.

It is important to compare the results of our method with the results of other methods. We also compare our results with those of the three state-of-art range image segmenters (i.e. the USF, WSU and UB, see (Hoover, Jean-Baptiste et al. 1996)).

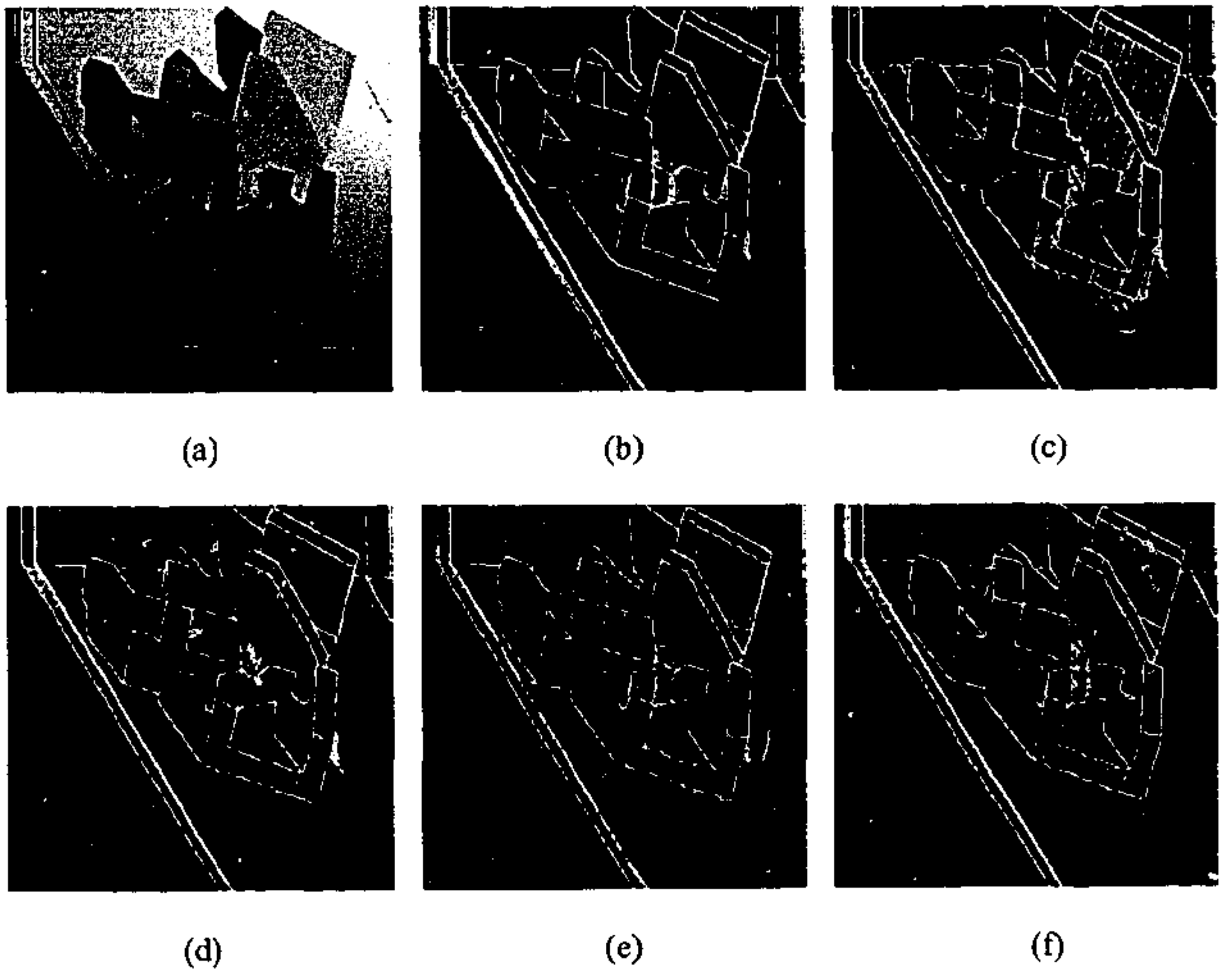

Figure 5.9: Comparison of the segmentation results for ABW range image (test.1) from the USF database. (a) Range image; (b) The result of ground truth; (c) The result by the USF; (d) The result by the WSU; (e) The result by the UB; (f) The result by the proposed method.

Consider Figure 5.9 and Figure 5.10: (a) is the range image and (b) is the edge map of the manually made ground truth segmentation result. The results obtained by all methods should be compared with the results of the ground truth. (c) is the results obtained by the USF. From Figure 5.9 (c) and Figure 5.10 (c), we can see the USF's results contained many noisy points. In both Figure 5.9 (d) and Figure 5.10 (d), the WSU segmenter missed surfaces. The WSU segmenter also under segmented the surface in Figure 5.10 (d). From Figure 5.9 (e) and Figure 5.10 (e), we can see the boundaries on the junction of surfaces were distorted relatively seriously. Our results are shown in Figure 5.9 (f) and Figure 5.10 (f). Compared with other methods, the proposed method performed best. Our method directly extracted the planar primitives. In the proposed method, the parameters requiring tuning are less than other traditional methods.

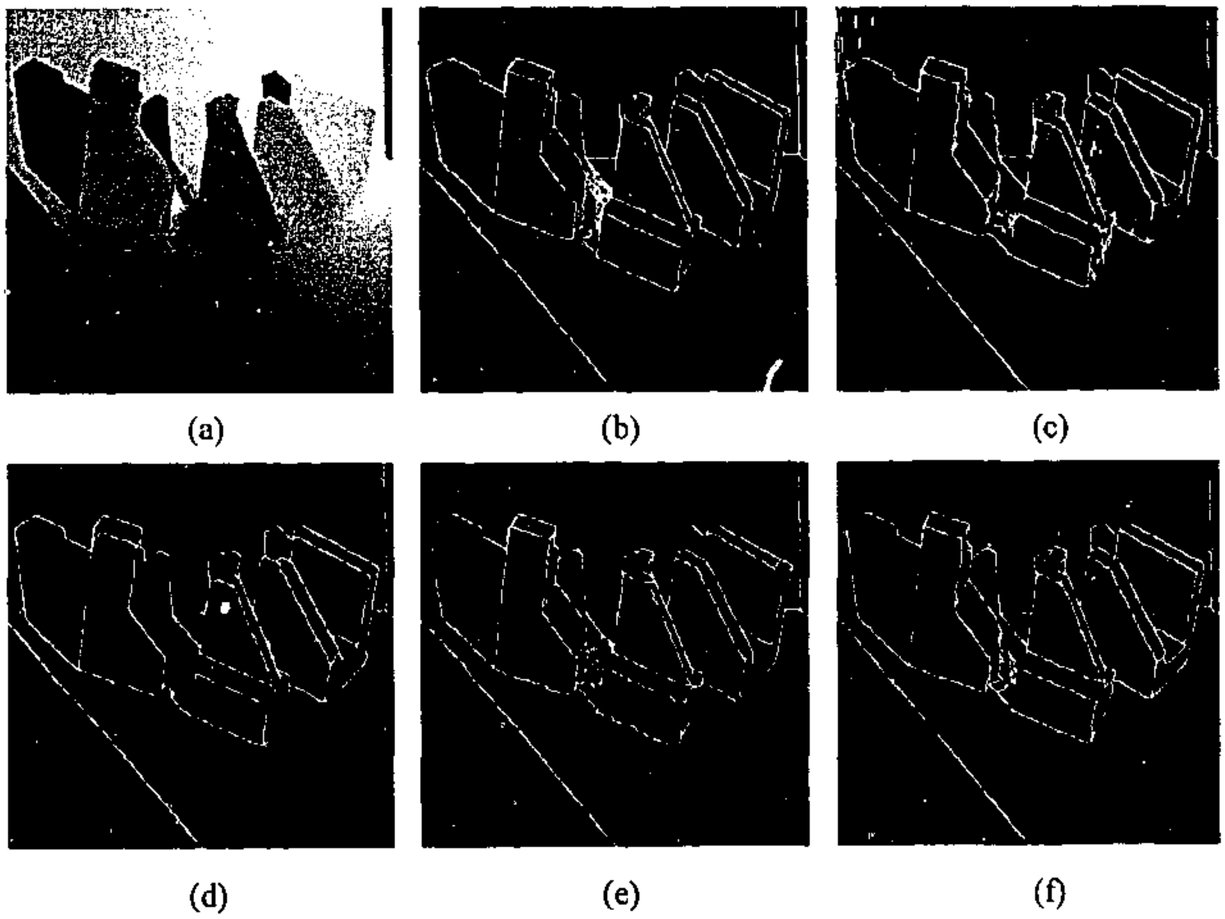

(a) (b) (c)

(d) (e) (f)

Figure 5.10: Comparison of the segmentation results for ABW range image (train 6) from the USF database. (a) Range image; (b) The result of ground truth; (c) The result by the USF; (d) The result by the WSU; (e) The result by the UB; (f) The result by the proposed method.

As stated before, adopting hierarchy-sampling technique in the proposed method greatly reduces its time cost. The processing time of the method is affected to a relatively large extent by the number of surfaces in the range images. The processing time for a range image including simple objects is faster than that for a range image including complicated objects. Generally speaking, it takes about 40 seconds (on an AMD800MHz personal computer programmed (un-optimized) in the C language) for segmenting a range image with less surfaces and about 80-100 seconds for a range image including more surfaces. This includes the time for computing normal information at each range pixel (which takes about 12 seconds).

5.6 Conclusion

In this chapter, we developed a quicker version of MDPE called QMDPE. The advantage of QMDPE is that only the probability density corresponding to the center of the converged mean shift window needs to be calculated; therefore the time cost to compute the probability density power is greatly reduced. Although QMDPE has a relatively lower tolerance to outliers than MDPE, QMDPE still has a better tolerance than most available estimators (such as M-estimators, LMedS, LTS, RANSAC, ALKS, and RESC). We recommend that when the number of data points are small (say less than 5000 points) and the task has a high reliance on the robustness of the estimator, MDPE is an ideal choice. On the other hand, when the task involves a large number of data points (for example, range image segmentation which often involves more than tens of thousands of data), and the speed is a relatively important factor to consider, it is better to choose QMDPE rather than MDPE.

The second contribution of this chapter is that we apply the new QMPDE to the computer vision task of segmenting range data. This part is more than a mere application of the estimator in a straightforward manner. There are a number of issues that need to be addressed when applying an estimator (any estimator) to such a problem. The solutions we have found, to these practical problems that arise in the segmentation task, should be of independent interest. The resulting combination of a highly robust estimator and a very careful application of that estimator, produces a very effective method for range segmentation.

Experimental comparisons of the proposed approach, and several other state-of-the-art methods, support the claim that the proposed method is more robust to outliers and can achieve good results even when the range images are contaminated by a large number of (impulse) noisy data points.

In (Roth and Levine 1990), the authors also employed a robust estimator—LMedS to segment range image. They firstly found the largest connected region bounded by edge pixels; then they used LMedS to fit the geometric primitive in the chosen region. They assumed the largest connected region contained only one geometric primitive. However, if the region includes more than two geometric primitives (for complicated range images), and each geometric primitive has less than 50% data in the region, the estimated primitive will be wrong because LMedS has only up to 0.5 breakdown point.

The algorithm proposed in this chapter is a model-based method and can directly extract planar primitives from the raw images. Because QMDPE is very robust to noise, the algorithm has the advantage that it can resist the influence of a large amount of random noise in the range image. Also, the proposed algorithm is robust to the presence of multiple structures. Since we sequentially removed the detected surfaces one by one, the average time to segment the range image will be affected by how many surfaces the range image includes. However, the computing time will not be greatly affected by the size of the range image as we use a sampling hierarchical technique.

Chapter 6

Variable-Bandwidth QMDPE for Robust Optical Flow Calculation

6.1 Introduction

One major task of computer vision is to compute the optical flow from image sequences (Horn and Schunck 1981; Nagel 1987; Fleet and Jepson 1990; Barron, Fleet et al. 1994; Black 1994; Black and Jepson 1996; Lai and Vemuri 1998; Memin and Perez 1998; Ong and Spann 1999; Farneback. 2000; Farneback 2001; Memin and Perez 2002). Accurate computation of optical flow is an important foundation for tasks, such as motion segmentation, extracting structure from motion, etc. Traditional methods of computing optical flow are non-robust. Which means that they will fail to correctly compute optical flow when the two assumptions: data conservation and spatial coherence, are violated. Clearly, these assumptions will be violated near motion boundaries, and when shadows, occlusions, and/or transparent motions are present.

During the last ten years, robust techniques, such as: M-estimators (Black and Anandan 1993; Black and Anandan 1996), Least Median Squares (LMedS) estimator (Bab-Hadiashar and Suter 1998; Ong and Spann 1999), Least Trimmed Squares (LTS) estimators (Ming and Haralick 2000), and robust Total Least Squares (TLS) estimator

(Bab-Hadiashar and Suter 1998) etc., have been employed to extract optical flow. Because these robust estimators can tolerate the influence of "bad" data, i.e. outliers, they usually obtain better results. Unfortunately, these robust estimators have a breakdown point no more than 50%. This means that when the data contain more than 50% outliers, these estimators will totally breakdown. Such may happen, for example, near motion boundary. In this chapter, we will provide, based on our previous work [see (Wang and Suter 2002a; Wang and Suter 2003b); also see chapter 4 and 5], a robust estimator—variable bandwidth QMDPE (vbQMDPE). Instead of using a fixed bandwidth as in QMDPE, vbQMDPE uses data-driven bandwidth selection. We apply the novel proposed vbQMDPE to the task of optical flow computation. We also correct the results of Bab-Hadiashar and Suter (Bab-Hadiashar and Suter 1998) for the Otte image sequence.

vbQMDPE is very robust if the percentage of outliers is less than 80%, outperforming most other methods in optical flow computation. Of course, any method can breakdown under extreme data: even LMedS and LTS can breakdown when clustered outliers are present - despite those outliers constituting less than 50% of the whole data (e.g., see section 4.4.2).

6.2 Optical Flow Computation

Let $I(x, y, t)$ be the luminance of a pixel at position (x, y) and time t, and $\mathbf{v} = (u, v)$ be the optical flow. The data conservation assumption implies (Fennema and Thompson 1979):

$$I(x, y, t)) = I(x + u\delta t, y + v\delta t, t + \delta t) \tag{6.1}$$

First order expansion yields the optical flow constraint (OFC) equation:

$$\frac{\partial I}{\partial x}u + \frac{\partial I}{\partial y}v + \frac{\partial I}{\partial t} = 0 \tag{6.2}$$

where $(\partial I/\partial x$, $\partial I/\partial y$, and $\partial I/\partial t)$ are partial derivatives of luminance I with respect to space and time at point $(x, y, t))$.

The residual at (x, y) can be written as:

$$r(u,v)=\frac{\partial I}{\partial x}u+\frac{\partial I}{\partial y}v+\frac{\partial I}{\partial t} \tag{6.3}$$

The error measure using the least squares (LS) within the small local neighbourhood R can be written as:

$$E_{LS}(u,v)=\sum_{(x,y)\in R}\left|r(u,v)\right|^2 \tag{6.4}$$

From equation (6.2), we can see there is only one equation but with two variables to estimate - the aperture problem. In order to constrain the solution, the local region R should be as large as possible. However, if R is too large, the spatial coherence assumption will be violated - the generalized aperture problem (Black and Anandan 1996). The affine motion model of image flow is sometimes used in preference to the constant flow model:

$$\begin{aligned} u &= a_0 + a_1 x + a_2 y \\ v &= a_3 + a_4 x + a_5 y \end{aligned} \tag{6.5}$$

Traditional (Least Squares) methods estimate the optical flow by minimizing the error measure in equation (6.4), assuming a flow model such as (6.5).

6.3 From QMDPE to vbQMDPE

In chapter 4 and 5, we proposed a robust estimator MDPE and its modification QMDPE which can both tolerate more than 50% outliers. However, these two robust estimators use a fixed bandwidth technique and thus they require the user to specify the bandwidth h for the kernel density estimation. In practical tasks, it will be attractive if the bandwidth can be data-driven.

Next, we will, based on QMDPE, provide a *variable bandwidth* QMDPE, called vbQMDPE.

6.3.1 Bandwidth Choice

One crucial issue in the non-parametric density estimation, and the mean shift method, is how to choose h (Wand and Jones 1995; Comaniciu, Ramesh et al. 2001; Comaniciu and Meer 2002a). We employ a method in (Wand and Jones 1995):

$$\hat{h} = \left[\frac{243R(K)}{35u_2(K)^2 n} \right]^{1/5} s \tag{6.6}$$

where$R(K) = \int_1 K(\zeta)^2 d\zeta$ and $u_2(K) = \int_1 \zeta^2 K(\zeta) d\zeta$, s is the sample standard deviation.

A robust median scale estimator is then given by (Rousseeuw and Leroy 1987):

$$s = 1.4826 \mathrm{med}_i \mathrm{x}_i \tag{6.7}$$

$\hat{h}$ will provide an above bound on the AMISE (asymptotic mean integrate error) optimal bandwidth $\hat{h}_{AMISE}$, thus we choose the bandwidth as $c\hat{h}$, c is a constant number ($0<c<1$) and is used to avoid over-smoothing (we are also aware that if the value of the bandwidth is too small, it will introduce artefacts).

The median scale estimator in equation (6.7) may be biased for non-symmetrical multi-model data and for data with more than 50% outliers. However, the influence of the bandwidth h on the final result is relatively weak as it is only used in the pdf estimation and the mean shift method.

6.3.2 The Algorithm of the Variable Bandwidth QMDPE

The vbQMDPE procedure can be written as follows:

1 Randomly choose one p-subset, estimate the model parameters by the p-subset, and calculate the residuals of all data points.

2 Adaptively choose the bandwidth h using the method described in section 6.3.1.

3 Apply the mean shift iteration in the residual space with initial window center zero. Thus, we obtain the center of converged window *Xc*.

4 Calculate the probability density $\hat{f}$ at the position *Xc* by equation (4.1) and (4.2).

5 Calculate the density power according to equation (5.1).

6 Repeat step (1) to step (5) many times. Finally, output the parameters with maximum density power.

"Variable bandwidth" means that the bandwidth *h* is variable for each randomly chosen *p*-subset - instead of using a fixed bandwidth as in our previous work (Wang and Suter 2002a; Wang and Suter 2003b). In order to improve the statistical efficiency, a weighted least square procedure (Rousseeuw and Leroy 1987) can be carried out as the final step.

6.3.3 Performance of vbQMDPE

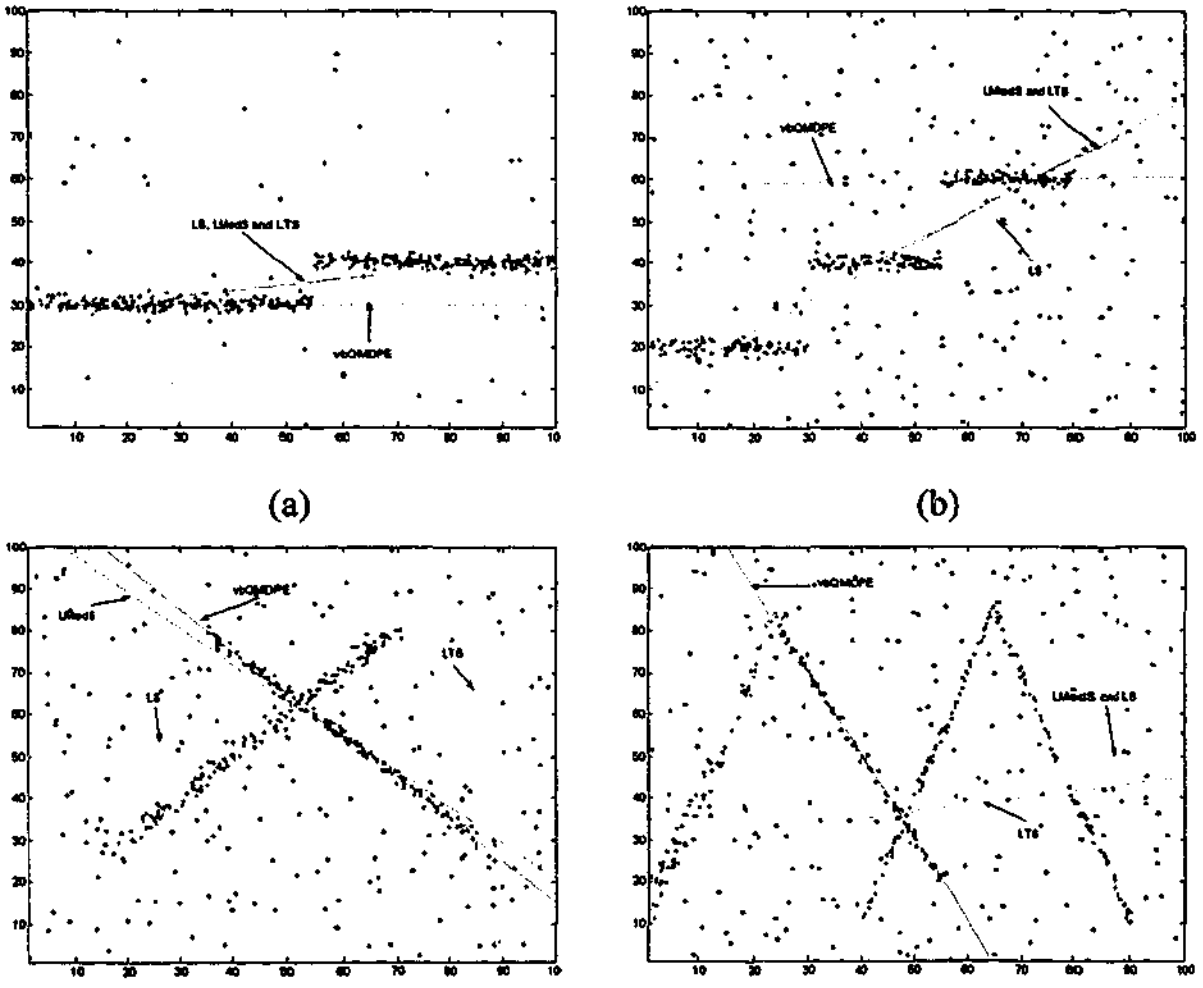

(a)

(b)

(c)

(d)

Figure 6.1: Comparing the performance of vbQMDPE, LS, LMedS, and LTS with (a) 55%; (b) 80%; (c) 70%; (d) 85% outliers.

We demonstrate that vbQMDPE is very robust to outliers by comparing it to several other traditional methods (the LS, LMedS and LTS methods, which are frequently employed in optical flow calculation).

First, we take a simple setting — line fitting. We generated four kinds of data (one step, two steps, two crossed lines, and four lines), each with a total of 500 data points. The signals were corrupted by Gaussian noise with zero mean and unit standard variance. Among the 500 data points, α data points were randomly distributed in the range of (0, 100). The i'th structure has n_i data points.

The four signals are as follows:

- One step: x:(0-55), y=30, n_1=225; x:(55-100), y=40, n_2=225; α=50.
- Two steps: x:(0-30), y=20, n_1=100; x:(30-55), y=40, n_2=100; x:(55-80), y=60, n_3=100; α=200.
- Two crossed lines: x:(20-70), y=x+10, n_1=150; x:(35-85), y=115-x, n_2=150; α=200.
- Four lines: x:(0-25), y=3x+10, n_1=75; x:(25-55), y=130-2x, n_2=20; x:(40-65), y=3x-110, n_3=75; x:(65-90), y=280-3x, n_4=75; α=370.

From Figure 6.1, we can see that LS is non-robust, and that LMedS and LTS failed to fit all the four signals. Only vbQMDPE correctly fitted all the four signals - not even breaking down when the data includes 85% outliers (Figure 6.1 (d)).

6.4 vbQMDPE and Optical Flow Calculation

The optical flow constraint (OFC) is a linear equation in u-v space. Each pixel gives rise to one such linear constraint and, in a noise-free setting, and assuming constant u and v, all lines intersect at a common point.

Two main difficulties in optical flow estimation are (Nesi, Del Bimbo et al. 1995):

- The discontinuities in the local velocity;
- The "aperture" problem.

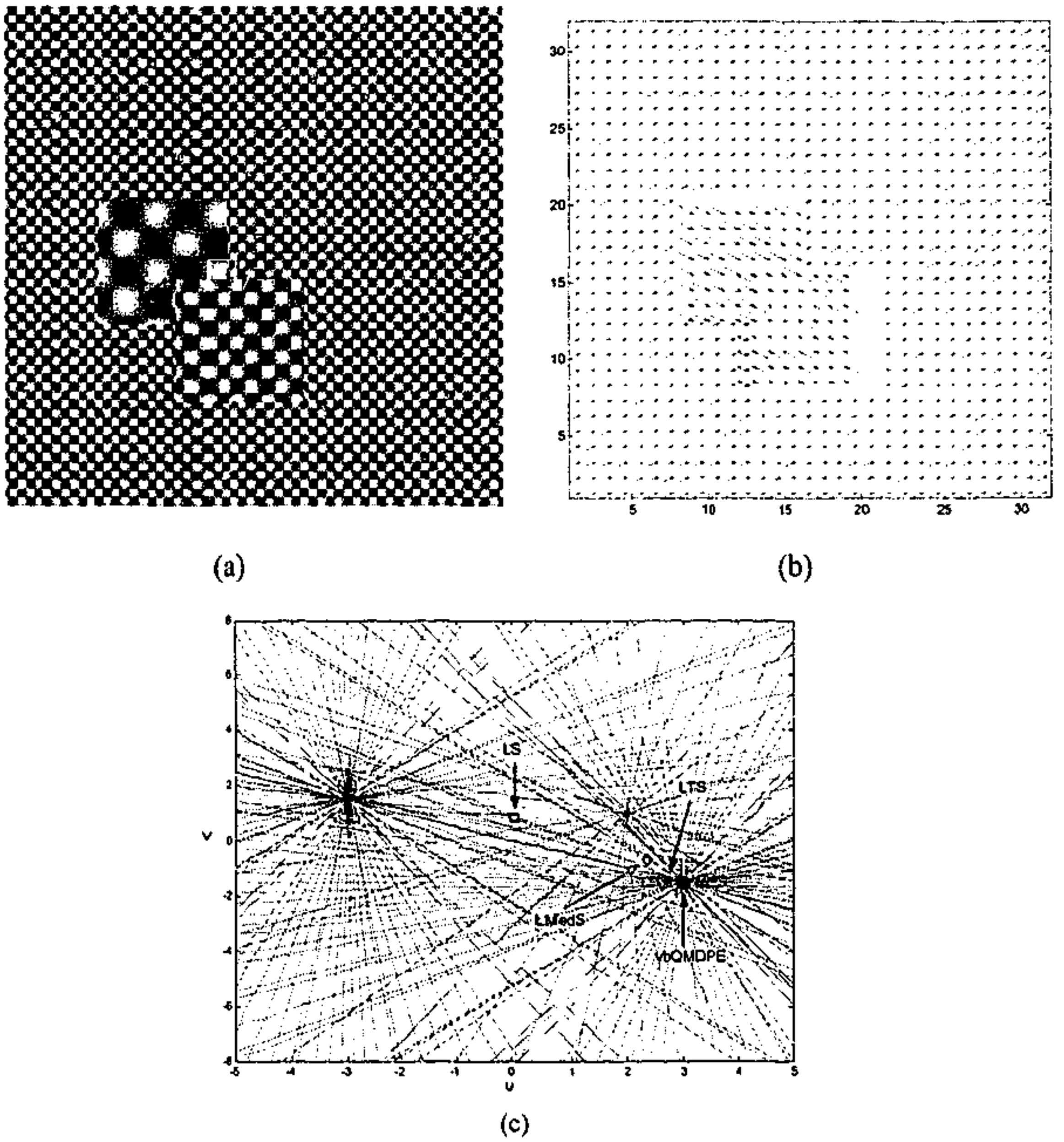

(a) (b)

(c)

Figure 6.2: One example of multiple motions.

The first difficulty is related to occlusions between image illumination discontinuities, moving objects or moving object boundaries. One solution to the second difficulty is to enlarge the local window so as to collect more constraint equations to over determine the optical; this will bring higher statistical efficiency. However, enlarging the window means more chance of including multiple motions (forming multiple clusters of intersecting lines e.g., Figure 6.2). Because traditional estimators (M-estimators, LMedS, LTS, etc.) have only up to 50% breakdown point, they may fail to compute optical flow when the data include multiple motion structures (i.e. the outliers occupy more than 50% of the data). In such cases, vbQMDPE performs well.

We generated an image sequence with two moving squares using the method similar to that in (Barron, Fleet et al. 1994). Figure 6.2 (a) shows one snapshot of the image sequence. The correct optical flow is shown in Figure 6.2 (b). The small window centered at (110, 136) in Figure 6.2 (a) includes three motions; each motion involves less than 50% data points. Its OFC plot, using symbolically determined derivatives of the image intensities I, is shown in Figure 6.2 (c). From Figure 6.2 (c), we can see that there are three motions included in the small window in Figure 6.2 (a). The optical flow of each motion (2.0, 1.0), (-3.0, 1.5), (3.0, -1.5) is marked by a red plus sign. The proposed robust estimator gives the correct optical flow estimation (3.0, -1.5). However, by the LMedS method, the estimated optical flow is (2.36, -0.71); and the estimated optical flow by the least trimmed squares and the least squares method is respectively (2.71, -1.43) and (0.06, 0.84).

6.4.1 Variable-Bandwidth-QMDPE Optical Flow Computation

The first step to compute optical flow is to estimate the spatio-temporal derivatives of the image brightness. We follow Bab-Hadiashar and Suter (Bab-Hadiashar and Suter 1998), and Nagel (Nagel 1995), by convolving the image brightness with derivatives of 3D spatio-temporal Gaussian function:

$$G(\mathrm{x}) = \frac{1}{(2\pi)^{3/2}\sqrt{|\Sigma|}} e^{-\frac{1}{2}\mathrm{x}^T\Sigma^{-1}\mathrm{x}} \tag{6.8}$$

where $\mathbf{x} = (x, y, t)^T$; Σ is the covariance matrix.

There are methods to estimate the derivatives near the discontinuities of optical flow (e.g., (Ye and Haralick 2000)). In our simple approach, we first estimate the derivatives of I with initial standard variance σ_0. Then, when the estimated derivatives (I_x, I_y, and I_t) are larger than a threshold, we simply re-compute the derivatives with half of the standard variance in that corresponding direction.

For each NxN patch of the image and chosen motion model (in our case, constant motion model and affine motion model), we solve for the flow using the vbQMDPE. The measure of reliability in (Bab-Hadiashar and Suter 1998) can be employed in our method.

6.4.2 Quantitative Error Measures for Optical Flow

When the "ground truth" optical flow of image sequences is known, the error analysis is performed by Barron's method (Barron, Fleet et al. 1994). The angular error measure is reported in degree:

$$E = \text{arcos}(\mathbf{v}_e , \mathbf{v}_c) \tag{6.9}$$

where $\mathbf{v}_e = (u,v,1)^T / \sqrt{u^2+v^2+1}$ and $\mathbf{v}_c$ is the true motion vector. The average and standard deviation of the errors are both reported.

6.5 Experimental Results on Optical Flow Calculation

The proposed algorithm has been evaluated on both synthetic and real images. Three well-known image sequences (the Diverging Tree sequence (which is obtained from ftp://csd.uwo.ca/pub/vision); the Yosemite sequence (which is obtained from ftp://csd.uwo.ca/pub/vision); and the Otte image sequence (which is obtained from http://i21www.ira.uka.de/image_sequences/)) are used (see Figure 6.3). Table 6.1 shows the comparison results the Diverging Tree sequence (Figure 6.3 (a)) – showing the proposed method gives the most accurate results for affine motion model. Even for the constant motion model, vbQMDPE still yields better results than most other comparative methods.

Figure 6.3 (b) shows one snapshot of the Yosemite sequence. Because the true motion of the clouds does not really reflect the image brightness changes, we exclude the clouds in our experiments. From Table 6.2, we can see that the proposed algorithm and Farneback's algorithms give the best overall results. The standard variance error of our results is less than that of Farneback's results (Farneback. 2000; Farneback 2001) for both constant and affine motion models. Although the averaged angle error of Farneback's results (Farneback. 2000) is better than our results for constant motion model, our results for affine motion model with larger local window outperform those results. However, the average angle error of Farneback's later version (Farneback 2001), which used an affine motion model and a combined a region growing segmentation algorithm, is better than ours. To our knowledge, it is the best result obtained so far in the field of optical flow computation for Yosemite sequence.

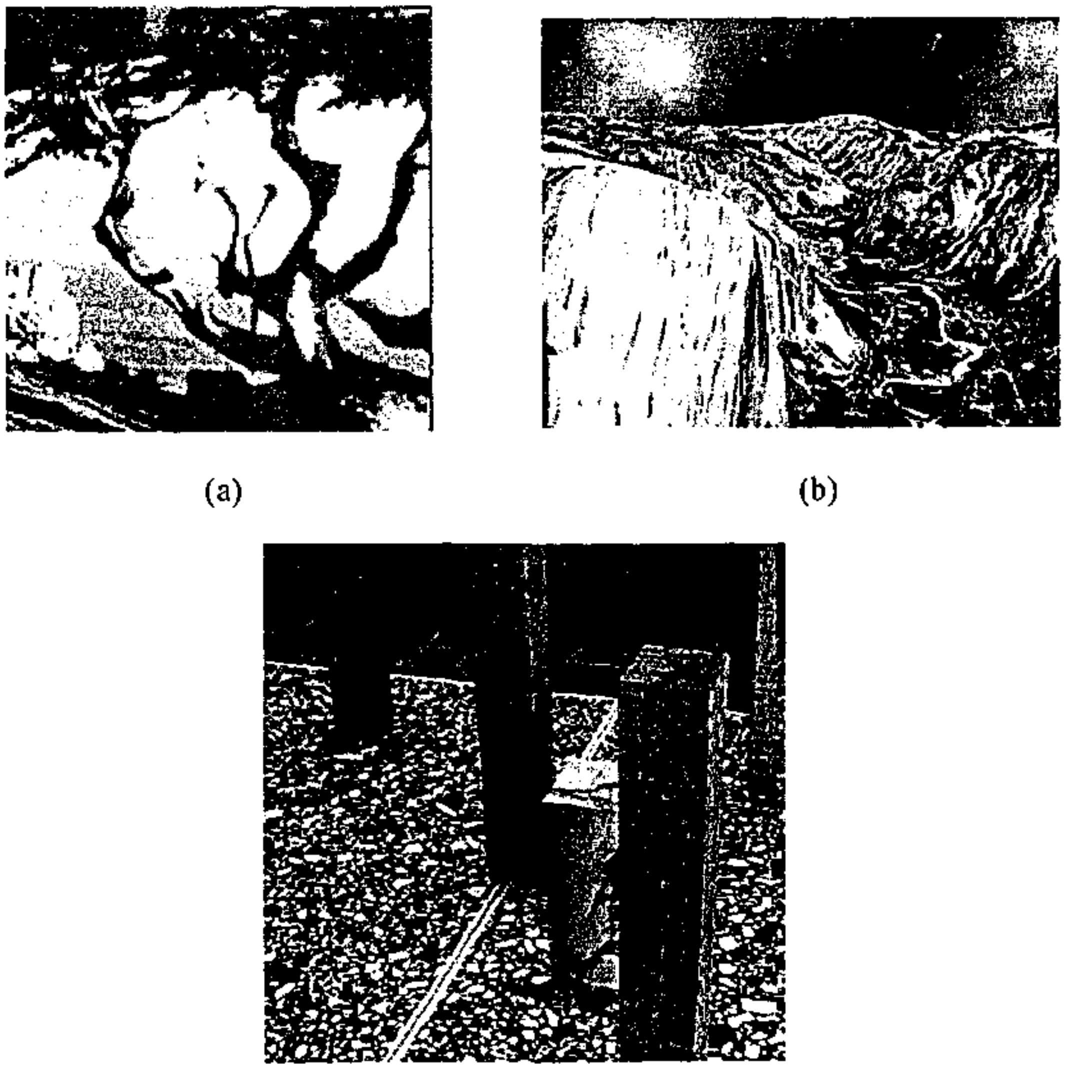

(a)

(b)

(c)

Figure 6.3: The snapshot of the three image sequences: (a) the Diverging Tree; (b) the Yosemite; and (c) the Otte sequence.

We also note that our results with affine motion model are better than those with constant motion model in both the Diverging Tree and the Yosemite. This is because the motion in two sequences is mostly diverging. For each pixel within a small local window, the optical flow changes. Thus, the affine motion model reflects the true situation better than the constant one.

The Otte sequence (Figure 6.3 (c)) is a real image sequence (Otte and Nagel 1995) and it is difficult because it includes many sharp discontinuities in both motion and depth. When we recomputed the optical flow for Otte image sequence (frame 35) by Bab-Hadiashar and Suter's code, we found that the results in (Bab-Hadiashar and Suter 1998) were wrongly reported (our results show an improved performance!). From Table 6.3, we can see our vbQMDPE outperforms all other published benchmarks

6.6 Conclusion

We have developed a novel robust estimator—variable bandwidth QMDPE, and we applied it to optical flow computation. By employing nonparametric density estimation and density gradient estimation techniques in parametric model estimation, the proposed method is very robust to outliers and is a substantial improvement over traditional methods. We expect we can do even better with a multi-resolution version of our approach.

Our code *without optimization* takes about 6 min on Yosemite image sequence on a 1.2GHz AMD personal computer, using 17x17 patches around each pixel and m is set to 30. The speed can be improved for less m and smaller patches but with worse accuracy. The mean number of mean shift iterations is about 3 for each p-subset.

Technique	Avg. error (degree)	Std. dev. (degree)	Density (%)
Horn and Schunck (original unthresholded)	12.02	11.72	100
Horn and Schunck (modified unthresholded)	2.55	3.67	100
Uras et.al. (unthresholded)	4.64	3.48	100
Nagel	2.94	3.23	100
Anandan	7.64	4.96	100
Singh (Step 1 unthresholded)	17.66	14.25	100
Singh (Step 2 unthresholded)	8.60	4.78	100
Least-Squares (block-based) method (in Ong and Spann, 1999)	1.98	2.81	100
vbQMDPE2 (σ_0=1.5, 11x11, m=30)	2.51	1.62	100
vbQMDPE6 (σ_0=1.5, 11x11, m=30)	1.46	1.03	100

Table 6.1: Comparative results on diverging tree: the first part of the table is the results reported by Barron et. al (1994) and Ong et. al (1999); the second part is the results obtained by the proposed algorithm (number 2 and 6 represent constant and affine motion models).

Technique	Avg. error	Std. dev.	Density
	(degree)	(degree)	(%)
Black (1994)	3.52	3.25	100
Szeliski and Coughlan (1994)	2.45	3.05	100
Black and Anandan (1996)	4.46	4.21	100
Black and Jepson (1996)	2.29	2.25	100
Ju et. al. (1996)	2.16	2.00	100
Memin and Perez (1998)	2.34	1.45	100
Memin and Perez (2002)	1.58	1.21	100
Lai and Vemuri(1998)	1.99	1.41	100
Bab-Hadiashar and Suter (WTLS2, 1998)	2.56	2.34	100
Bab-Hadiashar and Suter (WTLS6, 1998)	1.97	1.96	100
Farneback2 (2000)	1.94	2.31	100
Farneback6 (2000)	1.40	2.57	100
Farneback6 (2001)	1.14	2.14	100
vbQMDPE2 (σ_0=2.0, 17x17, m=30)	2.12	2.08	100
vbQMDPE6 (σ_0=2.0, 17x17, m=30)	1.54	1.99	100
vbQMDPE2 (σ_0=2.0, 25x25, m=30)	2.27	2.07	100
vbQMDPE6 (σ_0=2.0, 25x25, m=30)	1.34	1.69	100

Table 6.2: Comparative results on Yosemite (cloud region excluded): the first part is the results reported in the recently referenced literature; the second part is our results.

Technique	Avg. error (degree)	Std. dev. (degree)	Density (%)
Giachetti and Torre (1996)	5.33	-----	100
Bab-Hadiashar and Suter (WLS2, 1998)	3.39	6.55	100
Bab-Hadiashar and Suter (WLS6, 1998)	3.51	6.48	100
Bab-Hadiashar and Suter (WTLS2, 1998)	3.74	8.09	100
Bab-Hadiashar and Suter (WTLS6, 1998)	3.67	7.37	100
Bab-Hadiashar and Suter (WLS2, corrected)	3.02	5.98	100
Bab-Hadiashar and Suter (WLS6, corrected)	3.14	5.84	100
Bab-Hadiashar and Suter (WTLS2, corrected)	3.20	7.02	100
Bab-Hadiashar and Suter (WTLS6, corrected)	3.20	6.59	100
vbQMDPE2 (σ_0=2.0, 17x17, m=30)	2.64	4.98	100
vbQMDPE6 (σ_0=2.0, 17x17, m=30)	2.82	5.03	100
vbQMDPE2 (σ_0=2.0, 25x25, m=30)	2.21	4.16	100
vbQMDPE6 (σ_0=2.0, 25x25, m=30)	2.29	4.06	100

Table 6.3: Comparative results on Otte image sequences: the first part was reported by Bab-Hadiashar and Suter (1998); the second part is the corrected results; the third part is obtained by running the proposed algorithm.

Chapter 7

A Highly Robust Scale Estimator for Heavily Contaminated Data

It is not enough to (only) correctly estimate the parameters of a model to differentiate inliers from outliers; It is also important to robustly estimate the scale of inliers. In this chapter, we propose a new robust scale estimation technique: robust Two-Step Scale estimator (TSSE). The TSSE applies nonparametric density estimation and density gradient estimation techniques, to robustly estimate the scale of inliers for heavily contaminated data. The TSSE can tolerate more than 80% outliers and comparative experiments show its advantages over five other robust scale estimators: the median, the median absolute deviation (MAD), Modified Selective Statistical Estimator (MSSE), Residual Consensus (RESC), and Adaptive Least *K*th order Squares (ALKS).

7.1 Introduction

As emphasized in chapter 2, in computer vision tasks, it frequently happens that gross noise and pseudo outliers occupy the absolute majority of the data. Most past work aimed at presenting robust estimators with high breakdown point (Rousseeuw 1984; Yu, Bui et al. 1994; Stewart 1995; Miller and Stewart 1996; Lee, Meer et al. 1998), i.e. the estimator can correctly find the parameters of a model from the data which are heavily contaminated. However, correctly estimating the parameters of a model is not enough to differentiate inliers from outliers. Having a correct scale of inliers is crucial to the robust behaviour of an estimator. The success of some robust estimators is based on having correct initial scale estimate, or the correct setting of a particular parameter that is related to scale (e.g., RANSAC, Hough Transform, M-estimators etc.). Thus, their performance crucially depends on that user-provided scale-related knowledge. Robust scale estimation is often attempted during a post-processing stage of robust estimators (such as LMedS, LTS, etc.). Yet, although there are a lot of papers that propose robust estimators with high breakdown point for model fitting, robust scale estimation is relatively neglected.

In this chapter, we investigate the behaviour of several robust scale estimators that are widely used in computer vision community and show the problems of these scale estimation techniques. We also propose a new robust scale estimator: Two-Step Scale estimator (TSSE), based on the nonparametric density estimation and density gradient estimation techniques. TSSE can tolerate more than 80% outliers and outperform the five comparative scale estimators (The Median, MAD, ALKS, RESC, MSSE scale estimators).

This chapter is organized as follows: in section 7.2, we review previous robust scale techniques. In section 7.3, we propose a simple but efficient mean shift valley algorithm, by which the local valley can be found and propose the novel robust scale estimator: TSSE. TSSE is experimentally compared with five other robust scale estimators, using data with multiple structures, in section 7.4. We conclude in section 7.5.

7.2 Robust Scale Estimators

The emphasis in many past computer vision papers presenting robust estimators was on the high breakdown point (Rousseeuw 1984; Rousseeuw and Leroy 1987; Yu, Bui et al. 1994; Stewart 1995; Miller and Stewart 1996; Lee, Meer et al. 1998; Wang and Suter 2003b), i.e. the estimator that can correctly find the parameters of a model from the data which are heavily contaminated. Whether or not the inliers can be successfully differentiated from the outliers depends on two factors:

(1) Whether the parameters of a model are correctly found; and

(2) Whether the scale of inliers is correctly estimated.

Step (2), scale estimation plays an important role in the overall robust behaviour of these methods. Some robust estimators, such as M-estimators, RANSAC, Hough Transform, etc., put the onus on the "user" - they simply require some user-set parameters that are linked to the scale of inliers. Others, such as LMedS, RESC, MDPE, QMDPE, etc., use an auxiliary estimate of scale (after finding the parameters of a model) during a post-processing stage, which aims to differentiate inliers from outliers.

Given a scale estimate, s, the inliers are usually taken to be those data points that satisfy the following condition:

$$|r_i/s| < T \tag{7.1}$$

where r_i is the residual of i'th sample, and T is a threshold. For example, if T is 2.5 (1.96), 98% (95%) percent of a Gaussian distribution will be identified as inliers.

7.2.1 The Median and Median Absolute Deviation (MAD) Scale Estimator

Among many robust estimators, the sample median is one of the most famous estimators. The sample median is bounded when the data include more than 50% inliers. A robust median scale estimator is then given by (Rousseeuw and Leroy 1987):

$$M = 1.4826(1 + \frac{5}{n-p})\sqrt{\underset{i}{med}\, r_i^2} \tag{7.2}$$

where x_i is the residual of i'th sample, n is the number of sample points and p is the dimensions of parameter space (e.g., 2 for a line, 3 for a circle).

A variant, MAD, is also used to estimate the scale of inliers (Rousseeuw and Croux 1993):

$$\text{MAD}=1.4826\text{med}_i\{|x_i\text{-med}_j x_j|\} \tag{7.3}$$

The MAD estimator is very robust to outliers and has a 50% breakdown point. The outliers can be recognized by computing:

$$\frac{|x_i - med_j x_j|}{MAD_n} < T \qquad (7.4)$$

where T is a threshold.

The median and MAD are often used to yield initial scale values (before estimating the parameters of a model) for many robust estimators. These two methods can also serve as auxiliary scale estimators (after finding the parameters of a model) for other robust estimators.

Because the median and MAD have 50% breakdown points, they will break down when the data include more than 50% outliers. Both methods are biased for multiple-mode cases even when the data contains less than 50% outliers (see section 7.4).

7.2.2 · Adaptive Least K-th Squares (ALKS) Scale Estimator

As we have outlined in section 2.4.5, the authors of ALKS (Lee, Meer et al. 1998) employ the robust k scale estimation technique in ALKS by searching for a model minimizing the k-th order statistics of the squared residuals. The optimal value of the k is that which corresponds to the minimum of the variance of the normalized error (see equation (2.32)). The authors assume that when k is increased so that the first outlier is included, the increase of $\hat{s}_k$ is much less than that of $\hat{\sigma}_k$.

ALKS is limited in its ability to handle extreme outliers. Another problem we found (Wang and Suter 2003b) (also see chapter 4) in ALKS is its lack of stability under a small percentage of outliers.

7.2.3 Residual Consensus (RESC) Scale Estimator

In section 2.4.6, we discussed the RESC estimator (Yu, Bui et al. 1994). In that section, we concentrate on the estimation of the parameters, not on scale estimation. After finding a fit, RESC estimates the scale of the fit by directly calculating:

$$\sigma = \alpha\left(\frac{1}{\sum_{i=1}^{v} h_i^c - 1}\sum_{i=1}^{v}(ih_i^c\delta - \bar{h}^c)^2\right)^{1/2} \tag{7.5}$$

where $\bar{h}^c$ is the mean of all residuals included in the compressed histogram; α is a correct factor for the approximation introduced by rounding residuals in a bin of histogram to $i\delta$ (δ is the bin size of the compressed histogram); v is the number of bins of the compressed histogram.

However, we found the estimated scale is still overestimated for the reason that, instead of summing up squared differences between all individual residuals and the mean residual in the compressed histogram, equation (7.5) sums up the squared differences between residuals in each bin of compressed histogram and the mean residual in the compressed histogram.

To reduce this problem, we revise it as follows:

$$\sigma = \left(\frac{1}{\sum_{i=1}^{v} h_i^c - 1}\sum_{i=1}^{n_c}(r_i - \bar{h}^c)^2\right)^{1/2} \tag{7.6}$$

where n_c is the number of data points in the compressed histogram.

7.2.4 Modified Selective Statistical Estimator (MSSE)

Bab-Hadiashar and Suter (Bab-Hadiashar and Suter 1999) have used least k-th order (rather than median) methods and a heuristic way of estimating scale to perform range segmentation. After finding a fit, they tried to recognize the first outlier, by detecting the k-th residual jumps, which can indicate the unbiased scale estimate using the first k-th residuals in an ascending order:

$$\hat{\sigma}_k^2 = \frac{\sum_{i=1}^{k} r_i^2}{k-p} \tag{7.7}$$

where p is the dimension of the model.

They assume that when k is increased, the value of the k-th residual will jump when it comes from a different distribution. Thus, the scale can be estimated by checking the validity of the following inequality:

$$\frac{\sigma_{k+1}^2}{\sigma_k^2} > 1 + \frac{T^2 - 1}{k - p + 1} \tag{7.8}$$

Because this method does not rely on the k-th order statistics (it uses only the first k data points that has been classified as inliers), it is less biased when data include multiple-structural distribution.

However, though their method can handle large percentages of outliers and pseudo-outliers, it does not seem as successful in tolerating extreme cases

7.3 A Novel Robust Scale Estimator: TSSE

In this section, we will produce a mean shift valley (MSV) technique and then, we propose a highly robust scale estimator (TSSE), which is very robust to multiple-structural data.

7.3.1 Mean Shift Valley Algorithm

Although the mean shift method has been extensively exploited and applied in low level computer vision tasks (Cheng 1995; Comaniciu and Meer 1997; Comaniciu and Meer 1999b; Comaniciu and Meer 2002a) for its efficiency in seeking local *peaks* of probability density, sometimes it is very important to find the *valleys* of distributions. Based upon the Gaussian kernel, a saddle-point seeking method was published in (Comaniciu, Ramesh et al. 2002b). Here, we provide a more simple method to find local valleys in one dimensional function.

One characteristic of the mean shift vector is that it always points towards the direction of the maximum increase in the density. Thus the direction opposite to the mean shift vector will always point toward to a local minimum density. In order to find valley in density space, we define the mean shift valley vector $\mathrm{MV}_h(x)$ to point in the opposite direction to the peak:

$$\mathrm{MV}_h(x) = -\mathrm{M}_h(x) = x - \frac{1}{n_x} \sum_{x_i \in S_h(x)} x_i \tag{7.9}$$

Replace $\mathrm{M}_h(x)$ in (4.6) by $\mathrm{MV}_h(x)$, we can obtain:

$$\mathrm{MV}_h(x) \equiv -\frac{h^2}{d+2} \frac{\hat{\nabla} f(x)}{\hat{f}(x)} \tag{7.10}$$

$\mathrm{MV}_h(x)$ always points towards the direction of the maximum decrease in the density.

In practice, we find that the step-size given by the above equation may lead to oscillation. Thus we derive a recipe for avoiding the oscillations in valley seeking. Let $\{y_k\}_{k=1,2...}$ be the sequence of successive locations of the mean shift valley procedure, then we take a modified step by:

$$y_{k+1} = y_k + p \cdot MV_h(y_k) \tag{7.11}$$

where p is a correction factor, and $0 < p \leq 1$.

If the shift step at y_k is large, it causes y_{k+1} to jump over the local valley and thus oscillate over the valley. This problem can be avoided when we adjust the correction factor p so that $\mathrm{MV}_h(y_k)^T \mathrm{MV}_h(y_{k+1}) > 0$.

The mean shift valley algorithm can be described as:

1. Choose the bandwidth, h; set $p = 1$; and initialise the location of the window.

2. Compute the shift step vector $\mathrm{MV}_{\mathrm{h}}(y_k)$.

3. Compute y_{k+1} by equation (7.11) and $\mathrm{MV}_{\mathrm{h}}(y_{k+1})$.

4. If $\mathrm{MV}_{\mathrm{h}}(y_k)^{\mathrm{T}}\ \mathrm{MV}_{\mathrm{h}}(y_{k+1})>0$, go to step 5; Otherwise, we let $p=p/2$. Repeat step 3 and 4 until $\mathrm{MV}_{\mathrm{h}}(y_k)^{\mathrm{T}}\ \mathrm{MV}_{\mathrm{h}}(y_{k+1})>0$;

5. Translate the search window by $p \cdot MV_h(y_k)$.

6. Repeat step 3 to step 5 until convergence.

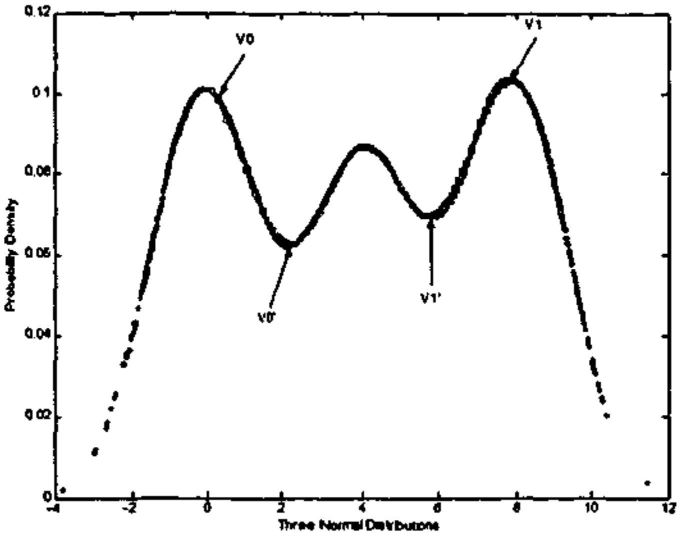

Figure 7.1: An example of the application of the mean shift valley method to find local valleys.

To illustrate the mean shift valley method, three normal modes (mode 1 includes 600 data points, mode 2 includes 500 data points, and mode 3 includes 600 data points) with total 1700 data points were generated in Figure 7.1. We selected two initial points: V0 (0.3) and V1 (7.8). The search window radius was chosen as 2.0. The mean shift valley method automatically found the local minimum densities (converged points). Precisely: V0' was located at 2.1831, and V1' was at 5.8898. The centers (V0' and V1') of the converged windows correspond to the local minimum probability densities. If we use V0' and V1' as two density thresholds, the whole data can be decomposed into three modes (see Table7.1).

	Mode 1		Mode 2		Mode 3	
	Mean	Number	Mean	Number	Mean	Number
Generated Data	0	600	4	500	8	600
Estimated Parameters	-0.0736	603	4.0419	488	7.9592	609

Table7.1: Applying the mean shift valley method to decompose data.

There is one exceptional case: when there are no local valleys (e.g., uni-modal), the mean shift valley method is divergent. This can easily be avoided by terminating when no samples fall within the window.

Next, we will apply the mean shift and mean shift valley methods, in (one-dimensional) residual space, to produce a highly robust scale estimator: Two-Step Scale Estimator.

7.3.2 Two-Step Scale Estimator (TSSE)

We base our method on the assumption that the inliers occupy relative majority, and are Gaussian distributed, but the whole data can include multiple-structural distribution. Thus, we propose a robust two-step method to estimate the scale of the inliers.

(1) Use mean shift, with initial center zero (in ordered absolute residual space), to find the local peak, and then use the mean shift valley to find the valley next to the peak. Note: modes other than the inliers will be disregarded as they lie outside the obtained valley.

(2) Estimate the scale of the fit by the median scale estimator using the points within the band centered at the local peak extending to the valley.

TSSE is very robust to outliers and can resist heavily contaminated data with multiple structures. In next section, we will compare the achievements of our method and other five methods. The experiments will show the advantages of the proposed method over other methods

7.4 Experiments on Robust Scale Estimation

In this section, we will investigate the behaviour of several state-of-the-art robust scale estimators that are widely used in computer vision community and show the weakness of these scale estimation techniques. We assume the parameters of the model have been correctly estimated. In the following experiments, we compare the proposed method — TSSE, with other five robust scale estimators: the median, MAD, ALKS, MSSE, and the revised RESC (according to revised equation 7.6). Comparative experiments show the proposed method achieves better results than the other five robust scale estimators.

The signals were generated as follows: The *i*'th structure has n_i data points, corrupted by Gaussian noise with zero mean and standard variance σ_i. α data points were randomly distributed in the range of (0, 100).

7.4.1 Normal Distribution

First, we generate a simple line signal: One line: x:(0-55), y=30, n_1=10000, σ_1=3; α=0, i.e., 100% inliers; After we applied the six robust scale estimators to the signal, we obtained the following estimates: Median (3.0258); MAD (3.0237); ALKS (2.0061); MSSE (2.8036); the revised RESC (2.8696); and TSSE (3.0258). Among these six comparative methods, the median, MAD, and TSSE gave the most accurate results. ALKS gave the worst result. This is because the robust estimate $\hat{s}_k$ is an underestimate of σ for all values of k (Rousseeuw and Leroy 1987) and because the criterion equation (2.32) estimates the optimal k wrongly. ALKS used only about 15% data as inliers. MSSE used 98% of the data points as inliers, which is reasonably good.

7.4.2 Two-mode Distribution

In this subsection, we analyse more complicated data. We generated a step signal so that the data include two structures, i.e. two lines.

A step signal: line1: x:(0-55), y=40, n_1=3000, σ_1=3; line2: x:(55-100), y=70, n_2=2000, σ_2=3; α=0.

The results that we obtained are as follows: the median (6.3541); MAD (8.8231); ALKS (3.2129); MSSE (2.8679); the revised RESC (2.9295); and TSSE (3.0791). Among these six methods, the median and MAD gave the worst results. This is because the median and MAD scale estimators assume the residuals of the whole data are at Gaussian distribution, which is violated in the signal (containing two modes). The other four robust scale estimators yield good results.

7.4.3 Two-mode Distribution with Random Outliers

Next, we again use the above one-step signal. However, we increased the number of outliers so that the data include 80% of outliers, i.e., n_1=1000; n_2=750; α=3250.

After applying the six methods, the estimated scale of the signal that we obtained are: the median (34.0962); MAD (29.7909); ALKS (7.2586); MSSE (27.4253); the revised RESC (24.4297); and TSSE (4.1427). From the obtained results, we can see that only the proposed method gave a reasonably good result, while all other five methods failed to estimate the scale of the inliers when the data involve a high percentage of outliers.

7.4.4 Breakdown Plot

7.4.4.1 A Roof Signal

We generate a roof signal containing 500 data points in total. A roof: x:(0-55), y=x+30, n_1, σ=2; x:(55-100), y=140-x, n_2=50; σ=2.

At the beginning, we assign 450 data point to n_l and the number of the uniform outliers α =0; Thus, the data include 10% outliers. Then, we decrease n_1, and at the same time, we increase α so that the total number of data points is 500. Finally, n_1=75, and α=375, i.e. the data include 85% outliers. The results are repeated 20 times.

Figure 7.2 shows that TSSE yielded the best results among the six comparative methods. The revised RESC method begins to break down when the outliers occupy around 60%. MSSE gave reasonable results when the percentage of outliers is less than 75%, but it broke down when the data include more outliers. Although the breakdown points of the median and the MAD scale estimators are as high as 50%, their results deviated from the true scale even when outliers are less than 50% of the data. They are biased more and more from the true scale with the increase in the percentage of outliers. ALKS yielded less accurate results than TSSE, and less accurate results than the revised RESC and MMSE when outliers are less 60%.

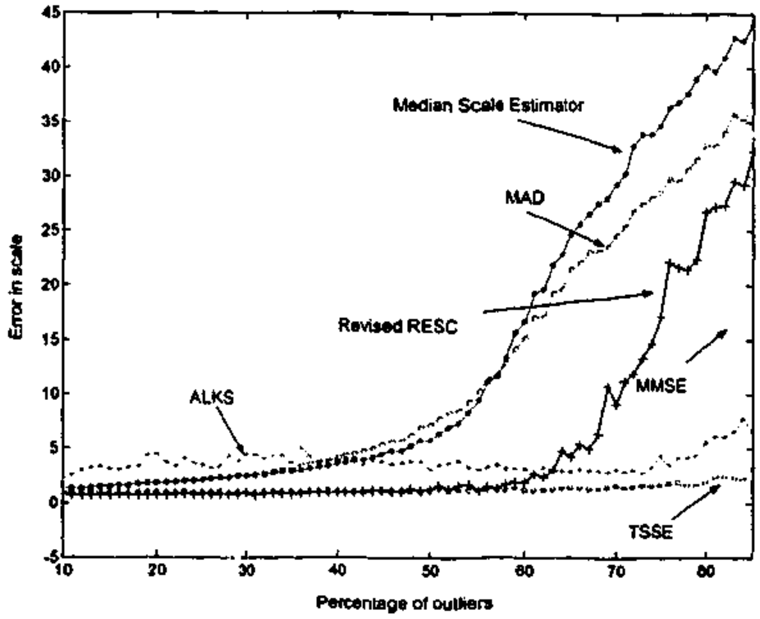

Figure 7.2: Breakdown plot of six methods in estimating the scale of a roof signal.

7.4.4.2 A Step Signal

We generated another signal: one-step signal that contains 1000 data points in total. One-step signal: x:(0-55), y=30, n_1, σ=2; x:(55-100), y=40, n_2=100; σ=2.

At the beginning, we assign n_1 with 900 data points and the number of the uniform outliers α =0; Thus, the data include 10% outliers. Then, we decrease n_l, and at the same time, we increase α so that the number of the whole data points is 1000. Finally, n_1=150, and α=750, i.e. the data include 85% outliers.

From Figure 7.3, we can see that TSSE gave the most accurate estimation of the scale of the signal. In contrast, the revised RESC begins to break down when the number of outliers is about 50% of the data. MSSE gave reasonable results when the percentage of outliers is less than 70%. However, it broke down when the data include more outliers. The median and the MAD scale estimators are more and more biased with the increase in the percentage of outliers for the two-structured signal. ALKS yielded less satisfactory results.

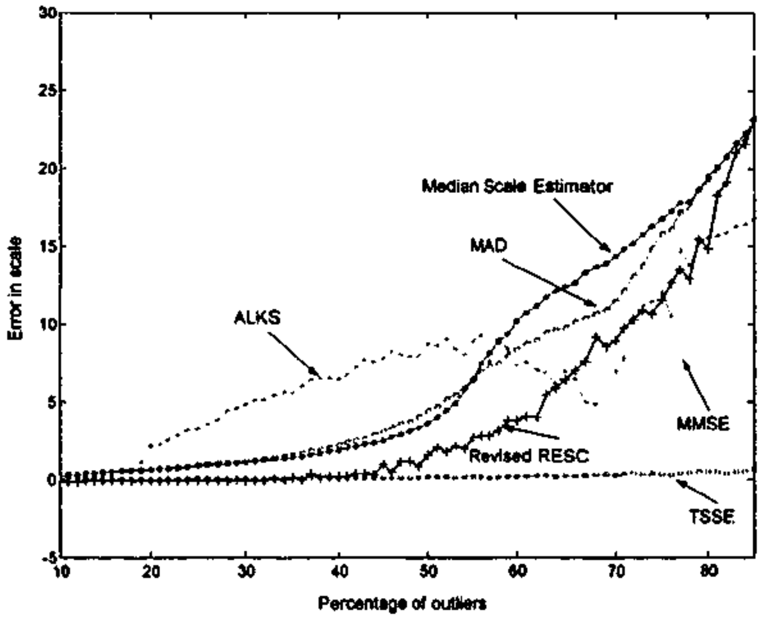

Figure 7.3: Breakdown plot of six methods in estimating the scale of a step signal.

Compared with Figure 7.2, we can see that the revised RESC, MSSE, and ALKS yielded less accurate results for small scale step signal than roof signal, but the results of the proposed TSSE are similar accurate for both types of signals. Even when the data include 85% outliers, the recovered scales of inliers by TSSE for the one-step signal are 2.95, which is reasonably good.

7.4.4.3 Breakdown Plot for Robust Scale Estimator

If the data have a Gaussian like distribution, the median scale estimator (7.1) is only one possible robust k scale estimator (2.31) (corresponding to k=0.5n). We investigated the achievements of the robust k scale estimator (assuming the correct parameters of a model have been found). Let:

$$S(q) = \frac{\hat{d}_q}{\Phi^{-1}[(1+q)/2]} \tag{7.12}$$

where q is set from 0 to 1. Thus S (0.5) is the median scale estimator.

We generated a one-step signal containing 500 data points in total. One-step signal: x:(0-55), y=30, n_1, σ=1; x:(55-100), y=40, n_2=50; σ=1. At the beginning, n_1 = 450 and α =0; Then, we decrease n_1, and at the same time, we increase α until n_1=50, and α=400, i.e. the data include 90% outliers.

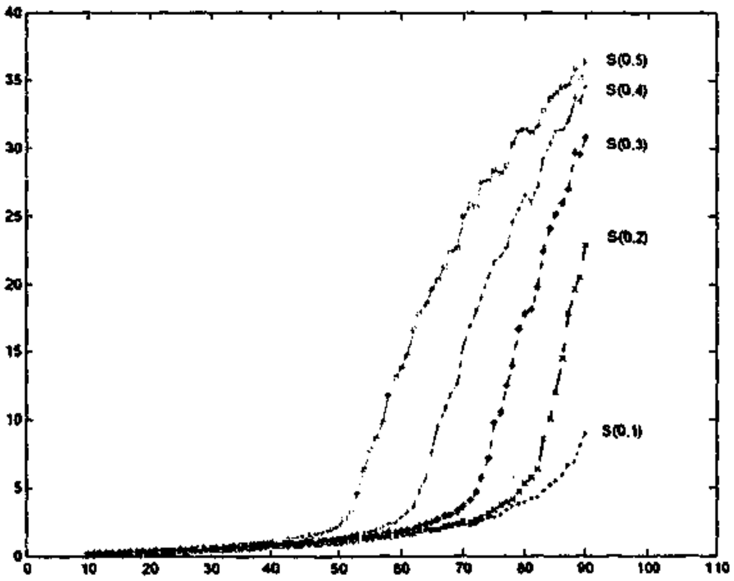

Figure 7.4: Breakdowr. plot of different robust k scale estimators.

As Figure 7.4 shows, after finding the robust estimate of the parameters of a model, the accuracy of S (q) is increased with the decrease of q. When the outliers are less than 50% of the whole data, the difference for different values of q is small. However, when the data include more than 50% outliers, the difference for various values of q is large. This provides a useful cue for robust estimators, which use the median scale method to recovery the scale of inliers.

7.4.4.4 Performance of TSSE

From the experiments in this section, we can see the proposed TSSE is a very robust scale estimator, achieving better results than the other five methods. However, we must acknowledge that the accuracy of TSSE is related to the accuracy of kernel density estimation. In particular, for very few data points, the kernel density estimates will be less accurate.

We also note that, for the purposes of this chapter (only), we assume we know the parameters of the model: this is so we can concentrate on estimating the scale of the residuals. However, in practice, one cannot directly estimate the scale: the parameters of a model also need to be estimated. In the next chapter, we will propose a new robust estimator—Adaptive Scale Sample Consensus (ASSC) estimator, which can estimate the parameters and the scale simultaneously.

7.5 Conclusions

In this chapter, we show that scale estimation for data, involving multiple structures and high percentages of outliers, is as yet a relatively unsolved problem. This provides an important warning to the computer vision community: it is necessary to carefully choose a proper scale estimator.

We also, based on the mean shift algorithm, propose a simple but efficient mean shift valley technique, which can be used to find local valley. Furthermore, we propose a promising robust scale estimator (TSSE), based on the mean shift and the mean shift valley techniques. The experiments are compared with five other state-of-the-art robust scale estimators, and show the advantages of TSSE over these methods, especially, when the data involve a high percentage of outliers and the noise level of inliers is large. TSSE is a very general method and can be used to give an initial scale estimate for robust estimators such as M-estimators, etc. TSSE can also be used to provide an auxiliary estimate of scale (after the parameters of a model to fit have been found) as a component of *almost any* robust fitting method such as Hough Transform (Hough 1962), MDPE (chapter 4) and QMDPE (chapter 5), etc.

Chapter 8

Robust Adaptive-Scale Parametric Model Estimation for Computer Vision

8.1 Introduction

Robust model fitting essentially requires the application of two estimators. The first is an estimator for the values of the models parameters. The second is an estimator for the scale of the noise in the (inlier) data. In the previous chapter, we proposed a novel robust scale estimation technique: the Two-Step Scale estimator (TSSE) and shown the performance of TSSE despite heavily contaminated data, assuming that the correct parameters of a model are available. However, in many practical cases, the parameters of a model and the scale of inliers need to be estimated simultaneously. In this chapter, based on our previous work (TSSE), we will propose a novel robust estimator: Adaptive Scale Sample Consensus (ASSC) estimator. The ASSC estimator combines Random Sample Consensus (RANSAC) and TSSE. ASSC also uses a modified objective function that depends upon both the number of inliers and the corresponding scale.

Discontinuous signals (such as parallel lines/planes, step lines/planes, etc.) often appear in computer vision tasks. A lot of work has been done to investigate the behaviour of robust estimators for discontinuous signals, e.g., (Miller and Stewart 1996; Stewart 1997; Stewart

1999; Chen and Meer 2002). Discontinuous signals are hard to deal with: e.g., most robust estimators break down and yield a "bridge" between the two planes of one step signal. ASSC is very robust to discontinuous signals and data with multiple structures, being able to tolerate more than 80% outliers.

The main advantage of ASSC over RANSAC is that prior knowledge about the scale of inliers is not needed. ASSC can simultaneously estimate the parameters of a model and the scale of inliers belonging to that model. Experiments on synthetic data show that ASSC has better robustness to heavily corrupted data than Least Median Squares (LMedS), Residual Consensus (RESC), and Adaptive Least K'th order Squares (ALKS). We also apply ASSC to two fundamental computer vision tasks: range image segmentation and robust fundamental matrix estimation. Experiments show very promising results.

At the latter part of this chapter, we extend ASSC to produce ASRC (Adaptive-Scale Residual Consensus) estimator. ASRC scores a model based on both the residuals of inliers and the corresponding scale estimate determined by those inliers. The difference between ASRC and ASSC is: in ASSC, all inliers are treated as the same, i.e., each inlier contributes 1 to the object function of ASSC. However, in ASRC, the sizes of the residuals of inliers are influential.

The main contributions of this chapter can be summarized as follows:

- By employing TSSE in a RANSAC like procedure, we propose a highly robust estimator: Adaptive Scale Sample Consensus (ASSC) estimator.

- Experiments presented show that ASSC is highly robust to heavily corrupted data with multiple structures and discontinuities (empirically, ASSC can tolerate more than 80% outliers), and that it outperforms several competing methods.

- ASSC is successfully applied in two fundamental and important computer vision tasks: range image segmentation and fundamental matrix estimation. The experiments show promising results.

- We extend ASSC to produce ASRC which improves the objective function of ASSC by weighting each inlier differently according to the size of the residual of that inlier. Experiments showing the advantages of ASRC over ASSC.

This chapter is organized as follows: in section 8.2, the robust ASSC estimator is proposed. In section 8.3, experimental comparisons, using both 2D and 3D examples, are presented. We apply ASSC to range image segmentation in section 8.4 and fundamental matrix estimation in section 8.5. We introduce ASRC and we provide some experiments showing the advantages of ASRC over ASSC in section 8.6. We state our conclusions in section 8.7.

8.2 Adaptive Scale Sample Consensus (ASSC) Estimator Algorithm

In section 2.4.3 we reviewed the RANSAC estimator. The criterion used by RANSAC is to maximize the number of data points within the user-set error bound. Clearly, this bound is related to the scale of the inliers (*S*). Mathematically, the RANSAC estimate can be written as:

$$\hat{\theta} = \arg\max_{\hat{\theta}} n_{\hat{\theta}} \tag{8.1}$$

where $n_{\hat{\theta}}$ is the number of points whose absolute residual in the candidate parameter space is within the error bound (i.e., $|r| \le 2.5S$)); $\hat{\theta}$ is the estimated parameters from one of the randomly chosen p-subsets.

The error bound in RANSAC is crucial to the performance of RANSAC. Provided with a correct error bound of inliers, the RANSAC method can find a model even when data contain a large percentage of gross errors. However, when the error bound is wrongly given, RANSAC will totally break down even when outliers occupy relatively small percentages of the whole data (see section 4.4.4.2). Thus the major problem with

RANSAC is that the technique needs priori knowledge of the error bound of inliers, which is not available in most practical vision tasks.

In this section, we will, based upon our previously proposed TSSE, propose an adaptive-scale robust estimator — ASSC. We assume that when a model is correctly found, two criteria should be satisfied:

- The number of data points (n_θ) near or on the model should be as large as possible;
- The residuals of the inliers should be as small as possible. Correspondingly, the scale (S_θ) should be as small as possible.

We therefore define our objective function as:

$$\hat{\theta} = \arg\max_{\hat{\theta}}(n_{\hat{\theta}} / S_{\hat{\theta}}) \qquad (8.2)$$

Note: when the estimate of the scale is fixed, equation (8.2) is another form of RANSAC with the score n_θ scaled by $1/S$ (i.e, a fixed constant for all p-subsets), yielding the same results as RANSAC. ASSC is more reasonable than RANSAC because the scale is estimated for each candidate fit, in addition to the fact that it no longer requires a user defined error-bound.

The ASSC algorithm is as follows:

(1) Randomly choose one p-subset from the data points, estimate the model parameters using the p-subset, and calculate the ordered absolute residuals of all data points.

(2) Choose the bandwidth by equation 6.6 and calculate an initial scale by a robust k scale estimator (equation 7.12) using q=0.2.

(3) Apply TSSE to the absolute sorted residuals to estimate the scale of inliers. At the same time, the probability density at the local peak $\hat{f}(peak)$ and local valley $\hat{f}(valley)$ are obtained by equation (4.1).

(4) Validate the valley. Let $\hat{f}(valley)/\hat{f}(peak) = \lambda$ (where $1>\lambda \geq 0$). Bεcause the inliers are assumed to have a Gaussian-like distribution, the valley is not sufficiently deep when λ is too large (say, 0.8). If the valley is sufficiently deep, go to step (5); otherwise go to step (1).

(5) Calculate the score, i.e., the objective function of the ASSC estimator.

(6) Repeat step (1) to step (5) many times. Finally, output the parameters and the scale S_1 with the highest score.

Because the robust k scale estimator is biased for data with multiple structures, the final scale of inliers S_2 should be refined when the scale S_1 obtained by TSSE is used. In order to improve the statistical efficiency, a weighted least square procedure ((Rousseeuw and Leroy 1987), p.202) is carried out after finding the initial fit.

Instead of estimating the fit involving the absolute majority in the data set, the ASSC estimator finds a fit having a relative majority of the data points. This makes it possible, in practice, for ASSC to obtain a high robustness so that it can tolerate more than 50% outliers. Indeed, the experiments in the next section show that the ASSC estimator is a very robust estimator for data with multiple structures and a high percentage of outliers.

8.3 Experiments with Data Containing Multiple Structures

In this section, both 2D and 3D examples are given. The results of the proposed method are compared with those of three other popular methods: LMedS, RESC, and ALKS. All of the four methods use the random sampling scheme ..rat is also at the heart of our method. Note: unlike the experiments in section 7.4, ḥ re *we do not (of course) assume any knowledge of the parameters of the models in the data. Nor are we aiming to find any particular structure. Due to the random sampling used, the methods will possibly return a different structure on different runs – however, they will generally find the largest structure most often (if one dominates in size).*

8.3.1 2D Examples

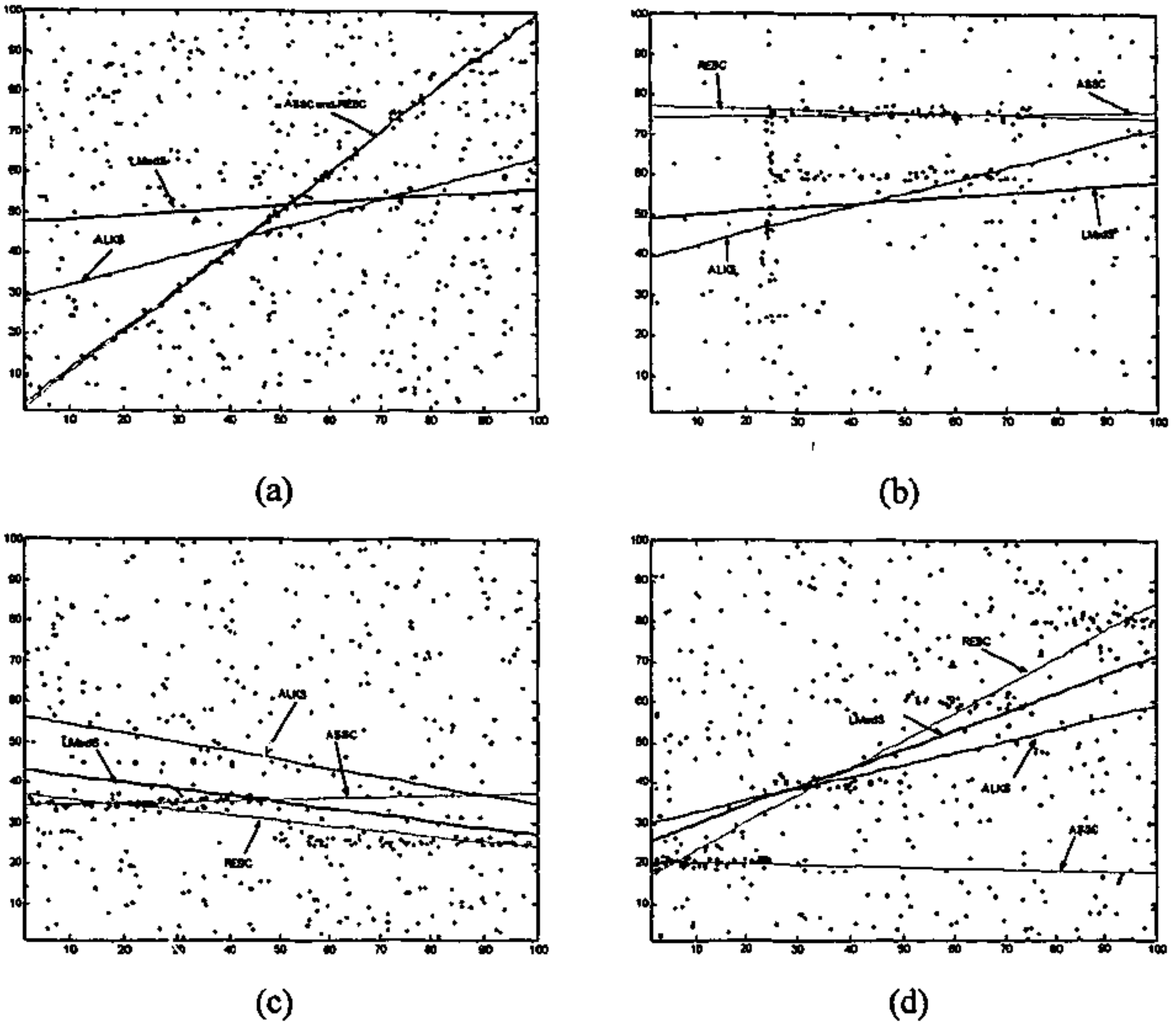

(a)

(b)

(c)

(d)

Figure 8.1: Comparing the performance of four methods: (a) fitting a line with a total of 90% outliers; (b) fitting three lines with a total of 88% outliers; (c) fitting a step with a total of 85% outliers; (d) fitting three steps with a total of 89% outliers.

We generated four kinds of data (a line, three lines, a step, and three steps), each with a total of 500 data points. The signals were corrupted by Gaussian noise with zero mean and standard variance σ. Among the 500 data points, α data points were randomly distributed in the range of (0, 100). The i'th structure has n_i data points.

(a) One line: x:(0-100), y=x, n_1=50; α=450; σ=0.8.

(b) Three lines: x:(25-75), y=75, n_1=60; x:(25-75), y=60, n_2=50; x=25, y:(20-75), n_3=40; α=350; σ=1.0.

(c) One step: x:(0-50), y=35, n_1=75; x:(50-100), y=25, n_2=55; α=370; σ=1.1.

(d) Three steps: x:(0-25), y=20, n_1=55; x:(25-50), y=40, n_2=30; x:(50-75), y=60, n_3=30; x:(75-100), y=80, n_4=30; α=355; σ=1.0.

In Figure 8.1, we can see that the proposed ASSC method yields the best results among the four methods, correctly fitting all four signals. Because LMedS has a 50% breakdown point, it failed to fit all the four signals. Although ALKS can tolerate more than 50% outliers, it failed in all four cases with very high outlier content. RESC gave better results than LMedS and ALKS. It succeeded in two cases (one-line and three-line signals) even when the data involved more than 88% outliers. However, RESC failed to fit two signals (Figure 8.1 (c) and (d)).

It should be emphasized that both the bandwidth choice and the scale estimation in the proposed ASSC method are data-driven. No priori knowledge about the bandwidth and the scale is necessary in the proposed method. This is a great improvement over the traditional RANSAC method where the user must set a priori scale-related error bound.

8.3.2 3D Examples

Two synthetic 3D signals were generated. Each contained 500 data points and three planar structures. Each plane contains 100 points corrupted by Gaussian noise with standard variance σ; 200 points are randomly distributed in a region including all three structures. A planar equation can be written as $Z=AX+BY+C$, and the residual of the point at (X_i, Y_i, Z_i) is $r_i=Z_i-AX_i-BY_i-C$. $(A, B, C; \sigma)$ are the parameters to estimate.

In contrast to the section 8.3.1, we now attempt to find *all* structures in the data. In order to extract all planes, we:

(1) Apply the robust estimators to the data set and estimate the parameters and scale of a plane;

(2) Extract the inliers and remove them from the data set;

(3) Repeat step 1 to 2 until all planes are extracted.

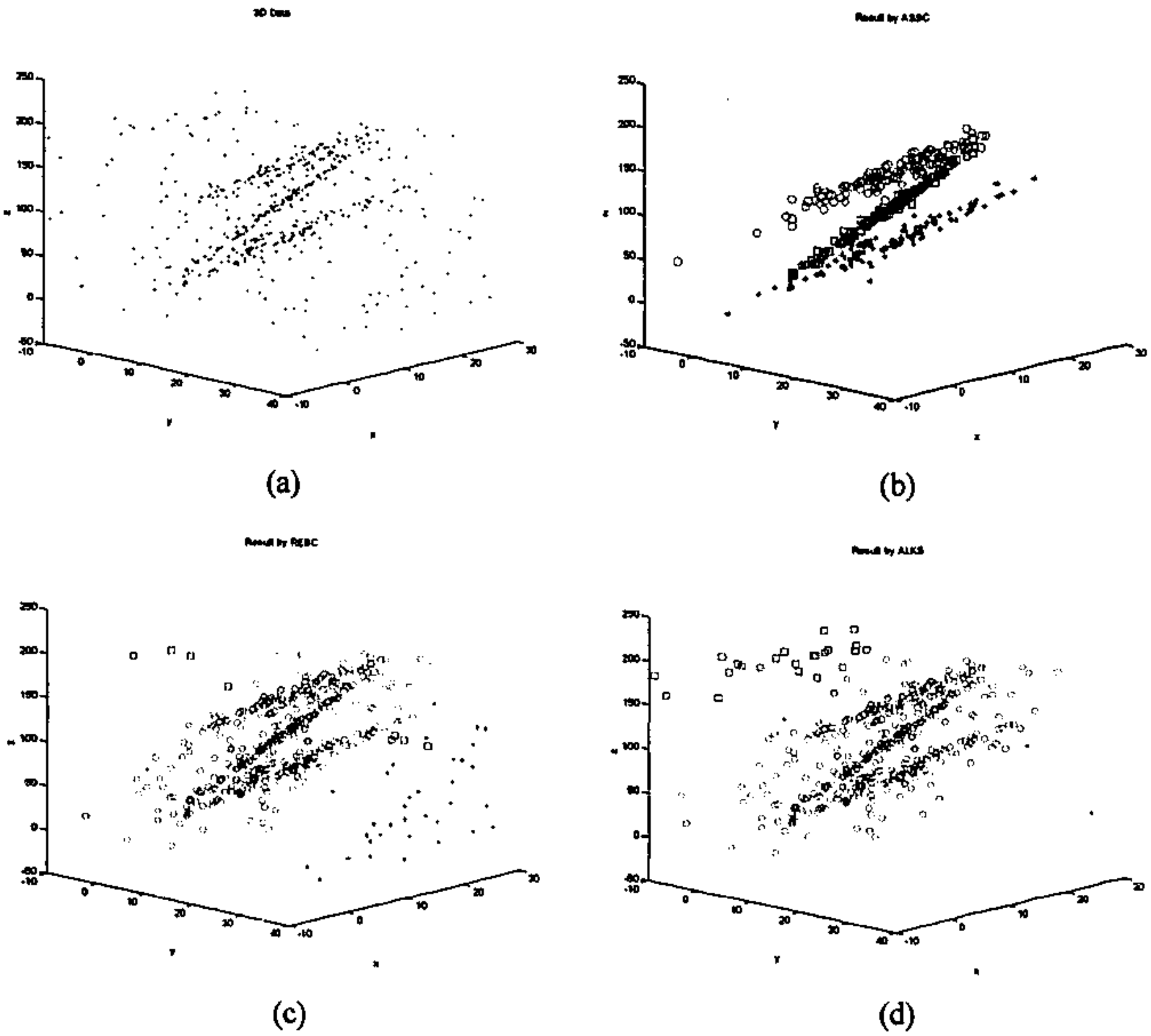

(a) (b) (c) (d)

Figure 8.2: First experiment for 3D multiple-structure data: (a) the 3D data; the results by (b) the ASSC method; (c) by RESC; and (d) by ALKS.

	Plane A	Plane B	Plane C
True values	(3.0, 5.0, 0.0; 3.0)	(2.0, 3.0, 0.0; 3.0)	(2.0, 3.0, 80.0; 3.0)
ASSC	(3.02, 4.86, 1.66; 3.14)	(2.09, 2.99, 0.56, 3.18)	(1.79, 2.98, 83.25, 3.78)
RESC	(3.69, 5.20, -7.94, 36.94)	(4.89, 13.82, -528.06,51.62) and (-2.88,-1.48, 189.62,0.47)	
ALKS	(2.74, 5.08, 1.63; 44.37)	(-7.20, 0.91,198.1; 0.007) and (-0.59,1.82,194.06; 14.34)	
LMedS	(1.22, 3.50,30.36, 51.50), (-0.11, -3.98, 142.80; 31.31) and (-9.59, -1.66,251.24;0.0)		

Table 8.1: Result of the estimates of the parameters (A, B, C; σ) provided by each of the robust estimators applied to the data in Figure 8.2.

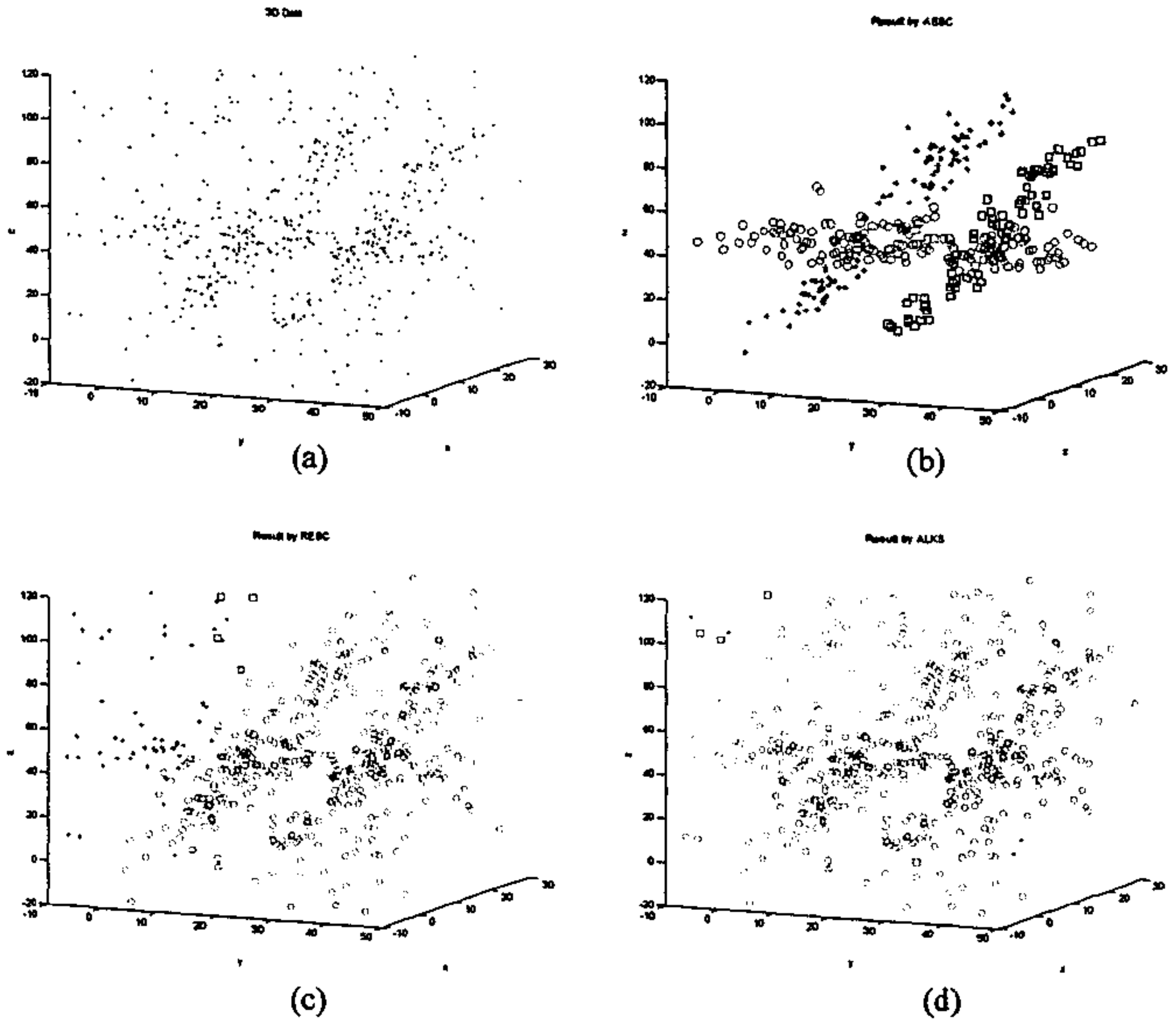

(a) (b)

(c) (d)

Figure 8.3: Second experiment for 3D multiple-structure data: (a) the 3D data; the results by (b) the proposed method; (c) by RESC; (d) and by ALKS.

	Plane A	Plane B	Plane C
True values	(0.0, 3.0, -60.0; 3.0)	(0.0, 3.0, 0.0; 3.0)	(0.0, 0.0, 40.0; 3.0)
ASSC	(0.00, 2.98, -60.68, 2.11)	(0.18, 2.93, 0.18, 3.90)	(0.08, 0.03, 38.26; 3.88)
RESC	(0.51, 3.04,-67.29;36.40)	(6.02,-34.00,-197.51;101.1) and (0.35, -3.85, 122.91, 0.02)	
ALKS	(-1.29, 1.03,14.35; 30.05), (-1.07, -2.07,84.31; 0.01) and (1.85, -11.19, 36.97; 0.08)		
LMedS	(0.25, 0.61,24.50, 27.06), (-0.04, -0.19, 92.27; 9.52) and (-0.12, -0.60,92.19; 6.89)		

Table 8.2: Result of the estimates of the parameters (A, B, C; σ) provided by each of the robust estimators applied to the data in Figure 8.3.

The red circles constitute the first plane extracted; the green stars the second plane extracted; and the blue squares the third extracted plane. The results are shown in Figure 8.2, Table 8.1; Figure 8.3 and Table 8.2 (the results of LMedS, which completely broke down for these 3D data sets, are only given in Table 8.1 and Table 8.2). Note for RESC, we use the revised form in equation (7.6) instead of equation (7.5) for scale estimate.

Similarly, in the second experiment (Figure 8.3 and Table 8.2), LMedS and ALKS completely broke down for the heavily corrupted data with multiple structures. RESC, although it correctly fitted the first plane, wrongly estimated the scale of the inliers to the plane. RESC wrongly fitted the second and the third planes. Only the proposed method correctly fitted all three planes (Figure 8.3 (b)) and estimated the corresponding scale for each plane.

The proposed method is computationally efficient. We perform the proposed method in MATLAB code with TSSE in Mex. When *m* is set as 500, the proposed method takes about 1.5 second for the 2D examples and about 2.5 seconds for the 3D examples in an AMD 800MHz personal computer.

8.3.3 The Breakdown Plot of the Four Methods

In this subsection, we perform an experiment to draw the breakdown plot of each method (similar to the experiment reported in (Yu, Bui et al. 1994). However, the data that we use is more complicated because it contains two types of outliers: clustered outliers and randomly distributed outliers).

We generate one plane signal with Gaussian noise having unit standard variance. Both clustered outliers and randomly distributed outliers are added to the data. The clustered outliers have 100 data points and are distributed within a cube. The randomly distributed outliers contain the plane signal and clustered outliers. The number of inliers is decreased from 900 to 100. At the same time, the number of randomly distributed outliers is increased from 0 to 750 so that the total number of the data points is kept 1000. Thus, the outliers occupy from 10% to 90% outliers. Examples for data with 20% and 70% outliers are shown in Figure 8.4 (a) and (b) to illustrate the distributions of the inliers and outliers.

If an estimator is robust enough to outliers, it can resist the influence of both clustered outliers and randomly distributed outliers even when the outliers occupy more than 50% of the data. In order to increase the stability of the result, we perform the experiments 20 times, using different random sampling seeds, for each data set involving different percentage of outliers (10% to 90%). An averaged result is show in Figure 8.4 (c-e).

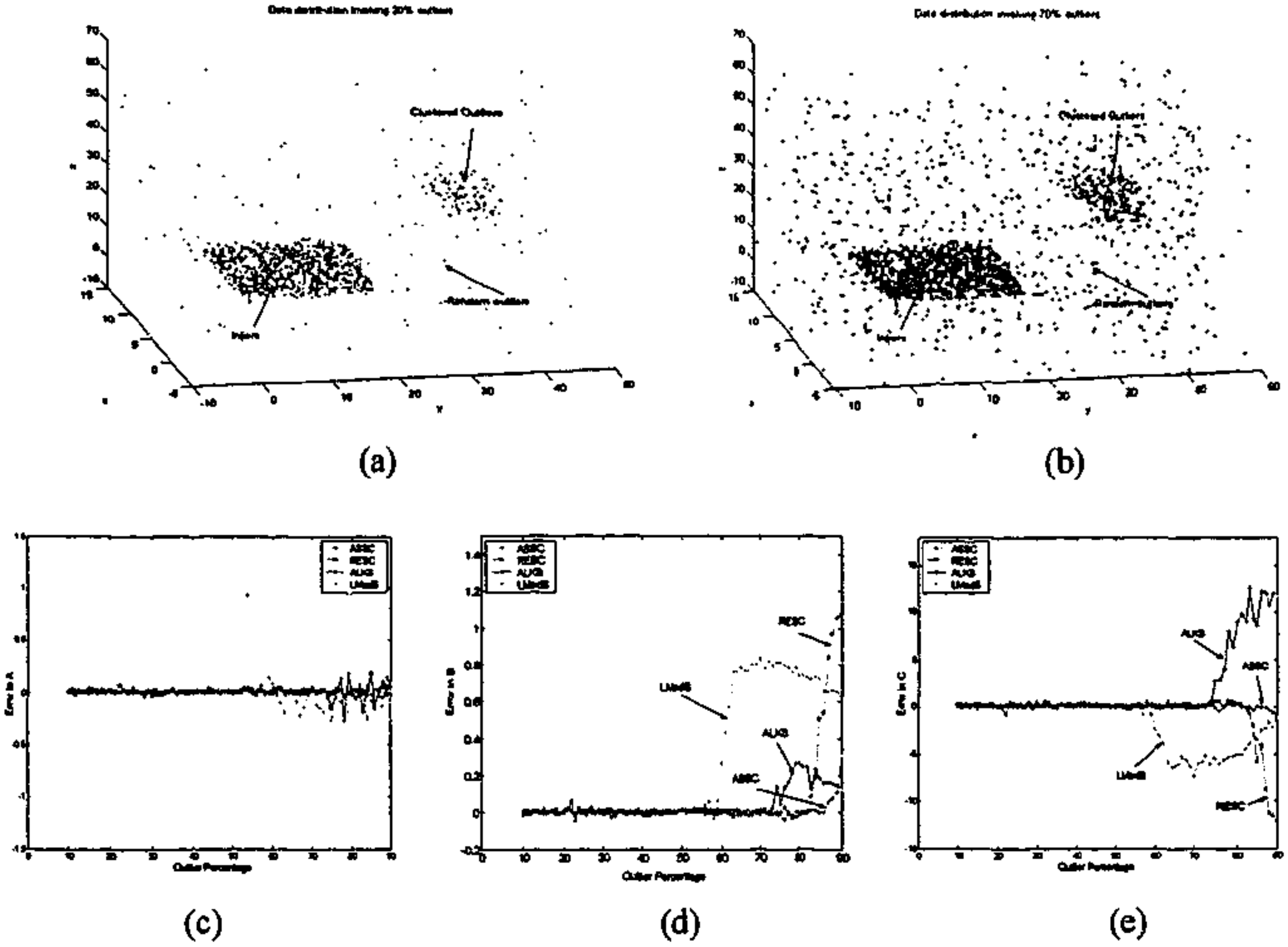

(a)

(b)

(c)

(d)

(e)

Figure 8.4: Breakdown plot of the four methods: (a) example of the data with 20% outliers; (b) example of the data with 80% outliers; (c) the error in the estimate of parameter A, (d) in parameter B, and (e) in parameter C.

From Figure 8.4 (c-e), we can see that our method obtains the best result. Because the LMedS has only 50% breakdown point, it broke down when outliers occupied more than 50% of the data (approximately). ALKS broke down when outliers had about 75%. RESC began to break down when outliers had more than 83% of the whole data; In contrast, the ASSC estimator is the most robust to outliers. It began to breakdown at 89% outliers. In fact, when inliers are about (or less than) 10% of the data, the assumption that inliers should occupy a relative majority of the data is violated. Bridging between the inliers and the clustered outliers tends to yield a higher score. Other robust estimators also suffer from the same problem.

8.3.4 Influence of the Noise Level of Inliers on the Results of Robust Fitting

Next, we will investigate the influence of the noise level of inliers on the results of the chosen four robust fitting methods. We use the signal shown in Figure 8.4 (b) with 70% outliers. However, we change the standard variance of the plane signal from 0.1 to 3, with increment 0.1.

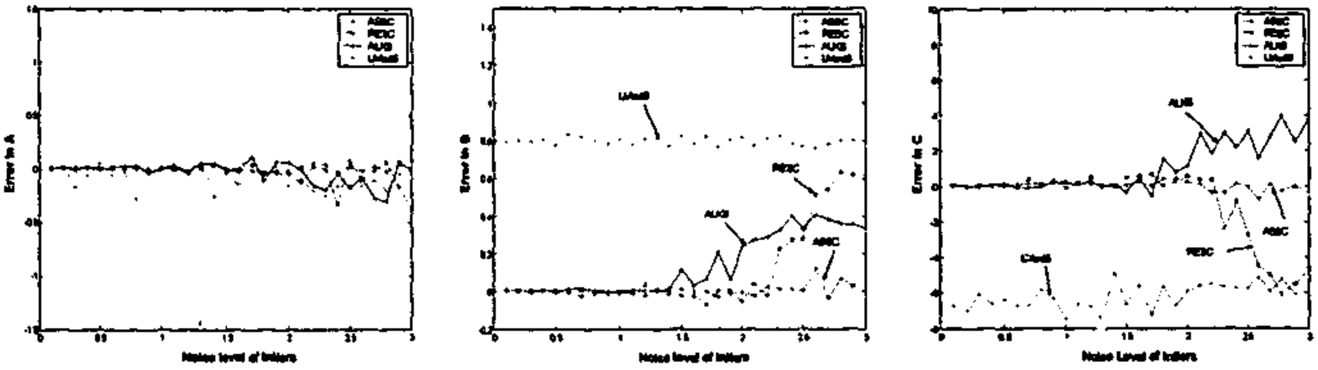

(a) (b) (c)

Figure 8.5: The influence of the noise level of inliers on the results of the four methods: plots of the error in the parameters *A* (a), *B* (b) and *C* (c) for different noise level.

Figure 8.5 shows that LMedS broke down first. This is because that LMedS cannot resist the influence of outliers when the outliers occupy more than a half of the data points. ALKS, RESC, and ASSC estimators all can tolerate more than 50% outliers. However, among these three robust estimators, ALKS broke down first. It began to break down when the noise level of inliers is increased to 1.7. RESC is more robust than ALKS: it began to break down when the noise level of inliers is increased to 2.3. The ASSC estimator shows the best achievement. Even when the noise level is increased to 3.0, the ASSC estimator did not break down yet.

8.3.5 Influence of the Relative Height of Discontinuous Signals

In this subsection, we will investigate the influence of the relative height of discontinuous signals on the performance of the four methods.

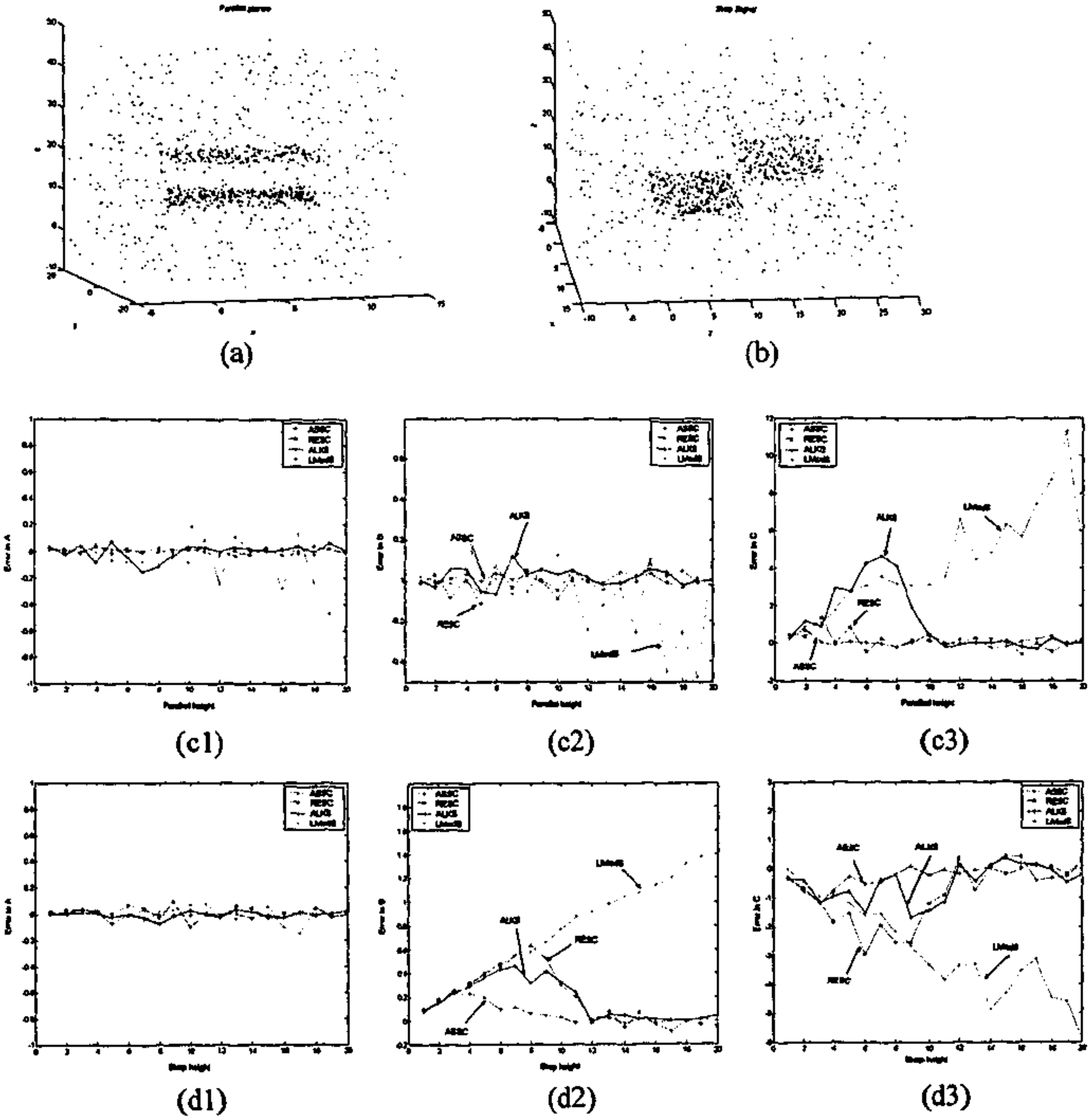

(a)

(b)

(c1)

(c2)

(c3)

(d1)

(d2)

(d3)

Figure 8.6: The influence of the relative height of discontinuous signals on the results of the four methods: (a) two parallel planes; (b) one step signal; (c1-c3) the results for the two parallel planes; (d1-d3) the results for the step signal.

We generate two discontinuous signals: one containing two parallel planes and one containing one-step planes. The signals have unit variance. Randomly distributed outliers covering the regions of the signals are added to the signals. Among the total 1000 data points, there are 20% pseudo-outliers and 50% random outliers. The relative height is increased from 1 to 20. Figure 8.6 (a) and (b) shows examples of the data distributions of the two signals with relative height 10. The averaged results (over 20 repetitions) obtained by the four robust estimators are shown in Figure 8.6 (c1-c3) and (d1-d3).

From Figure 8.6, we can see the tendency to bridge becomes stronger as the step decreases. LMedS shows the worst results among the four robust estimators. For the rest three estimators: ASSC, ALKS, and RESC, from Figure 8.6 (c1-c3) and (d1-d3), we can see that:

- For the parallel plane signal, the results by ALKS are affected most by the small step. RESC shows better result than ALKS. However, ASSC shows the best result.
- For the step signal, when the step height is small, all of these three estimators are affected. When the step height is increased from small to large, all of the three estimators show robustness to the signal. However, ASSC achieves the best results for small step height signals.

In next sections, we will apply the ASSC estimator to more "real world" computer vision tasks: range image segmentation and fundamental matrix estimation.

8.4 ASSC for Range Image Segmentation

The range image segmentation algorithm that we present here is based on the just introduced ASSC estimator. Although MDPE in chapter 4, has similar performance to ASSC, MDPE only outputs the parameters of the model as results. An auxiliary scale estimator is required to provide an estimate of the scale of inliers. ASSC, however, does not need any auxiliary scale estimator at the post-processing stage. It can estimate the scale of inliers during the process of estimating the parameters of a model.

8.4.1 The Algorithm of ASSC-Based Range Image Segmentation

We employ a hierarchical structure, similar to that in chapter 5. We begin with bottom level containing 64x64 pixels that are obtained by using regular sampling on the original 512x512 image. In each level of the hierarchy, we:

(1) Apply the ASSC estimator to obtain the parameters of plane and the scale of inliers.

(2) The inliers (in the top hierarchy) corresponding to the estimated parameters of plane and scale are then identified. If the number of inliers is less than a threshold, go to step (7). This step is different from the step (4) in section 5.4.2 in that the parameters of plane and the corresponding scale of inliers are obtained simultaneously in ASSC; while QMDPE needs an auxiliary scale estimator to obtain the scale of inliers.

(3) Use normal information to validate the inliers obtained in step (2). This step is similar to the step (5) in section 5.4.2. If the number of the validated inliers is small, go to step (7).

(4) Fill in the holes inside the maximum connected component from the validated inliers. The holes may appear because of sensor noise or because some points have large residuals and are beyond the range that is related to the estimated scale.

(5) Assign label to the points corresponding to the connected component from step (4) and remove the points from the data set that will be further processed. This happens in the top hierarchy.

(6) If a point is unlabelled and it is not a jump edge point, the point will be used as a "left-over" point. After collecting all these points, use the connected component algorithm to get the maximum connected component. If the number data points of the maximum connected component of "left-over" points is smaller than a threshold, go to step (7); otherwise, get the data for the current hierarchical level by regularly sampling on the maximum connected component obtained in this step, then go to step (1).

(7) Terminate the processing in the current level of the hierarchy and go to the higher-level hierarchy until the top of the hierarchy.

8.4.2 Experiments on Range Image Segmentation

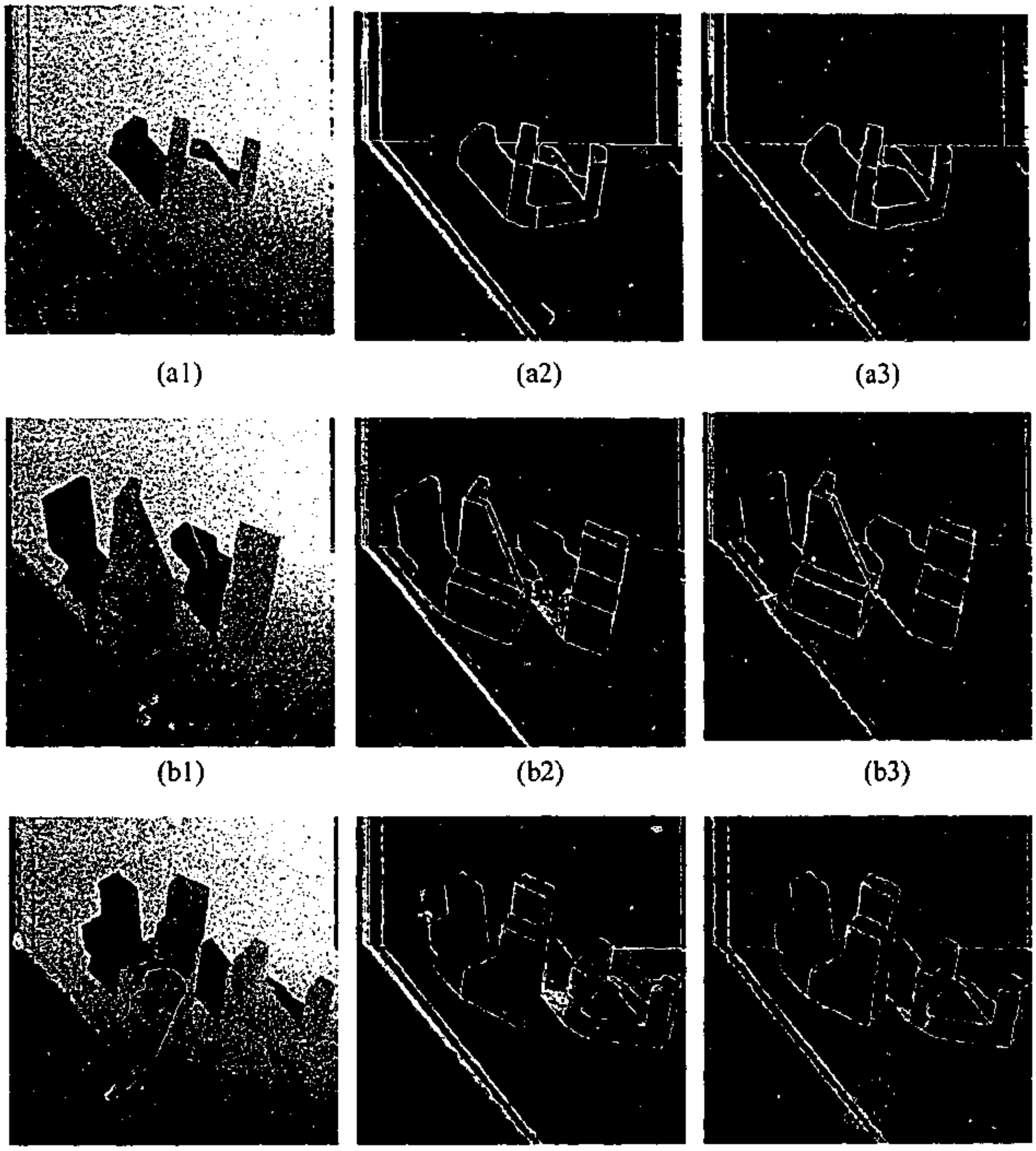

Figure 8.7: Segmentation of ABW range images from the USF database. (a1, b1, c1) Range image with 26214 random noise points; (a2, b2, c2) The ground truth results for the corresponding range images without adding random noise; (a3, b3.c3) Segmentation result by the proposed algorithm.

To show the performance of the proposed ASSC-based range image segmentation algorithm, we do experiments similar to those in section 5.5 by adding 26214 random noise points to the range images taken from the USF ABW range image database (test 16, test 7 and train 5).

As shown in Figure 8.7, all of the main surfaces (structures) were recovere'l by our method. Only a slight distortion appeared on some boundaries of neighbouring surfaces. Similar slight distortion also appears in the experimental results (by QMDPE) in chapter 5. This is because of the sensor noise and the limited accuracy of the estimated normal at each range point. Generally speaking, the more accurate the range data are, and the more accurate the estimated normal at range points is, the less the distortion is.

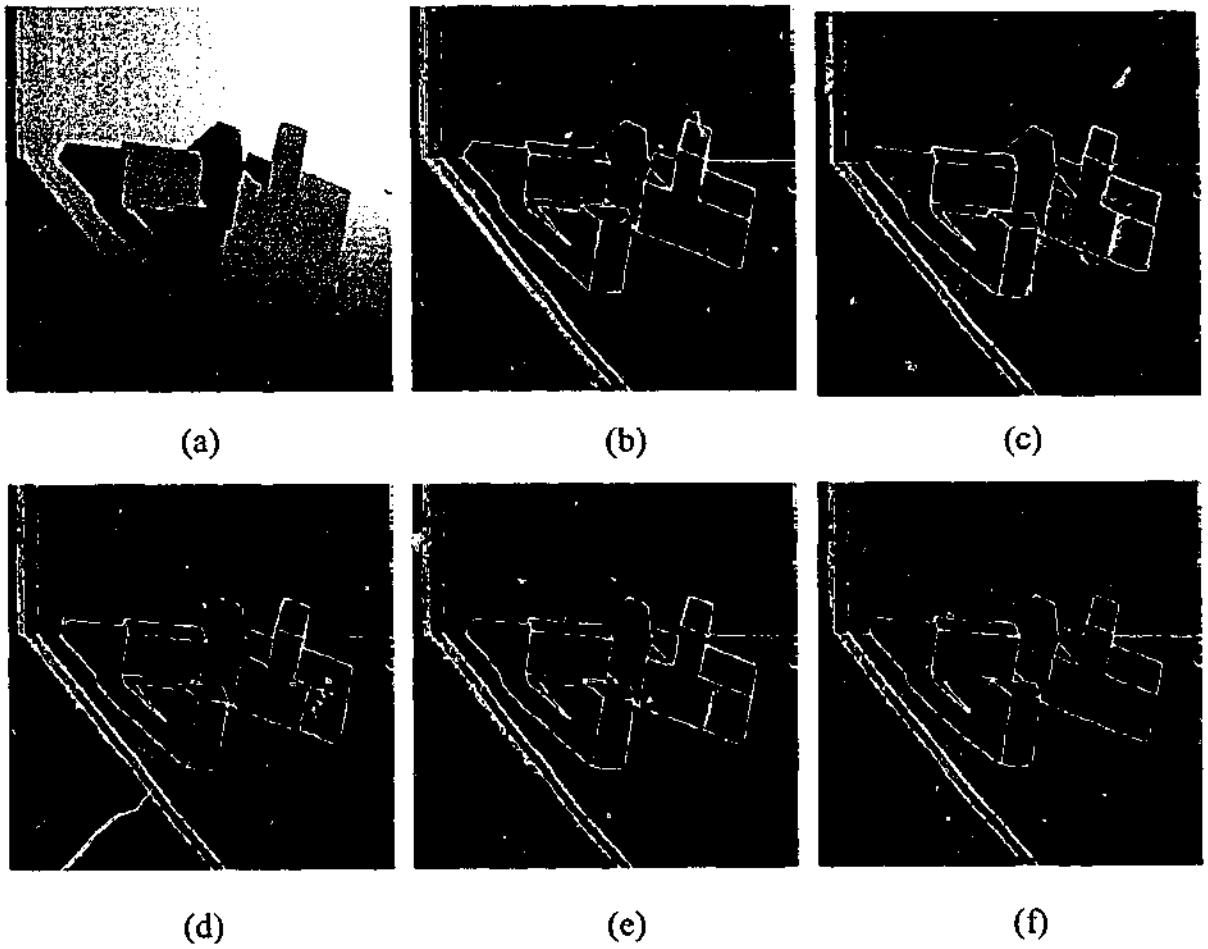

Figure 8.8: Comparison of the segmentation results for ABW range image (test 3) from the USF range image database. (a) Range image; (b) The result of ground truth; (c) The result by the USF;(d) The result by the WSU; (e) The result by the UE; (f) The result by the proposed method.

We also compare our results with those of the University of South Florida (USF), Washington State University (WSU), and the University of Edinburgh (UE) (Hoover, Jean-Baptiste et al. 1996) methods. Figure 8.8(c-f) and Figure 8.9 (c-f) show the results obtained by the four methods. From Figure 8.8 (c) and Figure 8.9 (c), we can see that the USF's results contained many noisy points. In both Figure 8.8 (d) and Figure 8.9 (d), the WSU segmenter missed one surface. The WSU segmenter also over segmented one surface in Figure 8.8 (d). Some boundaries on the junction of the segmented patch by the USF and WSU in Figure 8.9 (c) were relatively seriously distorted. The UE shows relatively better results than the USF and the WSU. However, some estimated surfaces are still noisy (see Figure 8.8 (e) and Figure 8.9 (e)). Compared with the other three methods, the proposed method achieved the best results. All surfaces are recovered and the segmented surfaces are relatively "clean". The edges of the segmented patches were reasonably good.

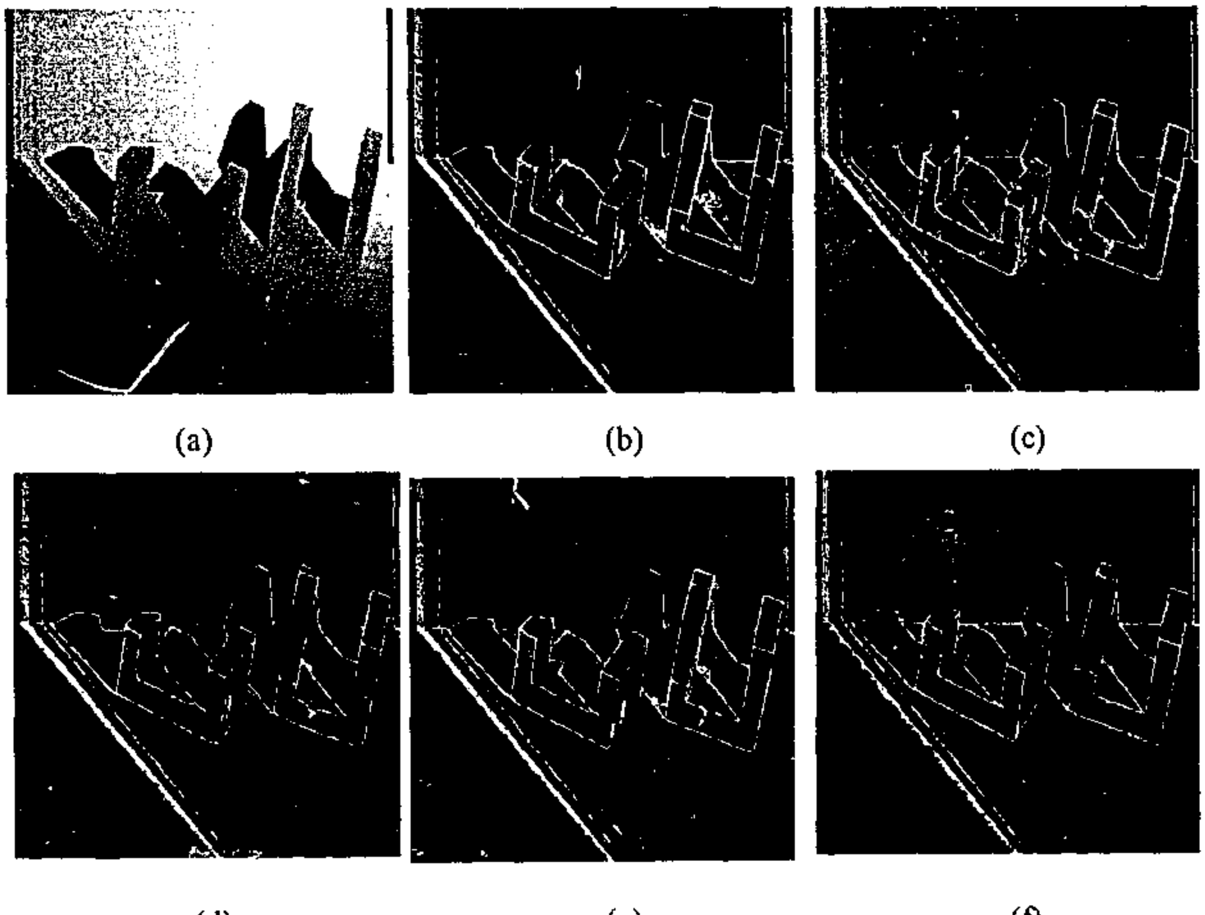
(a) (b) (c)

(d) (e) (f)

Figure 8.9: Comparison of the segmentation results for ABW range image (test 13) from the USF range image database. (a) Range image; (b) The result of ground truth; (c) The result by the USF; (d) The result by the WSU; (e) The result by the UE; (f) The result by the proposed method.

8.5 ASSC for Fundamental Matrix Estimation

8.5.1 Background of Fundamental Matrix Estimation

The fundamental matrix provides some constraints (related to epipolar geometry, projectivity, etc.) between corresponding points in multiple views. The estimation of the fundamental matrix is important for several problems: matching, recovering of structure, motion segmentation, etc.(Torr and Zisserman 2000). Since there possibly are mismatched pairs of points in the data, traditional method such as least squares estimator cannot yield accurate results. Even worse, the least squares estimator can breakdown. Robust estimators such as M-estimators, LMedS, RANSAC, MSAC and MLESAC have been applied to estimate the fundamental matrix to improve the accuracy of the results (Torr and Murray 1997).

Let {*x*$x_{i,}$} and {x_i'} (for *i*=1,...,*n*) to be a set of matched homogeneous image points viewed in image 1 and image 2 respectively. We have the following constraints for the fundamental matrix *F*:

$$x_i^{'T} F x_i = 0 \; and \; \det[F] = 0 \tag{8.3}$$

We employ the 7-point algorithm (Torr and Murray 1999) to solve for candidate fits using Sampson distance for the residual to a fitted fundamental matrix. For the *i*'th correspondence, the residual r_i using Simpson distance is:

$$r_i = \frac{k_i}{\left(k_x^2 + k_y^2 + k_{x'}^2 + k_{y'}^2\right)^{1/2}} \tag{8.4}$$

$$where\; k_i = f_1 x_i^{'} x_i + f_2 x_i^{'} y_i + f_3 x_i^{'} \varsigma + f_4 y_i^{'} x_i + f_5 y_i^{'} y_i + f_6 y_i^{'} \varsigma + f_7 x_i \varsigma + f_8 y_i \varsigma + f_9 \varsigma^2$$

8.5.2 The Experiments on Fundamental Matrix Estimation

First, we generated 300 matches including 120 point pairs of inliers with unit Gaussian variance and 160 point pairs of random outliers. In practice, the scale of inliers is not available. Thus, for RANSAC and MSAC, the median scale estimator, as recommended in (Torr and Murray 1999), is used to yield an initial scale estimate. The number of random samples is set to 10000. The experiment was repeated 30 times and the averaged values are shown in Table 8.3 . From Table 8.3, we can see that our method yields the best result.

	% of inliers correctly classified	% of outliers correctly classified	Standard variance of inliers
Ground Truth	100.00	100.00	1.0
ASSC	96.08	98.43	1.4279
MSAC	100.00	60.48	75.2288
RANSAC	100.00	0.56	176.0950
LMedS	100.00	61.91	65.1563

Table 8.3: An experimental comparison for data with 60% outliers.

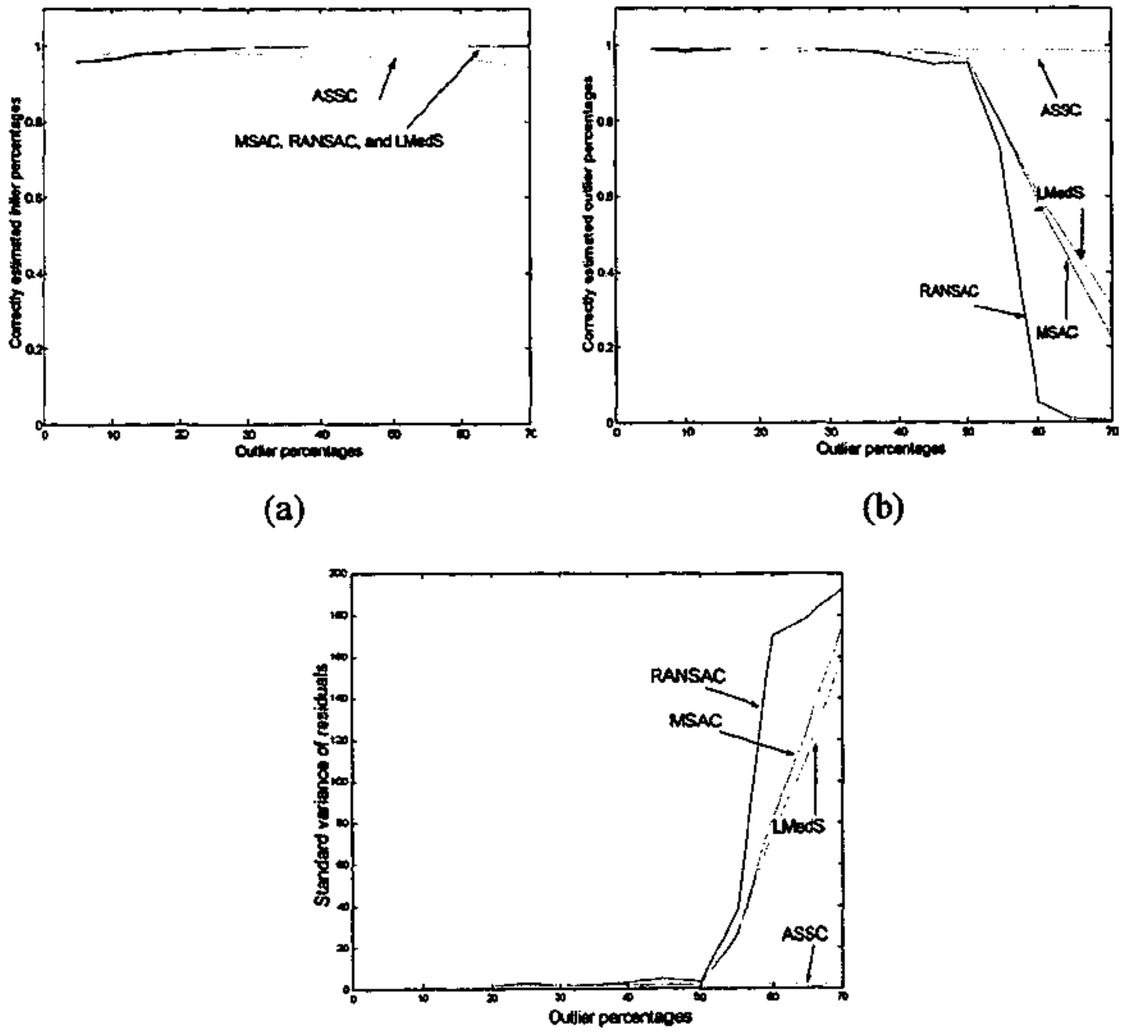

(a)

(b)

(c)

Figure 8.10: A comparison of correctly identified percentage of inliers (a), outliers (b), and the comparison of standard variance of residuals of inliers (c).

Next, we draw the *breakdown plot* of the four methods. Among the total 300 correspondences, the percentage of outliers is increased from 5% to 70% in increments of 5%. The experiments were repeated 100 times for each percentage of outliers. If a method is robust enough, it should resist the influence of outliers and the correctly identified percentages of inliers should be around 95% (T is set 1.96 in equation 7.1) and the standard variance of inliers should be near to 1.0 regardless of the percentages of outliers actually in the data. We set the number of random samples, m, to be high enough to ensure a high probability of success.

From Figure 8.10 we can see that MSAC, RANSAC, and LMedS all break down when the data involve more than 50% outliers. The standard variance of inliers identified by ASSC is the smallest of all of the estimates when the percentage of outliers is higher than 50%. Note: ASSC succeeds to find the inliers and outliers even when the outliers occupied 70% of the whole data.

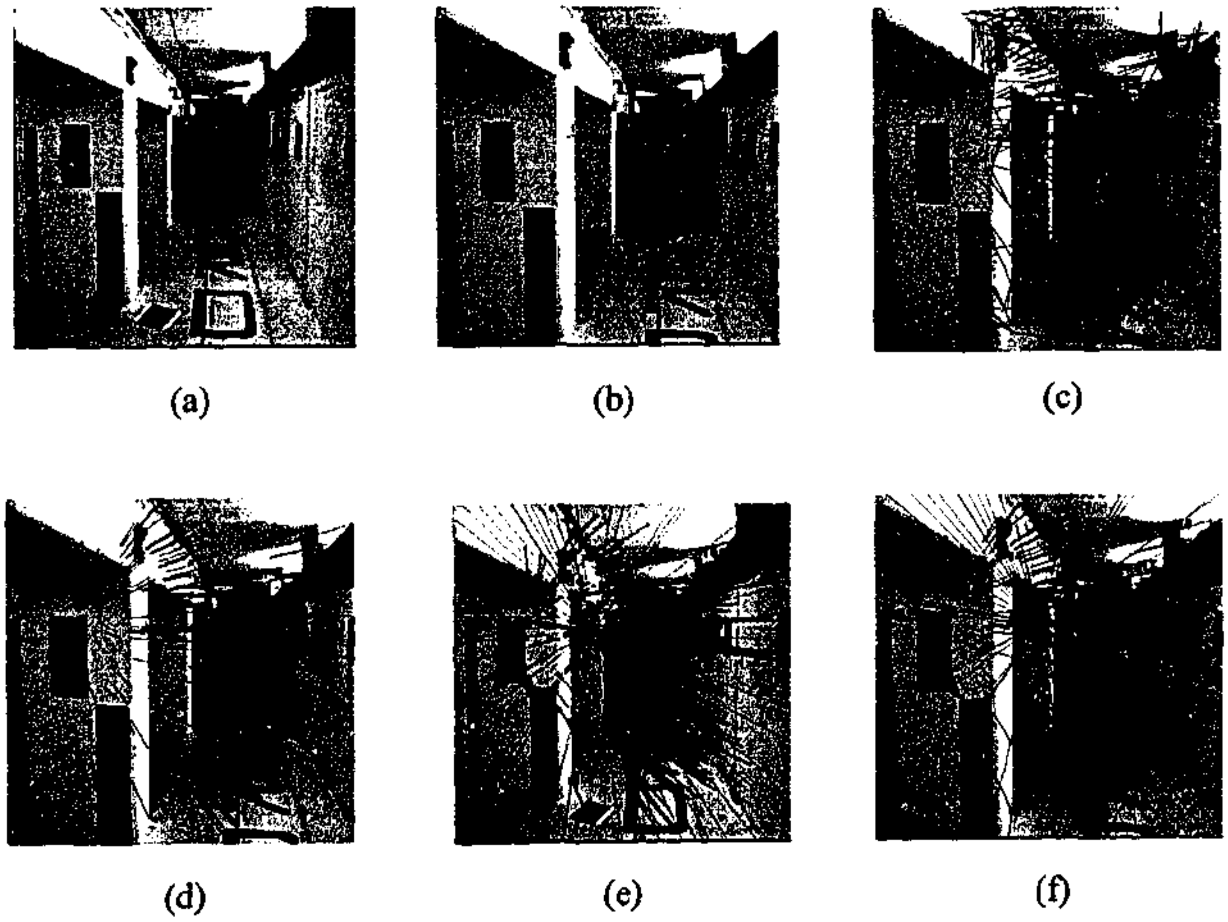
(a) (b) (c)

(d) (e) (f)

Figure 8.11: (a) (b) image pair (c) matches (d) inliers by ASSC; (e) (f) epipolar geometry.

	Number of inliers (i.e., matched correspondences)	Mean error of inliers	Standard variance of inliers
ASSC	201	0.0274	0.6103
MSAC	391	-1.3841	10.0091
RANSAC	392	-1.0887	10.1394
LMedS	372	-1.4921	9.5463

Table 8.4: Experimental results on two frames of the Corridor sequence.

To conclude, we apply the proposed method on real image frames. Two frames of the Corridor sequence (bt.003 and bt.006), which can be obtained from http://www.robots.ox.ac.uk/~vgg/data/ (Figure 8.11 (a) and (b)). Figure 8.11 (c) shows the matches involving 500 point pairs in total. The inliers (201 correspondences) obtained by the proposed method are shown in Figure 8.11 (d). The epipolar lines (we draw 30 of the epipolar lines) and epipole using the estimated fundamental matrix by ASSC are shown in Figure 8.11 (e) and (f). We can see that the proposed method achieves a good result. Because the camera matrices of the two frames are available, we can obtain the ground truth fundamental matrix and thus evaluate the errors. From Table 8.4, we can see that ASSC performs the best among the four methods.

8.6 A Modified ASSC (ASRC)

8.6.1 Adaptive-Scale Residual Consensus (ASRC)

In the previous experiments, we have seen the robustness of ASSC to outliers and multiple structures. However, all inliers in ASSC (equation 8.2), are treated as the same, i.e., each inlier contributes equivalently to the objective function of ASSC. Actually, inliers can have different influence on the results if we take into account the sizes of the residuals of inliers. Thus, we modify ASSC to yield a robust adaptive-scale residual consensus (ASRC) estimator.

$$\hat{\theta} = \arg\max_{\hat{\theta}}\left(\frac{\sum_{i=1}^{n_{\hat{\theta}}}(1-\left|r_{i\hat{\theta}} /(S_{\hat{\theta}}T)\right|}{S_{\hat{\theta}}}\right) \tag{8.5}$$

where $n_{\hat{\theta}}$ is the number of inliers which satisfies equation (7.1) for the fitted $\hat{\theta}$.

From equation (8.5), we can see that when the residual of a data point is zero, the point contributes 1 to the objective function of ASRC; when the residual of a data point is equal or larger than $S_{\hat{\theta}}T$, it does not contribute anything to the objective function of ASRC.

8.6.2 Experiments

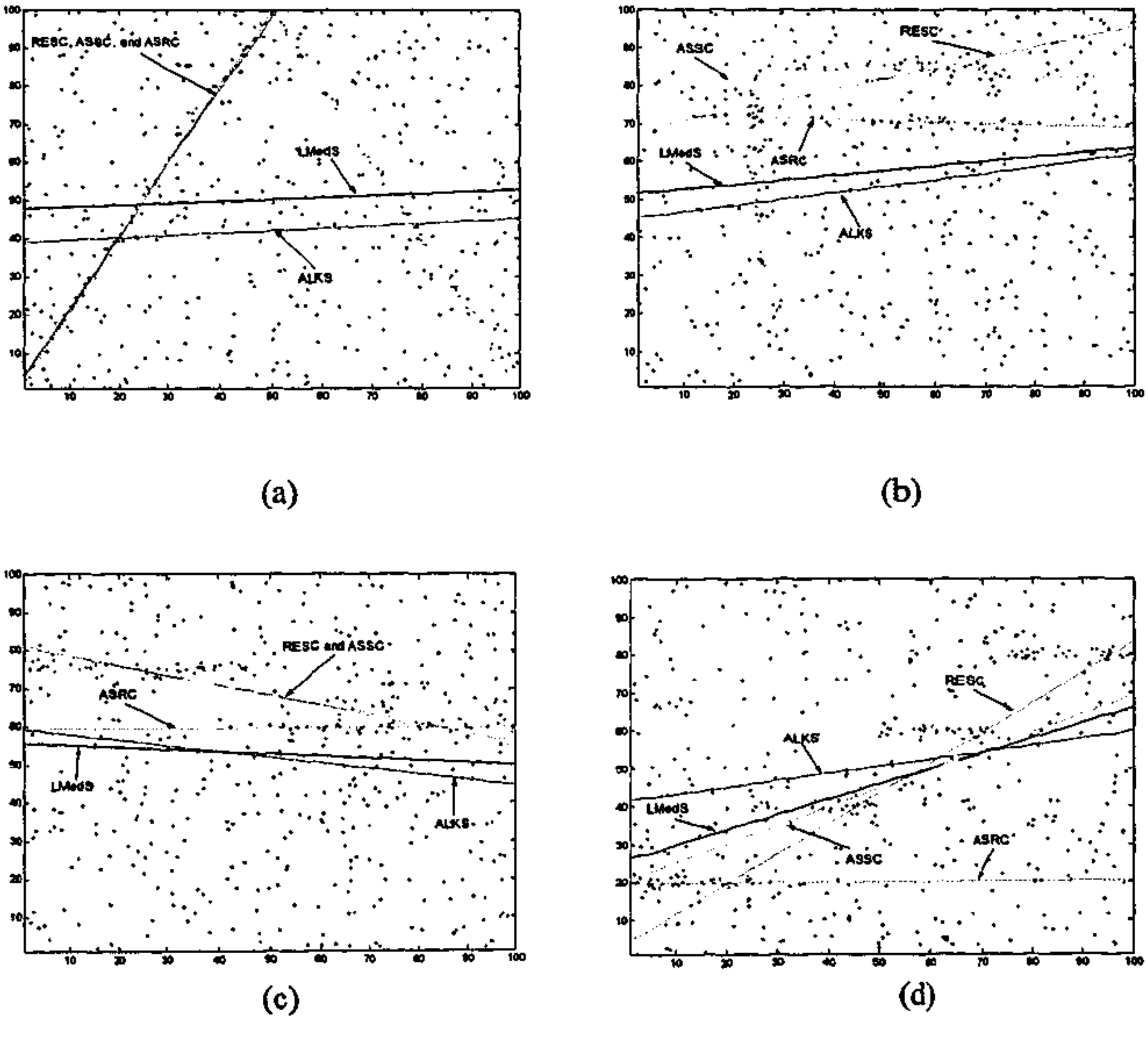

(a)

(b)

(c)

(d)

Figure 8.12: Comparing the performance of five methods: (a) fitting a roof with a total of 87% outliers; (b) fitting F-figure with a total of 92% outliers; (c) fitting a step with a total of 91% outliers; (d) fitting three-step with a total of 91% outliers.

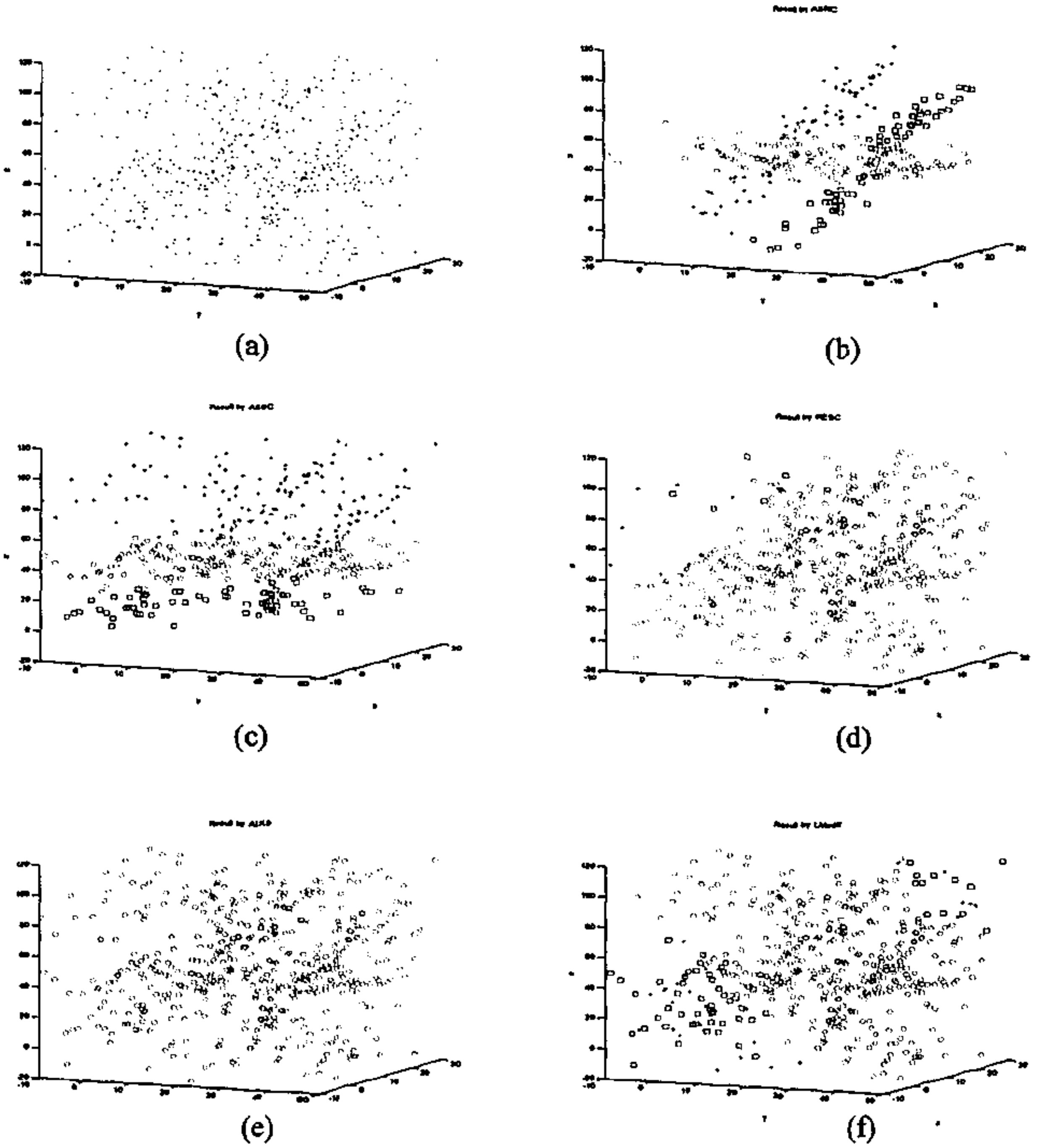

(a)

(b)

(c)

(d)

(e)

(f)

Figure 8.13: (a) the 3D data with 87% outliers; the extracted results by (b) ASRC; (c) ASSC; (d) RESC; (e) ALKS; and (f) LMedS.

In this subsection, we will carry out some experiments showing the advantages of ASRC over ASSC and other robust methods (RESC, ALKS, LMedS). We use data similar to that used in section 8.3.1 and section 8.3.2, but with more outliers.

From Figure 8.12 we can see that LMedS (50% breakdown point) failed to fit all four examples. Although ALKS is more robust than LMedS, it also failed to fit the four signals. RESC and ASSC succeeded in the roof signal (87% outliers), however, they both failed in the other three cases. In contrast, ASRC correctly fits all four signals. ASRC doesn't breakdown even when outliers occupy more than 90%, which is an improvement over ASSC.

From Figure 8.13 (d) and (e), we can see that RESC and ALKS, which claim to be robust to data with more than 50% outliers, failed to extract the three planes. This is because the estimated scales (by RESC and ALKS) for the first plane were wrong, which caused these two methods to fail to fit the second and third planes. Because the LMedS (in Figure 8.13 (f)) has only a 50% breakdown point, it completely failed to fit data with such high contamination — 80% outliers. ASSC, although it correctly fitted the first plane, wrongly fitted the second and the third planes. Only the ASRC method correctly fitted and extracted all three planes (Figure 8.13 (b)).

We also successfully applied the ASRC to range image segmentation and fundamental matrix estimation, which is similar to those in section 8.4 and 8.5. We recommend reading (Wang and Suter 2004) for details of those experiments.

8.7 Conclusion

In this chapter, we propose a very robust Adaptive Scale Sample Consensus (ASSC) estimator. The ASSC method has an objective function that considers both the number of inliers and the corresponding scale estimate for those inliers. ASSC is very robust to multiple-structural data containing high percentages of outliers (more than 80% outliers). The ASSC estimator is compared to several popular robust estimators: LMedS, RESC, and ALKS and ASSC can generally achieve better results.

Furthermore, we applied ASSC to two important computer vision tasks: range image segmentation and robust fundamental matrix estimation. However, the applications of ASSC are not limited to these two fields. The computational cost of the proposed ASSC method is moderately low, which makes it applicable to many computer vision tasks.

We also improved ASSC: ASRC improves the objective function of ASSC by weighting each inlier differently according to the residual of that inlier.

Although we have compared against several of the "natural competitors" from the computer vision and statistics literature (Fischler and Rolles 1981; Rousseeuw 1984; Yu, Bui et al. 1994; Lee, Meer et al. 1998), it is difficult to be comprehensive. For example, in (Scott 2001) the authors also proposed a method which can simultaneously estimate the model parameters and the scale of the inliers. In essence, the method tries to find the fit that produces residuals that are the most Gaussian distributed (or which have a subset that is most Gaussian distributed), and all data points are considered; In contrast, only the data points, within the band obtained by the mean shift and mean shift valley, are considered in our object function. Also, we do not assume the residuals for the best fit will be the best match to a Gaussian distribution.

In the latter stage of proposing ASSC/ASRC, we become aware that Gotardo, et al. proposed an improved robust estimator based on RANSAC and MLESAC (Gotardo, Bellon et al. 2003), and applied it to range image segmentation. However, like RANSAC, this estimator also requires that the user to set the scale-related tolerance a priori. In contrast, the proposed ASSC/ASRC method in this chapter does not require any priori information about the scale or tolerance. The parameters of a model and the corresponding scale of inliers are simultaneously obtained from the data.

Chapter 9

Mean Shift for Image Segmentation by Pixel Intensity or Pixel Color

9.1 Introduction

One major task of pattern ιecognition, image processing, and related areas: is to segment image into homogenous regions. Image segmentation is the first step towards image understanding and its success directly affects the quality of image analysis. Image segmentation has been acknowledged to be one of the most difficult tasks in computer vision and image processing (Cheng, Jiang et al. 2001; Comaniciu and Meer 2002a). Note: the type of image we refer to in this chapter (grey/color) is different from that of the range image we referred to in chapter 5 and chapter 8. A range image contains 3D geometry information. That is, the value of a pixel in the range image corresponds to a depth/range measurement.

Unlike other vision tasks such as parametric model estimation ((Wang and Suter 2003a; Wang and Suter 2003b), also see chapter 3-5 and chapter 8) , fundamental matrix estimation (Torr and Murray 1997), optical flow calculation ((Wang and Suter 2003c); also see chapter 6), etc., there is no widely accepted model or analytical solution for image segmentation. There probably is no one "true" segmentation acceptable to all different people and under different psychophysical conditions. Indeed, acceptable segmentations may have to be defined for the different requirements one may have. All of these increase the difficulty of the segmentation task.

A lot of image segmentation methods have been proposed during recent decades. Roughly speaking, these methods can be classified into (Cheng, Jiang et al. 2001): (1) Histogram thresholding (Kurugollu, Sankur et al. 2001); (2) Clustering (Comaniciu and Meer 1997; Zhang and Wang 2000; Chen and Lu 2001); (3) Region growing method (Adams and Bischof 1994); (4) Edge-based method (Nevatia 1977); (5) Physical-model-based method (Klinker, Shafer et al. 1990); (6) Fuzzy approaches (Pal 1992); and (7) Neural network based methods (Iwata and Nagahashi 1998).

We have employed the mean shift algorithm extensively in our previously presented robust methods. In this chapter, we directly apply the mean shift method to image segmentation based on the image intensity or on the image color. As we stated in chapter 4, the mean shift is a form of mode seeking (in essence). It achieves a degree of scale selectivity since it works with a smoothed estimate of the underlying density function. In the most commonly used form (Fukunaga and Hostetler 1975; Comaniciu and Meer 2002a), the window size and the smoothing are directly related to a quantity h that is the "bandwidth" choice for the kernel density estimator employed.

Although many authors of papers that employ the mean shift method have remarked that the value h needs to be chosen with care, the general impression given is that the results are not that sensitive to the choice of h and that one generally takes a pragmatic "hit and miss" affair. Thus, in the first part of this chapter we illustrate that there are two issues affected by the setting of h: the rather disastrous appearance of false peaks (where the application of the mean shift process will fail) and the choice of scale (affecting the significance of actual peaks in the underlying density – at large scales the density is very smoothed and local peaks are disregarded or merged). The latter behaviour is much more benign and, indeed, as it performs a type of controlled scale-space analysis, can be used to advantage. The former is to be avoided at all costs as it will result in completely arbitrary results. (This behaviour, though, is due to the *extreme quantized* data — such as histogramed data and thus it may not arise in all applications).

Thus, this chapter provides an important warning about the sensitivity of the mean shift to false peak noise due to the *quantization*. For simplicity, we choose the problem of histogram-based grey-level image segmentation. We show that one can rather simply predict values of *h* that will be problematic; and thereby, in this setting, we provide a means for a completely automated approach. This negates the need for the setting of a value for any parameter, including *h* (except that one may repeat the solution with a range of *h* to perform a type of scale space analysis).

The general mean shift algorithm considers only the global color (or intensity) information of the image, while neglecting the local color information. In the second part of this chapter, we propose a new method of color image segmentation considering both global information and local homogeneity. We introduce local homogeneity information into the mean shift segmentation algorithm. The proposed method applies the mean shift algorithm in the hue and intensity subspace of HSV. The cyclic property of the hue component is also considered in the proposed method. Experiments on natural color images show promising results.

The contributions of this chapter can be summarized as follows:

- We present the relationship between the grey-level histogram of an image and the mean shift method and analytically determine the conditions leading to the appearance of false peaks. We present an "unsupervised peak-valley sliding" algorithm for image segmentation.

- We introduce the local homogeneity concept into the mean shift method and propose a color image segmentation method considering the Cyclic Property of the Hue component.

- We carry out several experiments on both grey-level and color image and the results are promising.

9.2 False-Peak-Avoiding Mean Shift for Image Segmentation

The mean shift (MS) algorithm is sensitive to local peaks. In this subsection, we show both empirically and analytically that when using sample data, the reconstructed PDF may have false peaks. We show how the occurrence of the false peaks is related to the bandwidth h of the kernel density estimator, using examples of gray-level image segmentation. It is well known that in MS-based approaches, the choice of h is important. However, we provide a quantitative relationship between the appearance of false peaks and the value of h. For the gray-level image segmentation problem, we not only show how to avoid the false peak problem, but also we provide a complete unsupervised peak-valley sliding algorithm for gray-level image segmentation.

9.2.1 The Relationship between the Gray-Level Histogram of Image and the Mean Shift Method

If we are segmenting a gray-level image based upon only the intensity characteristic of pixels, the mean-shift equations can be rewritten in terms of the image intensity histogram:

$$\hat{f}(x) = \frac{d+2}{2nh^{d+2}c_d} \sum_{t_i \in S_h(x)} H(t_i)\left(h^2 - \|x - t_i\|^2\right) \tag{9.1}$$

where H(t$_i$) be the histogram on gray level t$_i$ (t$_i$ is an integer and $0 \le t_i \le 255$).

The kernel density function in equation (9.1) is related to discrete gray levels $\{t_i \mid t_i \in S_h(x)\}$ and the corresponding histogram $\{\mathrm{H}(\mathrm{t}_i) \mid \mathrm{t}_i \in \mathrm{S}_h(\mathrm{x})\}$.

Likewise:

$$\begin{aligned}\hat{\nabla} f(x) &= \frac{1}{n(h^d c_d)} \frac{d+2}{h^2} \left[\sum_{t_i \in S_h(x)} H(t_i)(t_i - x) \right] \\ &= \frac{\sum_{t_i \in S_h(x)} H(t_i)}{n(h^d c_d)} \frac{d+2}{h^2} \left(\frac{\sum_{t_i \in S_h(x)} H(t_i) t_i}{\sum_{t_i \in S_h(x)} H(t_i)} - x \right)\end{aligned} \tag{9.2}$$

The last term in equation (9.2) is called the sample mean shift $M_h(x)$ in discrete gray-level space:

$$M_h(x) = \frac{\sum_{t_i \in S_h(x)} H(t_i) t_i}{\sum_{t_i \in S_h(x)} H(t_i)} - x \tag{9.3}$$

Equation (9.3) is derived from the Epanechnikov kernel. (Note: reference (Yang and Liu 2001) employing a similar formulation used a Gaussian kernel - see equation (15) and (17) in that paper).

9.2.2 The False Peak Analysis

In implementing the mean shift approach in this setting, we found, to our surprise, in some cases there are a lot of peaks appearing between two consecutive gray levels near a local maximum density (see Figure 9.1 (a) and (b)). We call these peaks the false peaks. These false peaks will seriously affect the performance of the mean shift method, i.e. the mean shift is very sensitive to these noise peaks and the mean shift loop will stop at these false peaks instead of a real local maximum density.

Here we analytically determine the conditions leading to this problem. For simplicity, we choose a one-dimensional setting. (However, the analysis of the influence of false peak noise on the mean shift and the mean shift valley can also be extended to multi-dimensional case). Let $\hat{f}(t_k)$ be the kernel density estimate at gray level t_k; let $0 < \delta x < 1$; d=1; and c_d=2. Using equation (9.1) we have:

$$\hat{f}(t_k + \delta x) = \frac{3}{4nh^3} \sum_{t_i \in S_h(t_k + \delta x)} H(t_i)\left(h^2 - \|t_k + \delta x - t_i\|^2\right) \tag{9.4}$$

If h is an integer (h>0) and t_k+h<255, and considering t_i has to be a series of consecutive unsigned integer, we have $\{t_i \mid t_i \in S_h(t_k + \delta x)\} = \{t_i \mid t_i \in S_h(t_k)\} \cup \{t_i \mid t_i = t_k + h\}$.

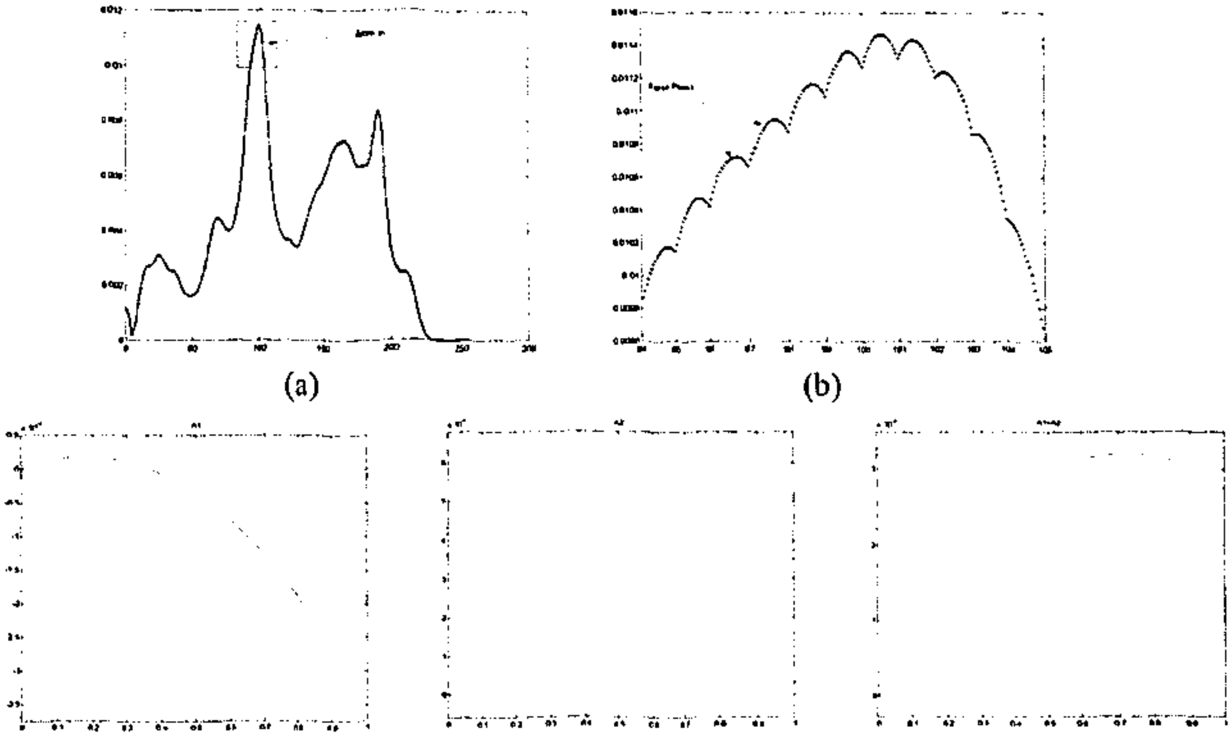

(a)

(b)

(c)

(d)

(e)

Figure 9.1: False peak noise. (a) Original probability density distribution with h equal to 5; (b) Zoom in a part of (a). Many false peaks introduced by *A1+A2* in Eq. (9.6); (c)-(e) *A1*, *A2*, and *A1+A2* in Eq. (9.6) with t_k=95.

The equation (9.4) can be rewritten as:

$$\begin{aligned}
\hat{f}(t_k+\delta x) &= \frac{3}{4nh^3}\left[\sum_{t_i\in S_h(t_k)} H(t_i)\left(h^2-\|t_k+\delta x-t_i\|^2\right)+H(t_k+h)(h^2-\|h-\delta x\|^2)\right] \\
&= \hat{f}(t_k)+\frac{3}{4nh^3}\left[\sum_{t_i\in S_h(t_k)} H(t_i)\left(-\|\delta x\|^2+2\delta x\left(\frac{\sum\limits_{t_i\in S_h(t_k)} H(t_i)t_i}{\sum\limits_{t_i\in S_h(t_k)} H(t_i)}-t_k\right)\right)+H(t_k+h)(-\|\delta x\|^2+2h\delta x)\right] \\
&= \hat{f}(t_k)+\frac{3}{4nh^3}\sum_{t_i\in S_h(t_k)} H(t_i)\left(-\|\delta x\|^2+2\delta x M_h(t_k)\right)+\frac{3}{4nh^3}H(t_k+h)(-\|\delta x\|^2+2h\delta x) \qquad (9.5)
\end{aligned}$$

We let:

$$A1=\frac{3}{4nh^3}\sum_{t_i\in S_h(t_k)} H(t_i)\left(-\|\delta x\|^2+2\delta x M_h(t_k)\right)$$

$$A2=\frac{3}{4nh^3}H(t_k+h)(-\|\delta x\|^2+2h\delta x) \qquad (9.6a)$$

When h>> δx , *A2* can be approximated as a linear equation (see Figure 9.1 (d)).

Equation (9.5) can be rewritten as:

$$\hat{f}(t_k + \delta x) = \hat{f}(t_k) + A1 + A2 \tag{9.6b}$$

Now we calculate the differentive of $\hat{f}(t_k + \delta x)$:

$$\begin{aligned}\frac{d\hat{f}(t_k + \delta x)}{d(\delta x)} &= \frac{3}{4nh^3} \sum_{t_i \in S_h(t_k)} H(t_i)\left(-2\delta x + 2M_h(i\quad\right) + \frac{3}{4nh^3} H(t_k + h)(-2\delta x + 2h) \\ &= \frac{3}{4nh^3}\left[-2\delta x\left(\sum_{t_i \in S_h(t_k)} H(t_i) + H(t_k + h)\right) + 2\left(\sum_{t_i \in S_h(t_k)} H(t_i)M_h(t_k) + H(t_k + h)h\right)\right]\end{aligned} \tag{9.7}$$

Setting (9.7) equal to zero, we obtain:

$$\delta x = \frac{\sum_{t_i \in S_h(t_k)} H(t_i)M_h(t_k) + H(t_k + h)h}{\sum_{t_i \in S_h(t_k)} H(t_i) + H(t_k + h)} \tag{9.8}$$

Substituting equation (9.3) into equation (9.8), and if $0 < \delta x < 1$, i.e. if:

$$\frac{\sum_{t_i \in S_h(t_k)} H(t_i)(t_k - t_i)}{H(t_k + h)} < h < \frac{\sum_{t_i \in S_h(t_k)} H(t_i)(t_k - t_i) + \sum_{t_i \in S_h(t_k)} H(t_i) + H(t_k + h)}{H(t_k + h)} \tag{9.9}$$

there will be a false peak appearing between two consecutive gray level, t_k and t_k+1.

For example, in Figure 9.1, when we apply the mean shift method with initial location at 95, we find the mean shift stopped at 95.7244, instead of the real local maximum density at 101. From equation (9.8), we obtained δx =0.7244, i.e. there is a false peak between 95 and 96.

We let *L* be the leftmost item in the in equation (9.9) and *R* be the rightmost item of (9.9); let $x_{MS(tk)}$ be the point which the mean shift converges to, from initial point at t_k, corresponding to the local peak. Thus if the condition: $L<h<R$ is satisfied, we can predict that there will be a false peak between t_k and t_k+1 (see Table 9.1).

h	L	R	δx	t_k	$x_{MS(tk)}$	False peak between t_k and t_k+1
5	-1.45	7.45	0.72	95	95.72	yes
6	-2.84	6.99	0.89	95	95.89	yes
7	-5.76	6.06	1.08	95	96.96	no
7	-5.10	7.45	0.96	96	96.96	yes
8	-9.68	3.95	1.30	95	97.94	no
8	-7.99	6.19	1.13	96	97.94	no
8	-7.42	8.96	0.94	97	97.94	yes

Table 9.1: False peaks prediction

The above analysis suggests that one could devise an approach that adaptively adjusts h depending upon whether false peaks are predicted. If a false peak is detected, we can use the following adjustment to avoid the influence of the false peak:

$$y_{k+1} = y_k + \text{ceil}(M_h(y_k)) \text{ for MS step} \tag{9.10a}$$

$$y_{k+1} = y_k + \text{floor}(MV_h(y_k)) \text{ for MSV step} \tag{9.10b}$$

9.2.3 An Unsupervised Peak-Valley Sliding Algorithm for Image Segmentation

Consider the peaks {P(i)} and valleys {V(i)}. V(0)=0 and V(n)=255. $V(0) \le P(1) < V(1) < .... < P(n) \le V(n)$. The proposed algorithm is described as follows:

(1) Initialise the bandwidth h and the location of search window.

(2) Apply the mean shift algorithm to obtain peak P_k with the initial window location $V_{k-1}+1$.

(3) Apply the mean shift valley method to obtain valley V_k with initial window location P_k+1.

(4) Repeat step (2) and (3) until P_k or V_k is equal to or larger than 255. The questions remains as to how many of these peaks are significant. We post-process by step (5).

(5) Validate peaks and valleys

(5a) Remove peaks too small compared with the largest.

(5b) Remove the smaller of two consecutive peaks if too close.

(5c) Calculate the normalized contrast (Albiol, Torrest et al. 2001) for a valley and two neighbouring peaks:

$$\text{Normalized Contrast} = \frac{Contrast}{Height} \tag{9.11}$$

where the *contrast* is the difference between the smaller peak and the valley. Remove the smaller one of the two peaks if this is small.

After step 5(a)-5(c), we obtain several significant peaks {PS(1),...PS(k)}. The valleys then are chosen as the minimum of the valleys between two consecutive significant peaks. Thus we have k-1 valleys {VS(1),...VS(k-1)}.

(6) Using the obtained valleys, finally obtain k segmented images by {[0, VS(1)], [VS(1), VS(2)], ... [VS(k), 255]}.

9.2.4 Experimental Results

In this section, we will use several examples to show the performance of the proposed method in segmenting images. Figure 9.2 demonstrates the segmentation procedures of the proposed method. Figure 9.2 (c)/(d) shows the obtained peaks and valleys before/after validation . Before the validation, there are ten peaks and ten valleys obtained. Near a local plateau, there will be some insignificant peaks and valleys. After applying step 5 in section 9.2.3, we finally obtained three validated valleys and thus we have four segmented images Figure 9.2 (e-h). The final result is shown in (i).

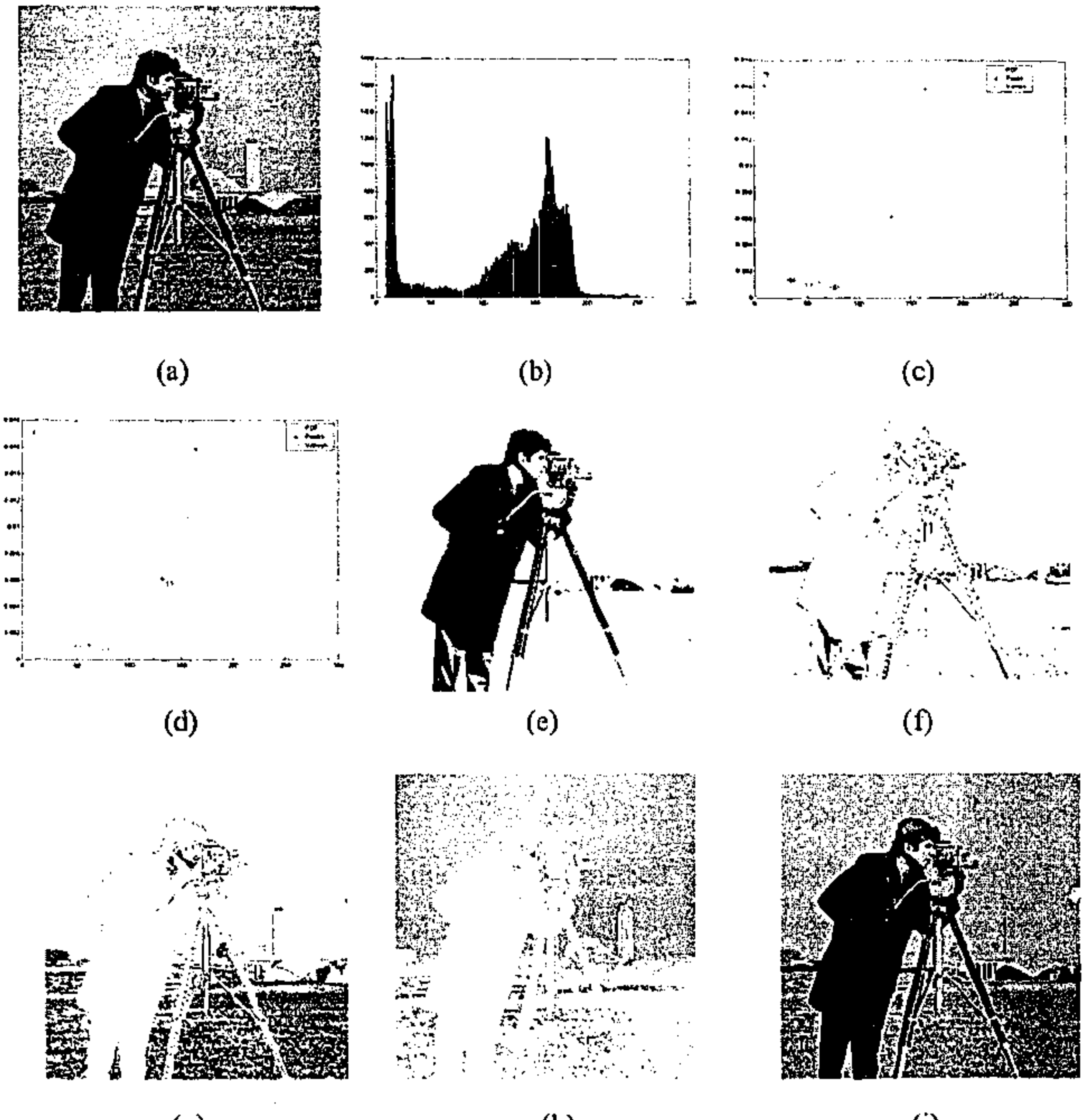

(a) (b) (c)

(d) (e) (f)

(g) (h) (i)

Figure 9.2: The segmentation results of the proposed method (h=7). (a) original image of the cameraman; (b) gray-level histogram; (c) peaks and valleys of $\hat{f}(x)$ before merging; (d) final peaks and valleys; (e)-(h) the resulting segmented images; (i) the final segmented image.

Figure 9.3 hows another experiment on a x-ray medical image. From Figure 9.3, we can see that the x-ray image has been successfully segmented: the background (Figure 9.3 (c)), the bone (Figure 9.3 (d)), and the tissues (Figure 9.3 (e) were extracted separately.

The computational speed of the proposed algorithm is efficient: about 0.27 second using MATLAB code on an AMD 800MHz personal computer.

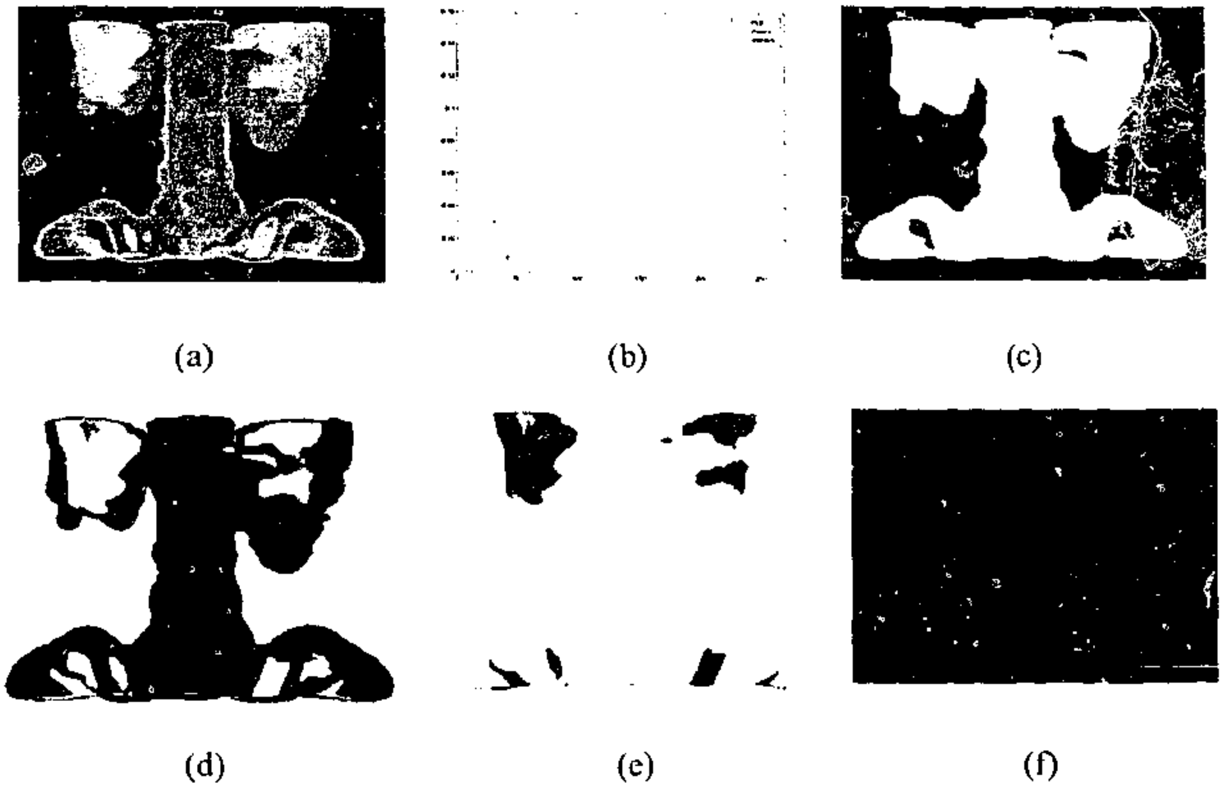

Figu^re 9.3: The application of the proposed method on medical images (*h*=2). (a) the original x-ray image; (b) the final peaks and valleys after validation; (c)-(e) the resulting segmented images; (i) the final segmented image.

9.3 Color Image Segmentation Using Global Information and Local Homogeneity

Clustering techniques identify homogeneous clusters of points in the feature space (such as RGB color space, HSV color space, etc.) and then label each cluster as a different region. The homogeneity criterion is usually that of color similarity, i.e., the distance between one cluster to another cluster in the color feature space should smaller than a threshold. The disadvantage of this method is that it does not consider local color information between neighbouring pixels.

In this section, we propose a new segmentation method introducing local homogeneity into a mean shift algorithm. Thus, our mean shift algorithm considers both global and local color information. The method is performed in "Hue-Value" two-dimensional subspace of Hue-Saturation-Value space (see section 9.3.1). Compared with those applying the mean shift algorithm in LUV or RGB color space, the complexity of the proposed method is lower. The proposed method also considers the cyclic property of the hue component and it does not need priori knowledge about the number of clusters and it detects the clusters unsupervised.

In (Cheng and Sun 2000), the authors also proposed a peak-finding algorithm. Unfortunately, it is heuristically based. One characteristic of the mean shift vector is that it always points towards the direction of the maximum increase in the density. The converged centres (or windows) correspond to modes (or centres of the regions of high concentration) of data. The mean shift algorithm has a solid theoretical foundation. The proof of the convergence of the mean shift algorithm can be found in (Comaniciu and Meer 1999b; Comaniciu and Meer 2002a).

9.3.1 HSV Color Space

Although RGB (Red, Green, and Blue) is a widely used color space to represent the color information in a color image, HSV (Hue, Saturation, and Value) is sometimes preferred as the color space. In the HSV color space, each color is determined by the values of HSV (see Figure 9.4). The first component, Hue, is a specification of the intrinsic color. The second component of the HSV triple, Saturation, describes, "how pure the color is". The last component of the HSV triple is a measure of "how bright the color is". The HSI (hue-saturation-intensity), the HSB (hue-saturation-brightness), and the HSL (hue-saturation-lightness) are variant forms of the HSV color space (Cheng, Jiang et al. 2001). This class of color space has been widely used in computer vision tasks (Cheng and Sun 2000; Zhang and Wang 2000; Sural, Qian et al. 2002). The reason that this class of color space is preferred to the RGB color space, is that it better represents human perception of colors. The advantages of hue over RGB are (Cheng and Sun 2000; Cheng and Y.Sun 2000; Cheng, Jiang et al. 2001):

- Hue is invariant to certain types of highlights, shading, and shadows;
- The segmentation is performed on only one dimension and results of segmentation have fewer segments than using RGB.

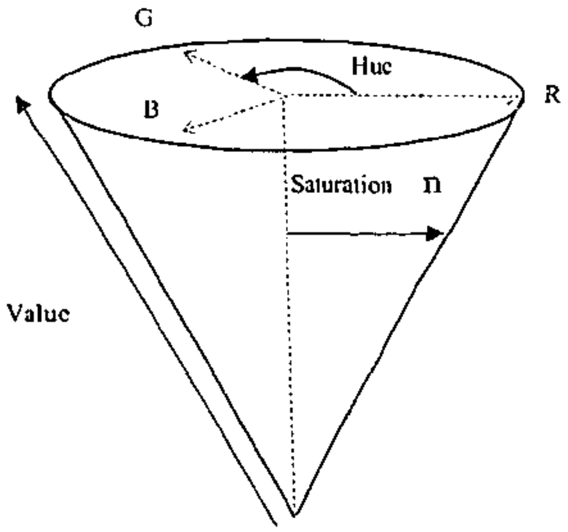

Figure 9.4: HSV color space.

In the HSV color space, Hue and value are the most important ones. Although the authors of (Cheng and Sun 2000) utilized both hue and intensity to segment color images, they segmented color images in one-dimensional intensity subspace and then, hierarchically, segmented the results (from the segmentation in the intensity subspace) in the hue subspace. Thus it is easy to over-segment the image. In this chapter, we apply the mean shift algorithm in hue-value two-dimensional subspace (both hue and intensity are considered simultaneously in our method). The hue and value are scaled so that they range from 0 to 255.

One thing worth mentioning is the cyclic property of the hue component. Because the hue is a value of angle, it has this cyclic property. The cyclic property of the hue will be considered in the mean shift algorithm and in classifying pixels to clusters (see section 9.3.2 and 9.3.3).

9.3.2 Considering the Cyclic Property of the Hue Component in the Mean Shift Algorithm

Because the hue is a value of angle, the cyclic property of the hue must be considered in the mean shift algorithm. The revised mean shift algorithm can be written as:

$$\mathrm{M}'_{\mathrm{h}}(\mathrm{x}) \equiv \frac{1}{n'_x} \sum_{X_i \in S'_h(x)} X_i - x \tag{9.12}$$

where the converging window center x is a vector of [H, V],

and

$$S'_h(x) = \begin{cases} |H_i - H| < h \& |V_i - V| < h, if\ h \leq H \leq 255 - h \\ (|H_i - H| < h||255 - H_i| < h - H) \& |V_i - V| < h, ifH - h < 0 \\ (|H_i - H| < h||255 - H| < h - H_i) \& |V_i - V| < h, ifH + h > 255 \end{cases}$$

(n'_x is the number of data points inside the hypersphere $S'_h(x)$).

When translating the search window, let x_{k+1}=[$\mathrm{H}_{\mathrm{k+1}}$,$\mathrm{V}_{\mathrm{k+1}}$]. We have:

$$H_{k+1} = \begin{cases} \frac{1}{n'_{x_k}} \sum_{H_i \in S'_h(H_k)} H_i, if\ 0 \leq \frac{1}{n'_{x_k}} \sum_{H_i \in S'_h(H_k)} H_i \leq 255 \\ \frac{1}{n'_{x_k}} \sum_{H_i \in S'_h(H_k)} H_i + 255, if\ \frac{1}{n'_{x_k}} \sum_{H_i \in S'_h(H_k)} H_i < 0 \\ \frac{1}{n'_{x_k}} \sum_{H_i \in S'_h(H_k)} H_i - 255, if\ \frac{1}{n'_{x_k}} \sum_{H_i \in S'_h(H_k)} H_i > 255 \end{cases} \quad \text{and} \quad V_{k+1} = \frac{1}{n'_{x_k}} \sum_{V_i \in S'_h(V_k)} V_i \tag{9.13}$$

9.3.3 The Proposed Segmentation Method for Color Images

Although the mean shift algorithm has been successfully applied to clustering (Cheng 1995; Comaniciu and Meer 1999b), image segmentation (Comaniciu and Meer 1997; Comaniciu and Meer 2002a), etc., it mainly considers global color information, while neglecting local homogeneity. In this chapter, we introduce a measure of local homogeneity (Cheng and Sun 2000) into the mean shift algorithm. The proposed method considers both global information and local homogeneity information as explained in the next section.

9.3.3.1 Local Homogeneity

In (Cheng and Sun 2000), a measure of local homogeneity has been used in one-dimensional histogram thresholding. The homogeneity consists of two parts: the standard deviation and the discontinuity of the intensities at each pixel of the image. The standard derivation S_{ij} at pixel P_{ij} can be written as:

$$S_{ij} = \sqrt{\frac{1}{n_w} \sum_{I_w \in W_d(P_{ij})} (I_w - m_{ij})^2} \tag{9.14}$$

where m_{ij} is the mean of n_w intensities within the window $W_d(P_{ij})$, which has a size of d by d and is centered at P_{ij}.

A measure of the discontinuity D_{ij} at pixel P_{ij} can be written as:

$$\mathrm{D_{ij}} = \sqrt{\mathrm{G}_x^2 + G_y^2} \tag{9.15}$$

where G_x and G_y are the gradients at pixel P_{ij} in the x and y direction.

Thus, the homogeneity H_{ij} at P_{ij} can be written as:

$$\mathrm{H_{ij} = 1\text{-}(S_{ij}/S_{max}) \times (D_{ij}/D_{max})} \tag{9.16}$$

From equation (9.16), we can see that the H value ranges from 0 to 1. The higher the H_{ij} value is, the more homogenous the region surrounding the pixel P_{ij} is.

In (Cheng and Sun 2000), the authors applied this measure of homogeneity to the histogram of gray levels. Here, we will show that the local homogeneity can also be incorporated into the popular mean shift algorithm.

9.3.3.2 Color Image Segmentation Method

Our proposed method mainly consists of three parts:

- Map the image to the feature space considering both global color information and local homogeneity.
- Apply the revised mean shift algorithm (section 9.3.2) to obtain the peaks.
- Post-processing and assign the pixels to each cluster.

The details of the proposed method are:

1. Map the image to the feature space.

We first compute the local homogeneity value at each pixel of the image. To calculate the standard variance at each pixel, a 5-by-5 window is used. For the discontinuity estimation, we use a 3-by-3 window. Of course, other window sizes can also be used. However, we find that the window sizes used in our case can achieve better performance and computational efficiency.

After computing the homogeneity for each pixel, we only use the pixels with high homogeneity values (near to 1.0) and neglect the pixels with low homogeneity values. We map the pixels with high homogeneity values in the hue-value two-dimensional space. Thus, both global and local information are considered.

2. Apply the mean shift algorithm to find the local high-density modes.

We randomly initialize windows (many enough) in HV space, with radius *h*. When the number of data points inside the window is large, and when the window center is not too close to the other accepted windows, we accept the window. After the initial window has been chosen, we apply the mean shift algorithm considering the cyclic property of the hue component to obtain the local peaks.

3. Validate the peaks and label the pixels.

After applying the mean shift algorithm, we obtain a lot of peaks. Obviously, these peaks are not all valid. We need some post-processing to validate the peaks. Thus we do by the following step.

- Eliminate the repeated peaks. Because of the limited accuracy of the mean shift, the same peak obtained by the mean shift may not be at the exact same location. Thus, we remove the repeated peaks that are very close to each other (e.g., their distance is less than 1.0).

- Remove the small peaks related to the maximum peaks. Because the mean shift algorithm only finds the local peaks, it may stop at small local peaks.

- Calculate the normalized contrast using equation (9.11). Remove the smaller one of the two peaks if the normalized contrast is small.

4. After obtaining the validated peaks, we assign pixels to its nearest clusters. In this step, the cyclic property of the hue component will again be considered. The distance between the *i*'th pixel to the *j*'th cluster is:

$$Dist(i,j) = \sqrt{\left(\alpha \min(\left|H_i - H_j\right|, \left|255 + H_j - H_i\right|\right)^2 + \left|V_i - V_j\right|^2} \qquad (9.17)$$

where α is a factor to adjust the relative weight of the hue component over the value component.

The authors of (Zhang and Wang 2000) employed the *k*-means algorithm to segment image. The disadvantage of such an approach is the requirement that the user must specify the number of the clusters. In comparison, the proposed method is unsupervised in that it needs no priori knowledge about the number of the clusters. We illustrate with the experiments in the next section.

9.3.4 Experiments on Color Image Segmentation

In this section, we test our color image segmentation method on natural color images.

In Figure 9.5, part of the procedures of the proposed method is illustrated and final segmentation results are given. Figure 9.5 (a) includes the original image "home". The points in HV space are displayed in Figure 9.5 (b) (no validation of local homogeneity) and (c) (after validation of local homogeneity). The tracks of the mean shift in HV space, with different initializations, are included in Figure 9.5 (d). The blue lines are the traces of the mean shift procedures; green dots are the centres of the converged windows by the mean shift procedures; and the red circles are the final peaks after validation. Figure 9.5 (e) gives the final segmentation results by the proposed method. From Figure 9.5 (e), we can see that our method obtains good segmentation results. The tree, the house, the roof, and the rim of the curtain and the house are all segmented out separately. The curtain and the sky are segmented to the same cluster. This is because the color of the curtain is blue, which is similar to the color of sky. From the point of view for color homogeneity, this result is correct.

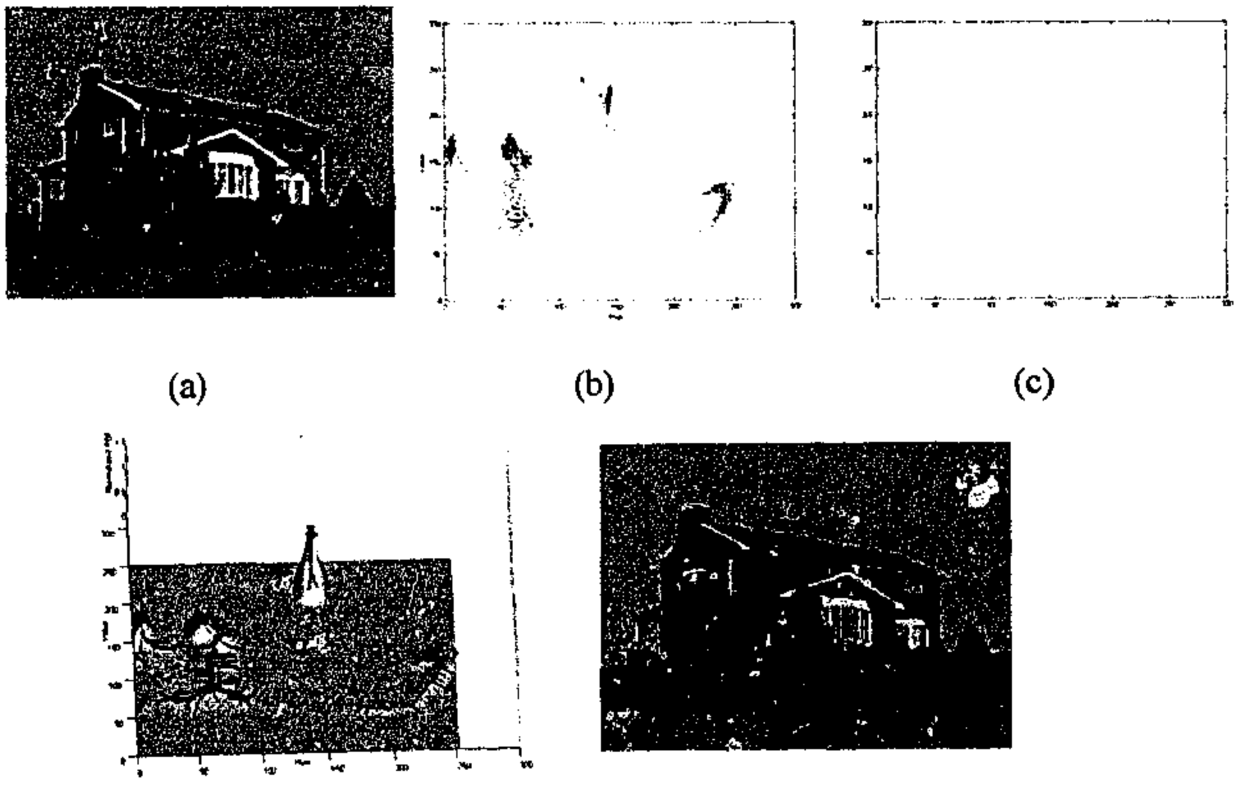

(a) (b) (c)

(d) (e)

Figure 9.5: (a) the original image "home"; (b) The hue-value feature space without considering local homogeneity; (c) The hue-value feature space considering local homogeneity; (d) procedures and results of the data decomposition by the mean shift algorithm with different initializations (e) the final results with seven colors obtained by the proposed method with h=9.

We also note that the grassland are segmented into two parts: on one hand, one can say the method over-segments the grassland because they both belong to the grassland; on the other hand, one can say the method correctly segment the grassland because the grassland can be seen to have different color. This again demonstrates that there is no unique solution to image segmentation.

In Figure 9.6 and Figure 9.7, we compare the proposed method with a method employing a similar scheme but without considering the local homogeneity and the cyclic property of the hue component

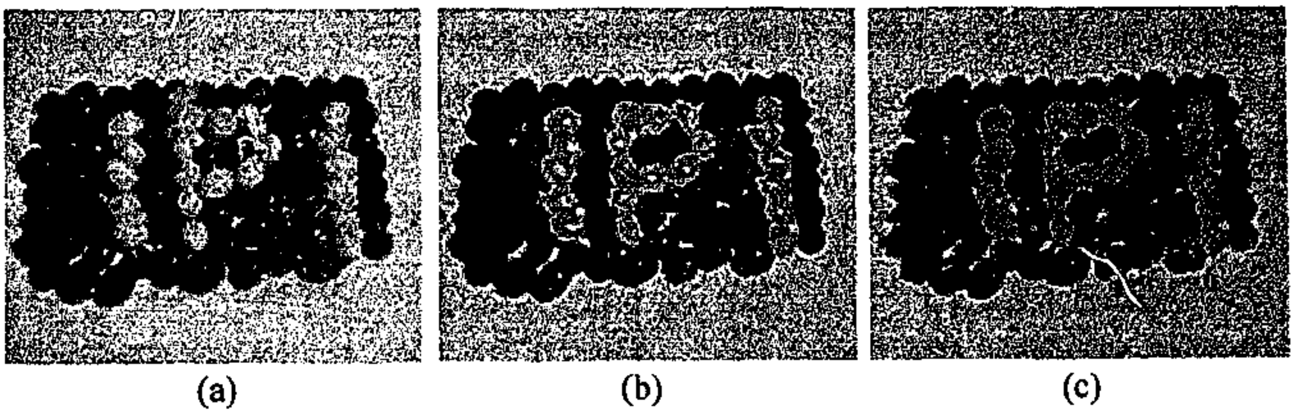
(a) (b) (c)

Figure 9.6: (a) the original image "Jelly beans"; (b) the final results with five colors obtained by the proposed method with h=7; (c) the results with seven colors without considering the local homogeneity and the cyclic property of the hue (h=7).

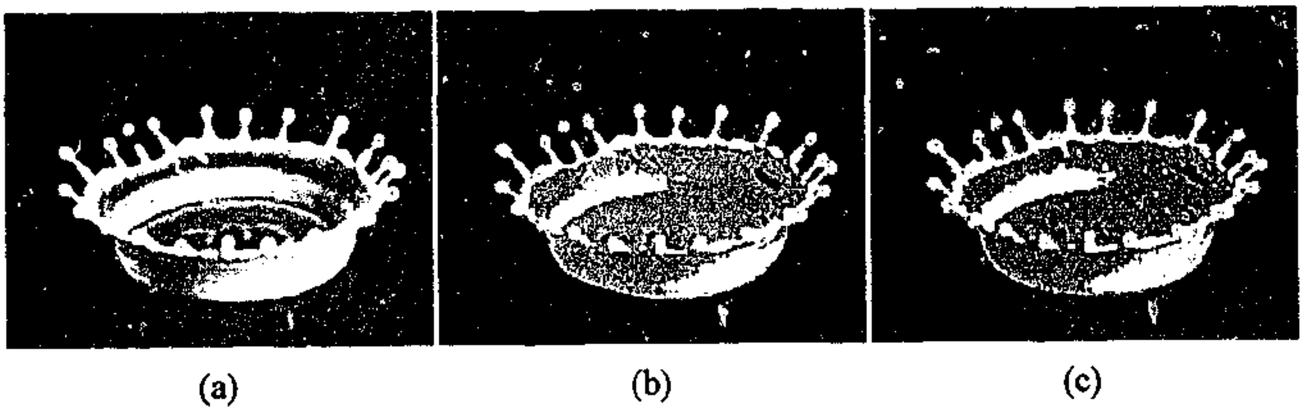
(a) (b) (c)

Figure 9.7: (a) the original image "Splash"; (b) the final results with three colors obtained by the proposed method with h=7; (c) the results with six colors without considering the local homogeneity and the cyclic property of the hue (h=7).

From Figure 9.6, we can see that the method which considers no the local homogeneity, nor the cyclic property of the hue component, over-segments the image of "Jelly beans" into seven colors; the blue beans fall into two clusters; part of the red beans are wrongly assigned to the black beans. In contrast, the proposed method correctly segments the "Jelly beans" images into five colors (four colors from beans and one color from background).

In Figure 9.7, we can see that the method without considering the local homogeneity and the cyclic property of the hue component over-segments the image of "Splash". The red background falls into two clusters; also, some pixels of the red background are wrongly assigned to the object in the image. In contrast, the proposed method considering the local homogeneity and the cyclic property of the hue component obtains good results. The image is effectively compressed to three colors.

9.4 Conclusion

The mean shift (MS) method is well known and popular: yet its sensitivity to false local peaks is virtually unrecognized. In this chapter, we analyse the influence of false peak noise on the MS and MSV method, in particular, we show how the occurrence of the false peaks is related to the bandwidth of the kernel density estimator (i.e., false peaks appear only when equation (9.9) is satisfied).

A novel unsupervised false-peak-avoiding peak-valley sliding algorithm for image segmentation is also presented in this chapter. We use the MS method to find peaks and the MSV method to find valleys. The peaks and valleys are alternatively found one by one. After validating the obtained peaks and valleys, we use the validated valleys as density thresholds to segment the image.

The "peak-valley sliding method" for identifying modes and anti-modes, is of interest in its own right. Moreover, the application of this method to automatically threshold multimodal gray-level images may also be of independent interest, as the method does not require the priori knowledge of the number of the peaks and valleys and it is computationally effective. This part of work inspired us to present the robust Two-Step

Scale (TSSE), the Adaptive-Scale Sample Consensus (ASSC), and the Adaptive-Scale Residual Consensus (ASRC) estimators in chapter 7 and chapter 8.

We also propose a novel color image segmentation method. We employ the concept of homogeneity, and the mean shift algorithm, in our method. Thus the proposed method considers both local and global information in segmenting the image into homogenous regions. We segment the image in the hue-value two-dimensional feature space. Thus, the computational complexity is reduced, compared with the methods that segment image in LUV or RGB three-dimensional feature space. The cyclic property of the hue component is considered in the mean shift procedures and in the labelling of the pixels of the image. Experiments show that the proposed method achieves promising results for natural color image segmentation.

Chapter 10

Conclusion and Future Work

Because of the presence of multiple structures in the image, we need approaches that are robust to (pseudo)-outliers in the sense of having a high breakdown point. Established techniques, in use, that meet this criterion are based upon random sampling: e.g., Least Median of Squares, Least Trimmed Squares, and RANSAC Random sampling techniques aim to explore the search space of possible solutions well enough to have at least one candidate which is determined solely by inliers (to a single structure in the data).

However, since one doesn't have an "oracle" to tell us which of the candidates are unpolluted by outliers; we require some form of model/fit scoring. In Least Median of Squares, this is obviously the median of the residuals. In RANSAC, it is the number of data residuals inside a certain bound. Of course, each form of model scoring has potential weaknesses. In Least Median of Squares, the median of the residuals of the entire data set (with respect to the candidate model) will obviously not be a good measure if the inliers to that model contain less than 50% of the total data. Generalizing to the k'th other statistic (rather than the Median) is one way out of this dilemma but now one either has to know in advance what value of k to use, or one has to attempt some form adaptation e.g., ALKS (which will perhaps be costly and limited in reliability).

Even still, it is overly optimistic to expect a single statistic (the k-th order residual, for Least Median of Squares and ALKS; or the number of inliers within a certain bound, for RANSAC) to be an entirely reliable/informative measure of the quality of a solution.

This observation has leaded us to seek alternative ways of scoring candidate models, so that greater robustness may be achieved. An early attempt (Wang and Suter 2002b; Wang and Suter 2003a) employed possible symmetry in the data set as one such statistic: though somewhat limited in versatility, such an approach definitely restores robustness in situations where standard Least Median of Squares will break down. Our recent estimators seek to use more information from the residual distribution. In particular, we have used Kernel Density estimation and Mean Shift Techniques (Wang and Suter 2002a; Wang and Suter 2003b; Wang and Suter 2003c) to formulate model fit scores that lead to empirically observed higher breakdown points than all existing methods. The scale of inliers can be an important factor that decides the performance of a robust estimator. Thus, our more recent methods (Wang and Suter 2003d; Wang and Suter 2003g) consider both the shape distribution of the residuals of inliers and the scale of inliers in formulating model fit scores.

In the work carried out in pursuit of this thesis, several novel ideas and methods/techniques were developed, and many of which result in publications (Wang and Suter 2002a; Wang and Suter 2002b; Suter, Chen et al. 2003; Wang and Suter 2003a; Wang and Suter 2003b; Wang and Suter 2003c; Wang and Suter 2003d; Wang and Suter 2003e; Wang and David 2003f; Wang and Suter 2003g; Suter and Wang 2004; Wang and Suter 2004) and five technical reports.

In summary, the main contributions of this thesis to the computer vision and pattern recognition community are:

1 We illustrate and analyze situations where LMedS and LTS to fail to correctly fit the data in the presence of clustered outliers. We introduce the concept of symmetry distance (SD) into model fitting, and propose a novel symmetry-based method—the Least Trimmed Symmetry Distance (LTSD) and apply it to model fitting.

2 We apply nonparametric density estimation and density gradient estimation techniques (the mean shift method) in parametric estimation, and provide a novel estimator, Maximum Density Power Estimator (MDPE), which can usually tolerate more than 85% outliers.

3 We modify the MDPE to produce a quicker version—Quick MDPE. Based on QMDPE, we propose a complete and model-based algorithm for range image segmentation.

4 We develop the QMDPE to produce variable bandwidth QMDPE (vbQMDPE) and apply it to robust optical flow calculation.

5 We investigate robust scale estimation and propose a novel and effective robust scale estimator: Two-Step Scale Estimator (TSSE).

6 We propose, by employing TSSE in a RANSAC like procedure, a highly robust estimator: Adaptive Scale Sample Consensus (ASSC) estimator. We apply ASSC to two important computer vision tasks: range image segmentation and fundamental matrix estimation.

7 We modify ASSC to produce ASRC (Adaptive Scale Residual Consensus), by which better achievements can be obtained.

8 We show how the occurrence of the false peaks is related to the bandwidth *h* of the kernel density estimator, and provide a quantitative relationship between the appearance of false peaks and the value of *h*. We also provide a complete false-peak-avoiding algorithm for gray-level image segmentation

9 We propose a new algorithm of color image segmentation considering both global information and local homogeneity.

10 We carry out a large number of experimental comparisons on both synthetic and real data. The results show the attractive advantages of our methods and provide a useful reference for the work of others in the future.

Limitations and future work:

Finally, we must remark on the shortcomings of the approaches we are hereby promoting. From a theoretical point of view, a lot remains to be studied. Though we promote our schemes in terms of "breakdown point", we acknowledge a number of issues in respect of this. We have not formally defined "breakdown point"; nor, consequently, have we in a way attempted to prove attainment of a high breakdown point. In these respects, our approach is intuitive and empirical.

However, we trust, despite these shortcomings, the technique we have described will be of use to the computer vision community (and wider) as the basis of proven practical methods which can be refined, and whose theoretical underpinnings can be explored.

Even though most of contributions of this thesis in term of new robust estimation lead to, in general purpose, methods/techniques that could be applied to many computer vision problems which can be formulated in a model fitting paradigm, for historical reasons (and limited time), we have not completed a uniform application to all problems investigation (e.g., we did not apply MDPE to fundamental matrix estimation). It would be interesting and useful to investigate such work in the future.

This thesis concentrates on the robust regression scheme including LMedS, RANSAC, etc. It does not employ the total least squares (TLS) scheme, nor does it use the geometric fitting (Kanatani 1996). It would be beneficial to explore the contributions of this thesis in such a framework.

Bibliography

Adams, R. and L. Bischof (1994). "Seeded Region Growing." IEEE Trans. Pattern Analysis and Machine Intelligence **16**: 641-647.

Albiol, A., L. Torrest and E. J. Delp (2001). An Unsupervised Color Image Segmentation Algorithm for Face Detection Applications. in Proceedings of International Conference on Image Processing. 681-684

Attneave, F. (1995). "Symmetry Information and Memory for Pattern." Am. J. Psychology **68**: 209-222.

Bab-Hadiashar, A. and D. Suter (1998). "Robust Optic Flow Computation." International Journal of Computer Vision **29**(1): 59-77.

Bab-Hadiashar, A. and D. Suter (1999). "Robust segmentation of visual data using ranked unbiased scale estimate." ROBOTICA, International Journal of Information, Education and Research in Robotics and Artificial Intelligence **17**: 649-660.

Barron, J. L., D. J. Fleet and S. S. Beauchemin (1994). "Performance of Optical Flow Techniques." International Journal of Computer Vision **12**(1): 43-77.

Bigun, J. (1988). Recognition of Local Symmetries in Gray Value Images by Harmonic Functions. Proc. Int'l Conf. Pattern Recognition. 345-347

Black, M. J. (1994). Recursive non-linear estimation of discontinuous flow field. Proc. of Third Europ. Conf. on Comp. Vis., ECCV-94. 138-145

Black, M. J. and P. Anandan (1993). A Framework for the Robust Estimation of Optical Flow. Fourth International Conf. on Computer Vision, Berlin, Germany. 231-236

Black, M. J. and P. Anandan (1996). "The Robust Estimation of Multiple Motions: Parametric and Piecewise-Smooth Flow Fields." Computer Vision and Image Understanding **63**(1): 75-104.

Black, M. J. and A. D. Jepson (1996). "Estimating Optical Flow in Segmented Images using Variable-order Parametric Models with local deformations." IEEE Trans. Pattern Analysis and Machine Intelligence **18**(10): 972-986.

Chen, H. and P. Meer (2002). "Robust Computer Vision through Kernel Density Estimation." A. Heyden et al. (Eds.), ECCV 2002, LNCS 2350, Springer-Verlag Berlin: 236-250.

Chen, T. Q. and Y. Lu (2001). "Color Image Segmentation--An Innovative Approach." Pattern Recognition **35**: 395-405.

Cheng, H. D., X. H. Jiang, Y.Sun and J. Wang (2001). "Color Image Segmentation: Advances and Prospects." Pattern Recognition 34: 2259-2281.

Cheng, H. D. and Y. Sun (2000). "A Hierarchical Approach to Color Image Segmentation Using Homogeneity." IEEE Trans. Image Processing 9(12): 2071-2082.

Cheng, H. D. and Y.Sun (2000). "A Hierarchical Approach to Color Image Segmentation Using Homogeneity." IEEE Trans. Image Processing 9(12): 2071-2082.

Cheng, Y. (1995). "Mean Shift, Mode Seeking, and Clustering." IEEE Trans. Pattern Analysis and Machine Intelligence 17(8): 790-799.

Comaniciu, D. and P. Meer (1997). "Robust Analysis of Feature Spaces: Color Image Segmentation." in Proceedings of 1997 IEEE Conference on Computer Vision and Pattern Recognition, San Juan, PR: 750-755.

Comaniciu, D. and P. Meer (1999a). "Mean Shift Analysis and Applications." in Proceedings 7th International Conference on Computer Vision, Kerkyra, Greece: 1197-1203.

Comaniciu, D. and P. Meer (1999b). "Distribution Free Decomposition of Multivariate Data." Pattern Analysis and Applications 2: 22-30.

Comaniciu, D. and P. Meer (2002a). "Mean Shift: A Robust Approach towards Feature Space A Analysis." IEEE Trans. Pattern Analysis and Machine Intelligence 24(5): 603-619.

Comaniciu, D., V. Ramesh and A. D. Bue (2002b). Multivariate Saddle Point Detection for Statistical Clustering. Europe Conference on COmputer Vision (ECCV), Copenhagen, Danmark. 561-576

Comaniciu, D., V. Ramesh and P. Meer (2000). Real-Time Tracking of Non-Rigid Objects Using Mean Shift. in Proceedings of 2000 IEEE Conference on Computer Vision and Pattern Recognition. 142-149

Comaniciu, D., V. Ramesh and P. Meer (2001). The Variable Bandwidth Mean Shift and Data-Driven Scale Selection. Proc. Eighth Int'l Conf. Computer Vision. 438-445

Danuser, G. and M. Stricker (1998). "Parametric Model Fitting: From Inlier Characterization to Outlier Detection." IEEE Trans. Pattern Analysis and Machine Intelligence 20(2): 263-280.

Duda, R. O. and P. E. Hart (1973). Pattern Classification and Scene Analysis. NowYork, John Wiley & Sons.

Farneback, G. (2001). Very high accuracy velocity estimation using orientation tensors, parametric motion, and simultaneous segmentation of the motion field. Computer Vision, 2001. ICCV 2001. Proceedings. Eighth IEEE International Conference on. 171-177

Farneback., G. (2000). Fast and Accurate Motion Estimation using Orientation Tensors and Parametric Motion Models. In Proceedings of 15th International Conference on Pattern Recognition, Barcelona, Spain. 135-139

Fennema, C. and W. Thompson (1979). "Velocity Determination in Scenes Containing Several Moving Objects." Computer Graphics and Image Processing 9: 301-315.

Fischler, M. A. and R. C. Rolles (1981). "Random Sample Consensus: A Paradigm for Model Fitting with Applications to Image Analysis and Automated Cartography." Commun. ACM 24(6): 381-395.

Fitzgibbon, A., M. Pilu and R. B. Fisher (1999). "Direct Least Square Fitting of Ellipses." IEEE Trans. Pattern Analysis and Machine Intelligence 21(5): 476-480.

Fitzgibbon, A. W., D. W. Eggert and R. B. Fisher (1995). "High-Level CAD Model Acquisition from Range Images." Technical Report, Dept. of Artificial Intelligence, Univ. of Edinburgh.

Fleet, D. J. and A. D. Jepson (1990). "Computation of Component Image Velocity from Local Phase Information." International Journal of Computer Vision 5(1): 77-104.

Flynn, P. J. and A. K. Jain (1988). Surface Classification: Hypothesis Testing and Parameter Estimation. Proc. IEEE Conf. Computer Vision and Pattern Recognition (CVPR '88), Ann Arbor, Mich. 261-267

Flynn, P. J. and A. K. Jain (1991). "BONSAI:3D Object Recognition Using Constrained Search." IEEE Trans. Pattern Analysis and Machine Intelligence 13(10): 1066-1075.

Fukunaga, K. and L. D. Hostetler (1975). "The Estimation of the Gradient of a Density Function, with Applications in Pattern Recognition." IEEE Trans. Info. Theory **IT-21**: 32-40.

Ghosal, S. and R. Mehrotra (1994). "Detection of Composite Edges." IEEE Trans. PA 13(1): 14-25.

Goldenshluger, A. and A. Zeevi (2004). "The Hough transform estimator." The Annals of Statistics: to appear.

Goldgof, D. B., T. S. Huang and H. Lee (1989). "A Curvature-Based Approach to Terrain Recognition." IEEE Trans. Pattern Analysis and Machine Intelligence 11: 1213-1217.

Gonzalez., R. C. and R. E. Woods. (1992). Digital Image Processing, Reading, Mass: Addison-Wesley.

Gotardo, P., O. Bellon and L. Silva (2003). Range Image Segmentation by Surface Extraction Using an Improved Robust Estimator. IEEE Conf. Computer Vision and Pattern Recognition, Madison, Wisconsin.

Gregory, R. L. (1970). "The intelligent Eye." New York:McGraw-Hill.

Gross, A. D. and T. E. Boult (1994). "Analyzing Skewed Symmetry." International Journal of Computer Vision **13**(1): 99-111.

Hampel, F. R., P. J. Rousseeuw and E. Ronchetti (1986a). "The Change-of-Variance Curve and Optimal Redescending M-Estimators." Journal of the American Statistical Associaion **76**: 643-648.

Hampel, F. R., P. J. Rousseeuw, E. Ronchetti and W. A. Stahel (1986b). Robust Statistics: The Approach Based on Influence Functions. New York, John Wiley & Sons.

Haralick, R. M. (1986). "Computer vision theory: The lack thereof." Computer Vision Graphics Image Processing **36**: 372-386.

Haralick, R. M. and L. G. Shapiro (1992). Computer and Robot Vision, Reading, Mass: Addison-Wesley.

Hill, R. W. (1977). Robust Regression When There Are Outliers in Carriers, Harvard University.

Hoffman, R. L. and A. K. Jain (1987). "Segmentation and Classification of Range Images." IEEE Trans. Pattern Analysis and Machine Intelligence 9(5): 608-620.

Holland, P. W. and R. E. Welsch (1977). "Robust Regression Using Iteratively Reweighted Least-Squares." Communications of Statistics-Theoretical Methods **A6**: 813-827.

Hoover, A., G. Jean-Baptiste and X. Jiang. (1996). "An Experimental Comparison of Range Image Segmentation Algorithms." IEEE Trans. Pattern Analysis and Machine Intelligence **18**(7): 673-689.

Horn, B. K. P. and B. G. Schunck (1981). "Determining optical flow." Artificial Intelligence **17**: 185-204.

Hough, P. V. C. (1962). Methods and means for recognising complex patterns. U.S. Patent 3 069 654.

Huber, P. J. (1973). "Robust Regression: Asymptotics, Conjectures and Monte Carlo." Annals of Statistics **1**: 799-821.

Huber, P. J. (1981). "Robust Statistics." New York, Wiley.

Illingworth, J. and J. Kittler (1988). "A survey of the Hough transform." Computer Vision, Graphics, and Image Processing **44**: 87-116.

Iwata, H. and H. Nagahashi (1998). "Active Region Segmentation of Color Image Using Neural Networks." Systems Comput. J. **29**(4): 1-10.

Jain, A. K. and R. C. Dubes (1988). Algorithms for Clustering Data. Englewood Cliffs, N.J.: Prentice Hall.

Jiang, X. Y. and H. Bunke (1994). "Fast Segmentation of Range Images into Planar Regions by Scan Line Grouping." Machine Vision and Applications 7(2): 115-122.

Kanatani, K. (1996). Statistical Optimization for Geometric Computation: Theory and Practice. Amsterdam, Netherlands, Elsevier Science.

Kirby, M. and L. Sirovich (1990). "Application of the Karhunen-Loeve Procedure for the Characterization of Human Faces." IEEE Trans. Pattern Analysis and Machine Intelligence 12(1): 103-108.

Klinker, G. J., S. A. Shafer and T. Kanade (1990). "A Physical Approach to Color Image Understanding." International Journal of Computer Vision 4: 7-38.

Kumar, R. and A. R. Hanson (1989). Robust estimation of camera location and orientation from noisy data having outliers. Proc. International Workshop on 3D Scenes, Austin, TX. 52-60

Kurugollu, F., B. Sankur and A. E. Harmani (2001). "Color Image Segmentation Using Histogram Multithresholding and Fusion." Image and Vision Computing 19: 915-928.

Lai, S. and B. Vemuri (1998). "Reliable and Efficient Computation of Optical Flow." International Journal of Computer Vision 29(2): 87-105.

Leavers, V. F. (1993). "Which Hough transform?" CVGIP: Image Understanding 58(2): 250-264.

Lee, K.-M., P. Meer and R.-H. Park (1998). "Robust Adaptive Segmentation of Range Images." IEEE Trans. Pattern Analysis and Machine Intelligence 20(2): 200-205.

Li, G. (1985). Robust regression. Exploring Data Tables, Trends and Shape, Chapter 8. D. C. Haoglin, F. Mosteller and J. W. Tukey, John Wiley.

Lumia, R., L. Shapiro and O. Zungia (1983). "A New Connected Components Algorithm for Virtual Memory Computer." Computer Vision, Graphics, and Image Processing 22(2): 287-300.

Mallows, C. L. (1975). On Some Topics in Robustness. Memorandum, Bell Telephone Laboratories, N.J.,, Murray Hill.

Marola, G. (1989). "On the Detection of the Axes of Symmetry of Symmetric and Almost Symmetric planar Images." IEEE Trans. Pattern Analysis and Machine Intelligence 11(1): 104-108.

Maronna, R. A., O. Bustos and V. Yohai (1979). Bias and Efficiency Robustness of General M-estimators for Regression with Random Carriers. Smoothing Techniques for Curve Estimation. T. Gasser and M. Rosenbaltt. New York, Springer Verlag: 91-116.

Meer, P., D. Mintz and A. Rosenfeil (1991). "Robust Regression Methods for Computer Vision: A Review." International Journal of Computer Vision 6(1): 59-70.

Memin, E. and P. Perez (1998). "Dense Estimation and Object-based Segmentation of the Optical Flow with Robust Techniques." IEEE Trans. Image Processing 7(5): 703-719.

Memin, E. and P. Perez (2002). "Hierarchical Estimation and Segmentation of Dense Motion Fields." Internation Journal of Computer Vision 46(2): 129-155.

Miller, J. V. and C. V. Stewart (1996). MUSE: Robust Surface Fitting Using Unbiased Scale Estimates. Proc. Computer Vision and Pattern Recognition, San Francisco. 300-306

Miller, W. (1972). Symmetry Groups and Their Applications. London, Academic Press.

Ming, Y. and R. M. Haralick (2000). Optical Flow From A Least-Trimmed Squares Based Adaptive Approach. Proc. 15th International Conference on Pattern Recognition. 1052-1055

Nagel, H. H. (1987). "On the Estimation of Optical Flow." Artificial Intelligence, 33: 299-324.

Nagel, H. H. (1995). "Optical flow estimation and the interaction between measurement errors at adjacent pixel positions." Internation Journal of Computer Vision 15: 271-288.

Nalwa, V. S. (1989). "Line-drawing Interpretation: Bilateral Symmetry." IEEE Trans. Pattern Analysis and Machine Intelligence 11(10): 1117-1120.

Neisser, U. (1967). "Cognitive Psychology." New York: Appleton-Century-Crofts.

Nesi, P., A. Del Bimbo and D. Ben-Tzvi (1995). "A Robust Algorithm for Optical Flow Estimation." Computer Vision and Image Understanding 62(1): 59-68.

Nevatia (1977). "A Color Edge Detector and Its Use in Scene Segmentation." IEEE Trans. System Man Cybernet SMC 7(11): 820-826.

Oh, W. G., M. Asada and S. Tsuji (1988). Model-Based Matching Using Skewed Symmetry Information. Proc. Int'l Conf. Pattern Recognition. 1043-1045

Ong, E. P. and M. Spann (1999). "Robust Optical Flow Computation Based on Least-Median-of-Squares Regression." Internation Journal of Computer Vision 31(1): 51-82.

Otte, M. and H. H. Nagel (1995). "Estimation of Optical Flow Based on Higher order Spatiotemporal Derivatives in Interlaced and Noninterlaced Image Sequences." Artificial Intelligence 78: 5-43.

Pal, S. K. (1992). "Image Segmentation Using Fuzzy Correlation." Inform. Sci. 62: 223-250.

Ponce, J. (1990). "On Charactering Ribbons and Finding Skewed Symmetries." Computer Vision, Graphics, and Image Processing 52: 328-340.

Rao, C. R. and Toutenburg (1999). Linear Models: Least Squares and alternatives. New York, Springer-Verlag.

Reisfeld, D., H. Wolfson and Y. Yeshurun (1992). Robust Detection of Facial Features by Generalized Symmetry. Proceedings International Conference on Pattern Recognition, Champaign. 117-120

Robin, P. L. (1999). "Further Five-Point Fit Ellipse Fitting." Graphical Models and Image Processing **61**: 245-259.

Roth, G. and M. D. Levine (1990). "Segmentation of Geometric Signals using Robust Fitting." Proc. 10th. International Conference on Pattern Recognition **1**: 826-831.

Roth, G. and M. D. Levine (1991). "A Genetic Algorithm for Primitive Extraction." Proc. 4th Int. Conf. on Genetic Algorithms: 487-494.

Rousseeuw, P. J. (1984). "Least Median of Squares Regression." Journal of the American Statistical Association **79**: 871-880.

Rousseeuw, P. J. and C. Croux (1993). "Alternatives to the Median Absolute Deriation." Journal of the American Statistical Associaion **88**(424): 1273-1283.

Rousseeuw, P. J. and A. Leroy (1987). "Robust Regression and outlier detection." John Wiley & Sons, New York.

Sampson, P. D. (1982). "Fitting Conic Sections to "Very Scattered" Data: An Iterative Refinement of the Bookstein Algorithm." Computer Graphics and Image Processing **18**: 97-108.

Scott, D. W. (2001). "Parametric Statistical Modeling by Minimum Integrated Square Error." Technometrics **43**(3): 274-285.

Siegel, A. F. (1982). "Robust Regression using Repeated Medians." Biometrika **69**: 242-244.

Silverman, B. W. (1986). Density Estimation for Statistics and Data Analysis. London, Chapman and Hall.

Stewart, C. V. (1995). "MINPRAN: A New Robust Estimator for Computer Vision." IEEE Trans. Pattern Analysis and Machine Intelligence **17**(10): 925-938.

Stewart, C. V. (1997). "Bias in Robust Estimation Caused by Discontinuities and Multiple Structures." IEEE Trans. Pattern Analysis and Machine Intelligence **19**(8): 818-833.

Stewart, C. V. (1999). "Robust Parameter Estimation in Computer Vision." SIAM Review **41**(3): 513-537.

Su, M. C. and C. H. Chou (2001). "A Modified Version of the K-Means Algorithm with a Distance Based on Cluster Symmetry." IEEE Trans. Pattern Analysis and Machine Intelligence **23**(6): 674-680.

Suk, M. and S. M. Bhanddarkar (1992). Three-Dimensional Object Recognition From Range Images. Tokyo, Springer-Verlag.

Sural, S., G. Qian and S. Pramanik (2002). Segmentation and Histogram Generation Using the HSV Color Space for Image Retrieval. International Conference on Image Processing (ICIP).

Suter, D., P. Chen and H. Wang (2003). Extracting Motion from Images: Robust Optic Flow and Structure from Motion. in Proceedings Australia-Japan Advanced Workshop on Computer Vision, Adelaide, Australia. 64-69

Suter, D. and H. Wang (2004). Robust Fitting Using Mean Shift: Applications in Computer Vision. M. Hubert, G. Pison, A. Struyf, and S. Van Aelst, editors, Theory and Applications of Recent Robust Methods, Statistics for Industry and Technology. Birkhauser, Basel. to appear

Thomas, P. H. and J. S. Simon (1992). "A Cautionary Note on the Method of Least Median Squares." The American Statistician 46(2): 79-83.

Tordoff, B. and D. W. Murray (2002). "Guided Sampling and Consensus for Motion Estimation." 7th European Conference on Computer Vision **Vol.I**: 82-96.

Torr, P. and D. Murray (1997). "The Development and Comparison of Robust Methods for Estimating the Fundamental Matrix." International Journal of Computer Vision **24**: 271-300.

Torr, P. and D. Murray (1999). "The Development and Comparison of Robust Methods for Estimating the Fundamental Matrix." International Journal of Computer Vision **24**: 271-300.

Torr, P. and A. Zisserman (2000). "MLESAC: A New Robust Estimator With Application to Estimating Image Geometry." Computer Vision and Image Understanding **78**(1): 138-156.

Wand, M. P. and M. Jones (1995). "Kernel Smoothing." Chapman & Hall.

Wang, H. and D. Suter (2002a). A Novel Robust Method for Large Numbers of Gross Errors. 7th International Conference on Control, Automation, Robotics And Vision (ICARCV02), Singapore. 326-331

Wang, H. and D. Suter (2002b). LTSD: A Highly Efficient Symmetry-based Robust Estimator. 7th International Conference on Control, Automation, Robotics And Vision (ICARCV02), Singapore.

Wang, H. and D. Suter (2003a). "Using Symmetry in Robust Model Fitting." Pattern Recognition Letters 24(16): 2953-2966.

Wang, H. and D. Suter (2003b). "MDPE: A Very Robust Estimator for Model Fitting and Range Image Segmentation." International Journal of Computer Vision: to appear.

Wang, H. and D. Suter (2003c). Variable bandwidth QMDPE and its application in robust optic flow estimation. Proceedings ICCV03, International Conference on Computer Vision, Nice, France. 178-183

Wang, H. and D. Suter (2003d). A Model-Based Range Image Segmentation Algorithm Using a Novel Robust Estimator. 3rd Int'l Workshop on Statistical and Computational Theories of Vision, Nice, France.

Wang, H. and D. Suter (2003e). False-Peaks-Avoiding Mean Shift Method for Unsupervised Peak-Valley Sliding Image Segmentation. The 7th International Conference on Digital Image Computing: Techniques and Applications (DICTA'03), Sydney, Australia. 581-590

Wang, H. and D. Suter (2003f). "Robust Adaptive-Scale Parametric Model Estimation for Computer Vision." submitted to IEEE Trans. Pattern Analysis and Machine Intelligence (in revised form).

Wang, H. and S. David (2003g). Color Image Segmentation Using Global Information and Local Homogeneity. The 7th International Conference on Digital Image Computing: Techniques and Applications (DICTA'03), Sydney, Australia. 89-98

Wang, H. and D. Suter (2004). Robust Fitting by Adaptive-Scale Residual Consensus. 8th European Conference on Computer Vision (ECCV04), Prague, Czech Republic. to appear

Wani, M. A. and B. G. Batchelor (1994). "Edge Region Based Segmentation of Range images." IEEE Trans. Pattern Analysis and Machine Intelligence 16(3): 314-319.

Weyl, H. (1952). Symmetry. Princeton, NJ, Princeton Univ. Press.

Yang, X. and J. Liu (2001). "Unsupervised Texture Segmentation with One-Step Mean Shift and Boundary Markov Random Fields." Pattern Recognition Letters 22: 1073-1081.

Ye, M. and R. M. Haralick (2000). Two-Stage Robust Optical Flow Estimation. IEEE Computer Society Conference on Computer Vision and Pattern Recognition. 623-628

Yu, X., T. D. Bui and A. Krzyzak (1994). "Robust Estimation for Range Image Segmentation and Reconstruction." IEEE Trans. Pattern Analysis and Machine Intelligence 16(5): 530-538.

Zabrodsky, H. (1993). Computational Aspects of Pattern Characterization-Continuous Symmetry, Hebrew Univ. Jerusalem, Israel.

Zabrodsky, H., S. Peleg and D. Avnir (1995). "Symmetry as a Continuous Feature." IEEE Trans. Pattern Analysis and Machine Intelligence 17(12): 1154-1166.

Zhang, C. and P. Wang (2000). A New Method of Color Image Segmentation Based on Intensity and Hue Clustering. International Conference on Pattern Recognition (ICPR).

Zhang, Z. (1997). "Parameter estimation techniques: a tutorial with application to conic fitting." Image and Vision Computing **15**: 59-76.